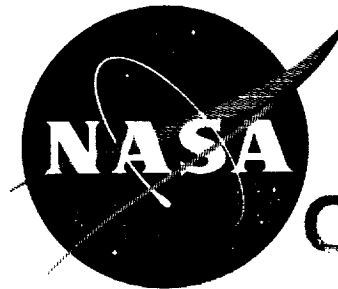


N 7 3 3 2 8 2 7

NASA CR 134483  
MDC E0784



**CASE FILE  
COPY**

**FINAL REPORT**

**FUSED SLURRY SILICIDE COATINGS  
FOR COLUMBIUM ALLOY REENTRY HEAT SHIELDS**

**Volume II Experimental and Coating Process Details**

by

**Barry Fitzgerald**

**MCDONNELL DOUGLAS ASTRONAUTICS COMPANY - EAST**

*Saint Louis, Missouri*

***August 1973***

prepared for

**NATIONAL AERONAUTICS AND SPACE ADMINISTRATION**

**NASA LEWIS RESEARCH CENTER**

**CONTRACT NAS3-14307**

**John P. Merutka, Project Manager**



1. Report No. CR-134483		2. Government Accession No.		3. Recipient's Catalog No.	
4. Title and Subtitle Fused Slurry Silicide Coatings for Columbium Alloy Reentry Heat Shields, Volume II, Experimental and Coating Process Details				5. Report Date August 1973	
				6. Performing Organization Code	
7. Author(s) Barry Fitzgerald				8. Performing Organization Report No. MDC E0784	
				10. Work Unit No.	
9. Performing Organization Name and Address McDonnell Douglas Astronautics Company - East St. Louis, Missouri 63166				11. Contract or Grant No. NAS3-14307	
				13. Type of Report and Period Covered Contractor Report	
12. Sponsoring Agency Name and Address National Aeronautics and Space Administration Washington, D.C. 20546				14. Sponsoring Agency Code	
15. Supplementary Notes Project Manager, John P. Merutka, NASA Lewis Research Center, Cleveland, Ohio					
16. Abstract Contained in this report are the experimental and coating process details of the work presented in CR-121216, Volume I, Evaluation Analysis. Also this report contains the process specifications which were developed for the formulation and application of the R-512E fused slurry silicide coating using either an acrylic or nitrocellulose base slurry system.					
17. Key Words (Suggested by Author(s)) oxidation resistant coatings columbium alloys fused slurry silicide coatings heat shields				18. Distribution Statement unclassified - unlimited	
19. Security Classif. (of this report) unclassified		20. Security Classif. (of this page) unclassified		21. No. of Pages 202	
				22. Price* \$3.00	

FOREWORD

This is the Final Technical Report on NASA-Lewis Research Center Contract NAS3-14307. The program, "Fused Slurry Silicide Coatings for Columbium Alloy Reentry Heat Shields," was conducted between June 1970 and February 1973.

Mr. John P. Merutka of NASA-Lewis Research Center's Material and Structures Division was the Project Manager. The McDonnell Douglas Astronautics Company - East Study Manager was Mr. Barry Fitzgerald.

The subcontract work on slurry process optimization was performed by HiTemCo under the technical direction of Barry Reznik with Sy Priceman assisting. Mr. Larry Sama is the Manager of Operations at HiTemCo and assisted in the preparation of the final report.

The contributions of the following individuals at MDAC-E are acknowledged: Dr. R. G. Gregory and J. K. Lehman, Strength Analysis and Rib Stiffened Panel Optimization Study; F. S. Pogorzelski, Panel Fabrication; M. B. Munsell, Reentry Simulation; and R. J. Schmitt, Emittance Measurements.

This report is divided into two volumes. Volume I, CR-121216, is the evaluation analysis summary; Volume II, CR-134483, presents the experimental and coating process details.



TABLE OF CONTENTS

<u>SECTION</u>	<u>PAGE</u>
I	
<u>EXPERIMENTAL DETAIL</u>	1
1.0 <u>ESTABLISHMENT OF TEST CONDITIONS</u>	2
1.1 Test Time	2
1.2 Test Temperature	2
1.3 Test Pressure	7
1.4 Stress Profile Selection	7
1.4.1 Rib Stiffened Panel Optimization Study	7
1.4.2 Stress Profile Consideration	10
1.4.3 Selection of Test Stress Levels	17
1.5 Acoustic Simulation	17
2.0 <u>COATING CHEMISTRY OPTIMIZATION STUDY FOR COLUMBIUM</u>	22
<u>ALLOYS C-129Y AND FS-85</u>	
2.1 Selection of Coating Chemistries	22
2.2 Screening Tests	25
2.3 Enhancement of Candidate Compositions	25
3.0 <u>SELECTION OF A COLUMBIUM ALLOY FOR REUSABLE HEAT SHIELD</u>	
<u>APPLICATIONS</u>	32
3.1 Total Hemispherical Emittance	32
3.2 Coating Structure and Chemistry	47
3.3 Reuse Capability	74
4.0 <u>COATING PROCESS OPTIMIZATION AND SCALE-UP STUDIES FOR</u>	
<u>RIB STIFFENED HEAT SHIELD PANELS</u>	87
4.1 Process Development	87
4.1.1 Screening Slurry Compositions	88
4.1.2 Slurry Support Studies	95
4.1.2.1 Fusion-Diffusion Cycle Latitude	95
4.1.2.2 Slurry Additive - Effect on	97
4.2 Process Scale-Up	101
4.2.1 Slurry Preparation	101
4.2.2 Coating Uniformity	104
4.2.3 Edge Coverage and Coating Reproducibility	106

TABLE OF CONTENTS (Continued)

<u>SECTION</u>		<u>PAGE</u>
	4.3 Process Verification	112
	4.3.1 Subsize Panels	112
	4.3.1.1 Fabrication	112
	4.3.1.2 Coating	114
	4.3.1.3 Testing	114
	4.3.2 Full Size Panels	131
5.0	<u>COATING PROCESS OPTIMIZATION AND SCALE-UP STUDIES FOR</u> <u>CORRUGATION STIFFENED HEAT SHIELD PANELS</u>	143
	5.1 Process Development	143
	5.1.1 Slurry Formulation	143
	5.1.2 Application Parameters	147
	5.1.3 Slurry Control Methods	148
	5.2 Process Scale-Up	153
	5.2.1 Coating Uniformity	153
	5.2.2 Coating Reproducibility	161
	5.3 Process Verification	163
	5.3.1 Subsize Panels	163
	5.3.1.1 Fabrication	163
	5.3.1.2 Coating	167
	5.3.1.3 Testing	169
	5.3.2 Full Size Panels	181
II	<u>C-5 COATING PROCESS SPECIFICATION</u>	192
III	<u>A-32 COATING PROCESS SPECIFICATION</u>	197
IV	<u>REFERENCES</u>	202

LIST OF PAGES

Title Page

ii -- xii

1 -- 202

ILLUSTRATIONS

<u>FIGURE</u>		<u>PAGE</u>
1-1	Reentry Profile Test Conditions for Tabs, Tensile, and Miniature Heat Shield Panels	3
1-2	Reentry Profile Test Conditions for Subsize Panels	4
1-3	Shuttle Entry Trajectory Parameters	5
1-4	Temperature on Lower Surface of High Cross Range Orbiter	6
1-5	Space Shuttle High Cross Range Orbiter Bottom Centerline Ultimate Pressures	8
1-6	Bending Strength of Rib Stiffened Panel Columbium FS-85	9
1-7	Minimum Gauge Skin is Optimum for the Rib Stiffened Concept	11
1-8	Columbium FS-85 Rib Stiffened Panel Design Curves	12
1-9	High Cross Range Orbiter Bottom Centerline Ultimate Pressure During Ascent	13
1-10	Ascent Differential Pressure Distribution and Location of Panel Design Points	14
1-11	Panel Strength and Flight Envelope	16
1-12	Acoustic Test Apparatus	20
1-13	Rib Stiffened Panel in Acoustic Fixture	21
2-1	Photomicrographs of Si-20Cr-5Ti and Si-20Ti-10Mo on 3 Columbium Alloy Substrates	23
2-2	Photomicrographs of Si-20Cr-20Fe and Si-40Cr-20Fe on Columbium Alloys C-129Y, FS-85 and Cb-752	24
2-3	Si-Cr-Fe Fused Silicide Coatings on C-129Y Alloy	28
2-4	Si-Cr-Fe Fused Silicide Coatings on FS-85 Alloy	29
2-5	Si-Cr-Fe Fused Silicide Coatings on Cb-752 Alloy	30
3-1	High Temperature Emissometer with Strip Sample Attachment	34
3-2	High Temperature Emissometer for Thin Gauge Specimens	35
3-3	Set-Up for Resistance Heating Sample from Base of Environmental Chamber	36
3-4	Results of Check on Iterative Method of Emittance Measurement	39
3-5	WC-3015/R-512E Total Normal Emittance at 2400°C (1300°C)	42
3-6	FS-85/R-512E Total Normal Emittance at 2400°F (1300°C)	43
3-7	Cb-752/R-512E Total Normal Emittance at 2400°F (1300°C)	43
3-8	C-129Y/R-512E Total Normal Emittance at 2400°F (1300°C)	43
3-9	B-66/R-512E Total Normal Emittance at 2400°F (1300°C)	44

ILLUSTRATIONS (Continued)

<u>FIGURE</u>		<u>PAGE</u>
3-10	C-129Y/Mod R-512E Emittance at 2400°F (1300°C) Versus Number of Reentry Cycles	46
3-11	FS-85/R-512E (A-32) Emittance at 2400°F (1300°C) Versus Number of Reentry Cycles	46
3-12	Photomicrographs of the Areas Examined with the Electron Microprobe on the Cb-752/R-512E System	52
3-13	Effect of Reentry Cycling on Niobium Distribution in the R-512E/Cb-752 Coating System	53
3-14	Effect of Reentry Cycling on Tungsten Distribution in the R-512E/Cb-752 Coating System	54
3-15	Effect of Reentry Cycling on Zirconium Distribution in the R-512E/Cb-752 Coating System	56
3-16	Effect of Reentry Cycling on Chromium Distribution in the R-512E/Cb-752 Coating System	57
3-17	Effect of Reentry Cycling on Iron Distribution in the R-512E/Cb-752 Coating System	58
3-18	Effect of Reentry Cycling on Silicon Distribution in the R-512E/Cb-752 Coating System	59
3-19	Photomicrographs of the Areas Examined with the Electron Microprobe on the FS-85/R-512E System	60
3-20	Effect of Reentry Cycling on Niobium Distribution in the R-512E/FS-85 Coating System	61
3-21	Effect of Reentry Cycling on Tantalum Distribution in the R-512E/FS-85 Coating System	62
3-22	Effect of Reentry Cycling on Tungsten Distribution in the R-512E/FS-85 Coating System	64
3-23	Effect of Reentry Cycling on Chromium Distribution in the R-512E/FS-85 Coating System	65
3-24	Effect of Reentry Cycling on Iron Distribution in the R-512E/FS-85 Coating System	66
3-25	Effect of Reentry Cycling on Silicon Distribution in the R-512E/FS-85 Coating System	67
3-26	Photomicrographs of the Areas Examined with the Electron Microprobe on the C-129Y/R-512E System	68
3-27	Effect of Reentry Cycling on Niobium Distribution in the R-512E/C-129Y Coating System	69
3-28	Effect of Reentry Cycling on Tungsten Distribution in the R-512E/C-129Y Coating System	70
3-29	Effect of Reentry Cycling on Hafnium Distribution in the R-512E/C-129Y Coating System	71

ILLUSTRATIONS (Continued)

<u>FIGURE</u>		<u>PAGE</u>
3-30	Effect of Reentry Cycling on Chromium Distribution in the R-512E/C-129Y Coating System	72
3-31	Effect of Reentry Cycling on Iron Distribution in the R-512E/C-129Y Coating System	73
3-32	Effect of Reentry Cycling on Silicon Distribution in the R-512E/C-129Y Coating System	75
3-33	Rib Stiffened Panel Specimen	76
3-34	Profile Simulation Test Facility	77
3-35	Panel Loading Distribution and Fixture	78
3-36	R-512E Coated C-129Y Rib Stiffened Heat Shield Panel After 100 Simulated Shuttle Reentries (External Pressure)	81
3-37	Rib and Skin Cross Sections of an R-512E Coated C-129Y Miniature Heat Shield Panel in the As Coated Condition	82
3-38	Rib and Skin Cross Sections of an R-512E Coated FS-85 Miniature Heat Shield Panel After 80 Reentry Exposures (Ext. Pressure)	83
3-39	Rib and Skin Cross Sections of an R-512E Coated Cb-752 Miniature Heat Shield Panel After 28 Reentry Exposures (Ext. Pressure)	84
4-1	C-4 Slurry Coverage	91
4-2	C-5 Slurry Coverage	92
4-3	A-16 Slurry Coverage	93
4-4	Effect of Diffusion Temperature and Time on Air Slow Cycle Life	96
4-5	Effect of Vehicle, Binder and Thixotropic Additives on the Coating Structure of R-512E on Cb-752 Alloy	98
4-6	Coating Uniformity Studies on 20" x 20" (50 cm x 50 cm) Flat Panel Mockup	102
4-7	Effect of Settling on Viscosity 1/4 In. (0.6 cm) Below Surface for Acrylic Base (A-22) and Nitrocellulose Base (C-5) Slurries	102
4-8	Coating Composition Uniformity on 20" x 20" (50 cm x 50 cm) Flat Stainless Mockup	103
4-9	Coating Uniformity Study on 20" x 20" (50 cm x 50 cm) Rib Stiffened Mockup	105
4-10	Dermatron Uniformity* Study As Dipped and (As Diffused) R-512E on Cb-752	106
4-11	Metallographic Uniformity Study on Cb-752 Corner Detail	107
4-12	The Use of Yellow Colorant on the Edge Overspray Slurry	109
4-13	Slurry Bead Applied to Edge After Dip Coating	109

## ILLUSTRATIONS (Continued)

<u>FIGURE</u>		<u>PAGE</u>
4-14	Edge Coverage R-512E on Cb-752 Alloy	111
4-15	Roller Probe for Thermoelectric NDT of Edge Coating Thickness	111
4-16	Coating at Rib Edge on 3" x 4" (7.5 cm x 10 cm) Cb-752 Panel	111
4-17	Rib Stiffened Columbiu Panel Specimen	113
4-18	Metallographic Coating Uniformity Study on R-512E Coated FS-85 Alloy Subsize Rib Stiffened Heat Shield Panel	115
4-19	Uniformity Study - R-512E Coated FS-85 Alloy 3" x 12" (7.5 cm x 30 cm) Rib Stiffened Panel	116
4-20	Astro Furnace and Loading Fixture Used for Reentry Simulation	118
4-21	Subsize Rib Stiffened Heat Shield Panel Creep Deflections	120
4-22	Creep Deflection Rate of Subsize Rib Stiffened Heat Shield Panels	121
4-23	Flight Simulation Testing of Panel No. 1	123
4-24	Flight Simulation Testing of Panel No. 2	124
4-25	Flight Simulation Testing of Panel No. 3	125
4-26	Flight Simulation Testing of Panel No. 4	126
4-27	Flight Simulation Testing of Panel No. 5	127
4-28	Heat Shield Panel No. 2 After 100 Cycles - External Pressure 1/4" (0.6 cm) from Rib Fracture	128
4-29	Heat Shield Panel No. 5 After 45 Cycles - External Pressure 1/4" (0.6 cm) From Rib Fracture	129
4-30	Green Coating Uniformity Study by Dermitron NDT - Panel 8C0	133
4-31	Final Coating Uniformity Study by Dermitron NDT - Panel 8C0	135
4-32	Final Edge Coating Thickness Uniformity Study by Thermoelectric NDT - Panel 8C0	136
4-33	Green Coating Uniformity Study by Dermitron NDT - Panel 8	137
4-34	Final Coating Uniformity Study by Dermitron NDT - Panel 8	138
4-35	Final Edge Coating Thickness Uniformity Study by Thermoelectric NDT - Panel 8	139
4-36	20" x 20" (50 cm x 50 cm) Rib Stiffened FS-85 Alloy Heat Shield Panel	141
4-37	Corner Detail 20" x 20" Rib Stiffened FS-85 Heat Shield Panel	142
5-1	Cross Section of 20" (50 cm) Long Corrugated Specimen Made 1" (2.5 cm) From Top with Respect to Dipping Direction of Specimen	144

ILLUSTRATIONS (Continued)

<u>FIGURE</u>		<u>PAGE</u>
5-2	Cross Section of 20" (50 cm) Long Corrugated Specimen Made 9" (23 cm) From Top with Respect to Dipping Direction of the Specimen	145
5-3	Cross Section of 20" (50 cm) Long Corrugated Specimen Made 15" (38 cm) From Top with Respect to Dipping Direction of Specimen	146
5-4	Effect of Settling on Viscosity 1/4" (0.6 cm) Below Surface for Acrylic Base A-22, A-28 and Nitrocellulose Base C-5 Slurries	149
5-5	Effect of Withdrawal Speed on Coating Thickness and Uniformity of 2" x 20" (5 cm x 50 cm) Strips in Acrylic Slurry A-28	150
5-6	Uniformity Study of 2" x 20" (5 cm x 50 cm) Strip in Acrylic Based Slurry A-29	151
5-7	18" (46 cm) Long Stainless Steel Corrugated Specimens	152
5-8	Green Coating Uniformity Study on Inside Surface of Skin, Single Face Corrugated Panels. For Nitrocellulose and Acrylic Based Slurry Air and Vacuum Dried (Note Coating Thinning Towards Edge).	154
5-9	Coating Uniformity Study on Corrugated Mockup Panel Panel 18 - A-29 Acrylic Based Slurry	155
5-10	Coating Uniformity Study on Corrugated Mockup Panel Panel 19 - C-5 Nitrocellulose Based Slurry	157
5-11	Coating Uniformity Study on Corrugated Mockup Panel Panel S-1 - A-32 (High Additive) Acrylic Based Slurry	158
5-12	Coating Uniformity Study on Corrugated Mockup Panel Panel 21 - A-29 Acrylic Based Slurry with Post 4 Wetting Agent	159
5-13	Coating Uniformity Study on FS-85 Alloy Si-20Cr-20Fe Coated Corrugated Panel Detail A-32 Acrylic Based Slurry	160
5-14	Green Coating Uniformity Study on 3" x 4" (7.5 cm x 10 cm) Corrugated FS-85 Alloy	161
5-15	Green Coating Uniformity Study on Subsize Corrugated FS-85 Alloy	162
5-16	Fired Coating Uniformity Study on 3" x 4" (7.5 cm x 10 cm) corrugated FS-85 Alloy Panel - Dermitron NDT	163
5-17	Fired Coating Uniformity Study on Subsize Corrugated FS-85 Alloy Panel - Dermitron NDT	164
5-18	Uniformity Study - R-512E Coated FS-85 Alloy Subsize Corrugated Panel	165
5-19	Coating Uniformity Study on Subsize Corrugated Heat Shield Panel	166

ILLUSTRATIONS (Continued)

<u>FIGURE</u>		<u>PAGE</u>
5-20	Single Pitch of Corrugated Heat Shield Panel Cross Section Drawing Showing Shape and Dimensions	168
5-21	Subsize Corrugation Stiffened Heat Shield Panel Creep Deflections	172
5-22	Flight Simulation Testing of Panel No. 2	174
5-23	Flight Simulation Testing of Panel No. 5	175
5-24	Flight Simulation Testing of Panel No. 7	176
5-25	Flight Simulation Testing of Panel No. 10	177
5-26	Flight Simulation Testing of Panel No. 12	178
5-27	Corrugation-Skin Joint of Panel No. 10 After 100 Reentry Cycles - Internal Pressure Environment	179
5-28	Skin Cross Section Between Welds of Panel No. 10 After 100 Reentry Cycles - Internal Pressure Environment	179
5-29	Straightening Bar Fixture in Place of Panel F-1 Prior to Dipping	183
5-30	Green Coating Uniformity by Dermatron NDT - Panel F-1	184
5-31	Final Coating Uniformity by Dermatron NDT - Panel F-1	185
5-32	Final Edge Coating Thickness Uniformity by Thermoelectric NDT - Panel F-1	186
5-33	Green Coating Uniformity by Dermatron NDT - Panel F-2	187
5-34	Final Coating Uniformity by Dermatron NDT - Panel F-2	188
5-35	Final Edge Coating Uniformity by Thermoelectric NDT - Panel F-2	189
5-36	General Appearance of Panels F-1 and F-2 After Coating	190
5-37	Closeup View of Corner Area of Panel F-1 After Coating	191



TABLES

<u>TABLE</u>		<u>PAGE</u>
2-1	Coating Chemistry Study Test Results	26
2-2	Oxidation Performance of Modified Coatings	27
3-1	Emittance Data R-512E Coated Columbium Alloys	40
3-2	Emittance Data Mod R-512E Coated C-129Y	45
3-3	Emittance Data Mod R-512E Coated FS-85	45
3-4	Test Matrix for Coating Chemistry and Structure Studies	48
3-5	Coating Surface Comparison of 100 Cycle Specimens to 50 Cycle Specimens by X-Ray Fluorescence	49
3-6	X-Ray Diffraction Results	50
3-7	Background Determinations	50
3-8	Miniature Rib Stiffened Heat Shield Panels Reuse Testing Results	79
3-9	Typical NDT Coating Thickness on R-512E Coated Rib Stiffened Panels	85
4-1	Materials Used for Slurry Preparation	87
4-2	Acrylic Base Screening Slurries	89
4-3	Nitrocellulose (L-18) Lacquer Slurries	90
4-4	Slurries with Post 4 Added to the Acrylic Vehicle	95
4-5	Coating Uniformity Studies A-22 Slurry, 2" x 20" (5 x 50 cm) Strips	95
4-6	Effect of Diffusion Temperature and Time on Coating Life	107
4-7	Effect of Slurry Additives on Slow Cyclic Air Oxidation of R-512E Coated Cb-752 Alloy	101
4-8	Effect of Edge Coating Method on Performance on R-512E Coating	110
4-9	Coating Thickness and Cyclic Life of Panel Sections	112
4-10	Coating Weight and Thickness Summary for Subsize FS-85 Rib Stiffened Panels	117
4-11	Deflection Measurements for Subsize Rib Stiffened Panels	119
4-12	NDT Dermatron Coating Thickness on R-512E Coated FS-85 Subsize Panels	130
5-1	Modified and Scaled-Up Acrylic Base Slurry Compositions	148
5-2	Comparison of an Acrylic Vs. Nitrocellulose Based Slurry on Coating Uniformity of Single Faced Corrugated Panels	153
5-3	Comparison of Air Vs. Vacuum Drying on Coating Uniformity of Single Faced Corrugated Panels	156

TABLES (Continued)

<u>TABLE</u>		<u>PAGE</u>
5-4	Effect of Thixotropic Additive Concentration on Coating Uniformity of Single Face Corrugated Panels with Acrylic Based Slurry	156
5-5	Coating Studies on 3" x 4" (7.5 cm x 10 cm) Panel Sections	167
5-6	Data Summary for Subsize FS-85 Corrugated Panels	169
5-7	Deflection Measurements for Subsize Corrugation Stiffened Heat Shield Panels	170
5-8	NDT Dermatron Coating Thickness on R-512E Coated FS-85 Subsize Corrugation Stiffened Panels	180

I

EXPERIMENTAL AND COATING PROCESS DETAIL

Equipment, test conditions and experimental details are described in this section.

The International System of Units, SI Units, is used as the secondary system of units in this report, parenthetically following the customary English Units. In the case of figures and tables, separate abscissa and ordinate scales or columns are given, one in SI Units, and one in customary English Units.

The SI Units used in this report, together with their symbols, are listed below:

<u>Physical Quantity</u>	<u>Name of Unit</u>	<u>Symbol</u>
Length	meter	m
Mass	gram	g
Time	second	s
Area	square meter	m <sup>2</sup>
Volume	cubic meter	m <sup>3</sup>
Density	grams per cubic meter	g/m <sup>3</sup>
Force	newton	N (kg•m/s <sup>2</sup> )
Pressure	newton per square meter	N/m <sup>2</sup>
Dynamic Viscosity	newton-second per square meter	N•s/m <sup>2</sup>
Work	joule	J (N•m)

The names of multiples and submultiples of the SI Units used were formed by the application of the following prefixes:

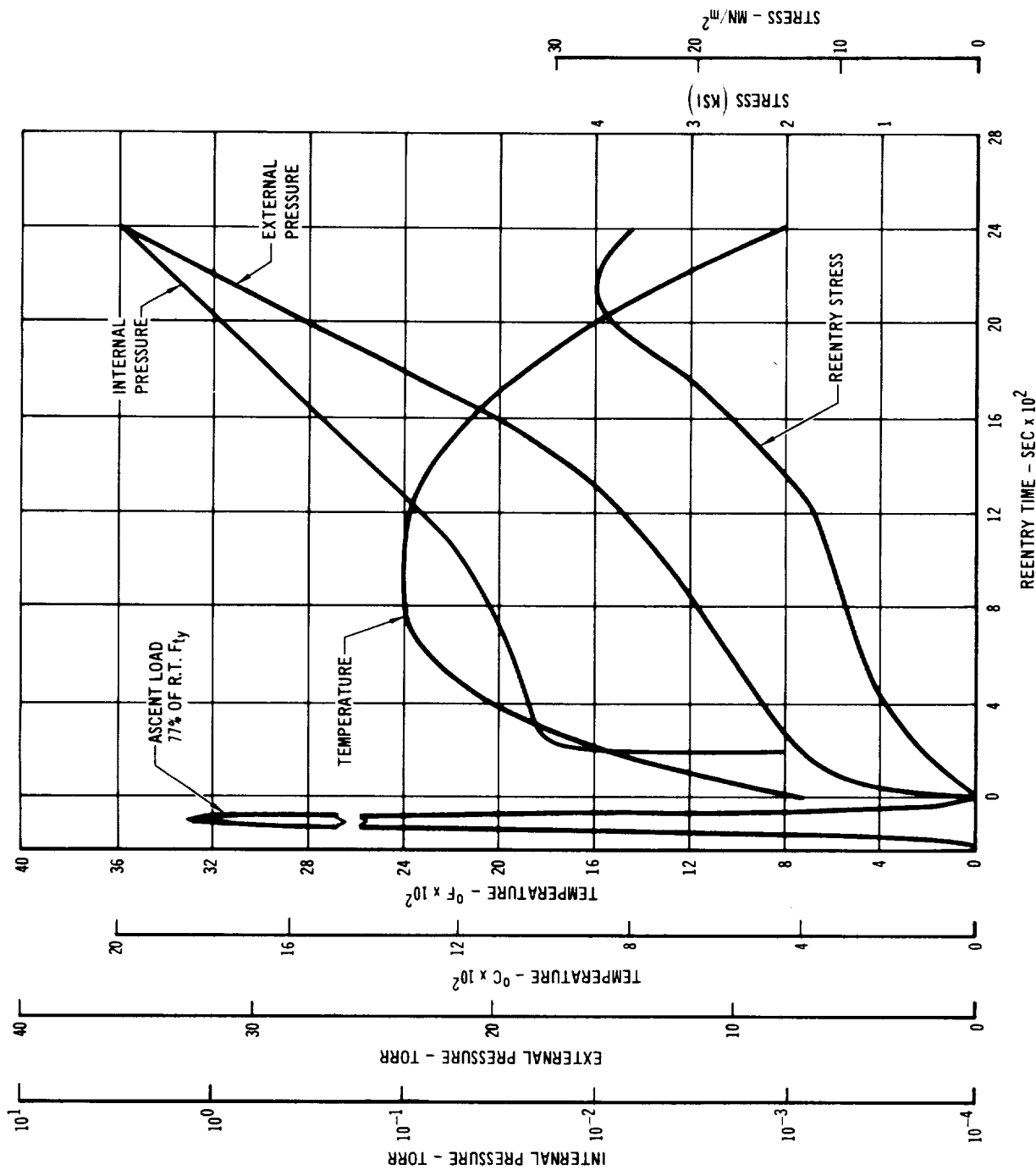
<u>Multiplying Factor</u>	<u>Prefix</u>	<u>Symbol</u>
10 <sup>6</sup>	mega	M
10 <sup>3</sup>	kilo	k
10 <sup>2</sup>	hecto	h
10 <sup>-2</sup>	centi	c
10 <sup>-3</sup>	milli	m
10 <sup>-6</sup>	micro	μ

## 1.0 TEST CONDITIONS

Reuse evaluation of fused slurry silicide coated columbium alloys involving tabs, tensile, and panel specimens required the selection of a set of test conditions for the flight profile simulation testing. These test conditions were selected to represent a Space Shuttle operational system. Instead of selecting a particular trajectory and point on a specific vehicle, the necessary parameters of time, temperature, pressure, and stress were studied separately. An attempt was made to insure that the full effect of each parameter would be imposed upon the test specimen in a realistic manner. The test conditions had to be representative of the general environmental conditions of the several Shuttle vehicles and missions under consideration, as well as of probable future vehicles. Each of the test parameters will be discussed separately and the rationale for its definition described. The initial test conditions selected are shown in Figure 1-1 and were used for evaluation of tabs, tensile specimens, and miniature heat shield panels. The flight simulation testing of a subsize rib stiffened panel required the use of a 7" (18 cm) diameter tube furnace. Since this furnace would not cool at the required rate, the profile was extended to 3600 sec elapsed time. The same temperature, pressure, and stress relationships were maintained throughout as shown in Figure 1-2. The total time above 2000°F (~ 1100°C) was 1200 sec, above 2200°F (~ 1200°C) was 780 sec, and at 2400°F (~ 1300°C) was 300 sec. The difference between the profiles occurred in the cooling time below 2000°F (~ 1100°C).

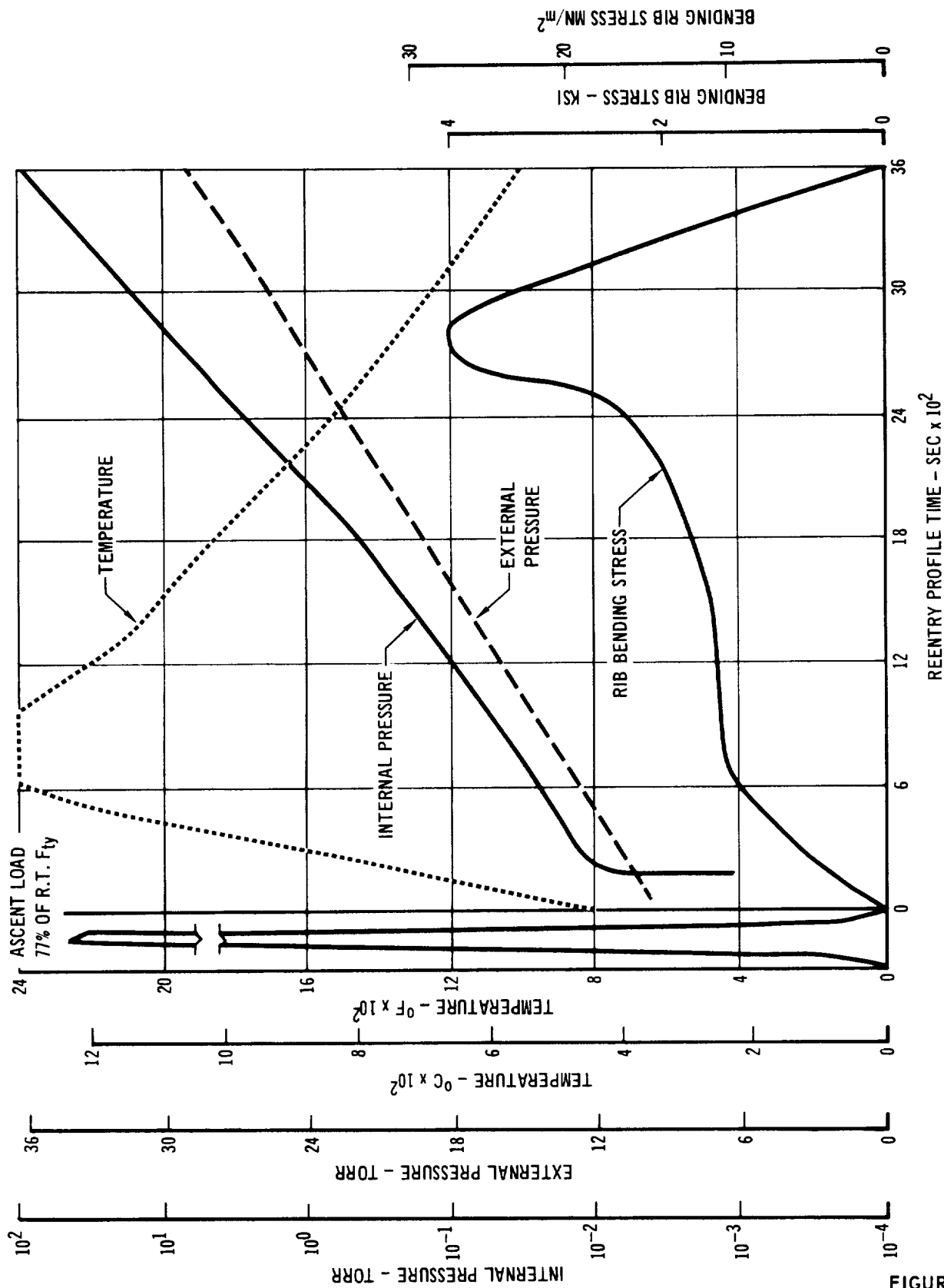
1.1 Test Time - The major influence on test duration was the selection of either a low or high cross range mission. A high cross range time of 2700 sec was chosen. This is longer than the majority of vehicles surveyed; however, the longer time is a conservative approach which also makes the test results applicable to a wider range of reentry vehicle systems. The extension of the time profile to 3600 sec was required during flight simulation of the subsize panels because of testing equipment limitations.

1.2 Test Temperature - A great many factors were considered in selecting the test temperature profile. Figure 1-3 illustrates some of the parameters surveyed and factors considered (Reference 1). The double peak condition illustrated in Figure 1-3 was selected as the most severe condition since it represents the greatest time at elevated temperature and also the greatest total heat input for equivalent maximum temperature of a single peak condition. Figure 1-4 shows the temperature as a function of time for the high cross range



REENTRY PROFILE TEST CONDITIONS FOR TABS, TENSILE, AND  
MINIATURE HEAT SHIELD PANELS

FIGURE 1-1



REENTRY PROFILE TEST CONDITIONS FOR SUB-SIZE PANELS

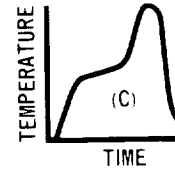
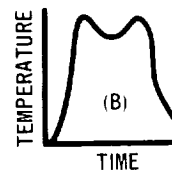
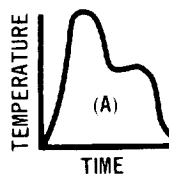
FIGURE 1-2

						PHASE B (DEVELOPED BY MDAC AS OF 8/1/70)		
	PHASE A		PRE-PHASE B (ORBITER "B" MOD 1)			HIGH CROSS RANGE MARK 1 SHAPE 2000°F INCLUDES DESIGN MARGINS	HIGH CROSS RANGE DRAW- BRIDGE LOW ALTITUDE DISPERSED INCLUDES DESIGN MARGINS	LOW CROSS RANGE LOW ALTITUDE DISPERSED 600 BANK NO DESIGN MARGINS
	LOW CROSS RANGE MSC-ILRV	HIGH CROSS RANGE (SAMSO)	LOW CROSS RANGE *	MEDIUM CROSS RANGE *	HIGH CROSS RANGE *			
CROSS RANGE (NMI) Km	231/428	2,000/3,700	350/650	1,260/2,340	1,700/3,160	1,500/2,790	2,180/4,050	140/260
DOWN RANGE (NMI) Km	2,000/3,700	9,800/18,200	2,800/5,200	5,400/10,000	6,500/12,000	6,300/11,700	6,500/12,000	2,100/39,000
W/C L S (W/S) K/m <sup>2</sup>	30/147	53/260	73/357	108/528	156/762	118/578	216/1,010	60/294
L/D	0.54	2.2	0.7	1.45	1.75	1.75	2.0	0.52
VEHICLE LENGTH (FT) m		160/48	170/51	170/51	170/51	156/47	148/44	148/44
ENTRY ANGLE (DEG)	-1.6	-1.5	-1.6	-1.6	-1.6	-1.6	-1.6	-1.6
ENTRY TIME (SEC)	1,260	3,100	1,138	2,079	2,523	2,590	2,755	720
ANGLE OF ATTACK (DEG)	60	43-20	53	31	23	14-20	18	60
MAXIMUM DYNAMIC PRESSURE (LBF/FT <sup>2</sup> ) N/m <sup>2</sup>	35-40 1675-1915	-	75/3,590	125/6,000	182/8,700	112/5,460	272/13,000	50/2,390
MAXIMUM SURFACE TEMPERATURE (°F) °C	2,200/1,200	2,200/1,200	2,100/1,150	2,100/1,150	2,100/1,150	2,000/1,100	2,200/1,200	2,200/1,200
TOTAL HEAT (A) (BTU/FT <sup>2</sup> MJ/m <sup>2</sup> )	7,600/86	44,00/504	-	-	-	15,989/18	22,275/253	5,340/61
TOTAL HEAT (B) (BTU/FT <sup>2</sup> MJ/m <sup>2</sup> )	-	-	-	-	-	17,623/200	31,950/404	5,315/60
TOTAL HEAT (C) (BTU/FT <sup>2</sup> MJ/m <sup>2</sup> )	-	-	6,116/69	14,699/167	16,994/192	15,055/171	18,305/209	4,892/55
TIME AT MAXIMUM TEMPERATURE (+20°)(A)(SEC)	60	60	-	-	-	140	100	75
TIME AT MAXIMUM TEMPERATURE (+20°)(A)(SEC)	-	-	-	-	-	250	230	100
TIME AT MAXIMUM TEMPERATURE (+20°)(C)(SEC)	-	-	20	250	70	50	60	35

\*  $\frac{X}{L} = 0.25$  WITH  $X = 42.5$  FT (14.3 m) AND  $L =$  DISTANCE FROM THE NOSE ALONG THE BOTTOM Q.

HEAT PULSE SHAPE

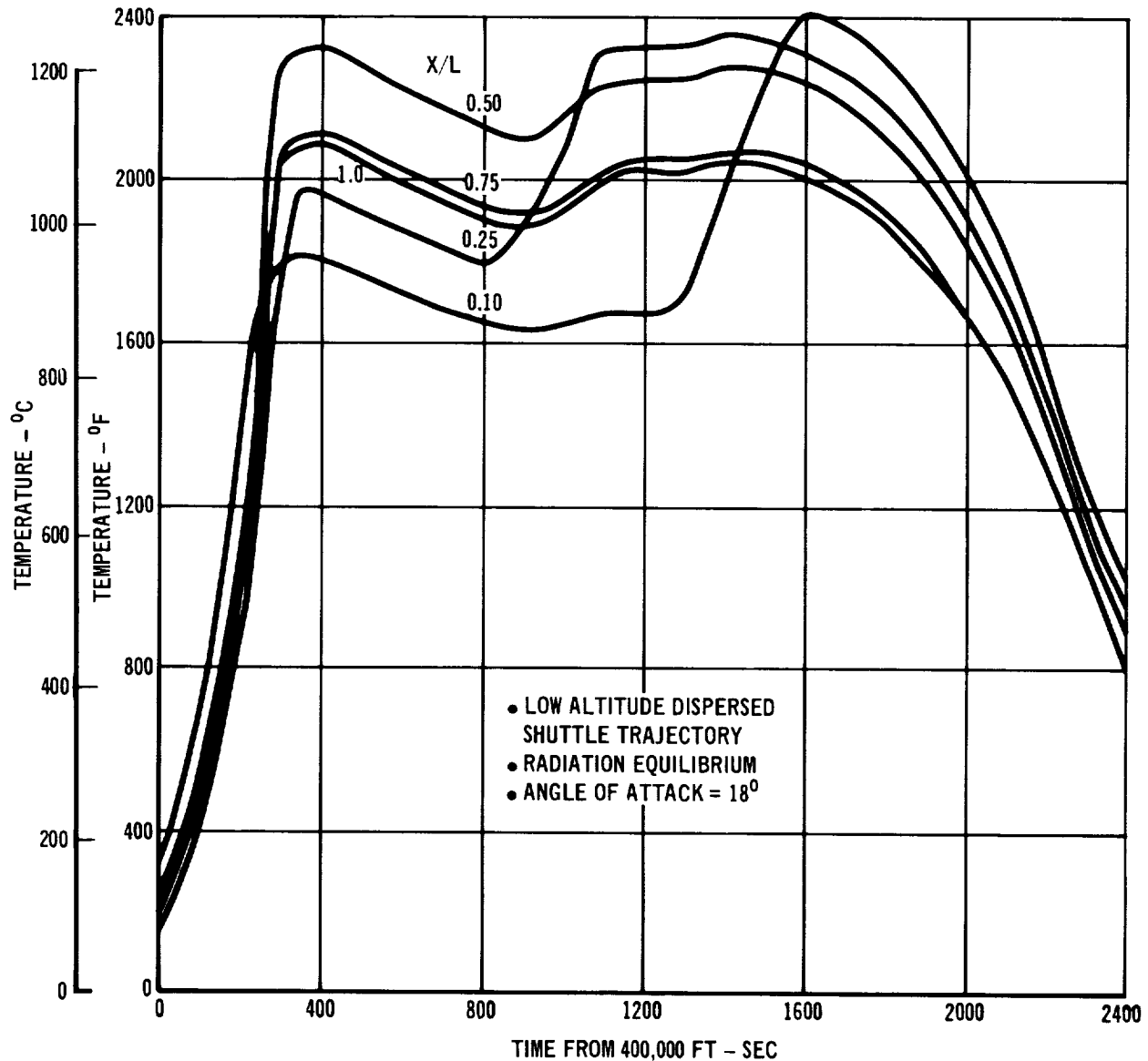
- (A) EARLY TEMPERATURE PEAK
- (B) DOUBLE TEMPERATURE PEAK
- (C) LATE TEMPERATURE PEAK



457-1158

SHUTTLE ENTRY TRAJECTORY PARAMETERS

FIGURE 1-3



TEMPERATURE ON LOWER SURFACE OF HIGH CROSS RANGE ORBITER

457-1160

FIGURE 1-4

orbiter which was used as a guide in selecting the test profile. A maximum temperature of 2400°F (1300°C) was selected, since it is equal to, or higher than, most temperatures surveyed. The selected temperature profile shown in Figure 1-1 employed a procedure of comparing the time at or above 2000°F (1100°C), 2200°F (1200°C), and 2400°F (1300°C) for several possible temperature profiles to insure that the selected conditions were broadly representative. The position of the peak and the cooling rate reflect the capabilities of the testing facility.

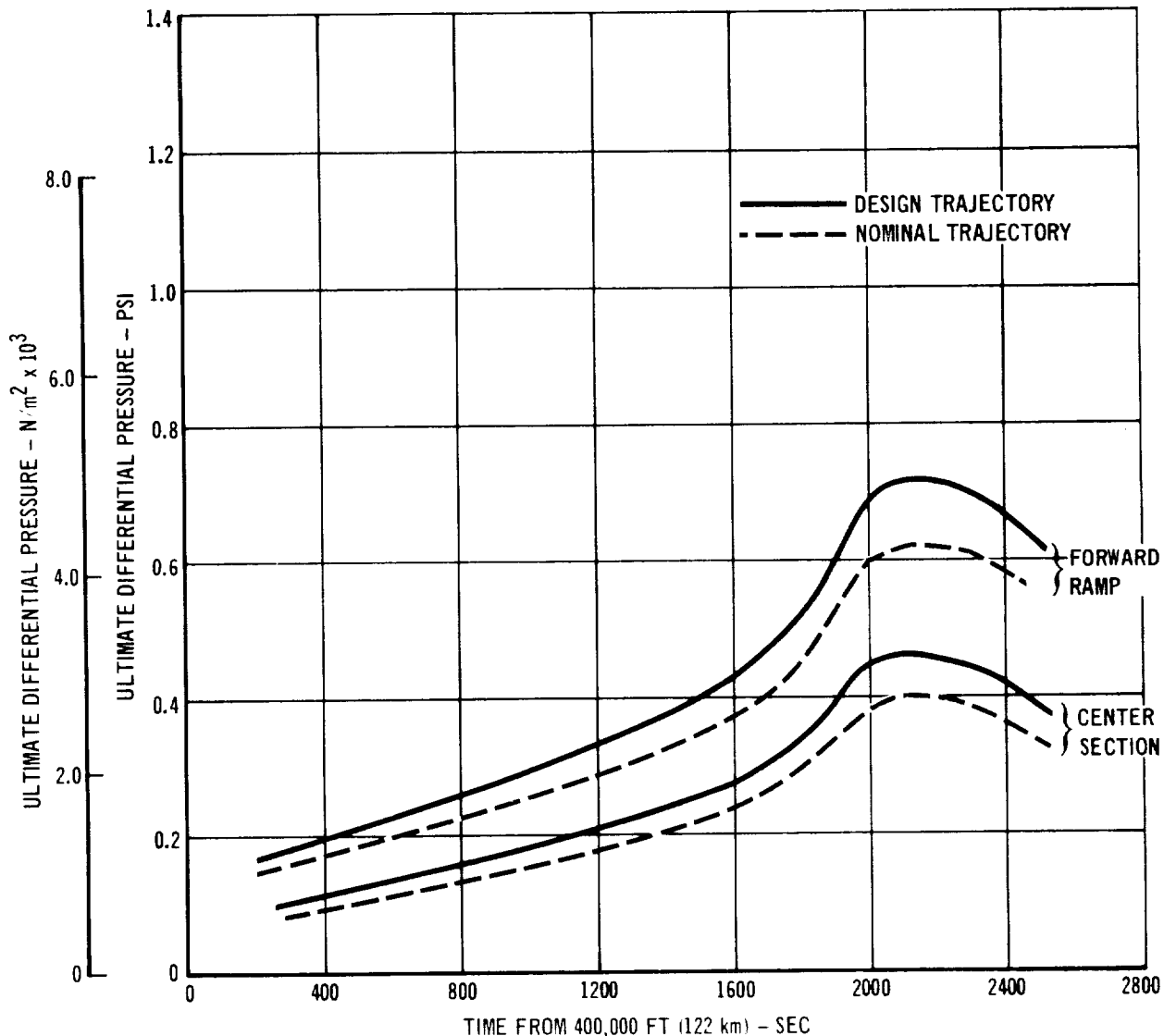


1.3 Test Pressure - The air pressure to be employed is an important testing parameter, because it strongly influences both coating protectiveness and base metal oxidation in areas of coating failure or damage. Both internal and external type pressure profiles were employed in testing and are shown in Figures 1-1 and 1-2. External pressures are those associated or present on the moldline surfaces of a vehicle during reentry. Internal pressures are those associated with the internal surfaces of heat shields and are normally considered to be ambient or equal to altitude. Loading on heat shields during actual reentry is produced by the difference in the external and internal pressure.

It was found that the external and internal pressure variations for various Shuttle orbiter vehicles and reentry conditions were subtle compared with coating performance. The coating and substrate oxidation mechanisms would be the same over the range of possible representative pressures that could be selected. Figure 1-5 shows the pressure on the lower surface of the high cross range Mark I Delta Orbiter. The design trajectory for the forward ramp was selected, since it was predicted to be the most severe test for substrate oxidation. The internal pressure profile is derived from a direct conversion of the expected altitude versus time plot of the Mark I Delta Orbiter. The external pressure curve is arrived at by adding the internal pressure to the forward ramp nominal differential pressure.

1.4 Stress Profile Selection - The proper stress or load to be applied to the panels is a very important environmental test condition because the stressing of the columbium substrate affects the protectiveness of the coating. The criterion for failure in the rib stiffened panel specimens was defined as the inability to carry the required loads. The exact design to be tested had to be defined before the critical load carrying member and the appropriate stress level could be determined. It was considered advantageous to optimize the rib stiffened design for a full size panel to determine the proper rib stress to employ. Fabrication of the sub- and full size rib stiffened panels for testing in the later stages required this design optimization study; therefore, the study was accomplished before a stress profile for the test conditions was made final.

1.4.1 Rib Stiffened Panel Optimization Study - A strength optimization study was conducted for rib stiffened columbium thermal protection system panels applicable to the Space Shuttle. Panel geometry is shown in Figure 1-6. Rib gage (w), skin gage (t), rib spacing (b) and rib height (h) were all varied to obtain

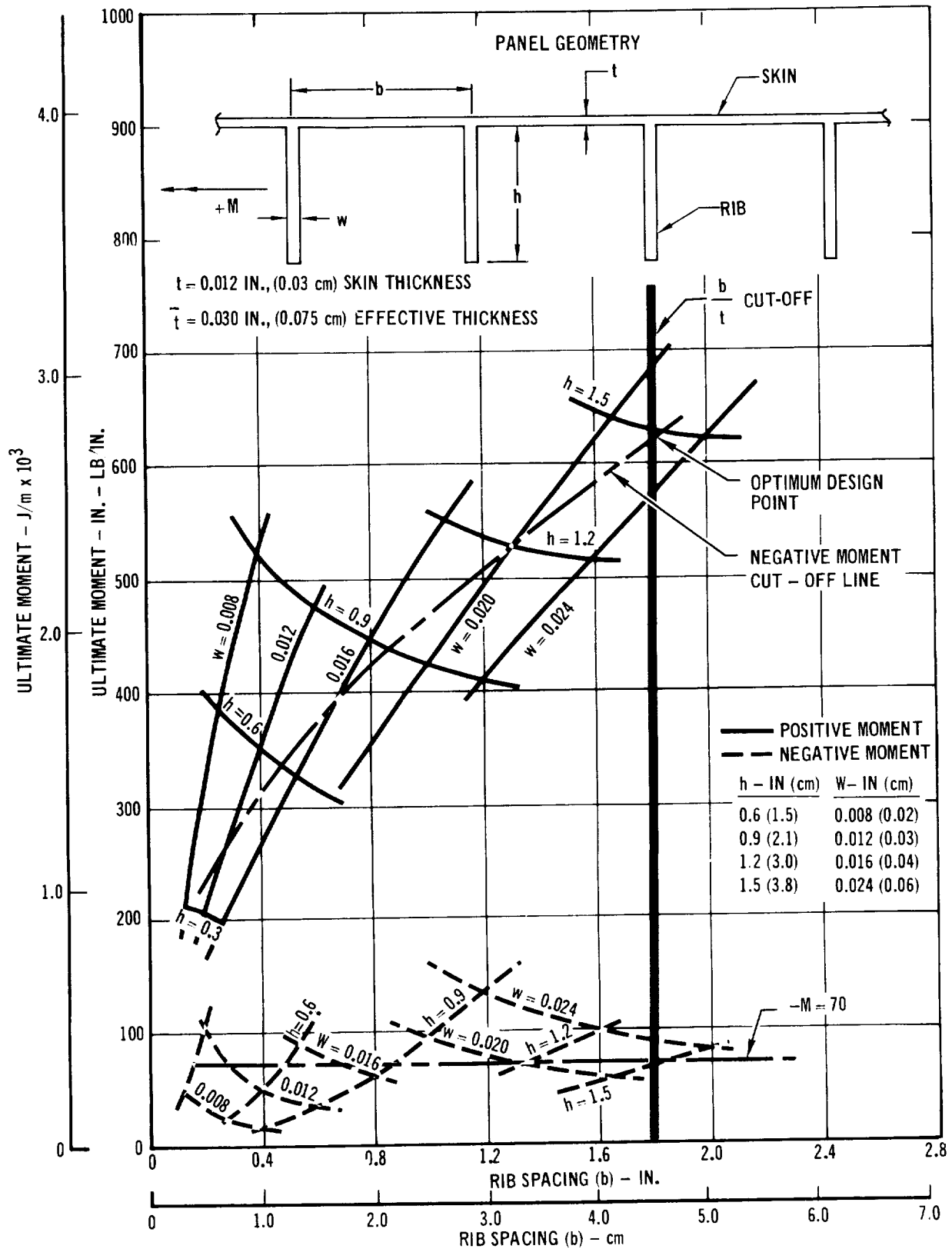


SPACE SHUTTLE  
HIGH CROSS RANGE ORBITER  
BOTTOM CENTERLINE ULTIMATE PRESSURES

FIGURE 1-5

minimum weight panels.

Figure 1-6 is an example of the working curves generated in the study. All data on Figure 1-6 are for a constant effective thickness (or weight) and a constant skin thickness. The upper curves show ultimate allowable positive bending strengths (causing compression in the skin) and the lower curves represent ultimate allowable negative bending strengths. A plastic bending analysis was used to determine ultimate positive bending strengths. Compression cap strength was based



BENDING STRENGTH OF RIB-STIFFENED PANEL  
COLUMBIUM FS-85

FIGURE 1-6

on crippling strength of the flat skin and of a portion of the rib above the neutral axis. The tension cap was assumed to operate at its ultimate tensile stress. Limit negative bending strength (causing compression in the rib) was based on an elastic analysis in which the allowable compressive stress in the rib was based on the rib buckling strength. Ultimate negative bending strength, shown in Figure 1-6, was obtained by multiplying limit strength by the safety factor of 1.4.

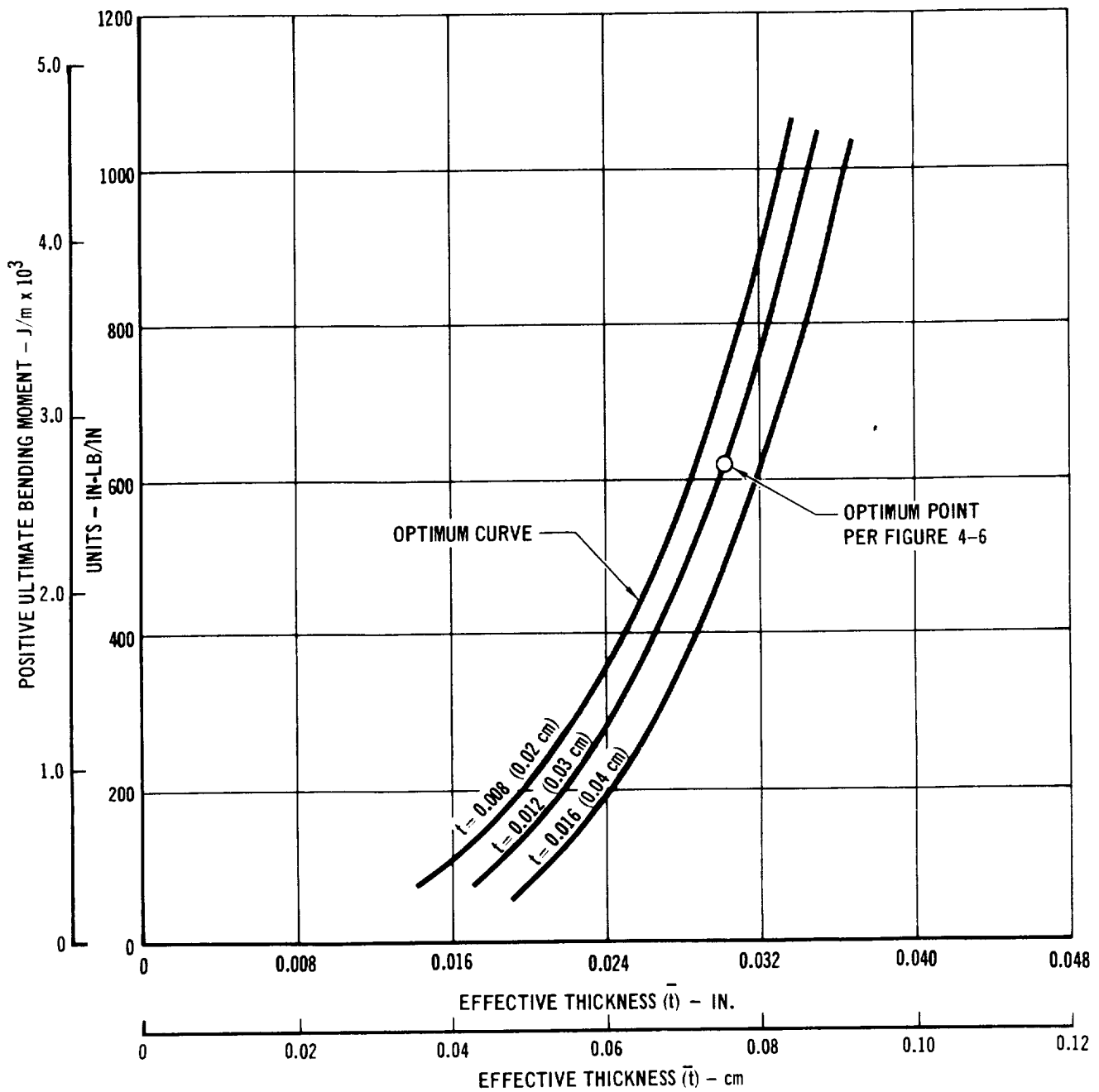
Constraints were established for the maximum  $b/t$  ratio and minimum negative bending strength. Based on previous experience with similar structures, a maximum  $b/t$  ratio of 150 was selected to minimize response to acoustic loading. A minimum allowable negative bending strength of 70 in-lb/in (310 J/m) was selected, which is based on  $1.4 \text{ lb/in}^2$  ( $9650 \text{ N/m}^2$ ) ultimate pressure active over a 20" (50 cm) span. The negative bending cutoff line, shown in Figure 1-6, was used to identify panel cross-sectional properties which meet the negative bending strength requirements. The optimum design moment for this weight is the maximum moment within the  $b/t$  cutoff constraint, and the negative moment cutoff line, as shown.

Figure 1-7 is made up from optimum moments determined from curves of the type shown in Figure 1-6 which have other effective skin thicknesses of 0.008, 0.012, and 0.016" (0.02, 0.03 and 0.04 cm). For any required moment allowable, the 0.008" (0.02 cm) skin thickness (minimum gage) yields the lowest weight design.

The resulting rib stiffened panel design curves are shown in Figure 1-8. These curves can be used to determine  $h$ ,  $w$ , and panel weight as a function of ultimate positive bending moment for columbium FS-85 panels at room temperature. Each design has an ultimate negative bending strength of 70 in-lb/in (310 J/m).

**1.4.2 Stress Profile Considerations** - The results of the rib stiffened panel design optimization study were combined with the Shuttle strength requirements and the effects of different alloys, Cb-752 and C-129Y, were considered.

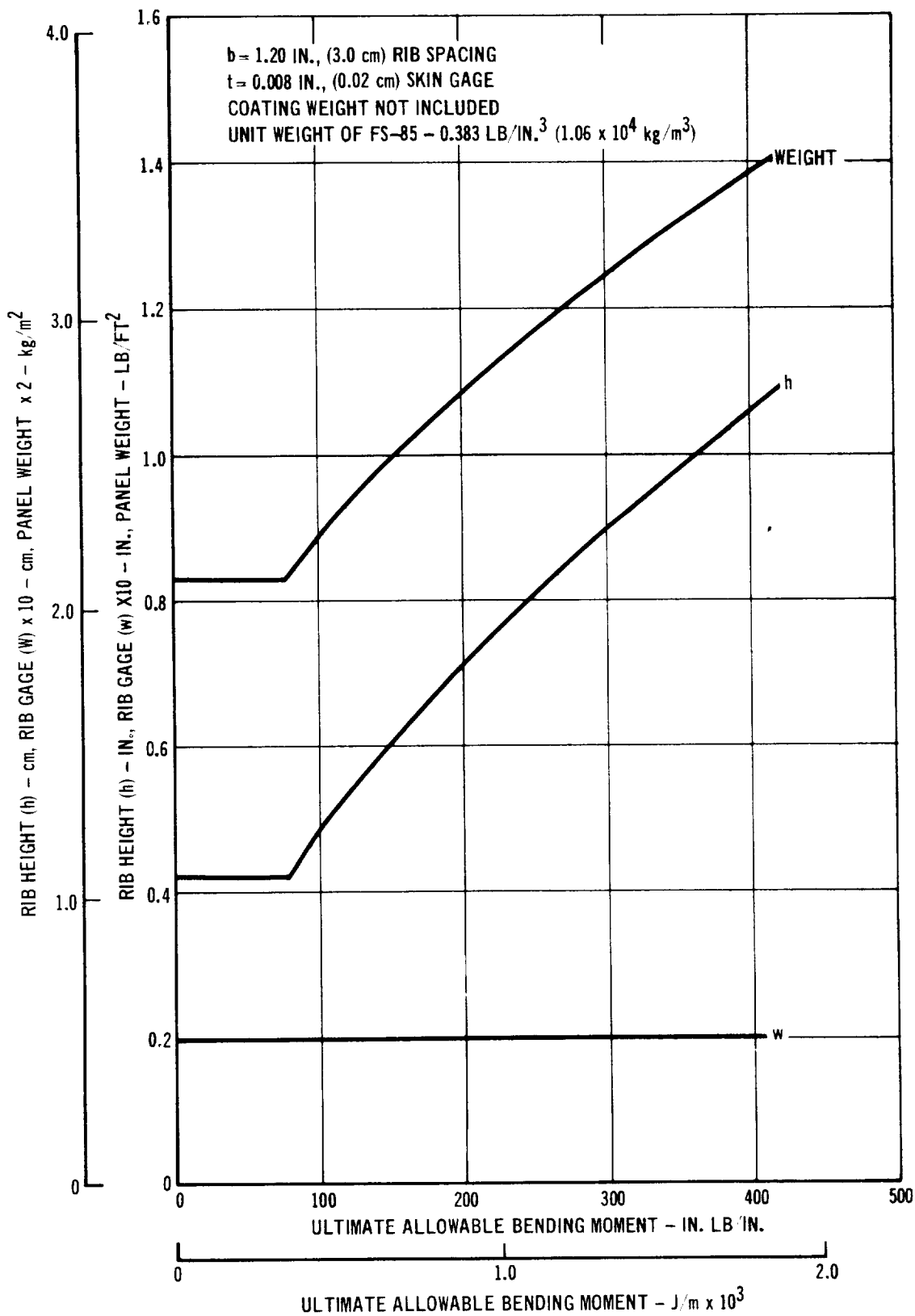
Ascent - Pressure variations along the high cross range orbiter lower fuselage centerline during ascent are illustrated in Figure 1-9. These pressures peak about 66 sec after lift-off, and are highest in the interaction region between the orbiter and booster. Curves are shown for both the nominal and design trajectories. The design trajectory is obtained by superimposing the effects of winds on the nominal trajectory. Design trajectory loads are used to size panels, whereas loads based on the nominal trajectory are employed in the reuse analysis of panels. Since a venting system was not defined, and ambient pressure is subject to



457-1164

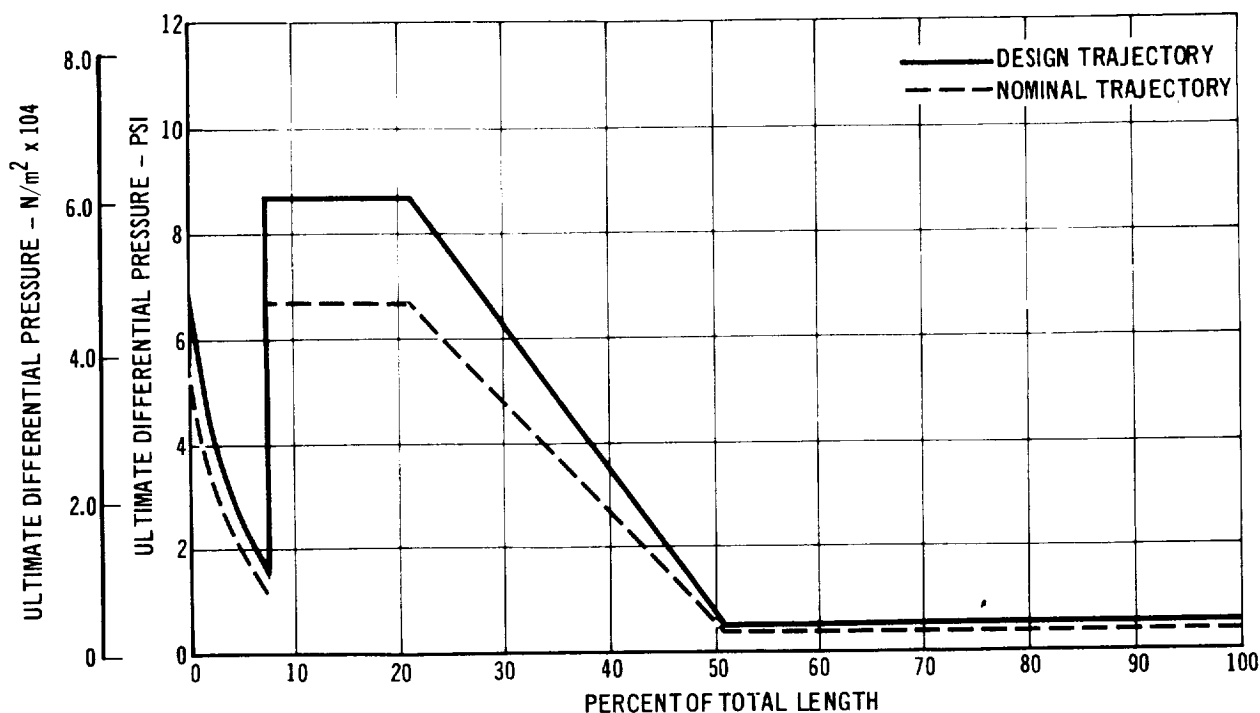
MINIMUM GAUGE SKIN IS OPTIMUM FOR THE RIB-STIFFENED CONCEPT

FIGURE 1-7



COLUMBIUM FS-85 RIB STIFFENED PANEL DESIGN CURVES

FIGURE 1-8



### HIGH CROSS RANGE ORBITER BOTTOM CENTERLINE ULTIMATE PRESSURE DURING ASCENT

457-1166

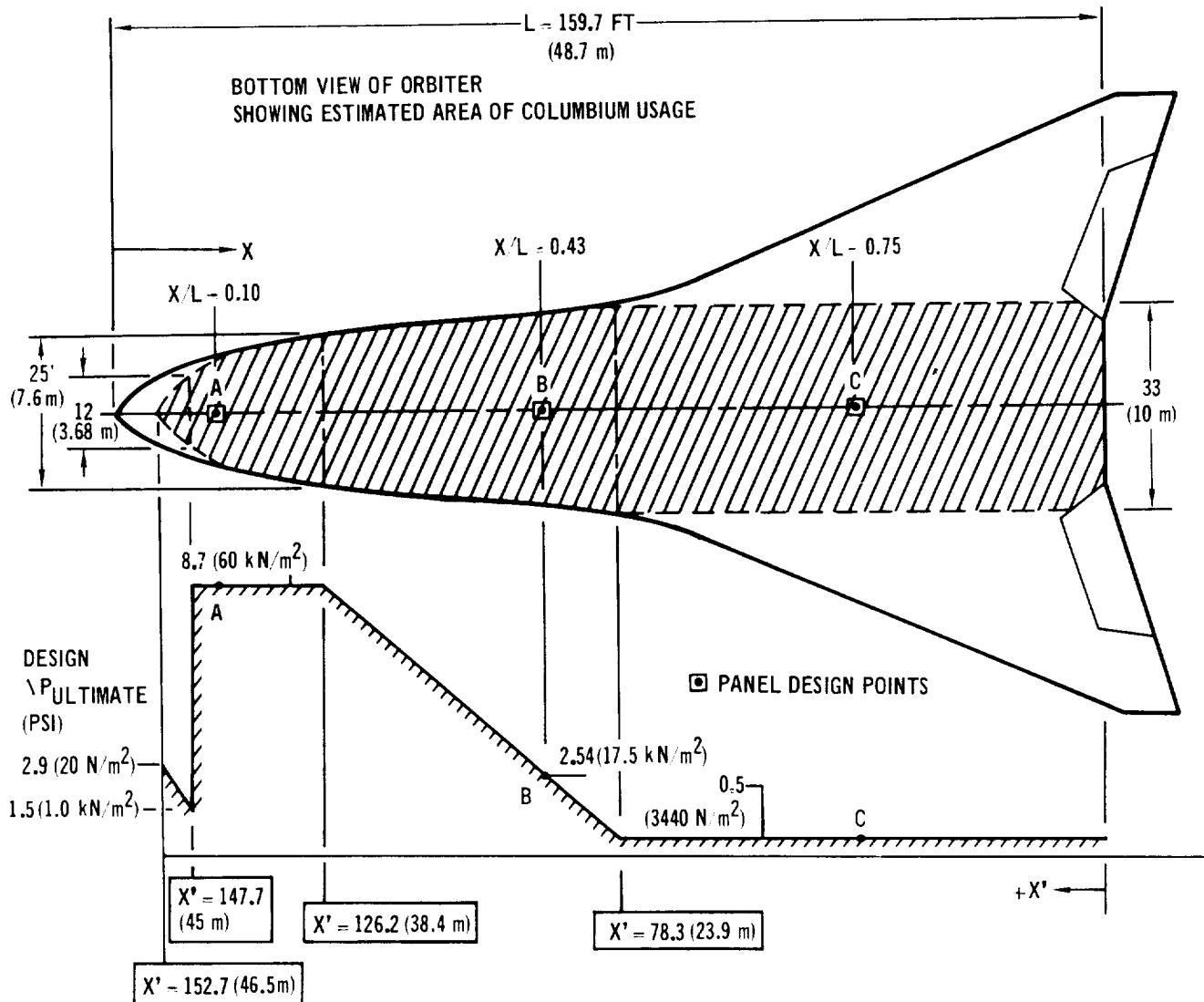
FIGURE 1-9

relatively rapid change during ascent, a 1-lb/in<sup>2</sup> (6900 N/m<sup>2</sup>) limit burst pressure was assumed to act on all panels. Although a small amount of aerodynamic heating occurs, room temperature material properties were used in designing for these pressure conditions.

Entry - Differential pressures on the bottom centerline of the high cross range orbiter occurring during entry are shown in Figure 1-5 for both nominal and design trajectories. The entry design trajectory was obtained by reducing the altitude of the nominal trajectory by 2500 ft (760m) at all velocities during entry. The temperature-time profiles during entry for the bottom centerline of this vehicle are given in Figure 1-4.

Cruise - Following entry and transition to airplane-type cruise operation, the Shuttle will be subjected to airloads typical of large aircraft. Pressure differentials across the fuselage panels may be as high as 1.75 lb/in<sup>2</sup> (12 kN/m<sup>2</sup>) ultimate. During this phase of the mission, panel temperatures remain relatively low.

Preliminary Design of Full Size Columbiu Panels - Three locations on the orbiter bottom centerline were selected for detailed analysis. The three locations are shown in Figure 1-10.



457-1167

**ASCENT DIFFERENTIAL PRESSURE DISTRIBUTION  
AND LOCATION OF PANEL DESIGN POINTS**

FIGURE 1-10

Panel A (at  $X/L = 0.10$ ) represents a region where all panels would be designed for ascent pressures. Highest ascent pressures (8.7 lb/in<sup>2</sup> (60 kN/m) ultimate)



occur in this area (as indicated in Figure 1-10). The resulting columbium rib stiffened panel cross section, along with a curve showing panel strength as a function of temperature, is shown in Figure 1-11, showing that Panel A, which was designed for the ascent condition, is not critical during entry.

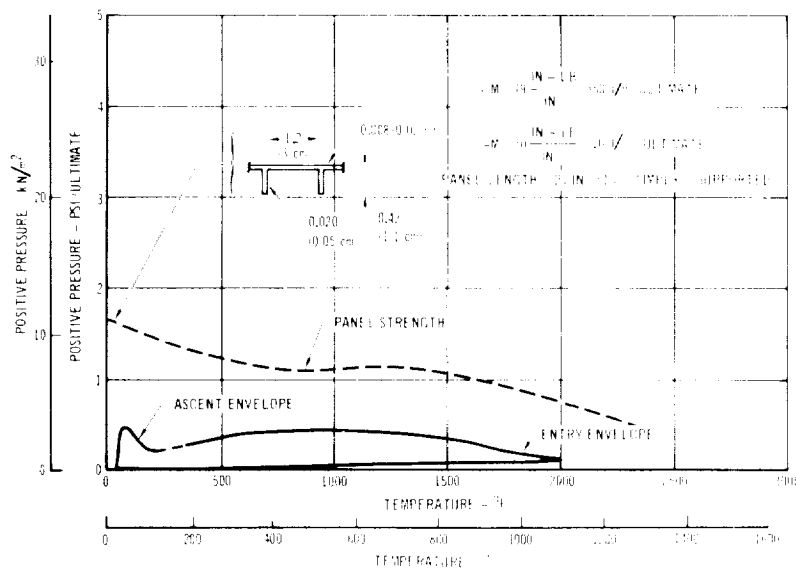
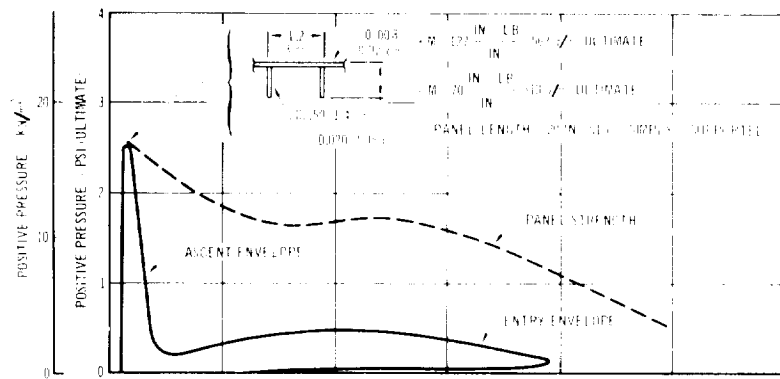
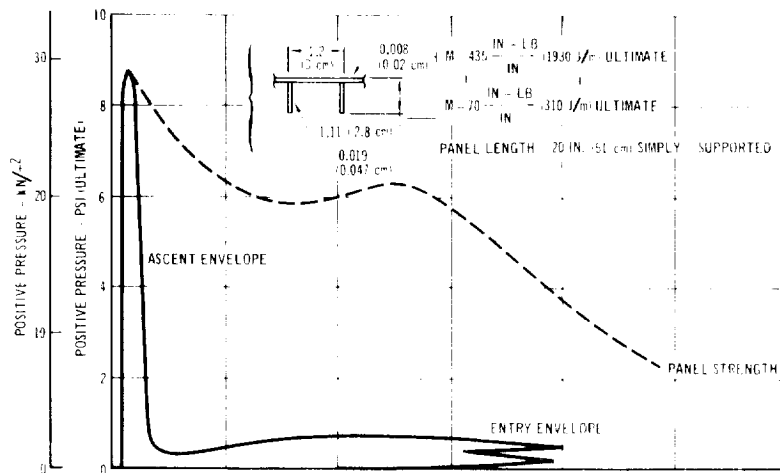
Panel B (at  $X/L = 0.43$ ) represents a panel subjected to the average ascent pressure. The design pressure for Panel B ( $2.54 \text{ lb/in}^2$  ( $17.5 \text{ kN/m}^2$ ) ultimate) resulted in the panel cross section shown in Figure 1-11. Ascent and entry envelopes shown in Figure 1-11 indicate again that the panel was not critical for entry.

Panel C (at  $X/L = 0.75$ ) is located in a region where pressures are lowest during ascent ( $0.5 \text{ lb/in}^2$  ( $3440 \text{ N/m}^2$ ) ultimate). This panel was actually designed for the negative pressure condition of  $1.4 \text{ lb/in}^2$  ( $9650 \text{ N/m}^2$ ) ultimate. The resulting cross section is shown in Figure 1-11. A margin of safety exists for both ascent and entry positive pressures.

Prior to the consideration of creep deflection in panel design, Panel B was selected as the most representative panel. (Panel A, which was designed for the highest ascent pressure, would not be subjected to high stresses during entry, and Panel C was designed for a burst pressure condition which would not occur on all flights.) Test stress levels for Panel B had not only to be based on the nominal trajectory, but had also to correspond to limit rather than ultimate loads. To illustrate this, the ascent test stress level is explained as follows:

- (1) The nominal ultimate pressure ( $1.96 \text{ lb/in}^2$  ( $13.5 \text{ kN/m}^2$ )) corresponding to the design ultimate pressure ( $2.54 \text{ lb/in}^2$  ( $17.5 \text{ kN/m}^2$ )) was obtained from Figure 1-9;
- (2) Dividing 1.96 by 1.4, the factor of safety, the nominal limit pressure ( $1.40 \text{ lb/in}^2$  ( $9650 \text{ N/m}^2$ )) was obtained;
- (3) Using the section properties of Panel B, the rib outer fiber stress ( $51,000 \text{ lb/in}^2$  ( $355 \text{ MN/m}^2$ )) for a  $1.50 \text{ lb/in}^2$  ( $9650 \text{ N/m}^2$ ) panel loading was calculated.

Following the same procedure while using nominal limit, the appropriate pressure stresses were calculated for the entry and cruise conditions. These results, illustrated in Figure 1-11, produced the stress-time profile originally selected for flight simulation tests. The temperature-time profile selected for testing (Figures 1-1 and 1-2) had temperatures higher than those used in this preliminary work which, as stated previously, caused us to initiate redesign work



PANEL STRENGTH AND FLIGHT ENVELOPE

FIGURE 1-11

based on panel creep deflection. Both ascent and entry stress levels for testing were revised as described below.

#### 1.4.3 Selection of Test Stress Levels

Ascent - During ascent, the nominal limit stress in the rib outer fiber of Panel B was  $51,000 \text{ lb/in}^2$  ( $355 \text{ MN/m}^2$ ). This value is approximately 77 percent of the room temperature yield strength of FS-85. Applying this same percentage to the yield strengths of Cb-752 and C-129Y gives the values 53 and 55 ksi ( $366$  and  $379 \text{ MN/m}^2$ ), respectively. Thus, to simulate nominal conditions on panels designed for ascent, each alloy requires a different stress level.

Entry - Analysis using currently available creep properties of the Cb-752, FS-85 and C-129Y alloys at the maximum test temperature,  $2400^\circ\text{F}$  ( $1300^\circ\text{C}$ ), showed that the maximum entry stresses in full size panels of these alloys would have to be limited to about  $4000 \text{ lb/in}^2$  ( $27.5 \text{ MN/m}^2$ ). This was based on the criterion that total permanent panel deflection, for a  $20" \times 20"$  ( $50 \times 50 \text{ cm}$ ) panel, after 100 flight cycles, must be limited to  $0.5"$  ( $1.27 \text{ cm}$ ). With this creep criterion, excessive creep deflections of full size panels (FS-85, Cb-752 and C-129Y) will not result until a stress of  $4000 \text{ lb/in}^2$  ( $27.5 \text{ MN/m}^2$ ) is exceeded.

1.5 Acoustic Simulation - A part of the flight simulation which was performed on each subsize heat shield panel was acoustic exposure to simulate the noise environment experienced during lift-off. Peak acoustic loading conditions are experienced for approximately 30 sec during each lift-off. In order to conserve time and be more economical, acoustic simulation was accomplished after a group of cycles, some as large as 20. The duration of the acoustic exposure was equal to 28.6 sec times the number of reentry cycles to which the panel was exposed. When a total of 100 reentry cycles had been accomplished, the total acoustic exposure time was 2860 sec. Since acoustic loading produces fatigue which is a cumulative condition, it was felt that grouping the acoustic tests is satisfactory and that the total time is the most important factor in the simulation.

Acoustic simulation utilizing the subsize panels presented a special problem because the responses of a subsize and full size panel to a Space Shuttle orbiter lift-off acoustic environment (approximately 156 dB) are quite different. The natural frequency of the subsize panel is considerably different than the natural frequency of a full size panel. Thus, a dB level at a certain frequency that would make one panel respond would not affect the other panel and hence, would not produce the same stresses in both the sub- and full size panels. Therefore, in order to learn about the effects of acoustics on coating performance and still run

a worthwhile test, it was decided to test to a certain stress level (induced by acoustics). A stress level which would cause fatigue failures was desired because something could be learned at the same time about the fatigue life of coated columbium structures.

After the time (2860 sec per 100 flights) at which peak acoustic loading would occur was known, selection of a stress level which would approach the fatigue life of R-152E coated FS-85 had to be made. The stress level which would cause fatigue failure exactly at 100 reentry cycles was sought for two reasons:

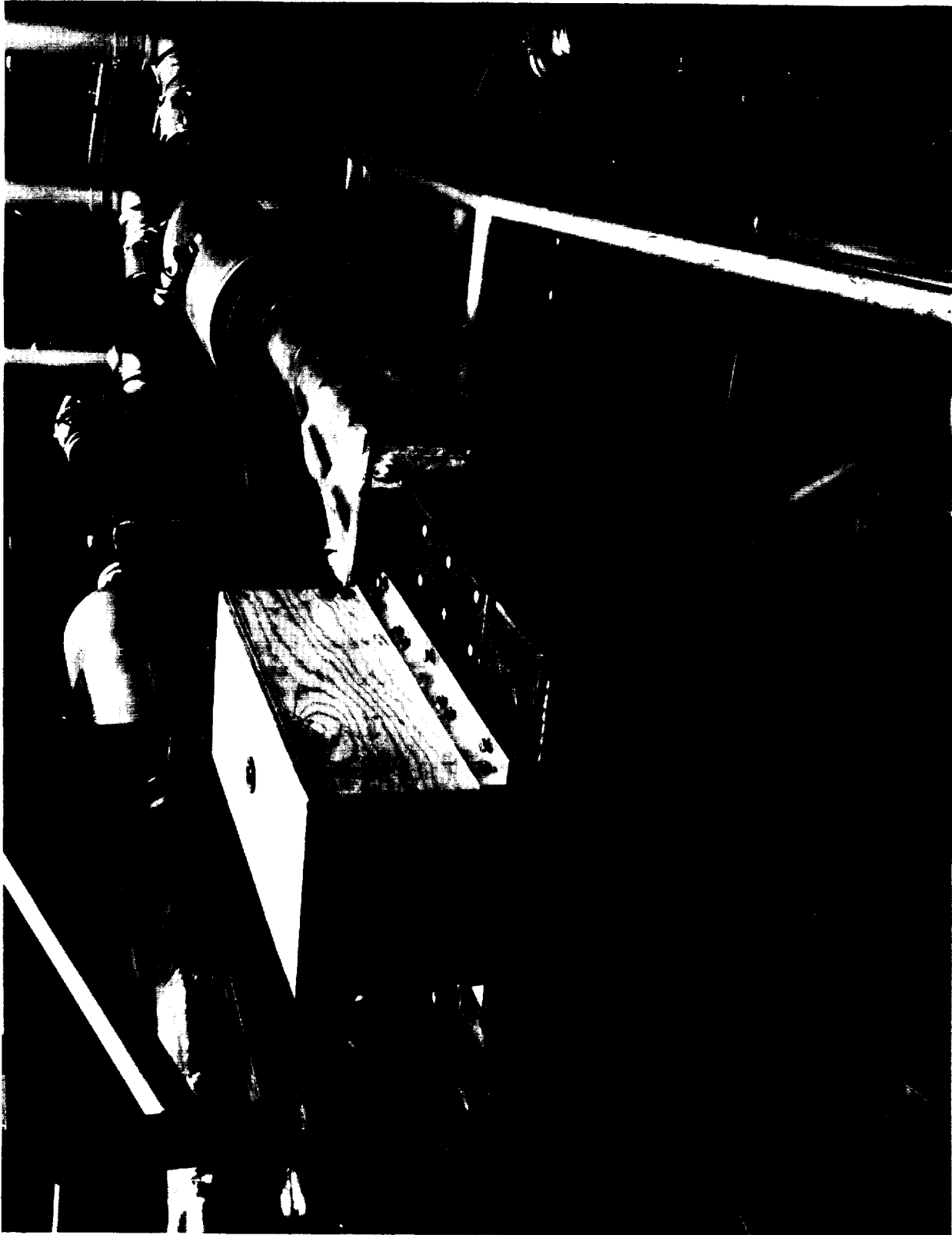
- (1) Reentry testing was scheduled to be stopped at 100 cycles, and fatigue failure at this point would give a good data point for fatigue life of coated columbium; and
- (2) A primary objective of this program was verification of 100 flight reuse capability of the fused slurry silicide coating, and proof of the ability of this coating to provide oxidation protection on a substrate up to its fatigue life would erase doubts about performance under these conditions.

Sufficient fatigue life data for coated columbium to allow confident selection of a stress level did not exist. Two available bits of data were used for stress level selection, one from extrapolated tension-tension fatigue life of aluminide coated Cb-752 and the other from vibrational fatigue of miniature rib stiffened panels generated under NASA Contract NAS8-26121, "Establishment of Requirements and Procedures for Field Repair of Thermal Protection Panels." These two bits of data agreed that 10,000 psi ( $69 \text{ MN/m}^2$ ) was approximately the stress level that would cause fatigue failure in about 760,000 cycles at room temperature. The 760,000 cycles was calculated from time (2860 sec) multiplied by natural panel frequency (265 cycles/sec). Natural panel frequency was determined by attaching a microminiature response accelerometer and a small electromagnetic vibration exciter to the specimen and conducting a frequency sweep. The resonance frequency of the specimen was obtained from the frequency response plot of the accelerometer.

The calibration was accomplished using FS-85 subsize rib and corrugation stiffened panels identical to the panels which would later be profile tested. The panel specimens were instrumented with a strain gage (3-element 45-degree strain rosette) in the center of the load area on the skin side for the rib stiffened panels and on the flats of the corrugations for the corrugated panels. The rib is the critical member in the rib stiffened panel design, with the rib stress being

2.5 times higher than the skin stress. The  $4000 \text{ lb/in}^2$  ( $27.5 \text{ MN/m}^2$ ) (rms) skin stress corresponds to the  $10,000 \text{ lb/in}^2$  ( $69 \text{ MN/m}^2$ ) (rms) limit stress of the ribs. A special acoustic fixture was fabricated to support the panels in a simple supported configuration. The fixture consisted of two rubber lined clamps mounted on each end of a steel plate. The panel was installed within the clamps of the fixture to obtain a panel floating condition. The rubber lining was used to prevent coating damage during acoustic loading. A double-walled test chamber of  $1 \text{ ft}^2$  ( $900 \text{ cm}^2$ ) cross-sectional area was positioned in front of an acoustic horn. The panel and fixture assembly was then installed in the test chamber. A box constructed of wood and filled with acoustic insulation was attached over the back of the panel to reduce the sound pressure incident upon the backside of the panel. Photographs of the panel and acoustic fixture assembly are presented as Figures 1-12 and 1-13.

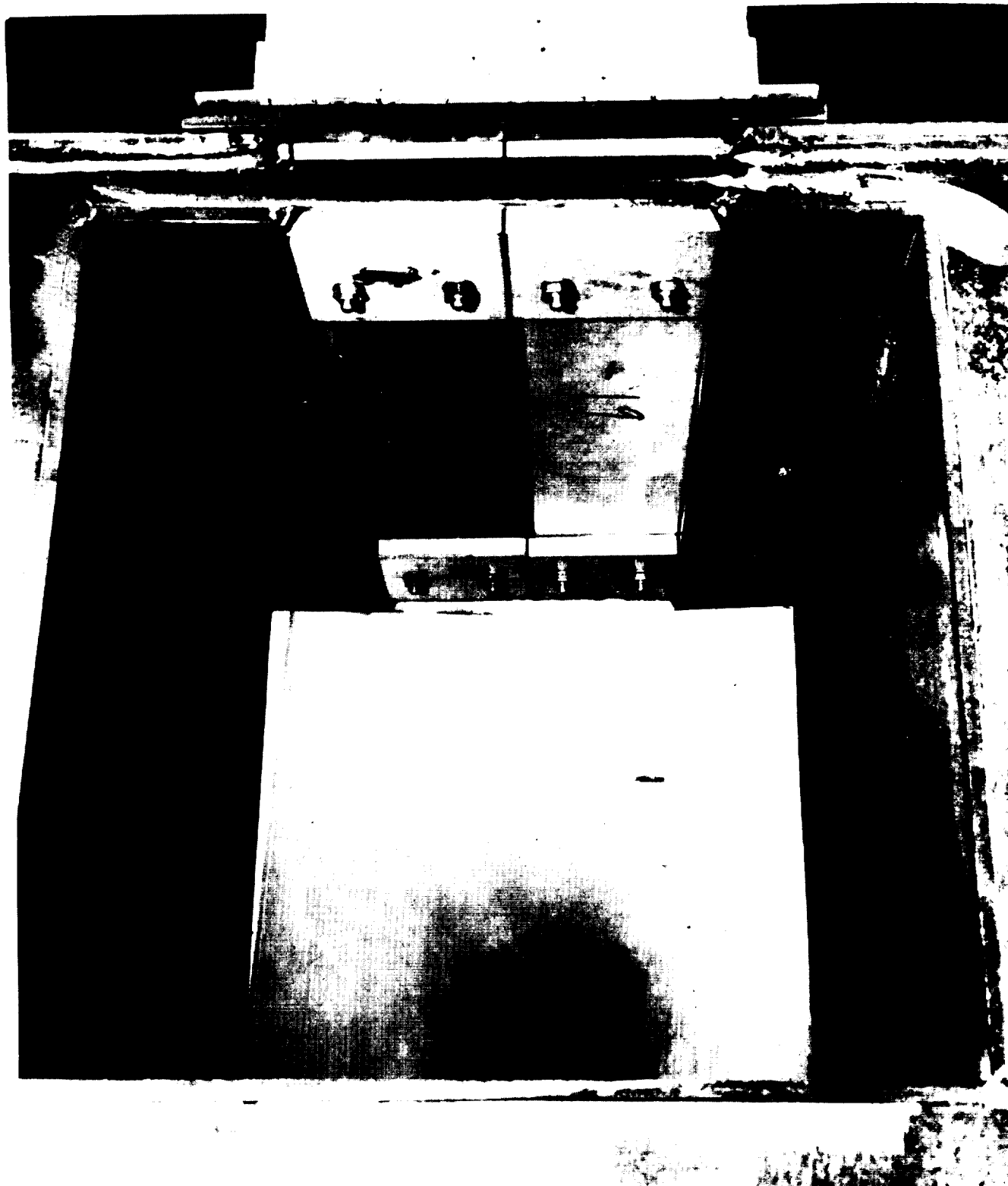
The calibration panel was initially excited sinusoidally from 50 to 500 Hz at an input acoustic level of 161 dB. Sinusoidal excitation was used to identify the panel's predominant bending frequencies. The outputs of the strain rosette and microphone were recorded on FM magnetic tape. The frequency response plots were obtained by using a log ratio computer which plotted the ratio of the recorded response strain amplitude to the recorded input pressure amplitude as a function of frequency. The signals were filtered using a dual-channel tracking filter employing 5 Hz bandwidth filters before obtaining the ratio. The exciter/acoustic system was fully attenuated below 50 Hz and above 500 Hz due to the characteristics of the system. The acoustic level on the rib calibration panel was increased until the rms stress level, determined from the output of the strain gage, measured  $4000 \text{ lb/in}^2$  ( $27.5 \text{ MN/m}^2$ ) (rms). An acoustic level of 167 dB was required to obtain  $4000 \text{ lb/in}^2$  ( $27.5 \text{ MN/m}^2$ ) (rms). The same basic procedure was used with the corrugated panel except the strain gage was connected directly to the area where  $10,000 \text{ psi}$  ( $69 \text{ MN/m}^2$ ) was desired. An acoustic level of 169 dB was required to obtain  $10,000 \text{ psi}$  ( $69 \text{ MN/m}^2$ ) in the corrugated panel. All subsequent panels (rib and corrugation stiffened) evaluated in the program were subjected to the same random acoustic environment as used for the calibration panels.



457-2834

ACOUSTIC TEST APPARATUS

FIGURE 1-12



RIB STIFFENED PANEL IN ACOUSTIC FIXTURE

FIGURE 1-13

457-2833

## 2.0 COATING CHEMISTRY OPTIMIZATION STUDY FOR COLUMBIUM ALLOYS C-129Y and FS-85

The object of this study was to select a coating chemistry for the C-129Y and FS-85 alloys that would offer better protection than the R-512E (Si-20Cr-20Fe) coating. The R-512E composition was "optimized" for D-43 and Cb-752 type alloys and might not provide equivalent protection to the other alloys which differ markedly in chemistry.

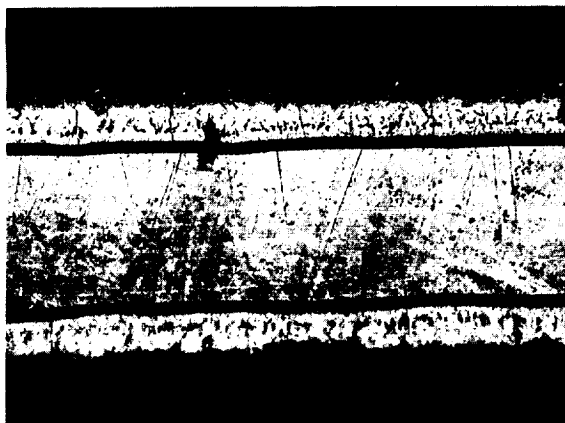
2.1 Selection of Coating Chemistries - FS-85 and C-129Y sheet materials 0.012" (0.03 cm) and 0.010" (0.025 cm) thick, respectively, were sheared into coupon type specimens 1/2" x 1" (1.25 cm x 2.5 cm). Cb-752 alloy specimens 0.020" (0.05 cm) thick were similarly fabricated.

Seven basic compositions (Si-20Cr-20Fe; Si-20Cr-5Ti; Si-40Cr-20Fe; Si-20Cr-10Mo; Si-20Cr-10W; Si-20Ti-10M; Si-20Ti-3V) were formulated and applied to batches of 10 of each alloy-coating combination by spraying. The unit weight of coating applied was adjusted to yield coatings having equivalent silicon contents of about 16.5 mg/cm<sup>2</sup>. All samples were given a standard fusion-diffusion treatment for one hour at 2580°F (1420°C). The 210 specimens were processed as a single batch in a large vacuum furnace.

Metallographic specimens representing each of the 21 coating/substrate combinations were prepared and examined. There is a wide variability in the way the different coatings wet and react with the three alloys. Four candidate coatings applied to the three alloys (Cb-752, FS-85, C-129Y) are shown in low magnification (100X) photomicrographs in Figures 2-1 and 2-2. Figure 2-1 shows the Si-20Cr-5Ti (R-512A) and Si-20Ti-10Mo coatings in combination with the 3 alloys. The Si-20Cr-5Ti on the C-129Y and FS-85 was uniform but was nonuniform on the Cb-752 alloy. The Si-20Ti-10Mo coating was fairly uniform only as applied to the FS-85 alloy. In combination with C-129Y and Cb-752 this coating was very nonuniform. In respect to coating thickness uniformity, these pictures are typical also of the Si-20Ti-3V, Si-20Cr-10Mo and Si-20Cr-10W coatings. The Si-Ti base coatings, however, were inferior to the Si-Cr base coatings in this regard.

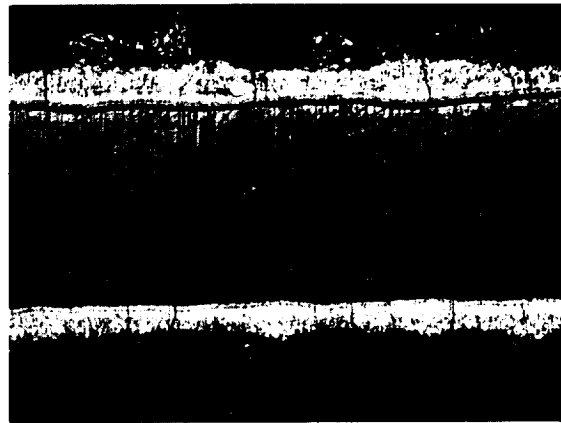
Figure 2-2 shows similar photomicrographs for the Si-20Cr-20Fe and Si-40Cr-20Fe coatings as applied to the same three alloys. The Si-20Cr-20Fe coating in combination with all three alloys was more uniform than any of the other coatings studied. The Si-40Cr-20Fe coatings were relatively nonuniform compared to the Si-20Cr-20Fe coatings although they were more uniform than the coatings outside of the Si-Cr-Fe system.





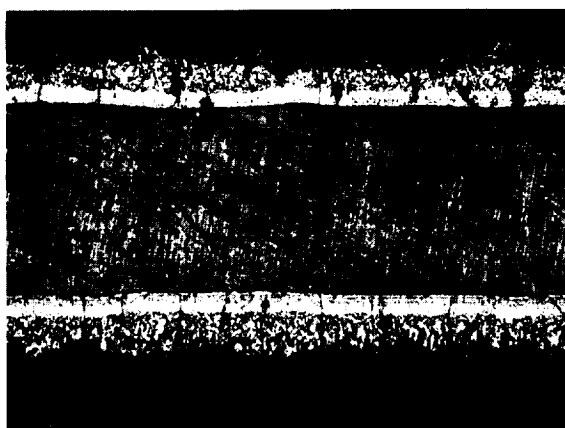
Si-20Cr-5Ti

C129Y



Si-20Ti-10Mo

C129Y



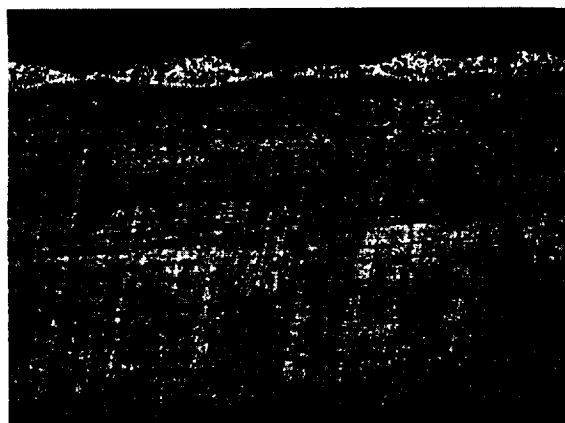
Si-20Cr-5Ti

FS85



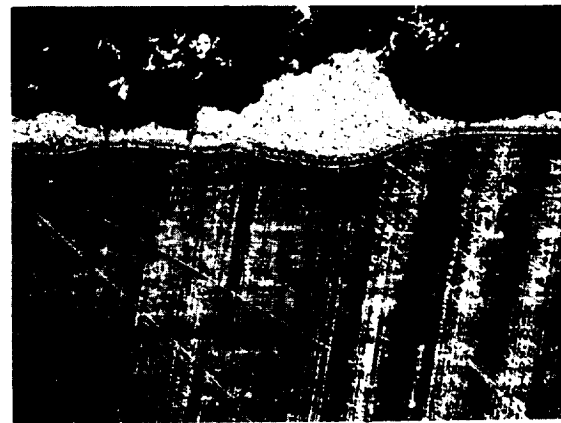
Si-20Ti-10Mo

FS85



Si-20Cr-5Ti

Cb752



Si-20Ti-10Mo

Cb752

PHOTOMICROGRAPHS OF Si-20Cr-5Ti AND Si-20Ti-10Mo ON 3 COLUMBIUM ALLOY SUBSTRATES  
(100 X)

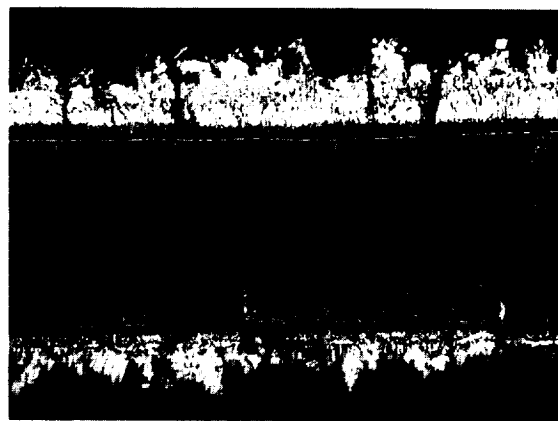
FIGURE 2-1

(100 X)



Si-20Cr-20Fe

C129Y



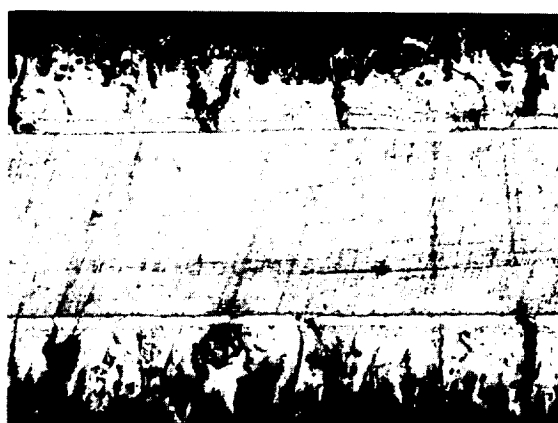
Si-40Cr-20Fe

C129Y



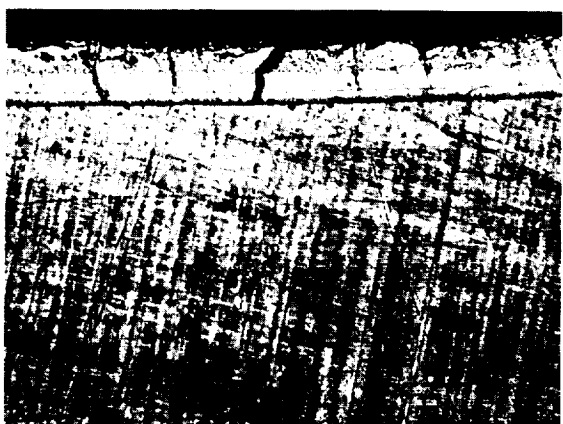
Si-20Cr-20Fe

FS85



Si-40Cr-20Fe

FS85



Si-20Cr-20Fe

Cb752



Si-40Cr-20Fe

Cb752

PHOTOMACROGRAPHS OF Si-20Cr-20Fe AND Si-40Cr-20Fe ON COLUMBIUM  
ALLOYS C129Y, FS85 AND Cb752

FIGURE 2-2

2.2 Screening Tests - All seven coating compositions as applied to the three alloys were subjected to oxidation performance screening tests. These tests consisted of slow cycle and reduced pressure profile (external and internal pressure).

Three samples of each coating-substrate combination were tested in slow cyclic testing at atmospheric pressure, at reduced pressures conforming to an internal reentry profile, and at reduced pressures conforming to an external pressure profile. The test profiles employed conform closely to those which were presented in Figure 1-1, with minor alterations necessitated by test equipment limitations. Those portions of the pressure profiles which could not be accommodated are not considered critical ones since the temperatures in both cases are 1600°F (870°C) or below.

The results of the tests are given in Table 2-1. On the basis of the atmospheric pressure tests the Si-20Cr-20Fe (R-512E) is superior to the other compositions tested for the C-129Y, FS-85 and Cb-752 alloys.

In the external pressure profile simulated reentry tests the R-512J (Si-20Fe-40Cr) coating gave the best overall performance on all three alloys. The R-512E coating also afforded good overall protection to all three alloys in this test. Two other coatings, Si-20Cr-10Mo and Si-20Cr-10W in combination with FS-85 also yielded protective lives in this test in the 200 cycle range. The results from this test show clearly that FS-85 is better protected than Cb-752 or C-129Y by the majority of compositions investigated here.

2.3 Enhancement of Candidate Compositions - The basic conclusion from the screening tests was that coating compositions which showed the most promise for increased life involved the chromium-iron modified coatings having increased chromium content. The three compositions selected for slow cycle (air), internal and external profile oxidation testing were Si-30Cr-20Fe, Si-35Cr-20Fe, and Si-40Cr-20Fe. The R-512E coating (Si-20Cr-20Fe) was used as a standard for all 3 alloys. Oxidation test results are shown in Table 2-2. The slow cyclic life in one atmosphere air was not strongly affected by the chromium content. The higher chromium coatings (> 30% Cr) did show increased life under reduced pressure profile oxidation. Temperature, 2400°F max. (1300°C) and pressure profiles used for these tests are the same as the ones which were used in the initial screening tests.

Metallographic specimens of the higher chromium content coatings were made. High magnification (400X) photomicrographs of Si-20Cr-20Fe, Si-30Cr-20Fe,

TABLE 2-1  
COATING CHEMISTRY STUDY TEST RESULTS

COATING COMP (w/o)	UNIT WT (mg/cm <sup>2</sup> )	BASE ALLOY	1 ATM SLOW CYCLIC TEST (NO. CYCLES TO FAILURE)	SIMULATED EXTERNAL PRESSURE PROFILE (NO. CYCLES TO FAILURE)	SIMULATED INTERNAL PRESSURE PROFILE (NO. CYCLES TO FAILURE)
Si-20Cr-5Ti	20.5	C129Y	71*, 71*, 71*	98(E), 98(E), 149(E)	TEST NOT CONDUCTED
	21	FS-85	71*, 71*, 71*	149(E), 149(E), 173(E)	
	21	Cb-752	71*, 71*, 71*	74(E), 109(E), 149(E)	
Si-20Ti-3V	22	C129Y	38(E), 38(E), 38(E)	74(E), 74(E), 74(E)	TEST NOT CONDUCTED
	25	FS-85	71(E), 38(E), 38(E)	98(E), 98(E), 98(E)	
	22.5	Cb-752	10(S), 10(S), 10(S)	28(S), 28(S), 28(S)	
Si-20Cr-20Fe	27	C129Y	71(S), 132(E), 179(E)	186(S,E), 136(S), 209(E)	200+, 200+, 200+
	26	FS-85	179(E), 179(E), 191(E)	128(E), 161(E), 186(E)	165(E), 165(E), 200+
	26.5	Cb-752	146(E), 179(E), 215(E)	186(E), 209(E), 209+	200+, 200+, 200+
Si-40Cr-20Fe	40	C129Y	19(E), 39(S), 30(E)	209(E), 209+, 209+	200+, 200+, 200+
	42	FS-85	7(E), 7(E), 7(E)	209+, 209+, 209+	200+, 200+, 200+
	43	Cb-752	18(E), 18(E), 30(E)	209+, 209+, 209+	200+, 200+, 200+
Si-20Cr-10Mo	23	C129Y	7(E), 30(E), 30(E)	32(E), 56(E,S), 64(E)	TEST NOT CONDUCTED
	25.5	FS-85	11(E), 30(E), 30(E)	180(E), 200(E), 200(E)	
	23	Cb-752	7(G), 7(G), 7(G)	32(S,E), 32(S), 32(S)	
Si-20Cr-10W	24	C129Y	30(E), 30(E), 36(E)	112(E), 138(E)	TEST NOT CONDUCTED
	24	FS-85	49(E), 49(E), 49(E)	200(E), 200+, 200+	
	24	Cb-752	18(S), 18(S), 18(S)	88(E), 112(E)	
Si-20Ti-10Mo	23	C129Y	6(S), 6(S)	17(E), 41(E), 41(E)	TEST NOT CONDUCTED
	23	FS-85	44(E), 56(E), 56(E)	41(E), 41(E), 41(E)	
	23	Cb-752	6(S), 6(S), 6(S)	17(E), 41(E), 41(E)	

\* ALL SAMPLES IN GROUP FAILED OVER WEEKEND. INDICATED TIME IS MAXIMUM. MINIMUM TIME IS 10 HOURS.

E - EDGE FAILURE

S - SURFACE FAILURE

G - GENERAL FAILURE

+ - NO FAILURE - TEST TERMINATED

Si-35Cr-20Fe, and Si-40Cr-20Fe coated C-129Y, FS-85, and Cb-752 are shown in Figures 2-3, 2-4 and 2-5. These pictures are not representative of the thickness uniformity of these coatings. Since it is possible to get a representative picture only with lower magnification micrographs such as Figures 2-1 and 2-2, the 400X micros are intended only to show typical microstructures and changes therein as a function of increasing chromium content. Although it may not be at all obvious at first glance, there is a 1-1.5 mil (25-38  $\mu$ m) thick  $\text{CbSi}_2$  layer on the Si-20Cr-20Fe coatings, a very thin, about 0.2 mil (5  $\mu$ m) discontinuous  $\text{CbSi}_2$  layer on the Si-30Cr-20Fe coatings and essentially no  $\text{CbSi}_2$  surface layers on the Si-35Cr-20Fe and Si-40Cr-20Fe coatings. Some observations and conclusions which

TABLE 2-2  
OXIDATION PERFORMANCE OF MODIFIED COATINGS

COATING	BASE ALLOY	CYCLIC LIFE*		
		AIR	EXTERNAL PRESSURE	INTERNAL PRESSURE
Si-20Cr-20Fe	Cb 752	180	200	200
	FS 85	183	158	180
	C 129 Y	127	177	200
Si-30Cr-20Fe	Cb 752	184	200	200
	FS 85	121	200	200
	C 129 Y	121	195	200
Si-35Cr-20Fe	Cb 752	200	200	200
	FS 85	142	200	200
	C 129 Y	127	200	200
Si-40Cr-20Fe	Cb 752	200	200	200
	FS 85	177	200	200
	C 129 Y	129	198	200

\*AVERAGE OF 3 SPECIMENS TESTED TO FAILURE OR 200 CYCLES

were made with respect to the coating study for FS-85 and C-129Y are presented in the following paragraphs.

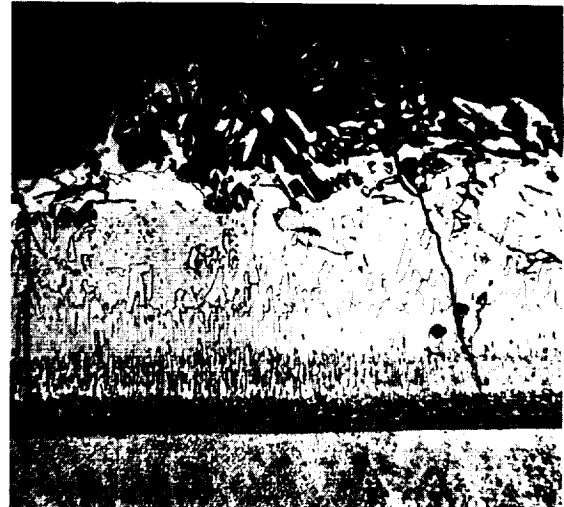
The Si-Cr-Fe coatings generally were more uniform than the others studied. Within this system the uniformity increased with decreasing chromium concentration. The Si-20Cr-20Fe was the only composition that gave reasonably uniform coating thickness coverage on all three alloys. Si-40Cr-20Fe coating is nonuniform, particularly on the C-129Y and Cb-752 alloys.

In the 1 atmosphere slow cyclic test, the Si-Cr-Fe coatings gave the best performance on all alloys. Si-35Cr-20Fe (Cb-752) and the Si-40Cr-20Fe (Cb-752) systems yielded 200+ cyclic lives on 3 samples each. The Si-30Cr-20Fe (Cb-752) systems yielded over 180+ cycles in this test. All Si-Cr-Fe coatings also gave good results in the test on C-129Y and FS-85; the latter alloy yielded more consistent results.

In the simulated external pressure profile tests, good results were obtained with the Si-Cr-Fe system coatings. All combinations of 3 alloys and 4 Si-Cr-Fe coating compositions yielded lives of about 200 cycles and the results correlate well with the result of the 1 atmosphere slow cyclic test. The results indicate that for this class of coating reduced pressure is a less rigorous although



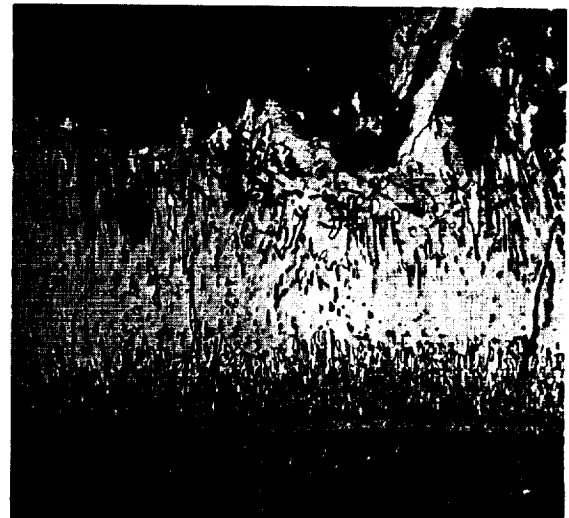
Si-20Cr-20Fe



Si-30Cr-20Fe



Si-35Cr-20Fe



Si-40Cr-20Fe

(400 X)

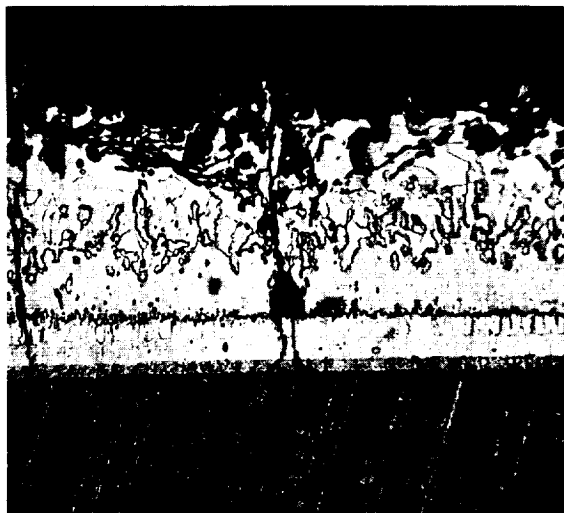
### Si-Cr-Fe FUSED SILICIDE COATINGS ON C-129Y ALLOY

FIGURE 2-3

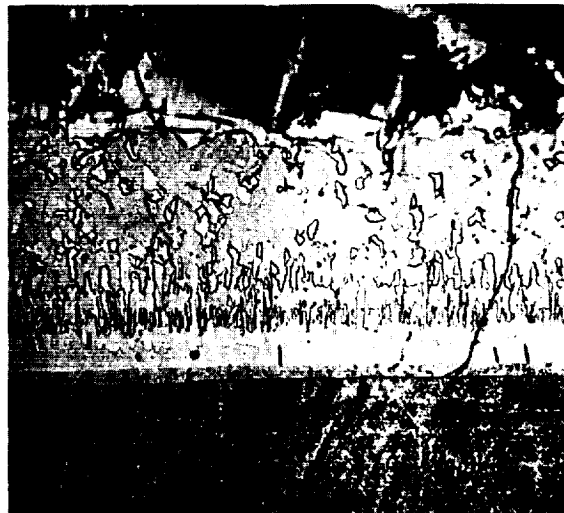
possibly a more representative test.

The Si-Cr-Fe coating compositions were tested in the simulated internal pressure profile test. All performed well, yielding lifetimes of 200+ cycles, except Si-20Cr-20Fe coated FS-85, which had 2 specimens failing after 165 cycles.

Metallographic analyses of oxidation tested specimens showed that the three test conditions resulted in formation of protective oxide layers on all Si-Cr-Fe



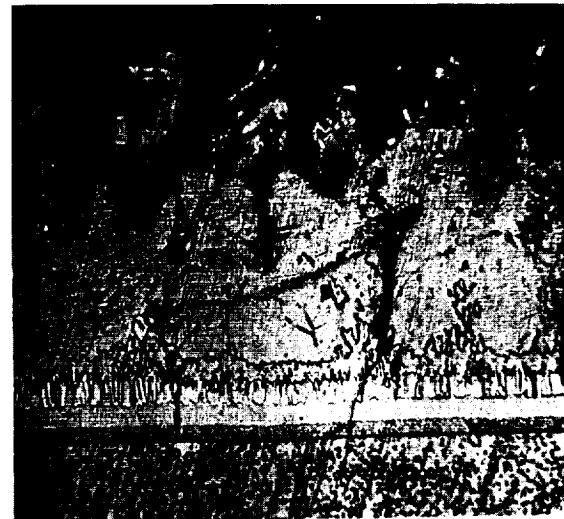
Si-20Cr-20Fe



Si-30Cr-20Fe



Si-35Cr-20Fe



Si-40Cr-20Fe

(400 X)

### Si-Cr-Fe FUSED SILICIDE COATINGS ON FS-85 ALLOY

FIGURE 2-4

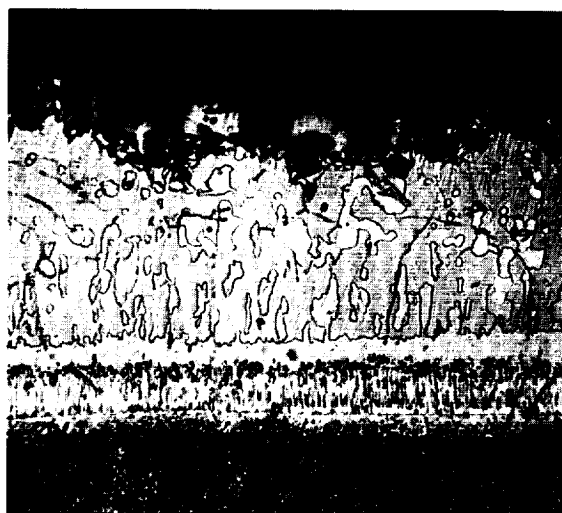
combinations examined. Oxidation in thermal stress cracks effectively sealed these cracks. In many, if not most, of the specimens tested to 200 cycles in 1 atmosphere and external pressure profile tests, oxidation at cracks penetrated the coating and resulted in very localized contamination. However, general contamination did not occur in any of these specimens as verified by 90° bend



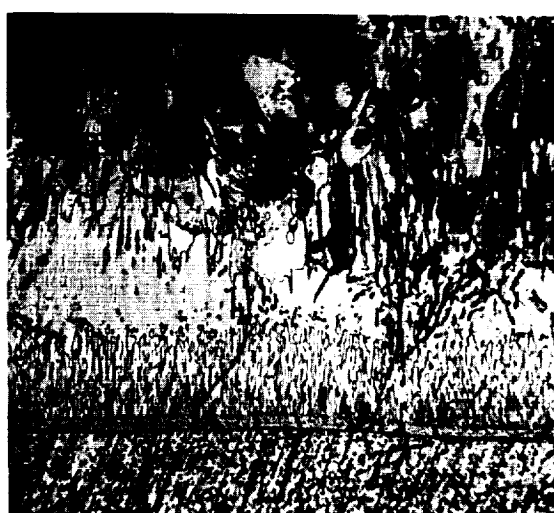
Si-20Cr-20Fe



Si-30Cr-20Fe



Si-35Cr-20Fe



Si-40Cr-20Fe

(400 X)

### Si-Cr-Fe FUSED SILICIDE COATINGS ON Cb-752 ALLOY

FIGURE 2-5

tests before sectioning for metallography. No such evidence of oxidation penetration was noted with specimens tested for 200+ cycles in the internal pressure profile test.

The Cb-752/Si-35Cr-20Fe system gave the overall best performance based on the test criteria employed. Almost equivalent results were recorded for the Cb-752/



Si-40Cr-20Fe system. The best performing coating on FS-85 was Si-40Cr-20Fe and the best performing coating on C-129Y was Si-35Cr-20Fe.

The decision was made not to change to the 35 or 40 Cr content coatings for the remainder of the program because the improvement in life was not considered significant enough to warrant a change. All background data had been generated with the 20Cr-20Fe system, and large batches of slurry had already been prepared using the 20Cr-20Fe composition.

### 3.0 SELECTION OF A COLUMBIUM ALLOY FOR REUSABLE HEAT SHIELD APPLICATIONS

The effects of multiple cycle reuse on coating emittance, coating chemistry and structure, and heat shield panel structural integrity were investigated to provide a broader performance base for optimum alloy selection.

A new technique for making total normal emittance measurements on sheet material without using a thermocouple attachment was developed. Changes in emittance due to reuse up to 100 simulated reentries were determined.

Coating chemistry and changes in chemistry, both surface and body, were examined utilizing x-ray diffraction, x-ray fluorescence, and electron microprobe techniques.

The emittance and coating chemistry studies were used in conjunction with the mechanical property data from Section 5.0, Vol. I, to select Cb-752, FS-85, and C-129Y as the alloys to be used in heat shield structural integrity studies.

Miniature rib stiffened heat shield panels of the three alloys were subjected to temperature, pressure, and stress profile testing to determine coating reusability, and structural performance. The FS-85 alloy was chosen for further evaluation using sub- and full size heat shield panels.

3.1 Total Hemispherical Emittance Measurements - Fifteen emittance specimens 3/8" (0.9 cm) wide x 8" (20 cm) long x .012" (0.03 cm) were fabricated from each of the columbium alloys (Cb-752, FS-85, C-129Y, B-66 and WC-3015). These specimens were coated by HiTemCo with the optimized and scaled-up R-512E coating process, except that no edge beading was used. The specimens were then exposed to 2400°F (1300°C) external pressure reentry cycling (see Figure 1-1). Exposure times varied from one to 100 cycles. Reentry cycling was performed in an Astro Furnace reentry simulator. Three specimens of each alloy were removed after 9, 24, 49 and 99 cycles of exposure. An additional cycle of exposure was accomplished in the emissometer during emittance measurements.

Initially, emittance measurements on the reentry exposure specimens were interrupted because difficulty was experienced when the surface of the reference sample (platinum) became contaminated by elements which were vaporized from the coated columbium sample. This was overcome by using a superalloy reference sample, but progress was then halted because of incompatibility between the platinum thermocouple and the coated columbium to which it was attached (by spot welding), even for the one cycle required to make emittance measurements. The coating was locally removed from the columbium and the thermocouples were attached directly to the columbium, but either the repair coatings were not compatible with the Pt wire

or the ceramic repair coatings changed the backside emittance which created a hot spot on the sample. Thus, the method of emittance determination via use of a reference sample was abandoned.

Because of the difficulties encountered in attaching thermocouples directly, a new method using ultraviolet pyrometry was developed to determine the emittance of thin, 0.010" (0.025 cm) coated columbium specimens. This method has been successfully used to determine total normal emittances of a variety of materials above 1400°F (760°C) without the need to attach thermocouples to the specimen.

The discussion which follows gives a brief description of the emissometer and measurement technique.

The major components of the High Temperature Emissometer can be seen in Figures 3-1 and 3-2. The Inconel blackbody is used for calibrating the thermopile and the UV pyrometer in terms of the blackbody temperature as measured by an attached thermocouple and the geometry of the blackbody cavity ( $\epsilon = .995$ ).

The sample is in the form of a strip (typically 3/8" (0.95 cm) wide x 8" (20 cm) long) which is fastened between two water-cooled copper electrodes in the Strip Sample Attachment (Figure 3-3). A power supply capable of supplying 300 amps at 6 vac is used to heat the sample. The electrode assembly is located in a vacuum chamber which is provided with a potassium bromide infrared window. Accumulation of contaminants on this window is monitored periodically by noting the response of the thermopile to a tubular Inconel blackbody, set at 1600°F (970°C) ( $\epsilon = .93$ ) located next to the sample.

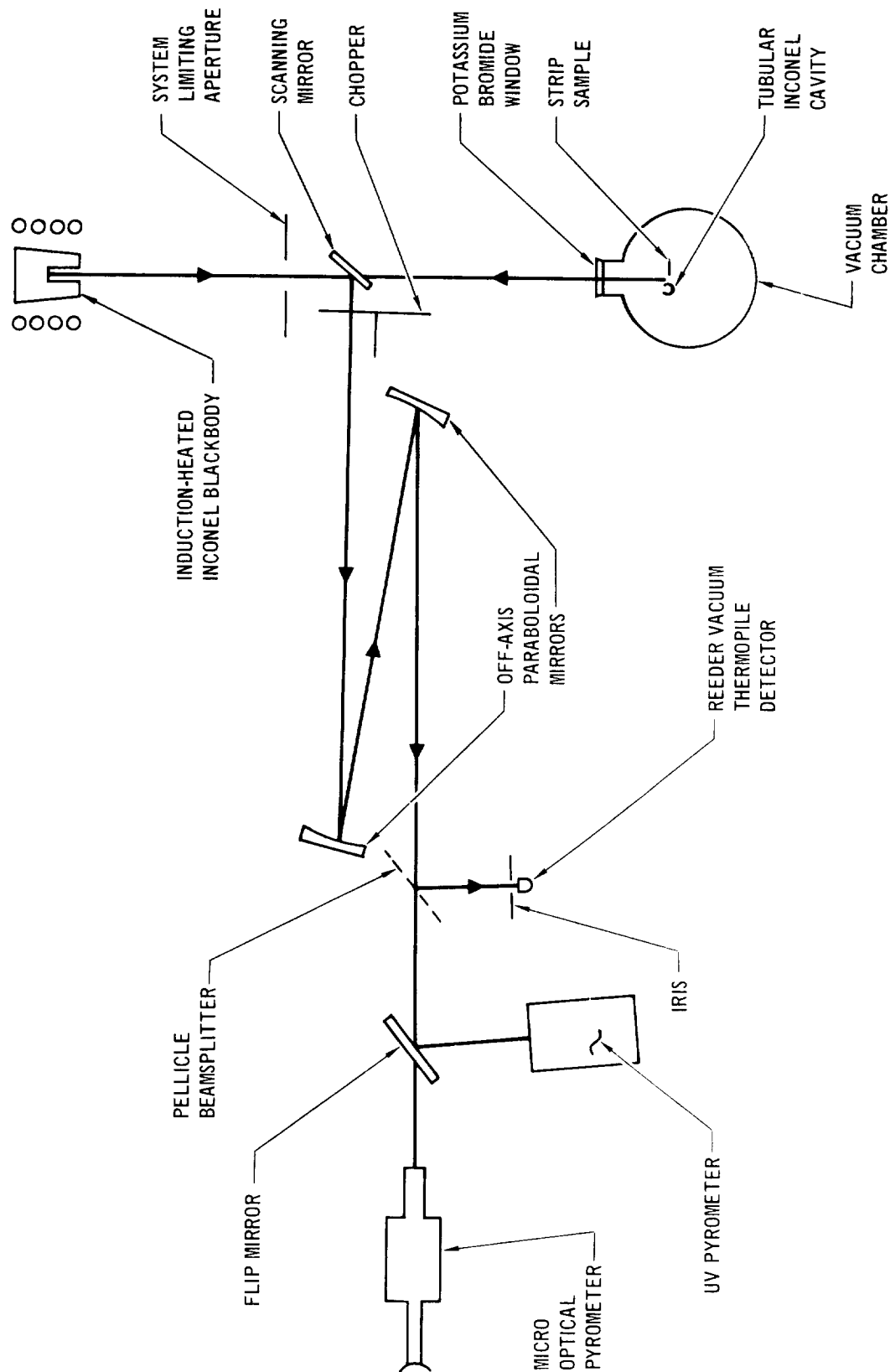
The optical transfer system consists of several mirrors and beam splitters and serves as the link between the other components. No lenses were used in this component.

A Reeder vacuum thermopile is the total radiation detector for the system. Its output was measured with a tunable microvoltmeter.

The UV pyrometer is a modified Barnes UV-1 with two temperature ranges. A differential voltmeter was used to measure the output.

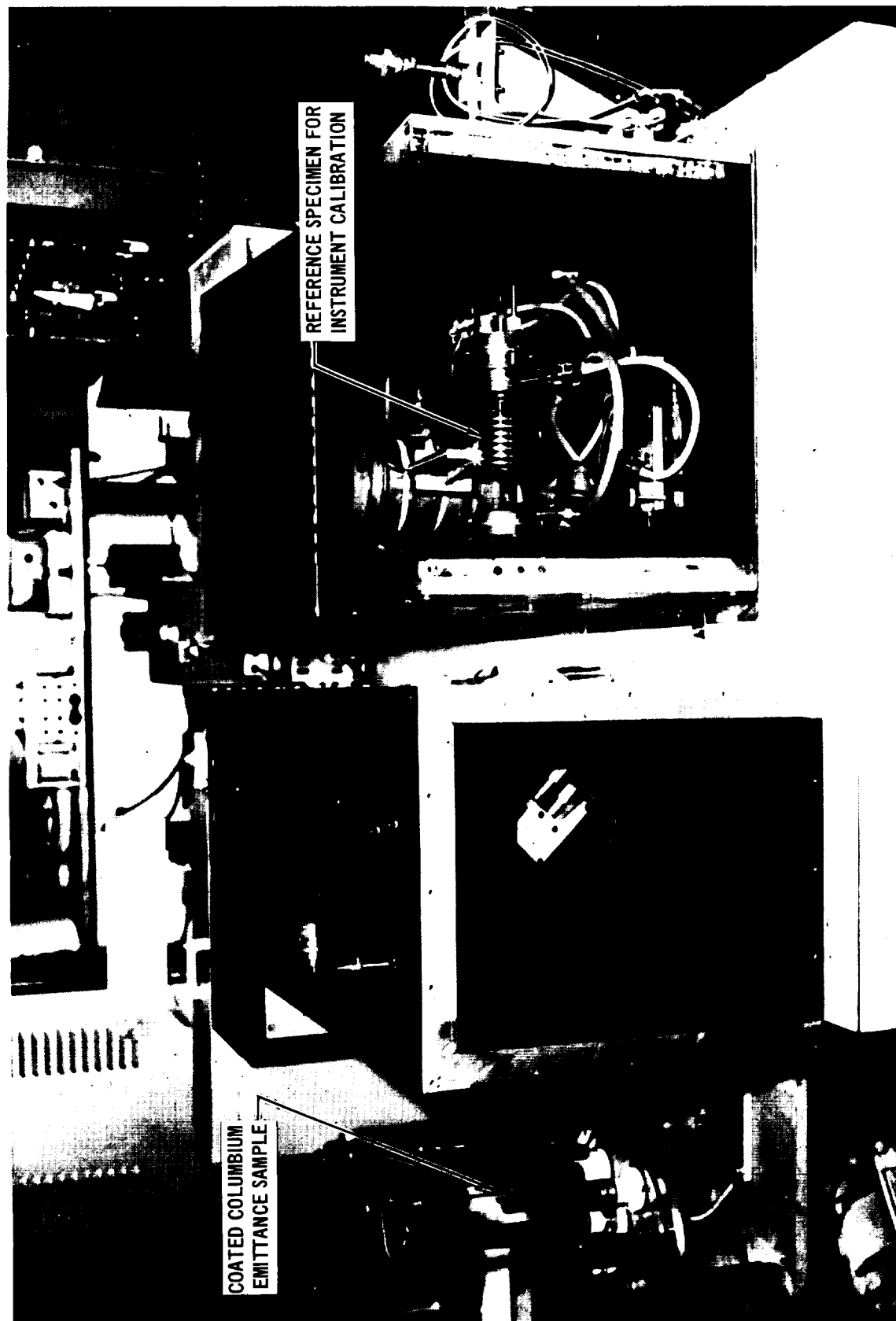
The Micro-Optical Pyrometer is a telescopic instrument used for visual alignment of the various components and to measure the brightness temperature of the sample. It also serves as a check on the thermocouples attached to the two blackbodies.

The following procedure was used to determine the true temperature of the sample and its emittance:



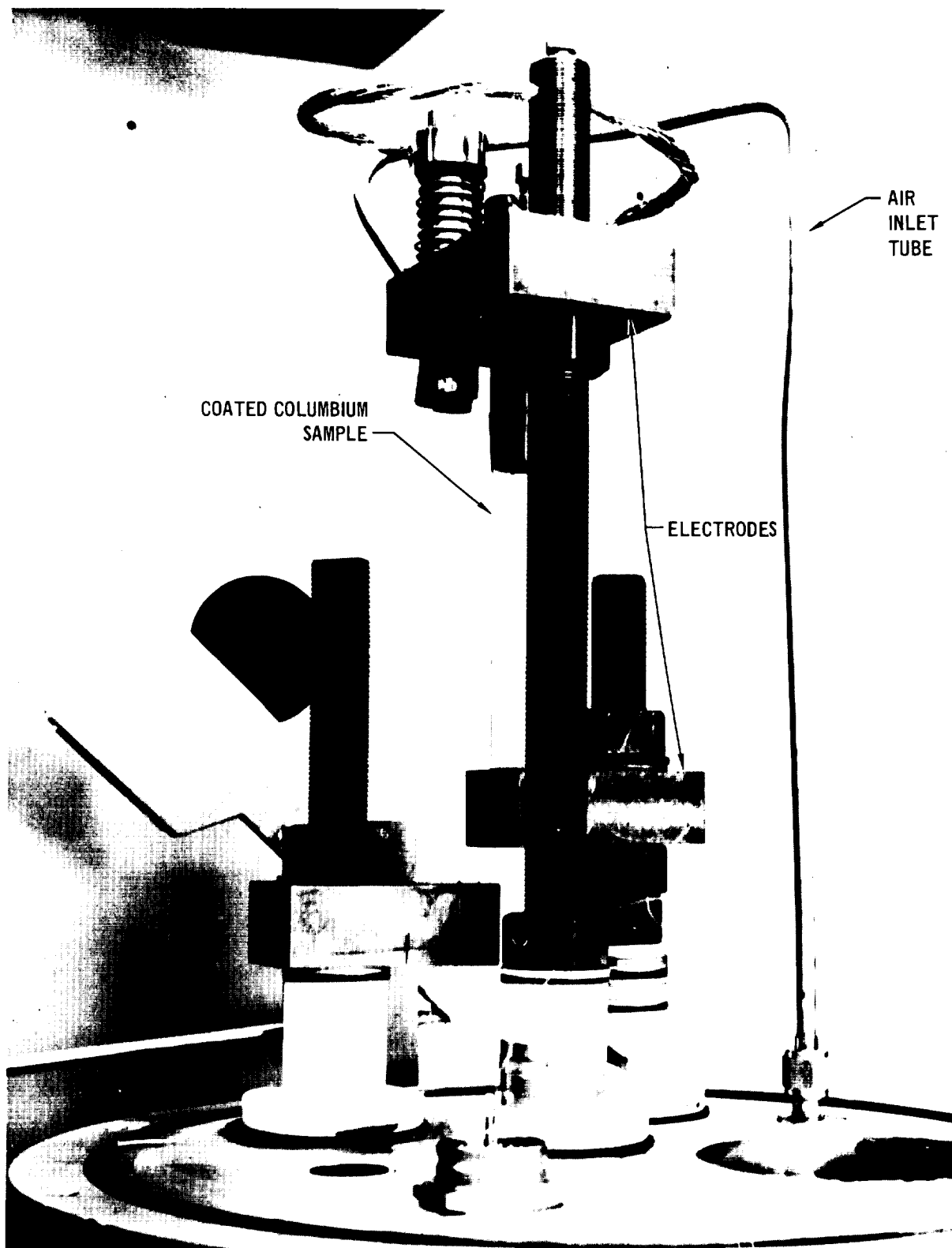
HIGH TEMPERATURE EMISSOMETER WITH STRIP SAMPLE ATTACHMENT

FIGURE 3-1



HIGH TEMPERATURE EMISSOMETER FOR THIN GAUGE SPECIMENS

FIGURE 3-2



SET-UP FOR RESISTANCE HEATING SAMPLE FROM BASE OF ENVIRONMENTAL CHAMBER

FIGURE 3-3

- (a) The sample is heated to 1400°F (760°C) or higher to obtain an on-scale reading from the UV pyrometer.
- (b) The voltage outputs from the UV pyrometer  $V_{uv}$  and the thermopile  $V_s$  detector are recorded as soon as the sample has reached thermal equilibrium.
- (c) The emittance of the sample is initially estimated at unity, and, from a calibration curve for the UV pyrometer, the temperature  $T_{s1}$  corresponding to  $V_{uv}$  is determined.
- (d) From the calibration curve for the thermopile voltage versus temperature of the Inconel blackbody, the system response  $V_{BB1}$  to a blackbody at temperature  $T_{s1}$  is determined.
- (e) A new estimate of the sample emittance is found from the following equation:

$$\epsilon_{s2} = \frac{V_s - V_{BGND}}{V_{BB1}} \quad (1)$$

where  $V_{BGND}$  = background thermopile output.

- (f) Next, use is made of the fact that the UV pyrometer is more sensitive to changes in emittance than to changes in temperature. The discrimination ratio of the UV pyrometer is defined as:

$$\eta(T) = \frac{\Delta\epsilon/\epsilon}{\Delta T/T} \quad (2)$$

where  $\Delta\epsilon/\epsilon$  = fractional change in emittance

$\Delta T/T$  = fractional change in temperature reading indicated by the UV pyrometer.

$\eta$  is experimentally determined by attenuating the radiation from the Inconel blackbody in known amounts during system calibration using neutral density filters. Equation (2) can be rewritten as follows:

$$\frac{T_{s2} - T_{s1}}{T_{s1}} = \frac{1}{\eta} \frac{\epsilon_{s1} - \epsilon_{s2}}{\epsilon_{s1}} \quad (3)$$

In our case, the initial estimate of the sample emittance,  $\epsilon_{s1}$ , is unity. Solving for  $T_{s2}$  gives a new estimate for the sample temperature.

- (g) Using  $T_{s_2}$  and the thermopile calibration, a new system response,  $V_{BB_2}$ , to the blackbody is determined.
- (h) Then, a new estimate of sample emittance is obtained from:

$$\epsilon_{s_3} = \frac{V_s - V_{BGND}}{V_{BB_2}} \quad (4)$$

- (i) Steps (f) through (h) are repeated until  $\epsilon_s$  and  $T_s$  converge.

As the initial estimate of  $T_s$  is low and that of  $\epsilon_s$  is high, several iterations are usually required to obtain convergence (to 1°F and  $5 \times 10^{-3}$  in emittance). The basic assumption of step (f) is that the sample is a graybody radiator. This assumption is generally valid for oxidized metals as well as slurry coated samples.

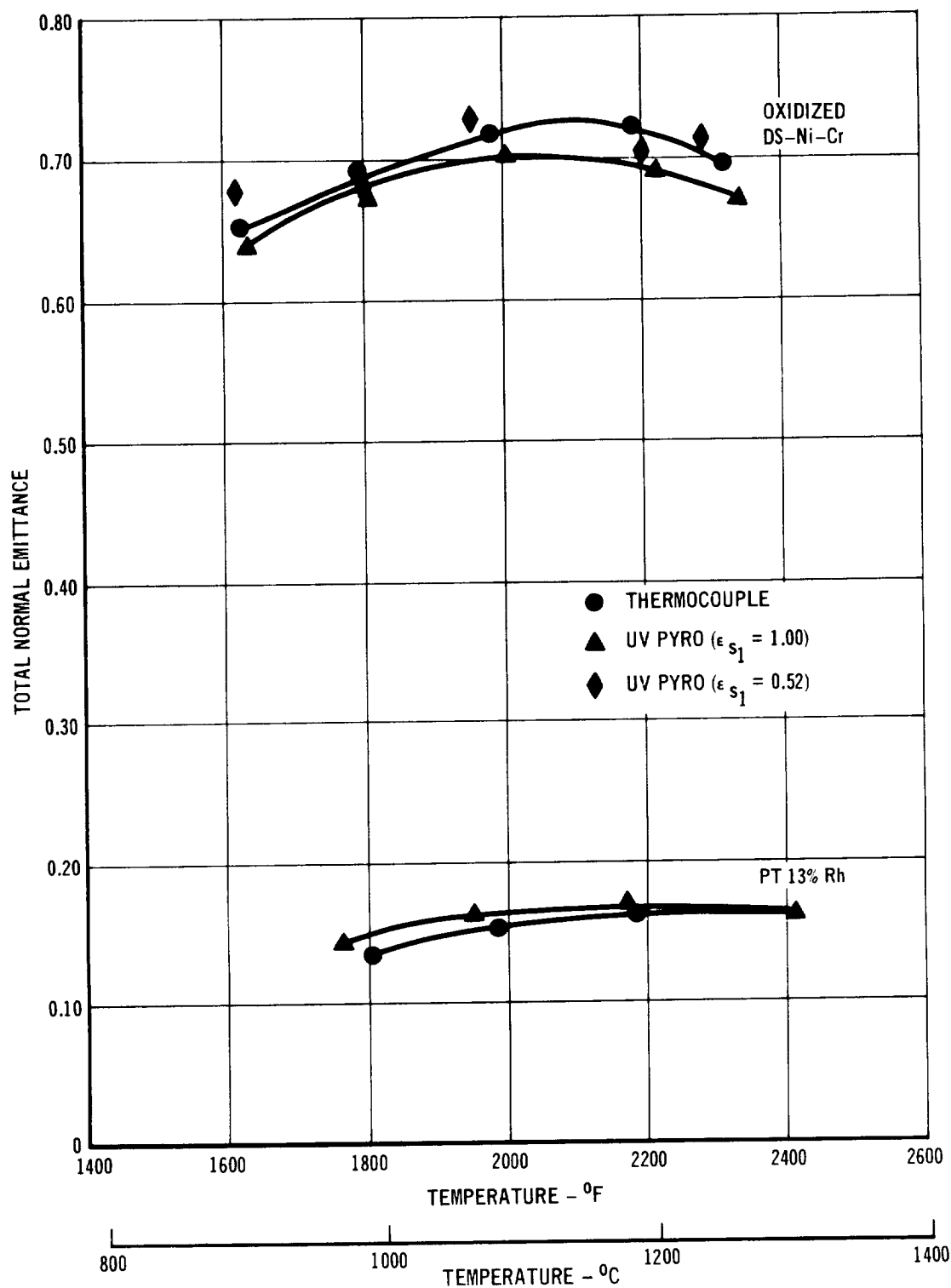
As a check on the accuracy of the iterative method, two samples (platinum and oxidized TD-Ni-Cr), each with attached thermocouples, were run. The results obtained from the iterative method and those obtained using the thermocouple data are shown in Figure 3-4. For the TD-Ni-Cr sample the iterative method was used twice, each time with a different initial emittance estimated. Least squares fits to the data show that the emittances obtained from the iterative method converge with those obtained from the thermocouple data to within  $\pm 0.02$ .

After receiving the required number of cycles, the R-512E coated columbium alloy samples were removed from the Astro Furnace and individually placed in the High Temperature Emissometer. Another cycle was run on each sample using resistance heating. The total normal emittance was measured at 1600, 2000, and 2400°F (870, 1100, and 1300°C) while the temperature increased and at 2000 and 1600°F (1100 and 870°C) during decreasing temperature. The iterative method was used to determine the emittance and temperature of the samples.

The total normal emittance for each sample at the three nominal temperatures indicated above are given in Table 3-1. Emittances are shown for each measurement made during the increasing and the decreasing temperature portions of the profile.

Figures 3-5 through 3-9 show the emittance data at 2400°F (1300°C) as a function of the number of cycles for each of the five alloys. The curves indicate the average emittance values. Independent emittance measurements on induction heated slugs of R-512E coated Cb-752 using both the integral reference cavity technique and the iterative method indicate that the standard deviation was 0.055. The emittances of the R-512E coated columbium alloys, except Cb-752, show initially





RESULTS OF CHECK ON ITERATIVE METHOD OF EMITTANCE MEASUREMENT

FIGURE 3-4

TABLE 3-1  
EMITTANCE DATA

TEMPERATURE AT WHICH ε WAS MEASURED DURING PROFILE EXPOSURE	Emittance of R-512E/B-66 System				
	NUMBER OF REENTRY CYCLES				
	1	10	25	50	100
1600°F (870°C)	0.952	0.873	0.960	0.829	0.949
	0.952	0.892	0.870	0.902	0.859
	0.950	—	0.863	0.867	0.848
2000°F (1100°C)	0.952	0.880	0.988	0.930	0.955
	0.951	0.920	0.891	0.925	0.858
	0.957	—	0.891	0.890	0.881
2400°F (1300°C)	0.963	0.844	0.940	0.967	0.969
	0.942	0.976	0.935	0.966	0.918
	0.955	—	0.885	0.887	0.929
2000°F (1100°C)	0.901	0.837	0.958	0.917	0.914
	0.911	0.879	0.894	0.906	0.893
	0.898	—	0.881	0.887	0.875
1600°F (870°C)	0.888	0.813	0.913	0.895	0.872
	0.872	0.864	0.863	0.896	0.868
	0.961	—	0.872	0.860	0.848

TABLE 3-1 (Continued)  
EMITTANCE DATA

TEMPERATURE AT WHICH ε WAS MEASURED DURING PROFILE EXPOSURE	Emittance of R-512E/C-129Y System				
	NUMBER OF REENTRY CYCLES				
	1	10	25	50	100
1600°F (870°C)	0.990	0.990	0.990	0.737	0.883
	—	0.819	0.846	0.853	0.808
	0.978	0.768	0.813	0.820	0.786
2000°F (1100°C)	0.975	0.975	0.990	0.799	0.922
	—	0.802	0.866	0.871	0.798
	0.940	0.819	0.860	0.860	0.840
2400°F (1300°C)	0.950	0.926	0.918	0.888	0.982
	—	0.941	0.926	0.926	0.906
	0.957	0.914	0.885	0.935	0.904
2000°F (1100°C)	0.865	0.864	0.918	0.802	0.914
	—	0.798	0.865	0.850	0.797
	0.878	0.810	0.868	0.868	0.844
1600°F (870°C)	0.851	0.886	0.837	0.747	0.864
	—	0.809	0.828	0.834	0.789
	0.848	0.799	0.813	0.834	0.793

FINAL REPORT

TABLE 3-1 (Continued)

EMITTANCE DATA

TEMPERATURE AT WHICH ε WAS MEASURED DURING PROFILE EXPOSURE	Emittance of R-512E/Cb-752 System				
	NUMBER OF REENTRY CYCLES				
	1	10	25	50	100
1600°F (870°C)	0.861	0.900	0.793	0.737	0.743
	0.782	0.850	0.764	0.795	0.766
	0.975	0.818	0.754	0.737	0.793
2000°F (1100°C)	0.839	0.865	0.833	0.882	0.773
	0.825	0.788	0.796	0.822	0.775
	0.914	0.835	0.798	0.784	0.840
2400°F (1300°C)	0.869	0.901	0.876	0.954	0.874
	0.890	0.878	0.880	0.907	0.893
	0.882	0.905	0.825	0.870	0.925
2000°F (1100°C)	0.775	0.853	0.832	0.879	0.756
	0.795	0.784	0.777	0.798	0.759
	0.736	0.787	0.785	0.770	0.833
1600°F (870°C)	0.774	0.910	0.807	0.855	0.723
	0.746	0.824	0.743	0.748	0.753
	0.683	0.773	0.743	0.733	0.794

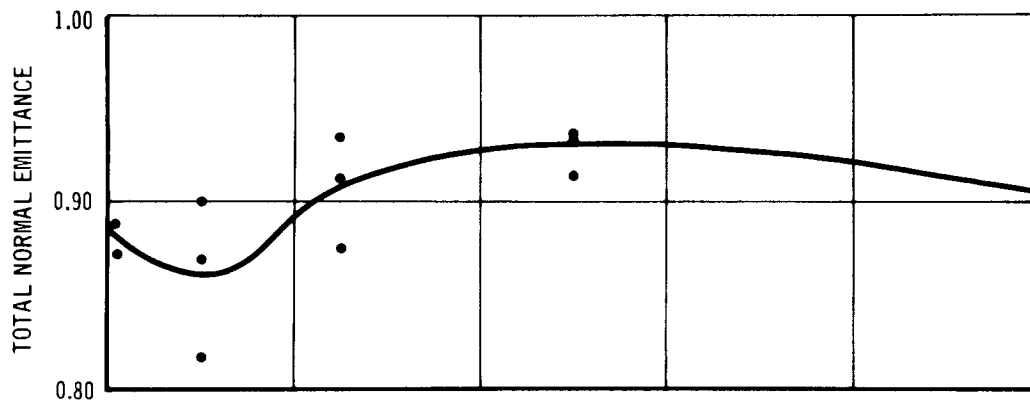
TABLE 3-1 (Continued)

EMITTANCE DATA

TEMPERATURE AT WHICH ε WAS MEASURED DURING PROFILE EXPOSURE	Emittance of R-512E/FS-85 System				
	NUMBER OF REENTRY CYCLES				
	1	10	25	50	100
1600°F (870°C)	0.918	0.937	0.818	0.873	0.845
	0.991	0.913	0.863	0.857	0.819
	0.944	0.849	0.936	0.810	0.863
2000°F (1100°C)	0.909	0.942	0.860	0.904	0.849
	0.895	0.857	0.858	0.879	0.877
	0.841	0.867	0.961	0.850	0.907
2400°F (1300°C)	0.930	0.887	0.847	0.922	0.916
	0.885	0.926	0.900	0.942	0.938
	0.850	0.832	0.944	0.902	0.948
2000°F (1100°C)	0.883	0.902	0.851	0.879	0.838
	0.803	0.834	0.854	0.874	0.873
	0.822	0.854	0.952	0.851	0.902
1600°F (870°C)	0.896	0.883	0.826	0.852	0.850
	0.816	0.857	0.852	0.850	0.827
	0.867	0.844	0.936	0.818	0.880

TABLE 3-1 (Continued)  
EMITTANCE DATA

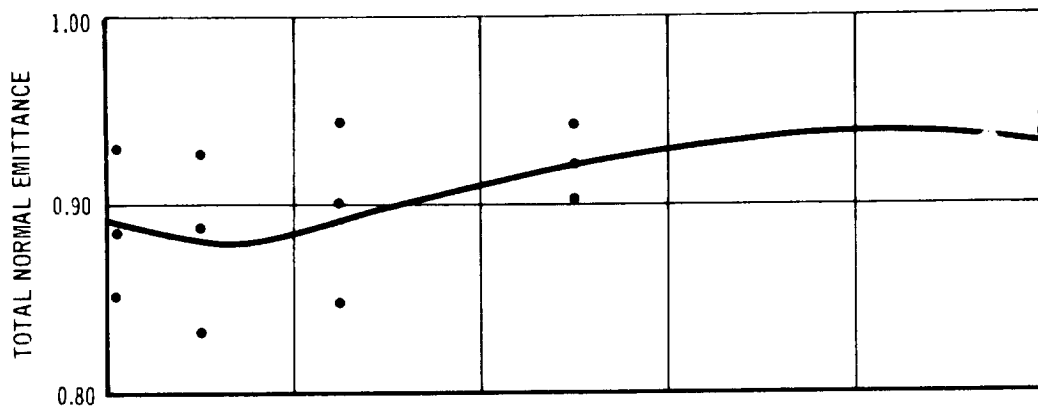
TEMPERATURE AT WHICH ε WAS MEASURED DURING PROFILE EXPOSURE	Emittance of R-512E/WC-3015 System				
	NUMBER OF REENTRY CYCLES				
	1	10	25	50	100
1600°F (870°C)	0.906	0.854	0.820	0.823	0.829
	—	0.791	0.788	0.810	0.765
	0.885	0.779	0.921	0.806	0.792
2000°F (1100°C)	0.892	0.882	0.858	0.889	0.829
	—	0.811	0.836	0.848	0.802
	0.918	0.808	0.946	0.838	0.859
2400°F (1300°C)	0.889	0.870	0.936	0.935	0.924
	—	0.900	0.876	0.935	0.881
	0.873	0.817	0.914	0.915	0.915
2000°F (1100°C)	0.796	0.833	0.868	0.886	0.841
	—	0.769	0.856	0.837	0.826
	0.814	0.799	0.899	0.824	0.857
1600°F (870°C)	0.764	0.763	0.830	0.824	0.828
	—	0.788	0.828	0.816	0.786
	0.738	0.783	0.836	0.788	0.798



WC-3015/R-512E TOTAL NORMAL EMITTANCE AT 2400°F (1300°C)

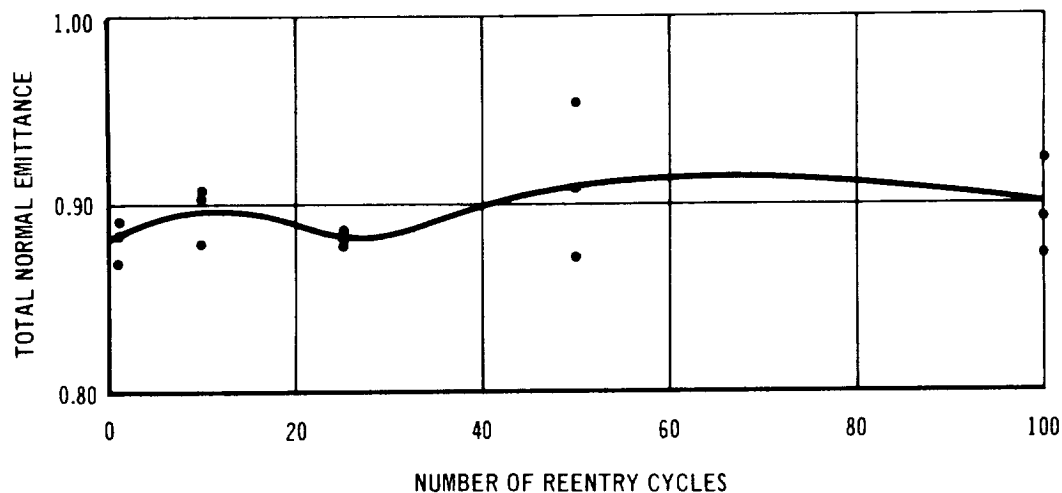
FIGURE 3-5

a decrease with increasing number of reentry cycles. This decrease, in most cases, amounts to only about .04. The decrease stops around 20 cycles and from then to 100 cycles shows a slight increase in emittance ending up slightly higher than for the first reentry cycle. The R-512E coated Cb-752 did not show an initial decrease



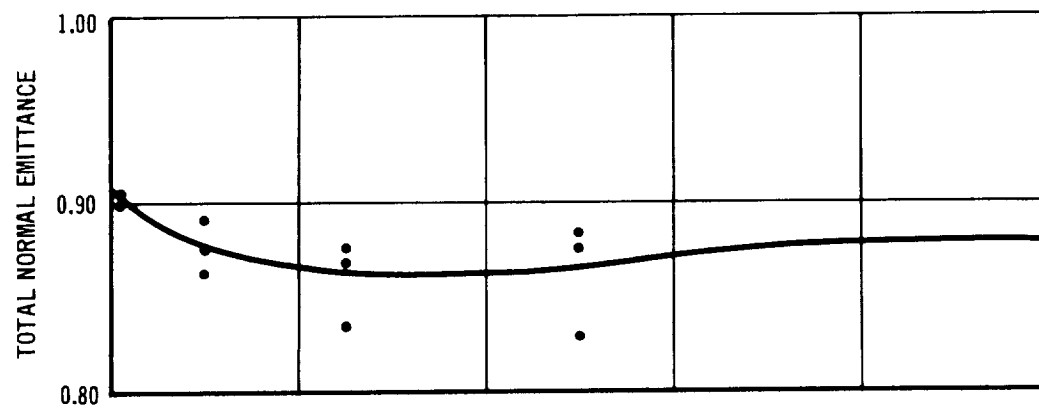
FS-85/R-512E TOTAL NORMAL EMITTANCE AT 2400°F (1300°C)

FIGURE 3-6



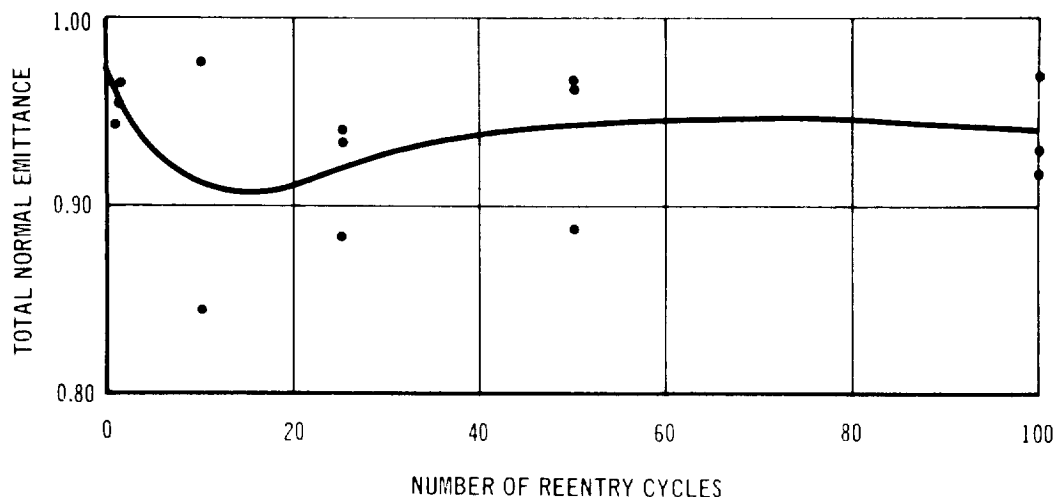
Cb-752/R-512E TOTAL NORMAL EMITTANCE AT 2400°F (1300°C)

FIGURE 3-7



C-129Y/R-512E TOTAL NORMAL EMITTANCE AT 2400°F (1300°C)

FIGURE 3-8



B66/R-512E TOTAL NORMAL EMITTANCE AT 2400°F (1300°C)

FIGURE 3-9

in emittance with cycling, but rather a slight increase. The emittance after 100 cycles for the R-512E/Cb-752 was approximately the same as that during the first cycle. The R-512E/FS-85 system showed the largest increase in emittance with cycling. The R-512E/Cb-752 had the lowest average emittance over the 100 cycles of reentry exposure, and R-512E/B-66 had the highest. These trends are based on curves which connect the averages of three measurements at 5 different temperatures. The range of emittance values at the various temperatures overlapped for almost all of the 5 temperatures. The largest range for a given temperature was approximately 15 percent; most of the ranges were within 7 percent.

Additional emittance tests were conducted to determine if R-512E coatings applied from acrylic base slurries and if modified (higher chromium content) coatings would affect emittance under reuse conditions.

Fifteen emittance specimens, 3/8" wide x 8" long x .012" (0.95 cm x 20 cm x 0.03 cm), were fabricated from each of the columbium alloys, FS-85 and C-129Y. The FS-85 specimens were coated by HiTemCo with the optimized and scaled-up R-512E coating process utilizing the A-32 acrylic-based slurry. The C-129Y specimens were coated with a modified R-512E coating. The modified coating, 45Si-35Cr-20Fe, developed from work described in Section 6.0 and contained more chromium (35 weight percent) and less silicon than the normal (20% chromium) R-512E coating. The specimens were exposed to reentry cycling for up to 100 cycles as previously described in this section. Total normal emittance measurements were made using the

iterative method as previously described. Results are shown in Tables 3-2 and 3-3.

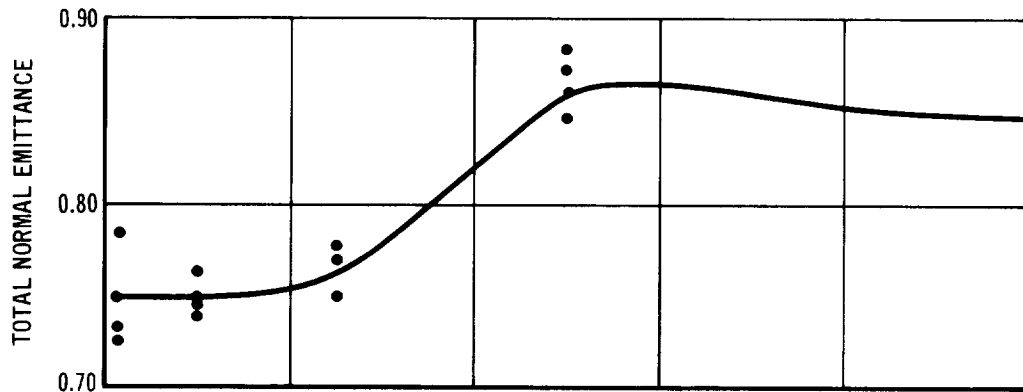
TABLE 3-2  
EMITTANCE DATA

TEMPERATURE AT WHICH $\epsilon$ WAS MEASURED DURING PROFILE EXPOSURE	EMITTANCE OF MODIFIED R-512E/ C-129Y SYSTEM NUMBER OF REENTRY CYCLES				
	1	10	25	50	100
1600°F (870°C)	0.548	0.835	0.869	0.848	0.855
	0.519	0.856	0.882	0.791	0.900
	0.728	0.854	0.874	0.849	0.791
2000°F (1100°C)	0.734	0.866	0.875	0.862	0.820
	0.732	0.858	0.889	0.795	0.856
	0.735	0.862	0.883	0.840	0.787
2400°F (1300°C)	0.736	0.742	0.750	0.882	0.876
	0.726	0.744	0.776	0.847	0.849
	0.785	0.762	0.771	0.874	0.822
2000°F (1100°C)	0.876	0.860	0.876	0.882	0.838
	0.868	0.870	0.884	0.829	0.839
	0.899	0.894	0.877	0.897	0.808
1600°F (870°C)	0.877	0.846	0.854	0.864	0.862
	0.840	0.863	0.877	0.863	0.886
	0.886	0.890	0.886	0.939	0.805

TABLE 3-3  
EMITTANCE DATA

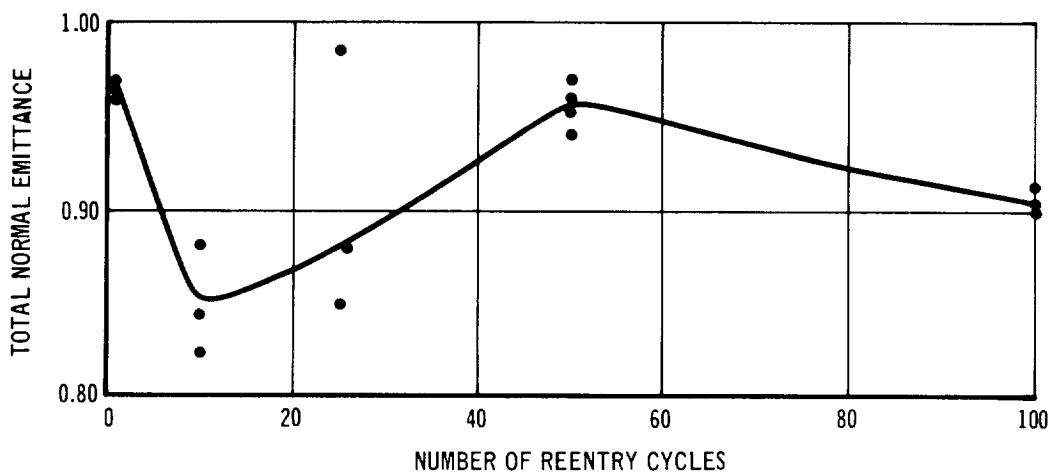
TEMPERATURE AT WHICH $\epsilon$ WAS MEASURED DURING PROFILE EXPOSURE	EMITTANCE OF R-512E/FS-85 SYSTEM (ACRYLIC) NUMBER OF REENTRY CYCLES				
	1	10	25	50	100
1600°F (870°F)	0.667	0.860	0.810	0.942	0.840
	0.728	0.842	0.840	0.791	0.865
	0.988	0.872	0.894	0.820	0.815
2000°F (1100°C)	0.864	0.829	0.820	0.949	0.871
	0.895	0.817	0.823	0.946	0.864
	0.945	0.861	0.902	0.895	0.907
2400°F (1300°C)	0.967	0.843	0.850	0.973	0.911
	0.968	0.824	0.798	0.942	0.912
	0.969	0.879	0.984	0.951	0.906
2000°F (1100°C)	0.913	0.837	0.863	0.934	0.872
	0.870	0.816	0.865	0.915	0.939
	0.886	0.870	0.827	0.967	0.903
1600°F (870°C)	0.931	0.866	0.880	0.930	0.835
	0.918	0.822	0.876	0.878	0.946
	0.928	0.894	0.809	0.813	0.834

The total normal emittance of the R-512E coating applied to FS-85 alloy from an acrylic-based slurry showed the same response to reentry cycling as the R-512E coating applied from a nitrocellulose-based slurry. Emittance values were very nearly the same after 10, 25, 50 and 100 cycles (Figures 3-10 and 3-11). Emittance during the first reentry exposure cycle was higher by about 0.07 for the coating applied from the acrylic-based slurry, which may be explained by the slightly rougher texture of this coating.



C-129Y/MOD R-512E EMITTANCE AT 2400°F (1300°C) VERSUS  
NUMBER OF REENTRY CYCLES

FIGURE 3-10



FS-85/R-512E (A-32) EMITTANCE AT 2400°F (1300°C) VERSUS  
NUMBER OF REENTRY CYCLES

FIGURE 3-11



Surprisingly, the modified R-512E (45Si-35Cr-20Fe) coating showed a lower emittance on the C-129Y alloy than did the normal R-512E (60Si-20Cr-20Fe) coating. This difference was about 0.12 for the first 25 reentry cycles, but essentially disappeared after 50 and 100 reentry cycles. It was thought that the higher chromium content of the modified coating would produce a higher emittance based on emittance studies conducted during an Air Force sponsored program (Reference 2). Closer examination of the Air Force studies revealed that the higher chromium content (25 and 30% Cr) coatings also had equivalent increases in iron content. It may be the increased iron content or the combined iron and chromium content which is responsible for higher emittance rather than the increase in chromium content alone.

The total hemispherical emittance of the fused slurry silicide coated columbium alloys is assumed to be equal to the total normal emittance. This assumption is based on confidence that the coating and/or coating oxide is a perfect diffuse emitter. Similar coatings and metal oxides, measured utilizing a directional emissometer, were found to be perfectly diffuse.

Good coating reliability for 100 flight reuse was demonstrated from reuse cycling of the emittance specimens. A total of 21 specimens were reentry cycled for 100 flights without any coating failures.

The effect of reuse on emittance of all five alloy/coating systems was small. Most alloy/coating systems showed an initial drop in emittance of about 5% up to the first 15 to 20 cycles, then a gradual increase until all of the loss had been recovered by 100 cycles. Differences in emittance between alloys were very subtle. The FS-85/R-512E system showed the largest increase in emittance from one cycle to 100 cycles.

3.2 Coating Structure and Chemistry - R-512E coated FS-85, C-129Y, Cb-752, B-66, and WC-3015 alloys were examined with the electron microprobe and by x-ray techniques to study the effects of reuse on coating structure and surface chemistry.

The specimens examined were portions of the tensile specimens which were used for determining the effects of reuse on mechanical properties. The portion of the specimens used was the area between the loading hole and the reduced cross section. Specimens, their reentry cycle history, and the analytical tests that were performed on each, are shown in the Table 3-4 test matrix.

Those specimens that were examined with x-ray techniques were placed directly in the instrument and exposed to radiation. The specimens that were examined with

TABLE 3-4  
TEST MATRIX FOR CHEMISTRY AND STRUCTURE STUDIES

SPECIMEN	NO. OF CYCLES	COMPOSITION (NOMINAL)	XRD EXAM	XRF EXAM	ELECTRON PROBE LINE SCANS							
					Si	Cr	Fe	Nb	W	Zr	Ta	Hf
C-62	0	5 Zr, 10 W, BAL. Nb	-	-	X	X	X	X	X	X	-	-
C-27	50	5 Zr, 10 W, BAL. Nb	X	X	X	X	X	X	X	X	-	-
C-89	100	5 Zr, 10 W, BAL. Nb	X	X	X	X	X	X	X	X	-	-
F-70	0	11W, 28 Ta, 1Zr, BAL. Nb	-	-	X	X	X	X	X	-	X	-
F-77	50	11W, 28 Ta, 1Zr, BAL. Nb	X	X	X	X	X	X	X	-	X	-
F-84	100	11W, 28 Ta, 1Zr, BAL. Nb	X	X	X	X	X	X	X	-	X	-
Y-43	0	10W, 10Hf, 0.1Y, BAL. Nb	-	-	X	X	X	X	X	-	-	X
Y-12	50	10W, 10Hf, 0.1Y, BAL. Nb	X	X	X	X	X	X	X	-	-	X
Y-18	100	10W, 10Hf, 0.1Y, BAL. Nb	X	X	X	X	X	X	X	-	-	X
B-38	50	5Mo, 5V, 1 Zr, BAL. Nb	X	X	-	-	-	-	-	-	-	-
B-81	100	5Mo, 5V, 1 Zr, BAL. Nb	X	X	-	-	-	-	-	-	-	-
W-8	50	30 Hf, 4Ti, 15W, BAL. Nb	X	X	-	-	-	-	-	-	-	-
W-4	100	30 Hf, 4Ti, 15W, BAL. Nb	X	X	-	-	-	-	-	-	-	-

the electron microprobe required additional preparation. These specimens were first coated with a thin layer of gold by vapor deposition. This coating provided a conductive layer which allowed a thick nickel plating to be formed. The thick nickel plating prevented rounding of the edges during the polishing operation. The nickel plated specimens were mounted in copper-filled Bakelite prior to polishing.

A qualitative surface comparison between the 50 and 100 cycle test specimens of each alloy for each element detected was made by x-ray fluorescence. Elements having an atomic number less than 22 could not be detected with the equipment used. This of course includes silicon, probably the major constituent. The qualitative comparisons are presented in Table 3-5. The major revelation of this examination was the detection of copper on all coated alloys except the FS-85. The presence of copper is accounted for as a result of the mounting material. The FS-85/R-512E system showed an increase in both of the coating modifiers on the surface while the rest of the systems did not have this tendency. The C-219/R-512E material showed a loss in coating modifiers (Cr and Fe) due to continued cycling. A base metal alloy addition, hafnium, showed an increased concentration in the coating. It would seem to be beneficial for long coating life to retain the coating modifiers.

TABLE 3-5

COATING SURFACE COMPARISON OF 100 CYCLE SPECIMENS TO  
50 CYCLE SPECIMENS BY X-RAY FLUORESCENCE

SAMPLE TYPE	ELEMENTS										
	Nb	Fe	Cr	W	Zr	Ta	Hf	Y	Cu	Mo	V
Cb-752	NC	NC	d	d	NM	NC	-	-	NC	-	-
FS-85	NC	i	l	NC	-	d	-	-	-	-	-
C129 Y	d	d	dD	D	-	d	i	NM	d	-	-
B-66	d	d	i	d	NM	d	-	-	NC	d	il
WC-3015	NC	NC	i	i	-	i	i	-	NC	-	-

NM - DETECTED BUT COULD NOT BE MEASURED

NC - NO CHANGE

d - SLIGHT DECREASE

dD - MODERATE DECREASE

D - RELATIVELY LARGE DECREASE

i - SLIGHT INCREASE

il - MODERATE INCREASE

l - LARGE INCREASE

Semiquantitative determination of the relative amounts of the surface compounds identified by the use of x-ray diffraction is presented in Table 3-6. In no instance were all of the compounds indicated by the x-ray patterns identified. There was a large quantity of data and the patterns were very complex. All alloy/coating systems showed the  $\text{CrCbO}_4$  compound. The B-66 and FS-85 showed large increases in this compound due to an exposure of 50 flight cycles. This is consistent with the x-ray fluorescence data which showed an increase in chromium content. Cb-752 was the only system in which  $\text{SiO}_2$  could be detected, although  $\text{SiO}_2$  certainly should be present in the other systems.

Background measurements and standard count rates were obtained to determine the optimum setting at which to operate the electron microprobe. The background and standard count rates for the elements involved in the electron microprobe analysis are given in Table 3-7.







The prepared specimens were then examined with the electron microprobe by the method of linear scanning. There were six elemental scans recorded for each specimen. Identification of the specimens and the elements scanned are presented in Table 3-4.

Several factors peculiar to the electron microprobe must be considered when the data is examined. One of the more important is the fact that the x-ray

# FINAL REPORT

TABLE 3-6

## X-RAY DIFFRACTION RESULTS

SAMPLE	Cr Nb O <sub>4</sub>	Si O <sub>2</sub>
C-27 C-89		
B-38 B-81		N.D.
F-77 F-84		N.D.
Y-12 Y-18		N.D.
W-8 W-4		N.D.

N.D. - NOT DETECTED

RELATIVE INTENSITY OF SURFACE PHASES

INCREASE INTENSITY SHOWN IN THIS DIRECTION 

TABLE 3-7

## BACKGROUND DETERMINATIONS

ELEMENT BEING ANALYZED

	Si	Cr	Fe	Nb	W	Zr	Ta	Hf
Si	20,000	70	15	65	15	30	15	15
Cr	40	8,500	25	40	30	40	25	30
Fe	45	55	5,500	65	30	50	30	30
Nb	55	70	30	2,500	40	70	30	30
W	70	60	60	45	1,200	50	50	55
Zr	80	110	30	140	35	2,500	30	35
Ta	350	90	45	325	55	250	1,500	50
Hf	85	450	45	120	50	90	60	1,600

COUNT RATE ON PURE STANDARD OF (CPS)

background values vary for each element setting and for each base metal. Furthermore, x-ray lines from one element may overlap the x-ray lines being detected from other elements and thus give a false intensity value. Because of intensity considerations, it is not always possible to fully eliminate all overlaps.

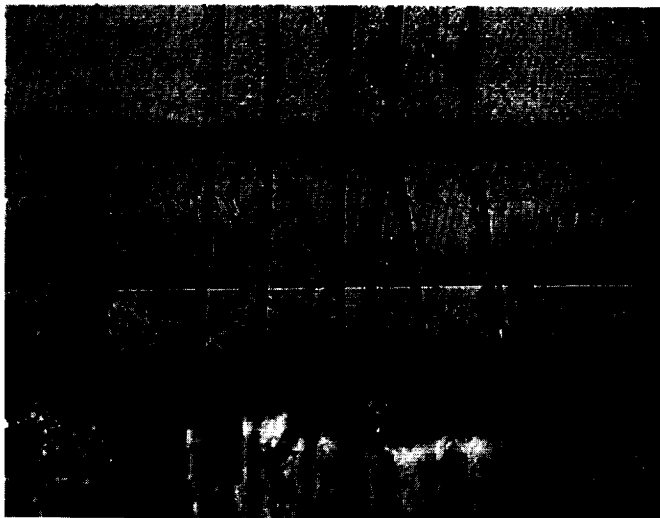
The intensity values obtained by the linear scans were converted to probe ratios by subtracting a background count and dividing by the intensity of a pure standard. The background value was determined by setting the spectrometer 2° off the peak setting and recording the intensity from a pure standard. However, it must be remembered that the actual background value changes as the composition of the sample changes. Still the values shown on the line scan graphs are not quantitative. The values must be corrected for absorption by the matrix of the x-rays emitted by the element examined, for fluorescence of x-rays of the element examined by x-rays from the elements in the matrix, and for effects due to the atomic number of the element being examined. Taking all of these effects into consideration, the accuracy of the probe ratio cannot be better than  $\pm 10\%$ . That is, the probe ratio can be as much as  $\pm 10\%$  of the actual weight percent composition. All of these factors must be considered upon examination of the linear scans presented. The linear scans do show, in a qualitative manner, how the distribution of each element varies across the coating.

Cb-752 - Photomicrographs of three Cb-752/R-512E specimens examined are shown in Figure 3-12. The three specimens were "as coated," "after 50 reentry cycles," external pressure, and "after 100 cycles," external pressure. The lines present in the photographs are caused by the deposition of diffusion pump oil by the microprobe electron beam. Therefore, these lines show the location and path of the microprobe linear scans.

In the "as coated" (Figure 3-13) condition the niobium content of the R-512E coating on Cb-752 was fairly constant throughout the coating at about 25%. After 50 cycles of exposure, the content dropped in the outer most 1/2 mil (13  $\mu\text{m}$ ) of coating. This decrease spread during the next 50 cycles to approximately 3/4 mil (19  $\mu\text{m}$ ) in depth, with spikes of high concentration up to 45%. The niobium content near the coating/metal interface showed a gradual increase into the coating. This is consistent with expected diffusion.

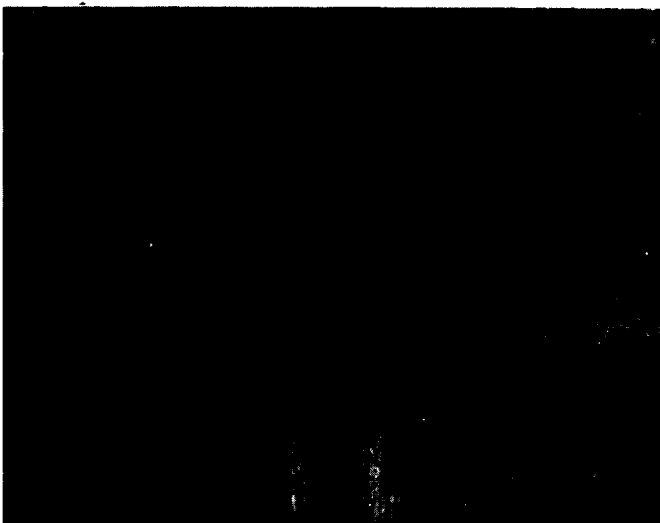
The tungsten content in the coating of the "as coated" (Figure 3-14) sample showed a peak concentration of 6-7%, 1/4 mil (6  $\mu\text{m}$ ) in from the surface with a gradual decline to about 1% at the interface. This peak remained about the same

500X



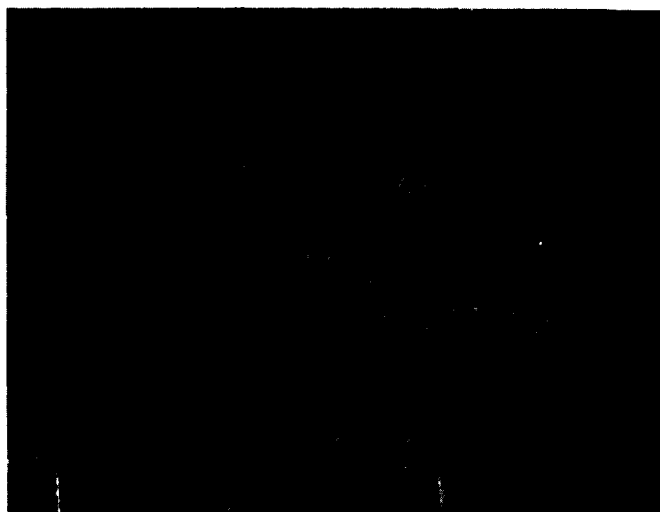
SAMPLE C-89 AFTER 100 REENTRY CYCLES

500X



SAMPLE C-27 AFTER 50 REENTRY CYCLES

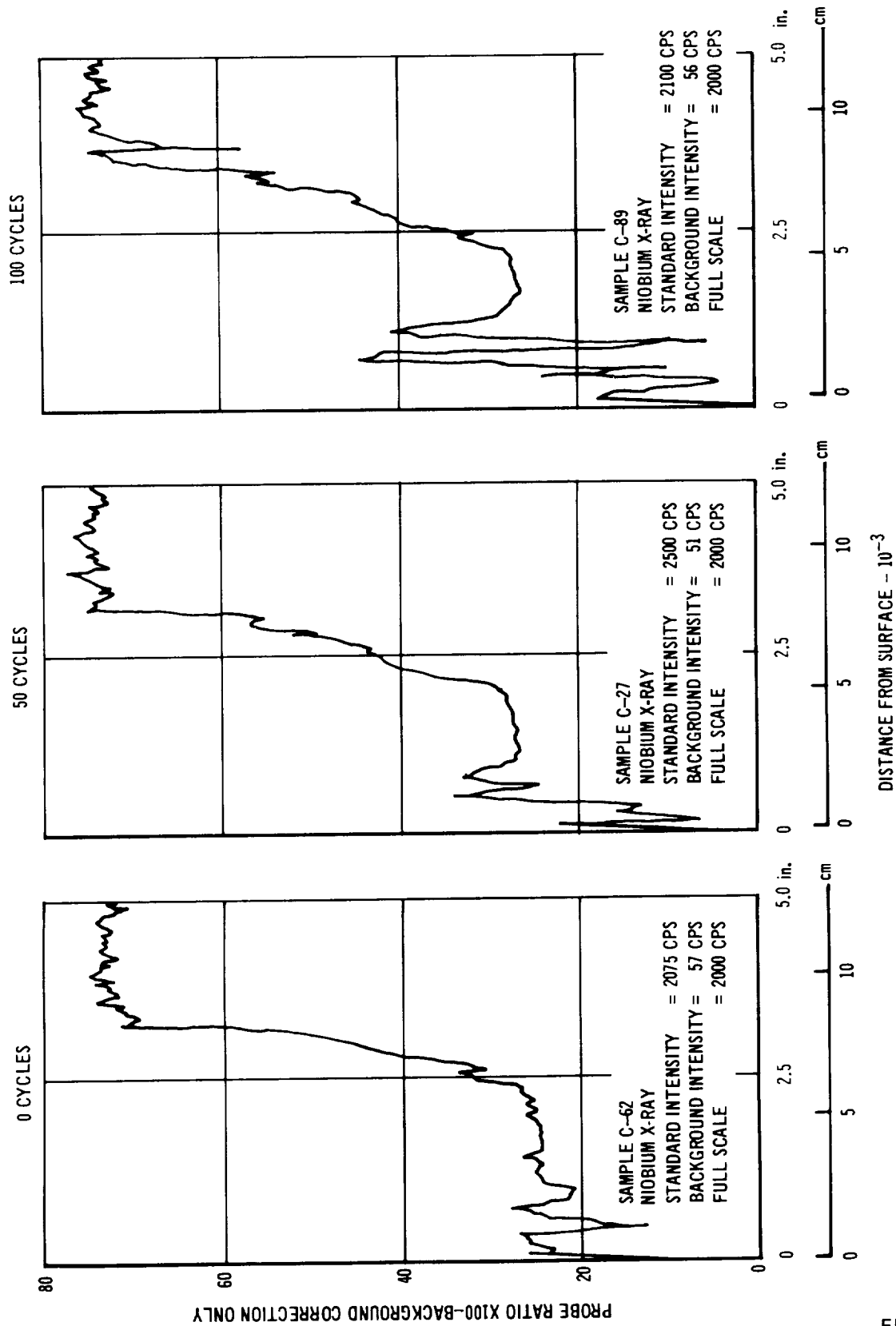
500X



SAMPLE C-62 AS COATED

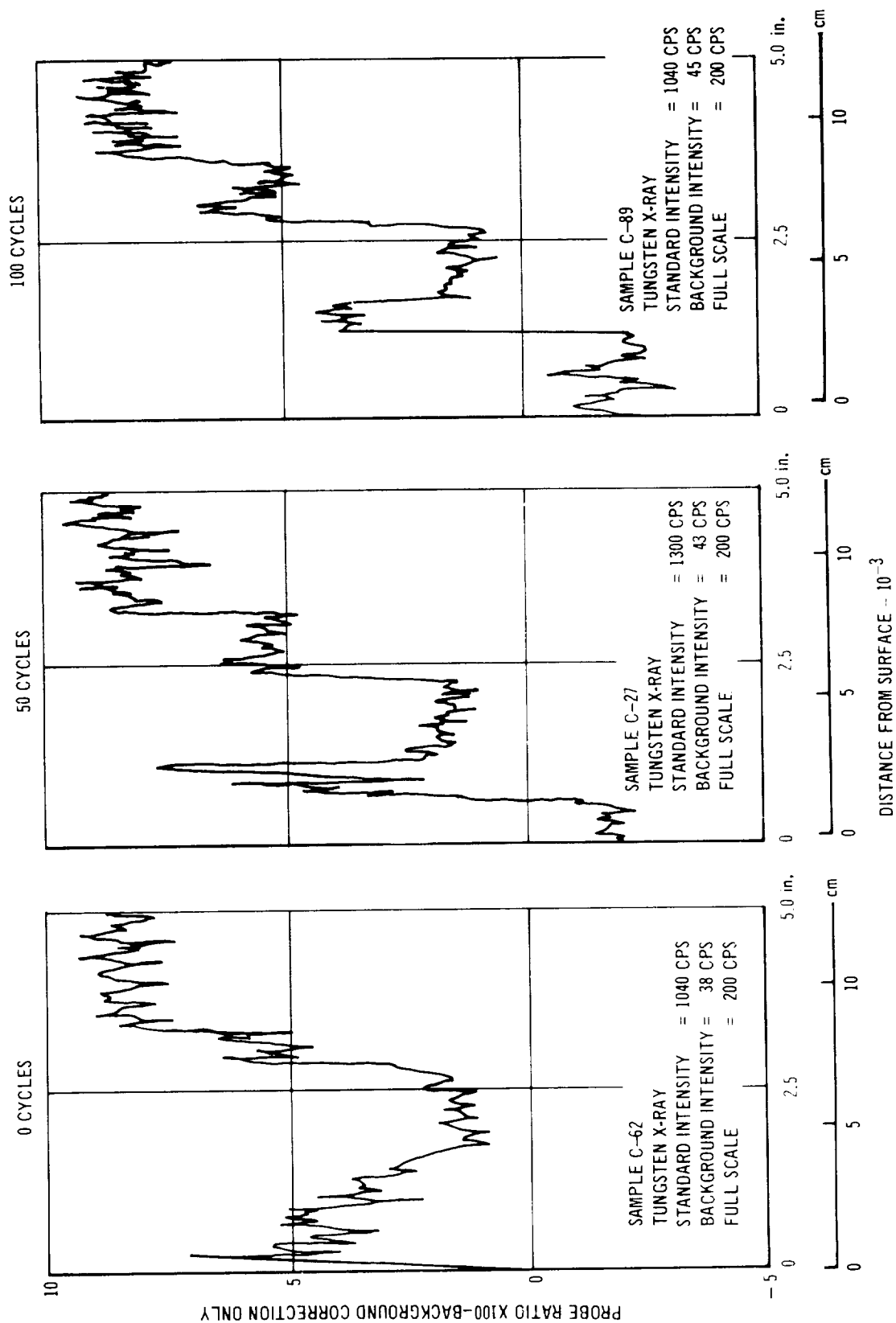
PHOTOMICROGRAPHS OF THE AREAS EXAMINED WITH THE  
ELECTRON MICROPROBE ON THE Cb-752/R-512E SYSTEM

FIGURE 3-12



EFFECT OF REENTRY CYCLING ON NIOBIUM DISTRIBUTION  
IN THE R-512E/Cb752 COATING SYSTEM

FIGURE 3-13



EFFECT OF REENTRY CYCLING ON TUNGSTEN DISTRIBUTION  
IN THE R-512E/Cb752 COATING SYSTEM

FIGURE 3-14



but shifted in to a depth of 1 mil (25  $\mu$ m) after 50 cycles. This peak concentration was located at a depth of 1-1/2 mils (38  $\mu$ m) after 100 cycles and was about 4%.

The zirconium content showed a gradual decrease from a content of 2.5% at the interface to 0 at the surface of the coating for the "as coated" (Figure 3-15) condition. The 0 content point continued to shift back from the surface with increased exposure; 3/4 mil (19  $\mu$ m) after 50 cycles and 1-1/4 mils (31  $\mu$ m) after 100 cycles.

The chromium in the coating (Figure 3-16) was very segregated with respect to zones in the coating, up to 15-20% in some zones, down to almost nothing in others. The zone with the highest concentration was very narrow, about 1/4 mil (6  $\mu$ m), but grew to 1/2 mil (13  $\mu$ m) after 100 cycles. It moved toward the surface during cycling, starting at about 1 mil (25  $\mu$ m) from the surface moving to within 1/4 mil (6  $\mu$ m) of the surface after 100 cycles.

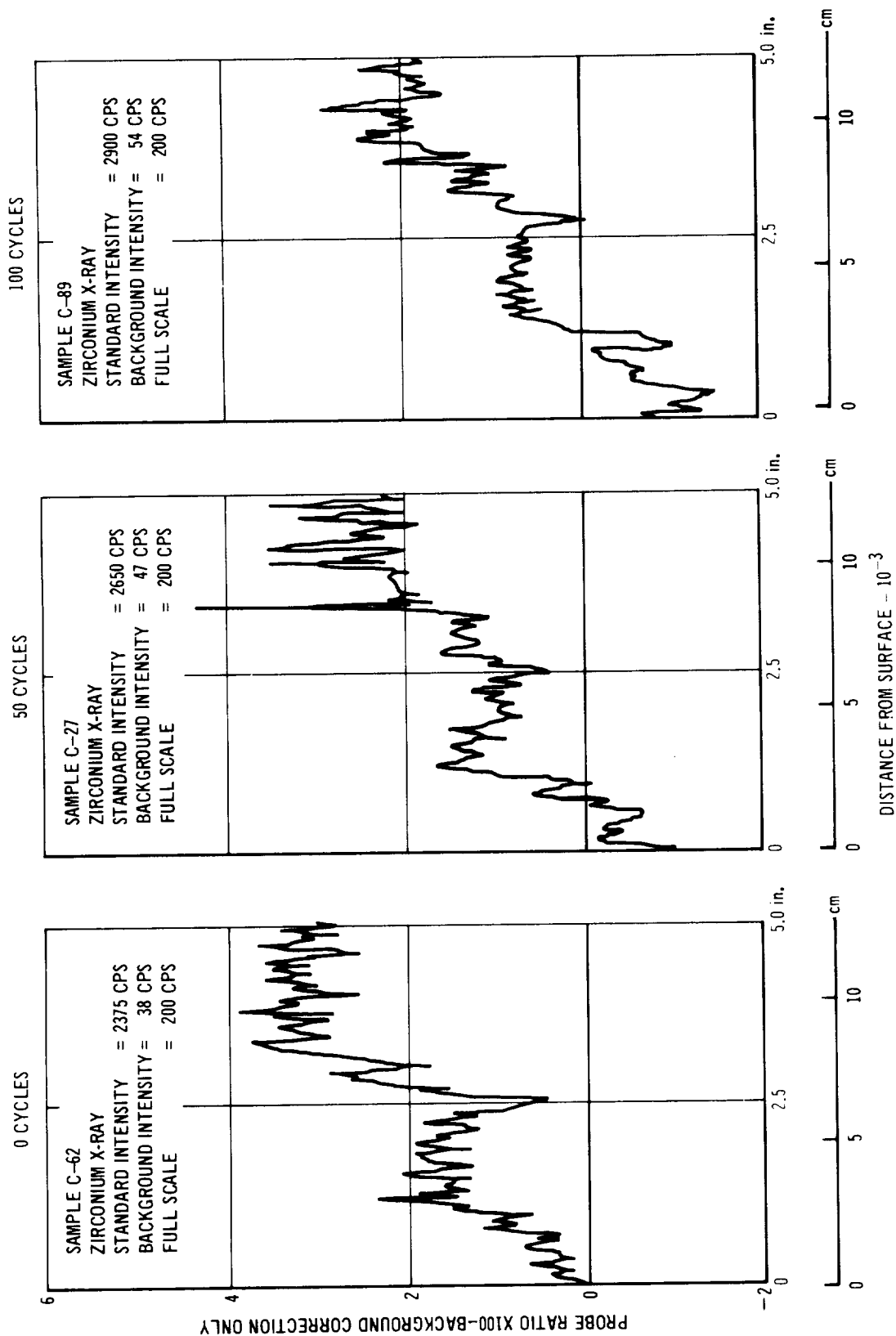
In the "as coated" condition (Figure 3-17) the iron content was also segregated in the coating zones with the majority of the iron, being in one zone (third zone from the metal/coating interface). With cycling the iron all concentrated into one large zone in the coating. The content decreased some from the surface, but in general, remained fairly constant.

The silicon content (Figure 3-18) showed two major peaks of concentration, one close to the surface and one close to the interface, both about equal at 25%. After cycling for 50 cycles the peak at the interface disappeared. The next 50 cycles of exposure produced little change in the silicon distribution. From the "as coated" condition to 100 cycles of exposure the sharp drop in the silicon content at the interface continued to drift outward, leaving iron, chromium, tungsten, zirconium and niobium.

FS-85 - Photomicrographs of the three FS-85/R-512E specimens examined are shown in Figure 3-19. The three specimens were "as coated," "after 50 reentry cycles," external pressure, and "after 100 reentry cycles," external pressure.

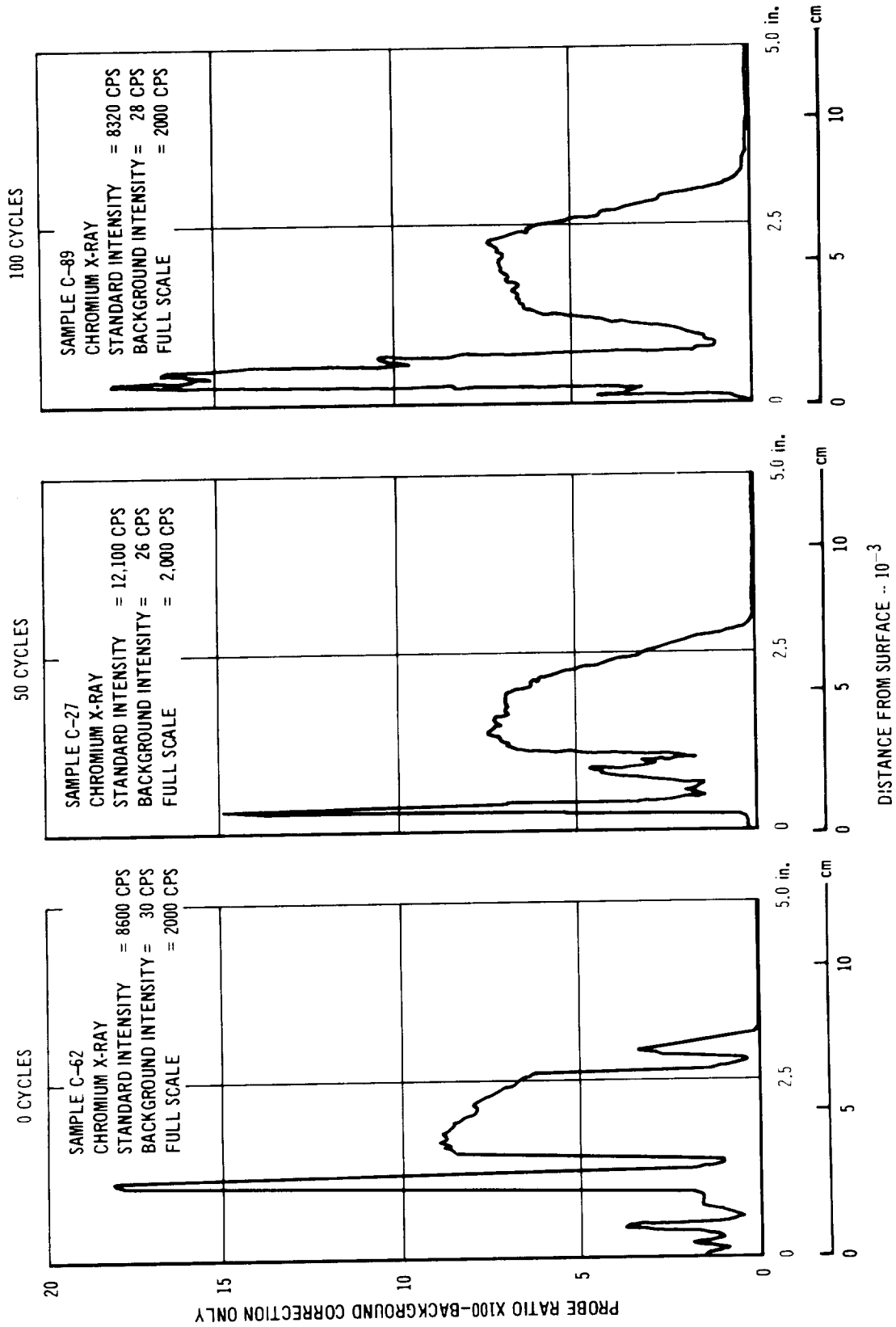
The niobium concentration of the "as coated" (Figure 3-20) coating was fairly uniform at about 18%. With cycling the concentration decreased at the surface to about 10% back to a depth of 1/2 mil (13  $\mu$ m) after 100 cycles. From 2-1/2 mils (63  $\mu$ m) on to the interface the concentration showed a gradual increase to the level in the base alloy.

The tantalum distribution in the coating (Figure 3-21) was very similar to the niobium. The concentration was fairly stable at about 13%. There was some reduction in concentration at the surface after 50 cycles, but this was recovered during the next 50 cycles.



EFFECT OF REENTRY CYCLING ON ZIRCONIUM DISTRIBUTION  
IN THE R-512E/Cb752 COATING SYSTEM

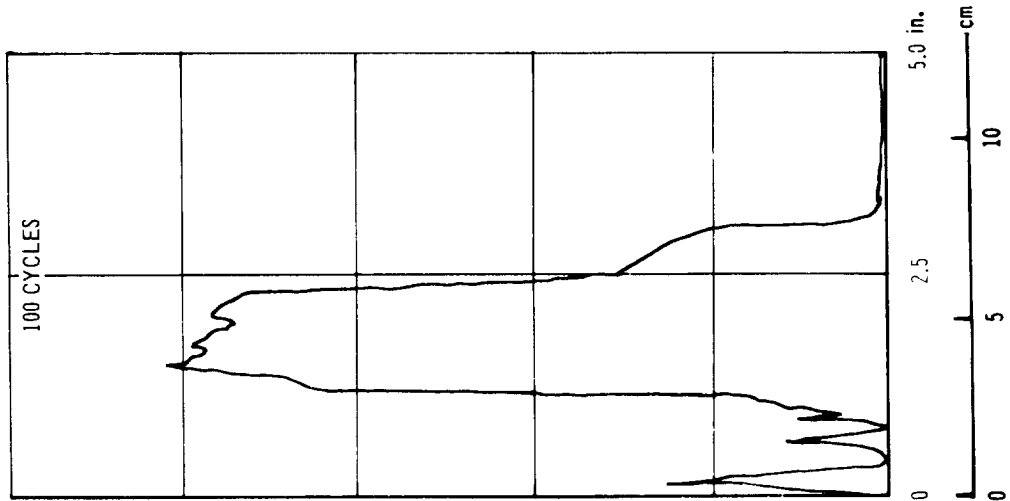
FIGURE 3-15



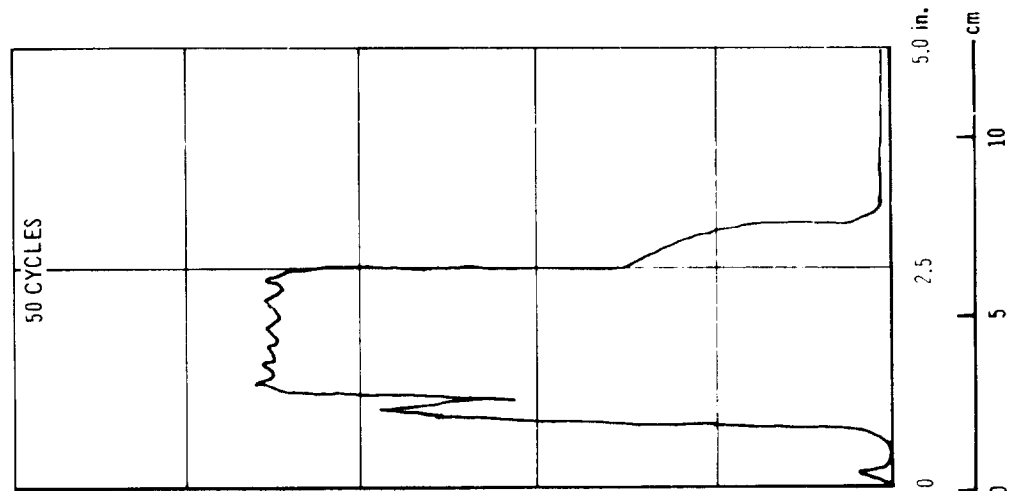
EFFECT OF REENTRY CYCLING ON CHROMIUM DISTRIBUTION  
IN THE R-512E/Cb752 COATING SYSTEM

FIGURE 3-16

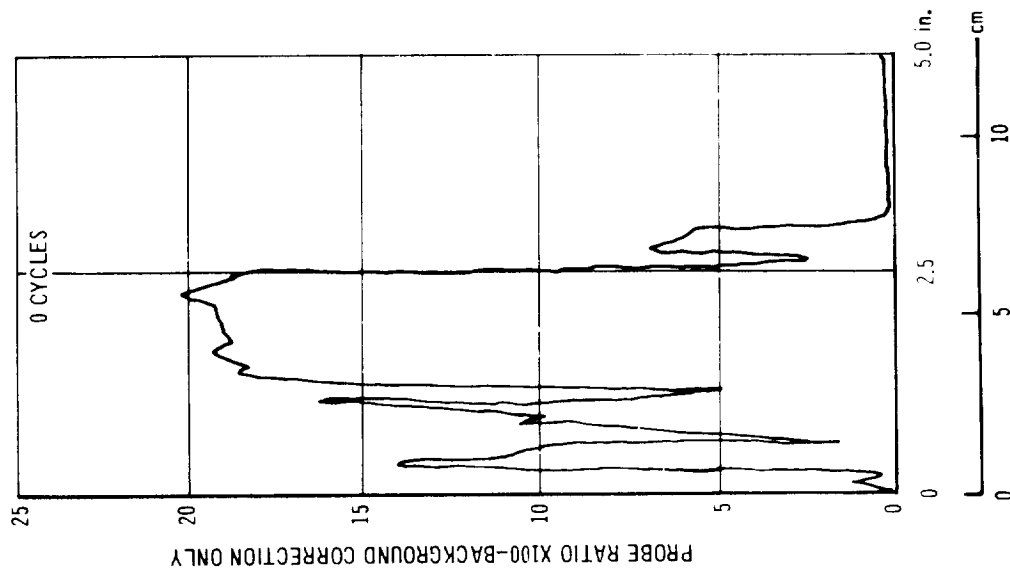
SAMPLE C-89  
IRON X-RAY  
STANDARD INTENSITY = 5450 CPS  
BACKGROUND INTENSITY = 28 CPS  
FULL SCALE = 2000 CPS



SAMPLE C-27  
IRON X-RAY  
STANDARD INTENSITY = 4500 CPS  
BACKGROUND INTENSITY = 21 CPS  
FULL SCALE = 1000 CPS

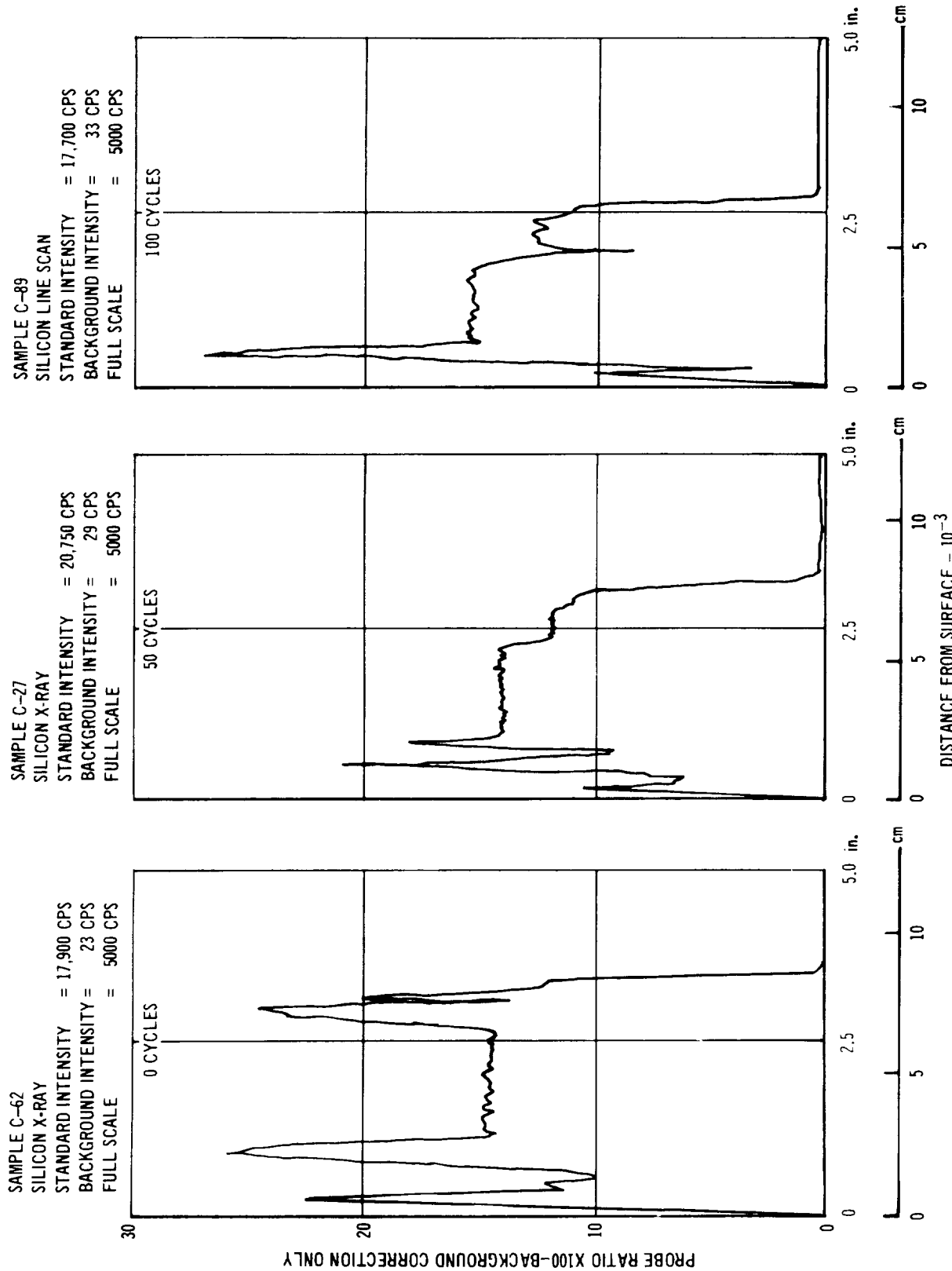


SAMPLE C-62  
IRON X-RAY  
STANDARD INTENSITY = 5900 CPS  
BACKGROUND INTENSITY = 28 CPS  
FULL SCALE = 2000 CPS



EFFECT OF REENTRY CYCLING ON IRON DISTRIBUTION  
IN THE R-512E/Cb752 COATING SYSTEM

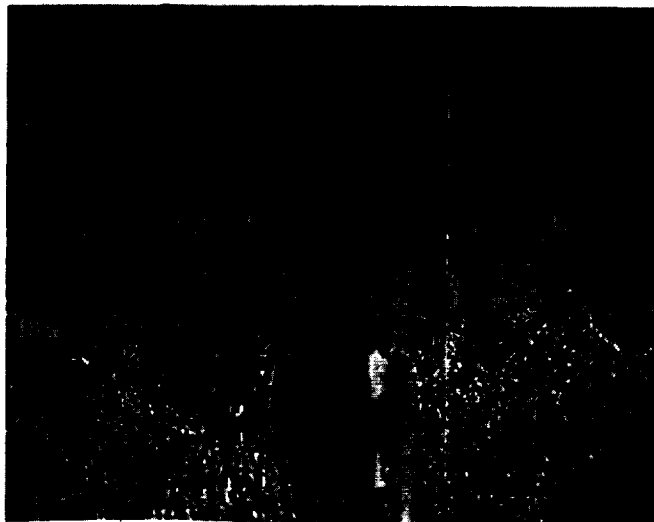
FIGURE 3-1



EFFECT OF REENTRY CYCLING ON SILICON DISTRIBUTION  
IN THE R-512E/Cb752 COATING SYSTEM

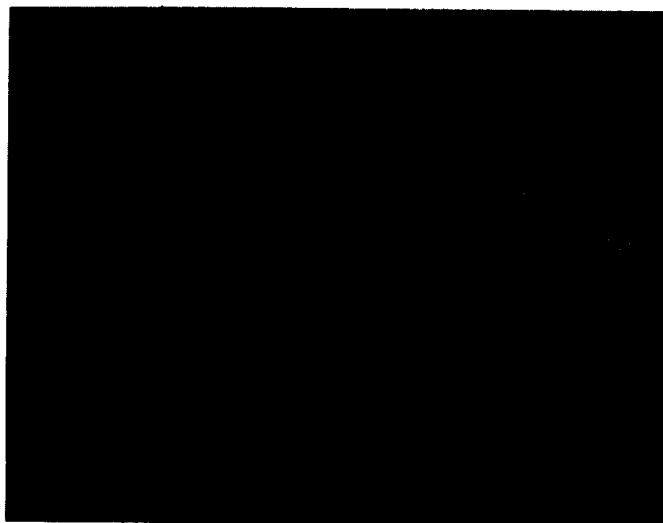
FIGURE 3-18

500X



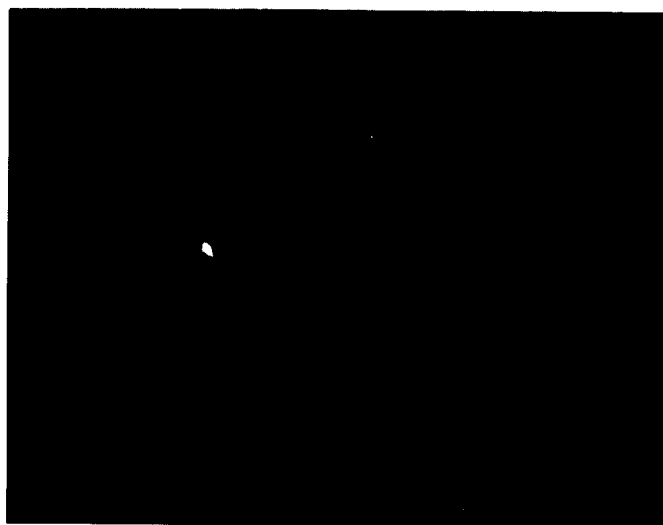
SAMPLE F-84 AFTER 100 REENTRY CYCLES

500X



SAMPLE F-77 AFTER 50 REENTRY CYCLES

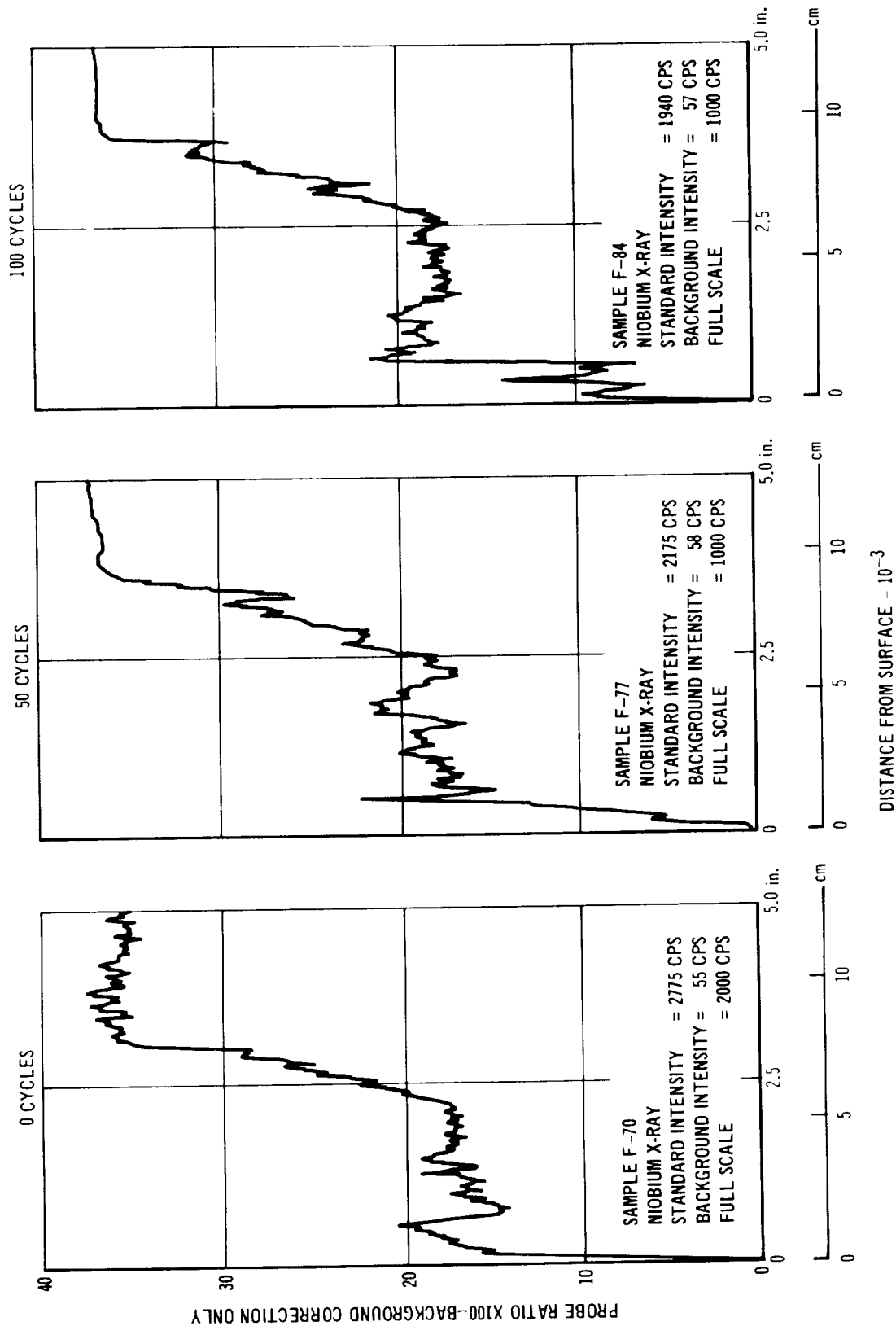
500X



SAMPLE F-70 AS COATED

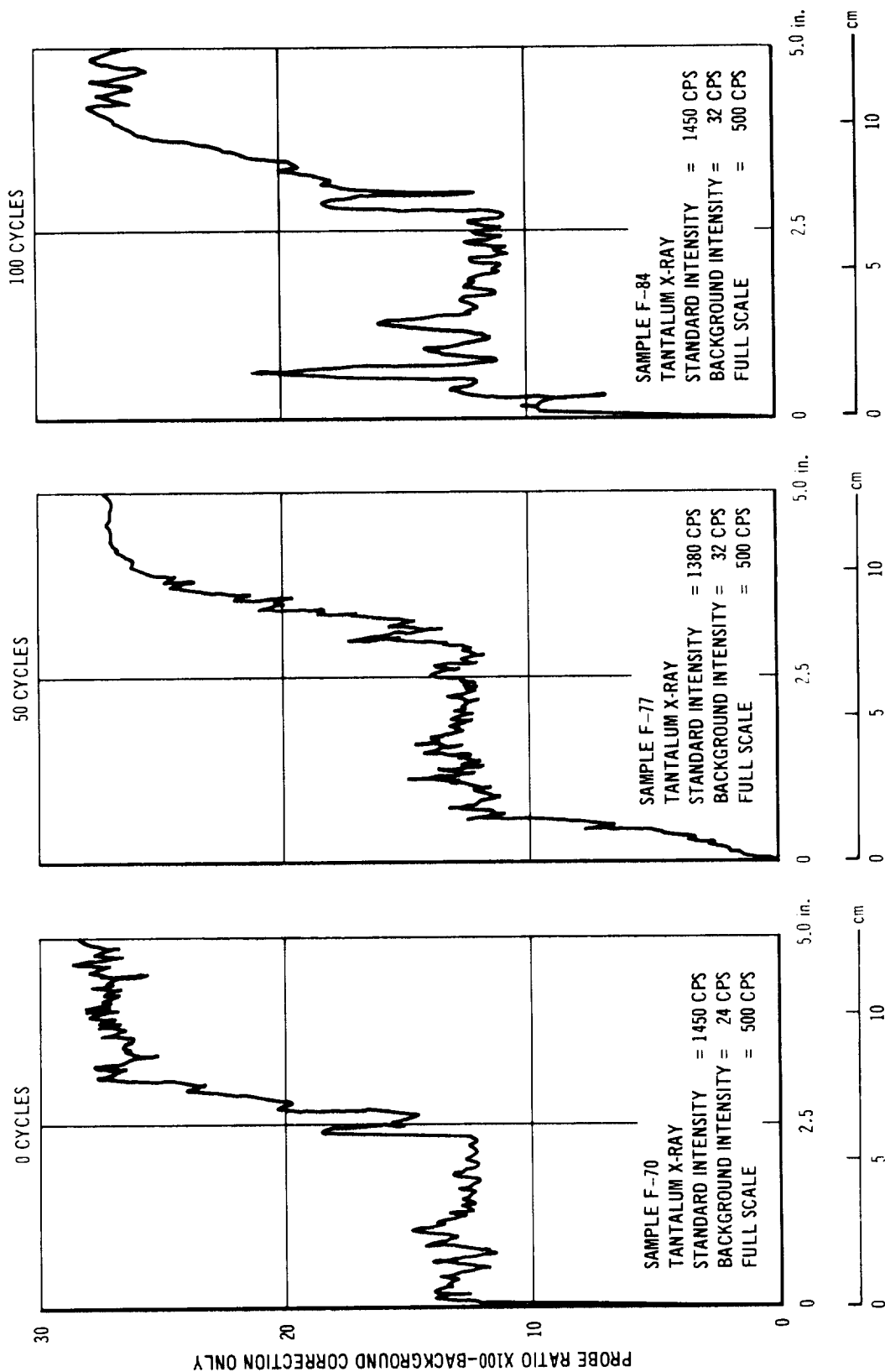
PHOTOMICROGRAPHS OF THE AREAS EXAMINED WITH THE  
ELECTRON MICROPROBE ON THE FS-85/R-512E SYSTEM

FIGURE 3-19



EFFECT OF REENTRY CYCLING ON NIOBIUM DISTRIBUTION  
IN THE R-512E/FS-85 COATING SYSTEM

FIGURE 3-20



EFFECT OF REENTRY CYCLING ON TANTALUM DISTRIBUTION  
IN THE R-512E/FS-85 COATING SYSTEM

FIGURE 3-21



The tungsten distribution (Figure 3-22) in the coating changed very little with cycling except for about a 1/2 mil (13  $\mu$ m) pull back from the surface. The peak contents within the outer 3/4 mil (19  $\mu$ m) of coating did increase from 5-6% to 8-9% after 100 cycles of exposure.

The chromium concentration (Figure 3-23), as in the Cb-752/R-512E system, segregated with respect to coating zones, but was stable with respect to cycling.

The iron concentration (Figure 3-24) was segregated with respect to the coating zones and showed a tendency to concentrate toward the center of the coating after 100 cycles of exposure.

The silicon distribution (Figure 3-25) was also quite stable with some drop-off in concentration at the surface as the number of cycles increased.

C-129Y - Photomicrographs of the three C-129Y/R-512E specimens examined are shown in Figure 3-26. The three specimens were "as coated," "after 50 reentry cycles," external pressure, and "after 100 reentry cycles," external pressure.

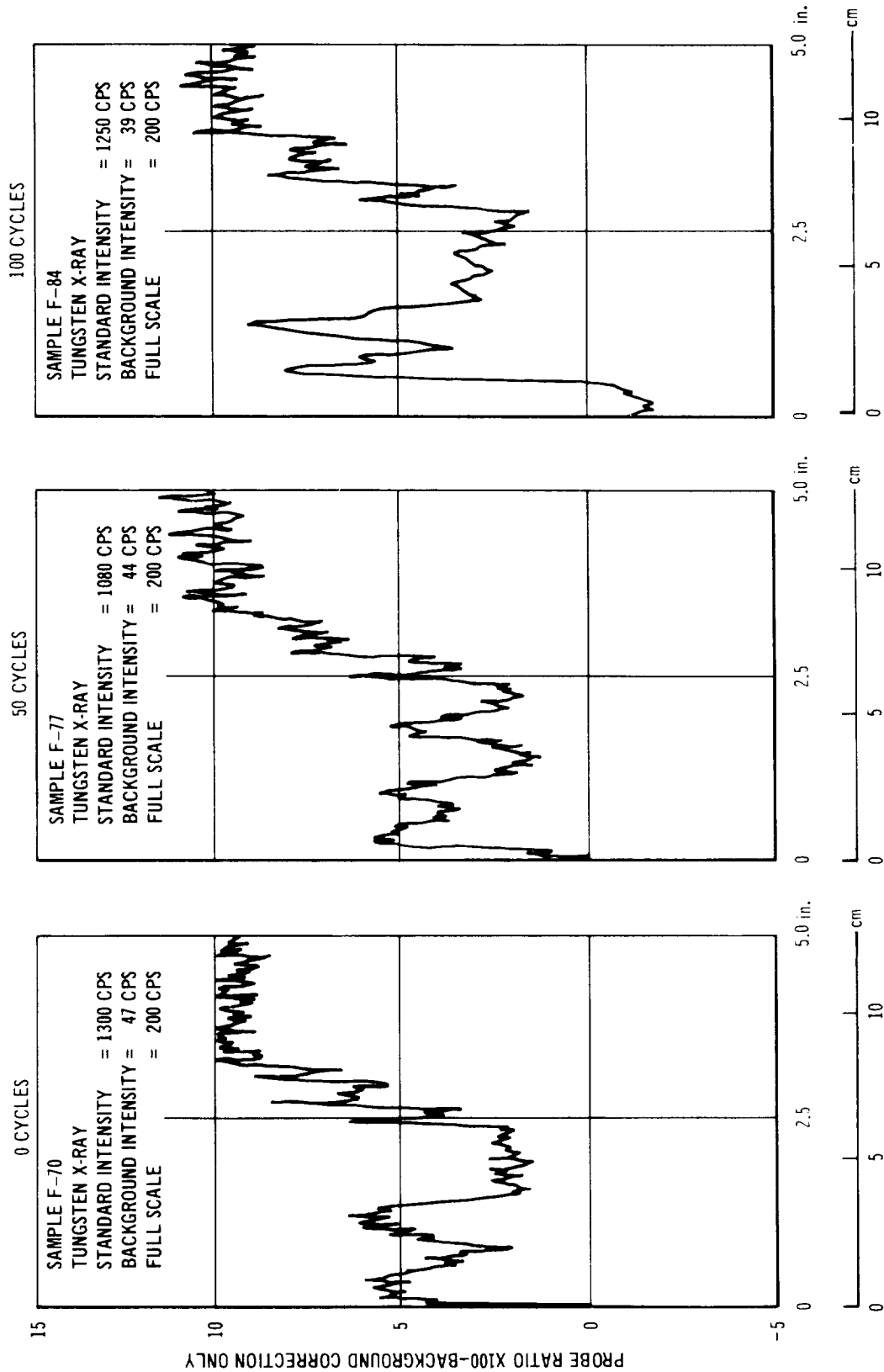
The niobium content of the coating in all three conditions (Figure 3-27) remained fairly stable at about 23%. However, the distribution was somewhat segregated with respect to the coating zones, ranging from 2% to 35%. There was no detectable shift of the niobium back from the surface as cycling progressed.

The tungsten content of the coatings (Figure 3-28) shifted back from the surface about 1/2 mil (13  $\mu$ m) after 50 cycles, but remained there during the next 50 cycles. From 10% tungsten content in the base metal the coating had peak concentrations of about 6%.

The hafnium distribution in the coatings changed very rapidly (Figure 3-29) with depth from the surface. Concentration cycled from 0 to about 7%. The hafnium was segregated with respect to coating zones. In the "as coated" condition there was a layer of about 5% concentration next to the surface. After 50 cycles this had disappeared to nothing and the next layer of concentration was at about 1 mil (25  $\mu$ m) in depth. This shifted out about 1/2 mil (13  $\mu$ m) toward the surface during the next 50 cycles.

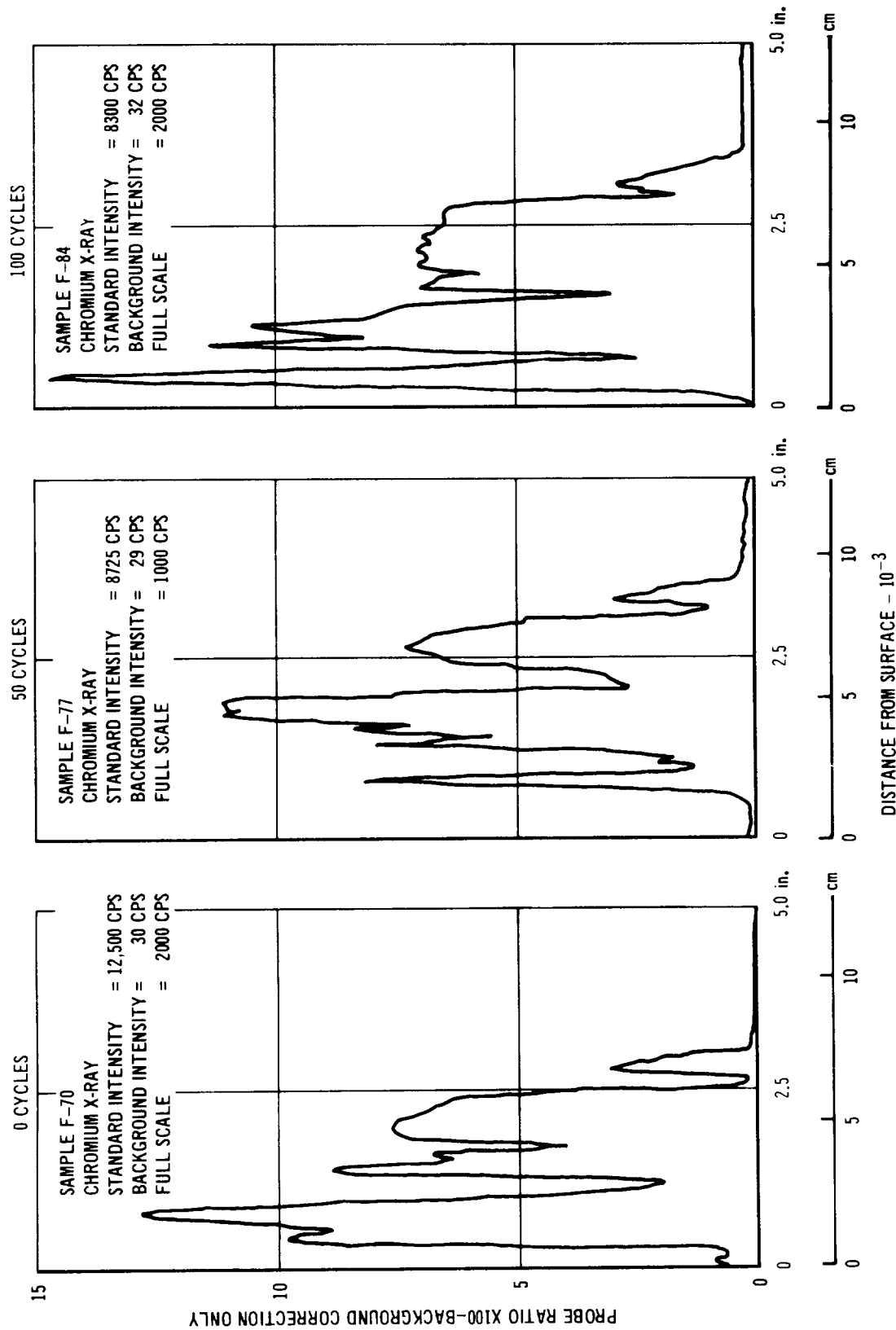
The chromium distribution in the coating was quite segregated, but remained rather stable throughout the cycling (Figure 3-30). Peak concentration was around 20%, minimum was about 1%.

The iron content was very segregated with respect to coating zones (Figure 3-31) but was also quite stable with respect to cycling.



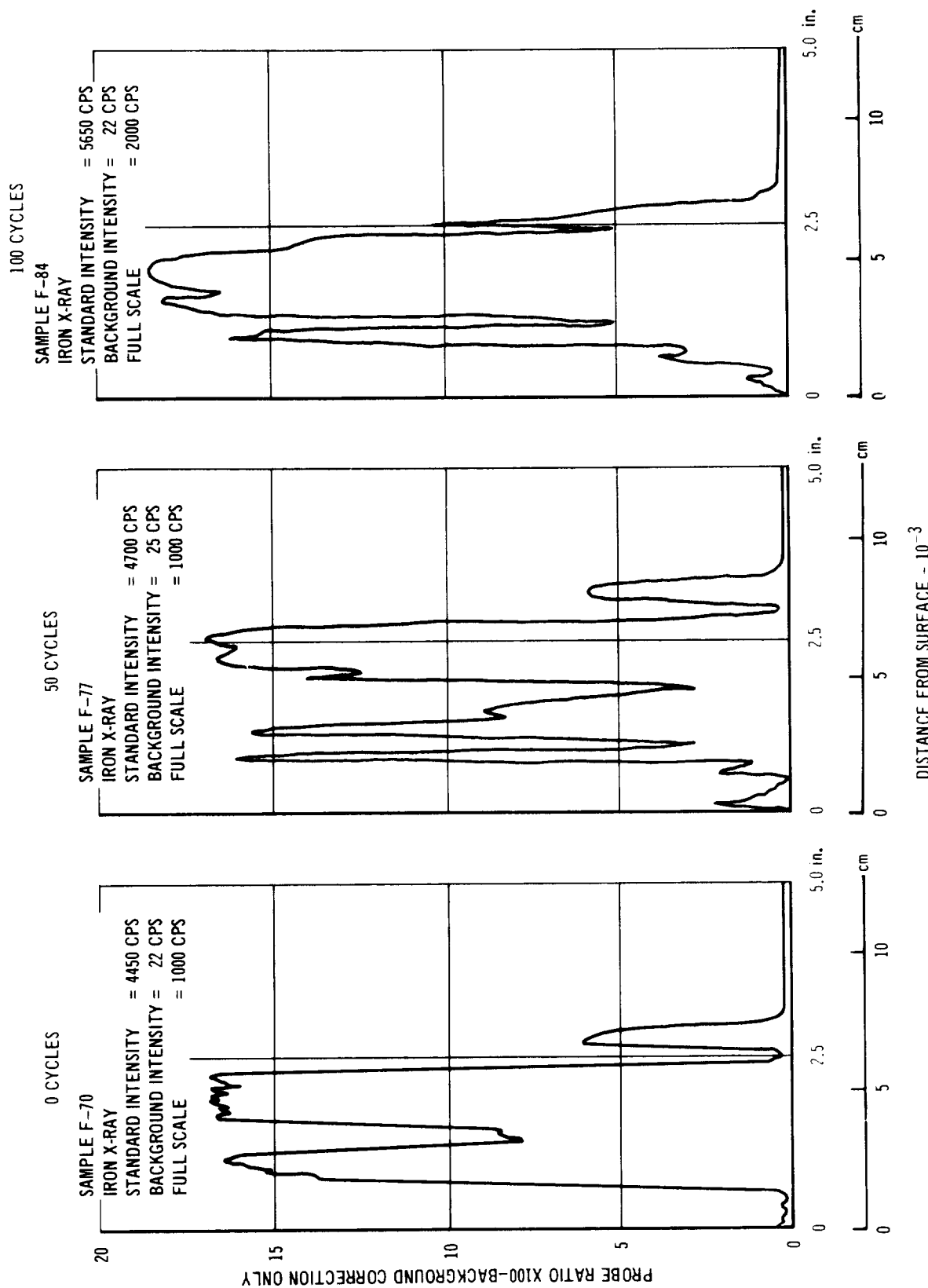
EFFECT OF REENTRY CYCLING ON TUNGSTEN DISTRIBUTION  
IN THE R-512E/FS-85 COATING SYSTEM

FIGURE 3-22



EFFECT OF REENTRY CYCLING ON CHROMIUM DISTRIBUTION  
IN THE R-512/FS-85 COATING SYSTEM

FIGURE 3-23

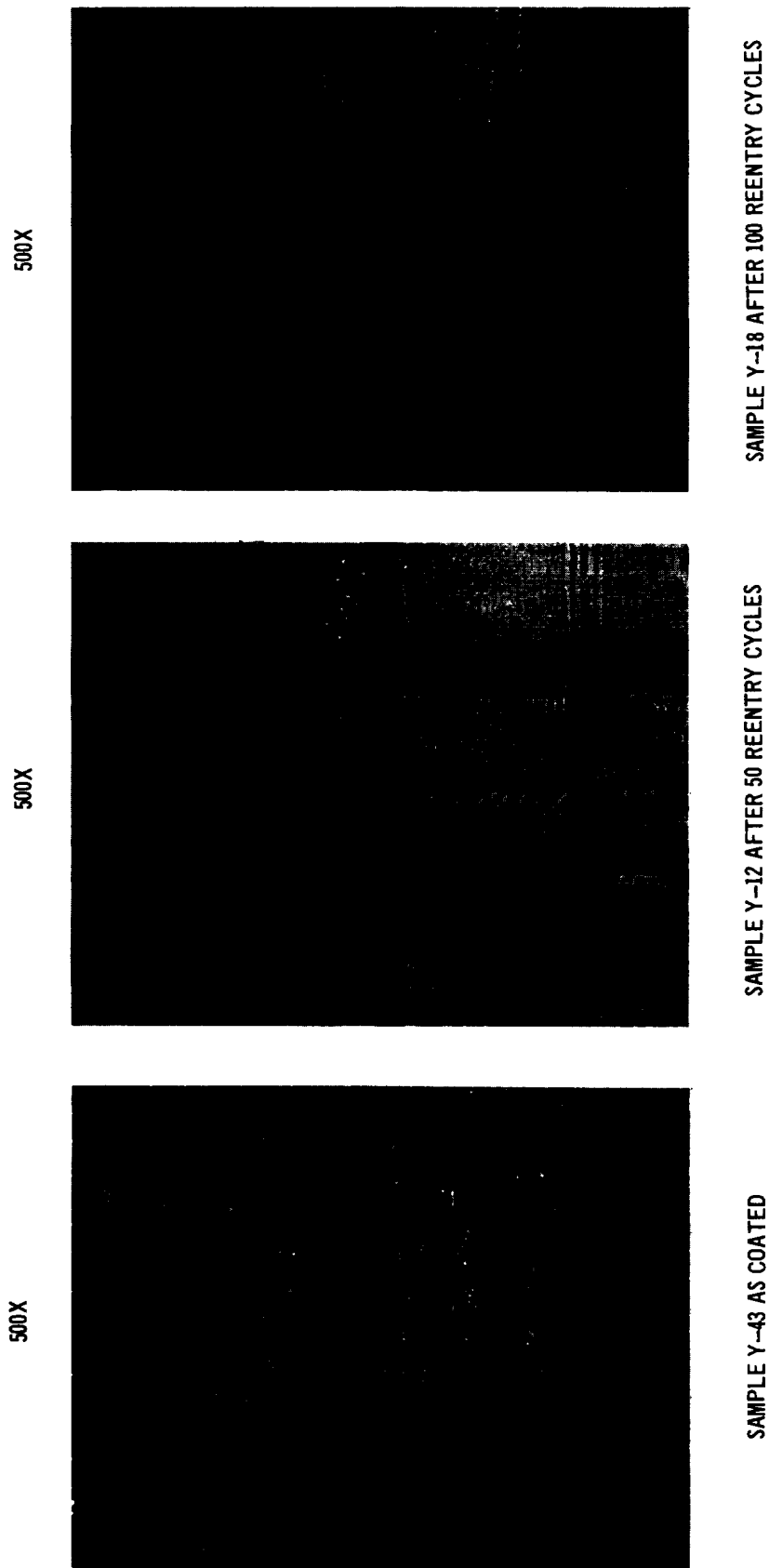


EFFECT OF REENTRY CYCLING ON IRON DISTRIBUTION  
IN THE R-512/FS-85 COATING SYSTEM

FIGURE 3-24

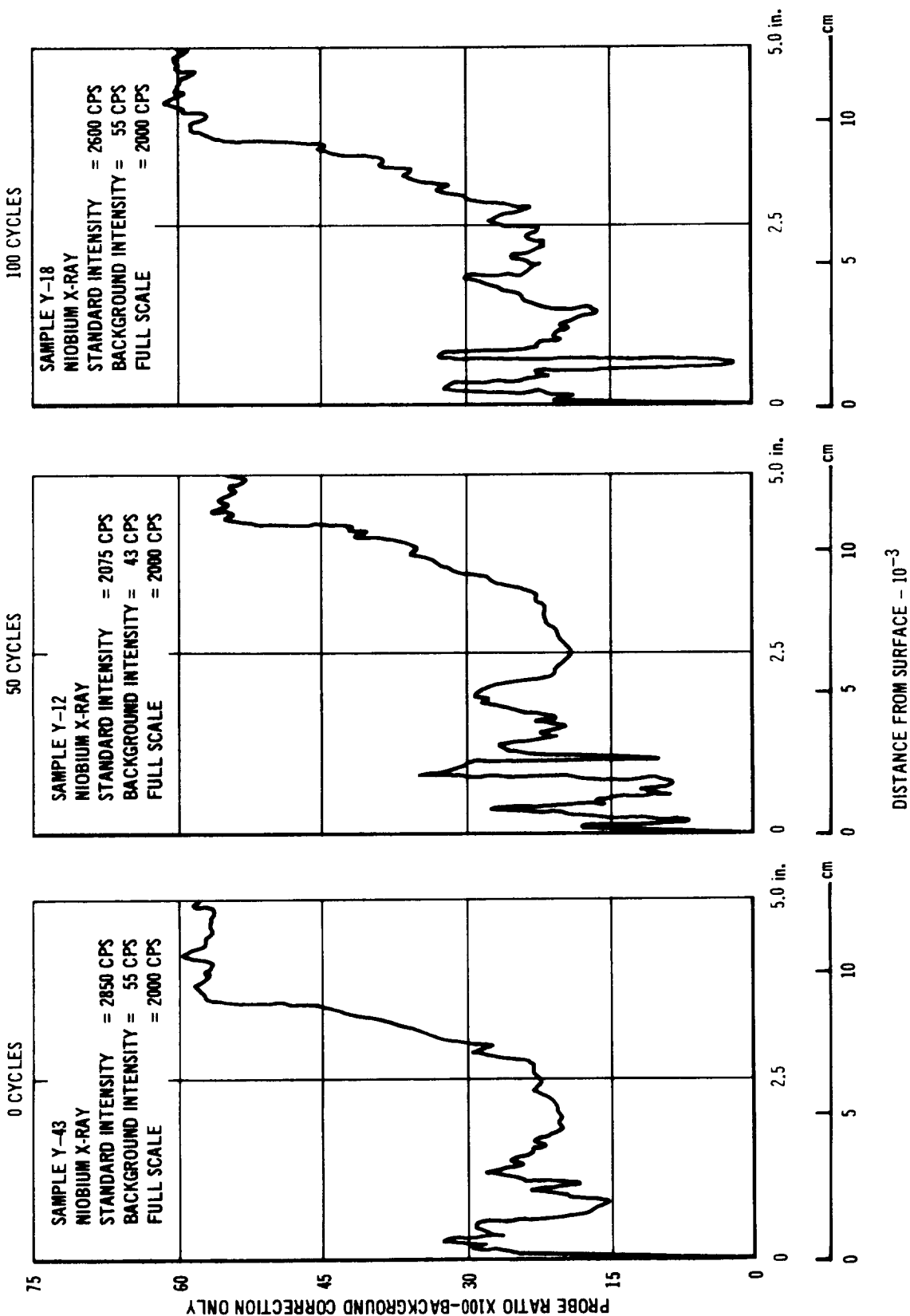


FIGURE 3-25



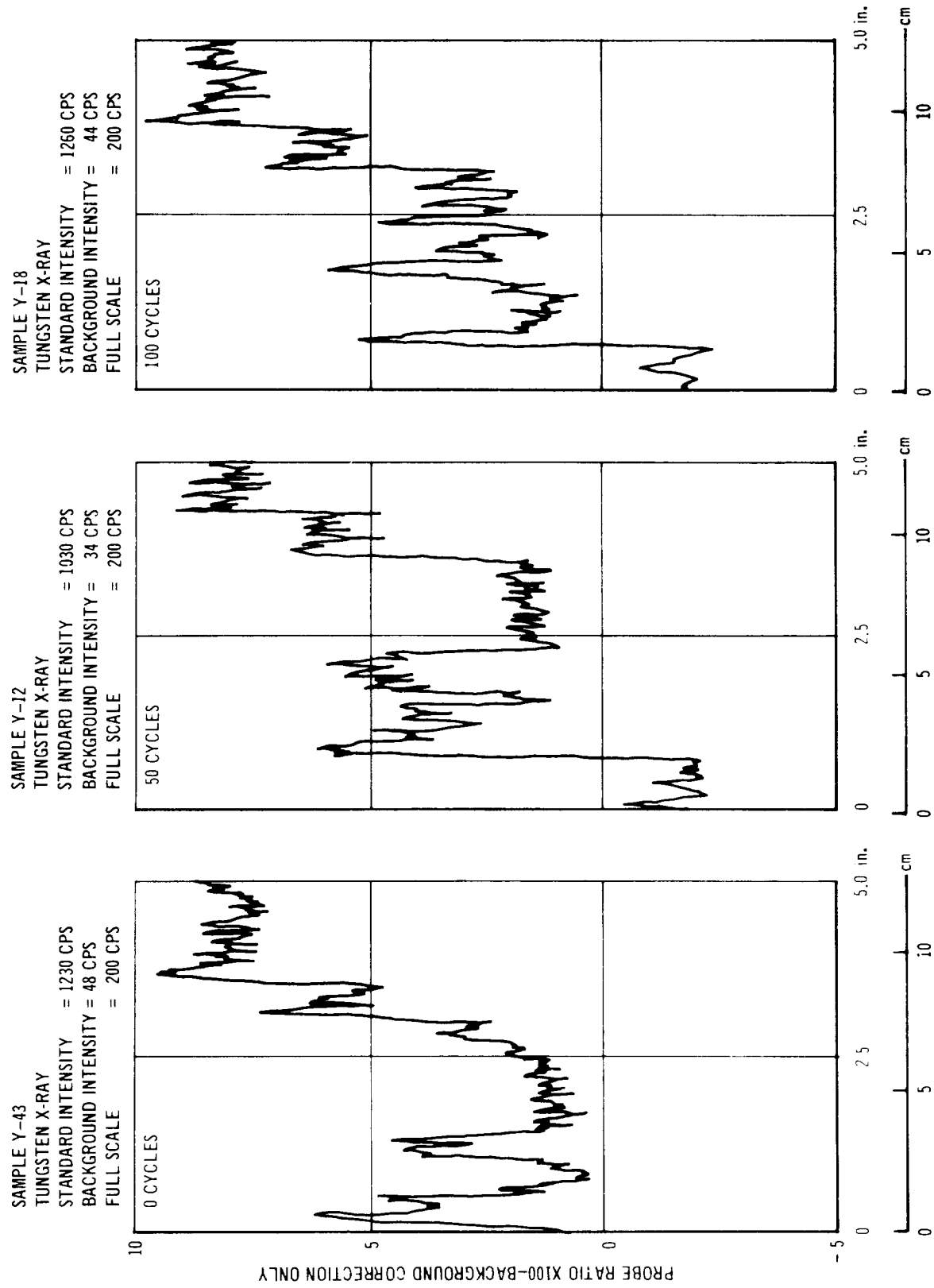
PHOTOMICROGRAPHS OF THE AREAS EXAMINED WITH THE  
ELECTRON MICROPROBE ON THE C-129Y/R-512E SYSTEM

FIGURE 3-26



EFFECT OF REENTRY CYCLING ON NIOBIUM DISTRIBUTION  
IN THE R-512E/C-129Y COATING SYSTEM

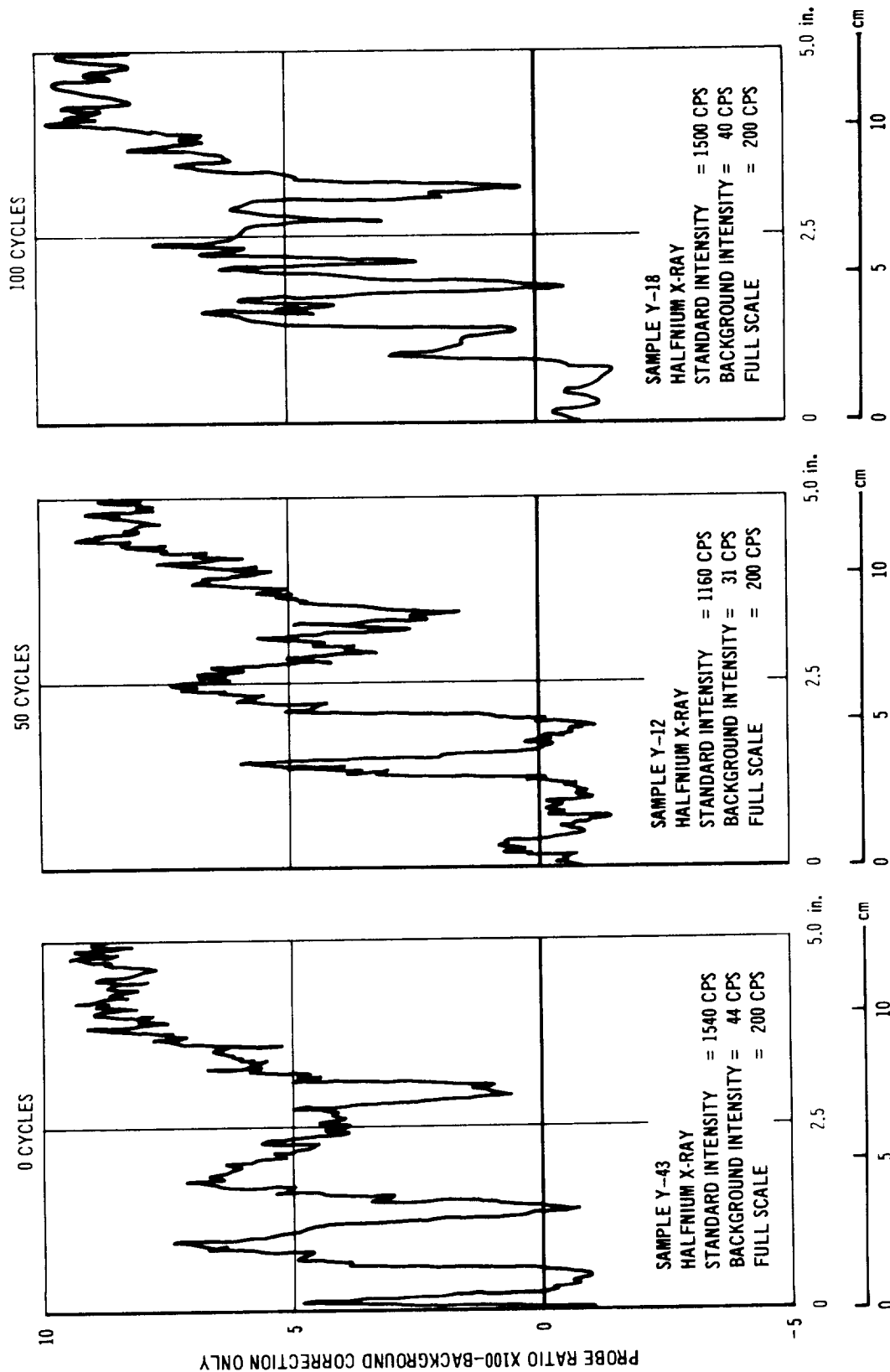
FIGURE 3-27



EFFECT OF REENTRY CYCLING ON TUNGSTEN DISTRIBUTION  
IN THE R-512E/C-129Y COATING SYSTEM

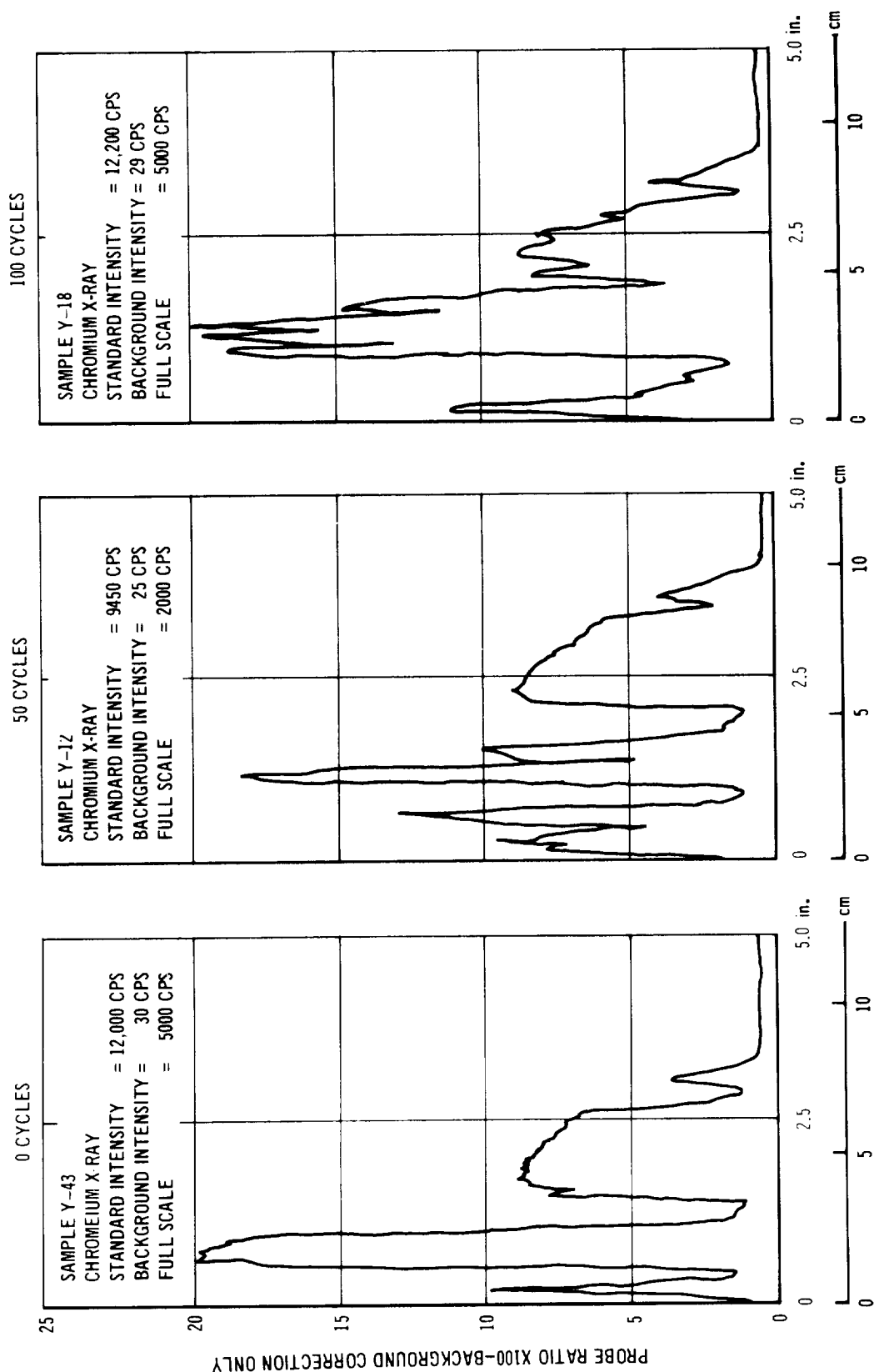
FIGURE 3-28





EFFECT OF REENTRY CYCLING ON HALFNIUM DISTRIBUTION  
IN THE R-512E/C-129Y COATING SYSTEM

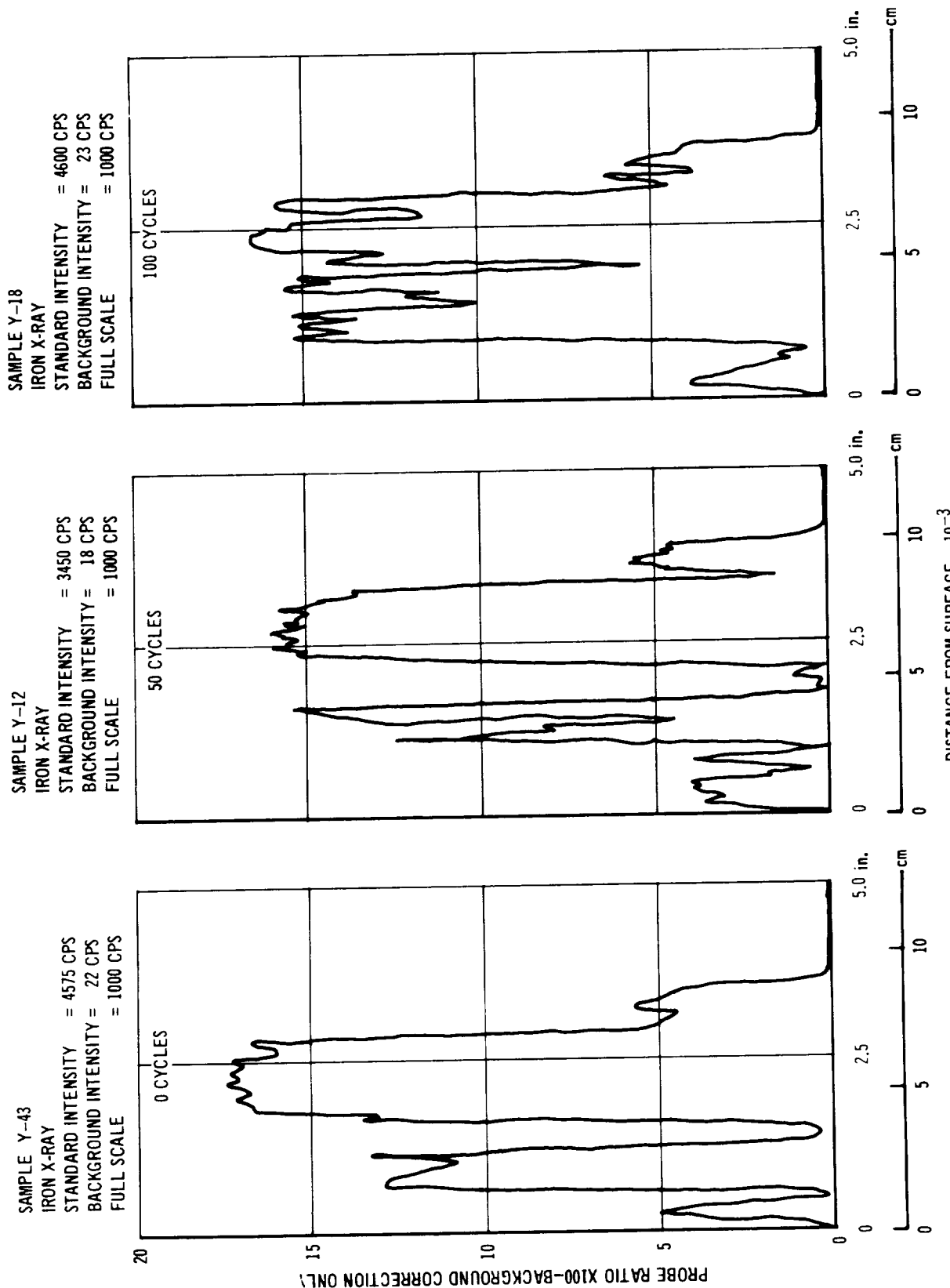
DISTANCE FROM SURFACE - 10<sup>-3</sup>



DISTANCE FROM SURFACE - 10<sup>-3</sup>

EFFECT OF REENTRY CYCLING ON CHROMIUM DISTRIBUTION  
IN THE R-512E/C-129Y COATING SYSTEM

FIGURE 3-30



EFFECT OF REENTRY CYCLING ON IRON DISTRIBUTION  
IN THE R-512E/C-129Y COATING SYSTEM

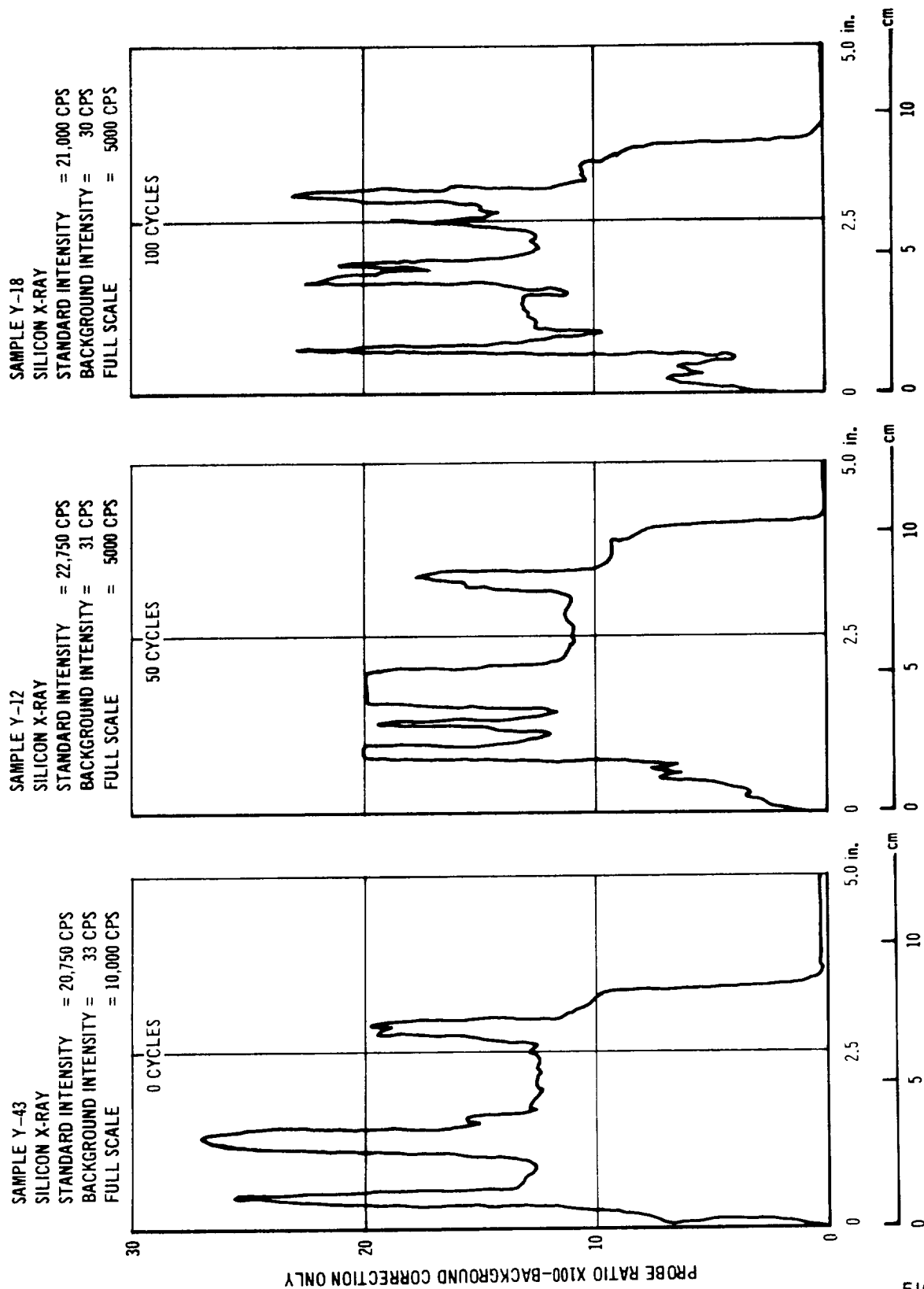
FIGURE 3-31

The silicon distribution was segregated with respect to coating zones, but did not dip below 10% in concentration (Figure 3-32). The silicon distribution did not shift much during cycling.

The major conclusion that can be drawn from the electron microprobe analysis is the excellent stability of the elements in the R-512E coated FS-85 with respect to reentry cycling. This coating/alloy combination should provide longer life because of this stability. The R-512E coating on Cb-752 showed the most shifting and moving of elements with respect to reentry cycling.

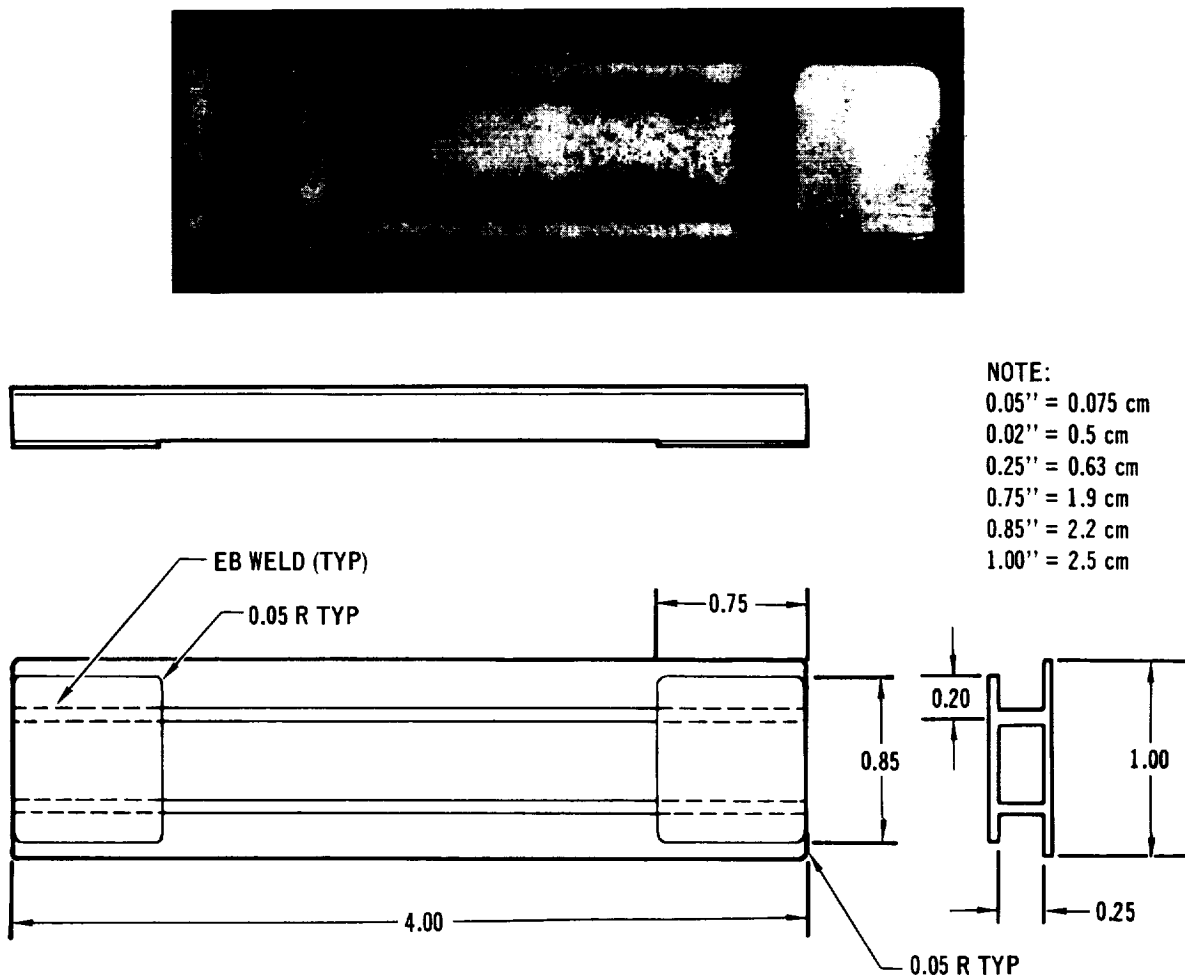
**3.3 Reuse Capability** - Test results from mechanical property studies, coating chemistry optimization studies, chemistry and structure studies, and emittance studies were reviewed to choose the three alloys most suitable for heat shield panel application. The three columbium alloys selected were FS-85, Cb-752, and C-129Y. These alloys coated with the R-512E coating were evaluated under Space Shuttle reentry conditions in the form of miniature, 1" x 4" (2.5 cm x 10 cm), rib stiffened heat shield panels to determine the alloy with the best reuse capability.

The miniature panel specimen selected was one employed in past coating evaluations (Reference 2) which fit into an existing test facility. The panel test specimen and loading fixture had to fit inside a 1-3/4" (4.4 cm) diameter tube, whose 6" (15 cm) long working hot zone permitted a uniform temperature in the central 4" (10 cm). The specimen was thus restricted to a 1 x 4 x 0.25" (2.5 x 10 x 0.635 cm) size. Figure 3-33 shows the rib stiffened panel configuration and dimensions. Five panels of each alloy (Cb-752, FS-85 and C-129Y) were fabricated. After detail parts preparation and chemical cleaning, the ribs were joined to the skins by blind electron beam welding through the skin. Finally, the loading plates were electron beam welded to each end of the ribs and the edges of the panel were radiused. The panels were coated with the R-512E coating by HiTemCo and subjected to temperature-pressure-stress profile conditions typical of those for a Space Shuttle reentry (see Figure 1-1). Temperature and pressure conditions were provided by a resistance heated tube furnace while stress on the panels was provided simultaneously from a scissors-type loading fixture. The profile simulation testing was conducted in the profile simulator shown in Figure 3-34. The load was applied to the panel specimens using a four point loading fixture fabricated from FS-85 alloy columbium and protected with the R-512E coating. The loading fixture and the bending moment distribution it produced are shown in Figure 3-35. The loading fixture containing the specimen was then positioned in



EFFECT OF REENTRY CYCLING ON SILICON DISTRIBUTION  
IN THE R-512E/C-129Y COATING SYSTEM

FIGURE 3-32



NOTES:

- (1) PANEL SKIN 0.008" (0.02 cm) AFTER COATING
- (2) PANEL RIBS 0.016" (0.04 cm) AFTER COATING
- (3) ALL DIMENSIONS ARE IN INCHES.

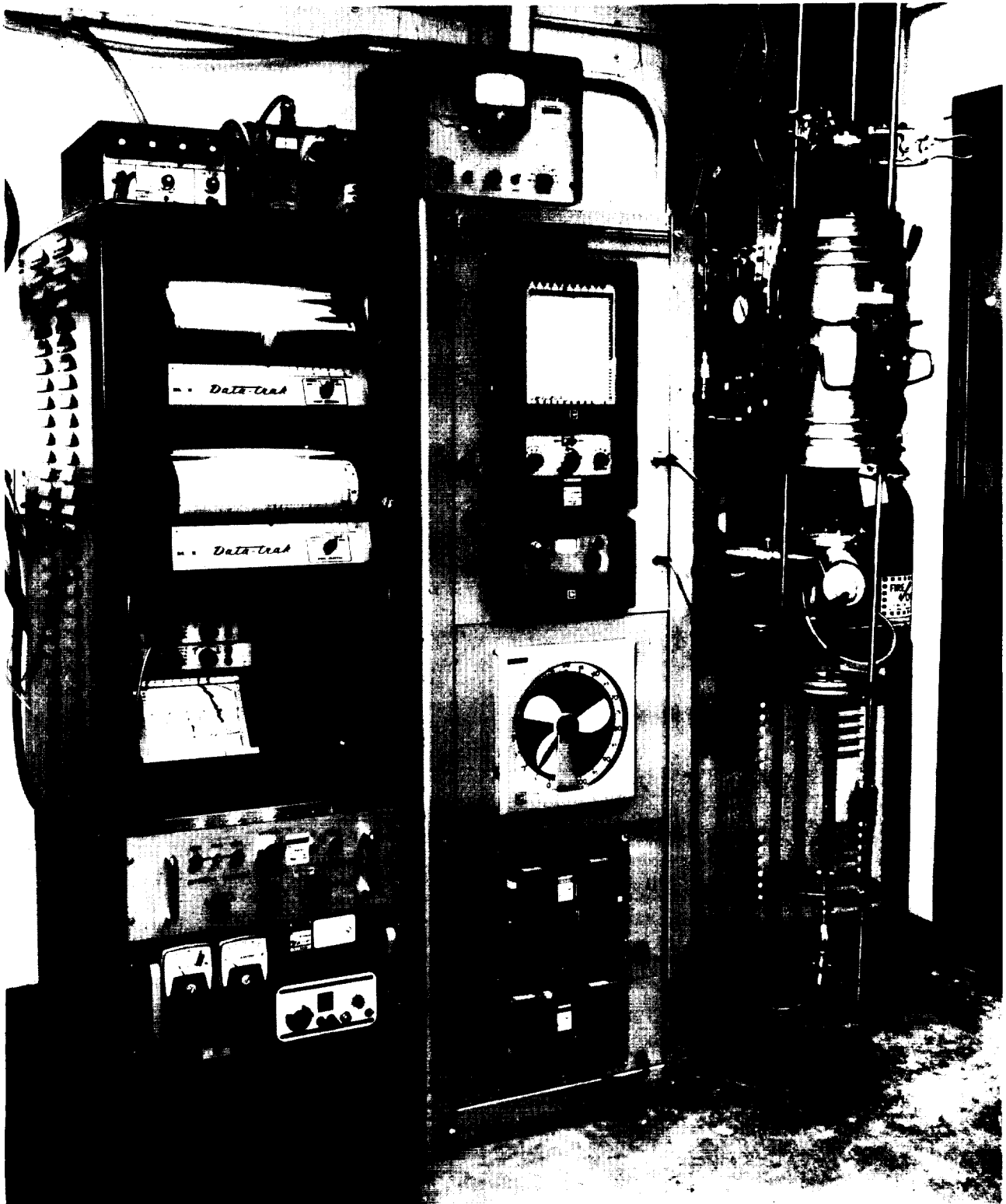
RIB STIFFENED PANEL SPECIMEN

457-1154

FIGURE 3-33

the furnace and secured to the loading drive mechanism. The boost load was applied and released, and the facility then automatically followed the time, temperature, pressure, and stress profile. After returning to approximately room temperature, the boost load was reapplied and the entire procedure repeated. After each 10 cycles, the panel was removed and visually examined to determine the extent of oxidation and to check for crack initiation. Creep deflection measurements were made after each 10 profile cycles.

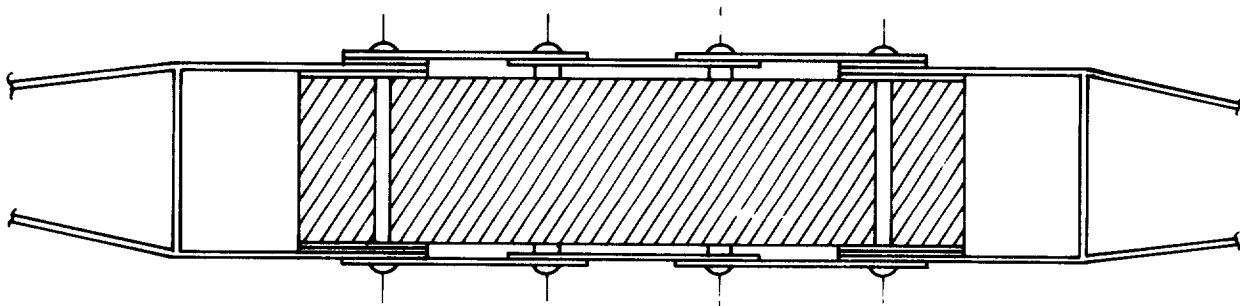
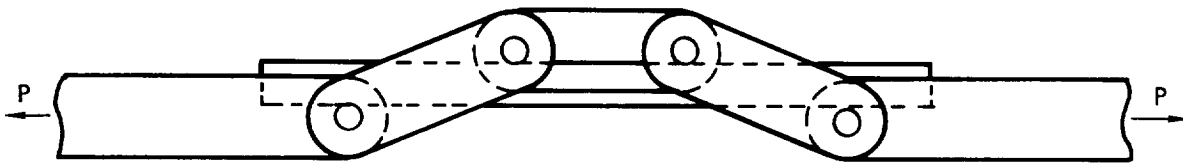
Five panels each of R-512E coated FS-85 and Cb-752 and four panels of C-129Y were tested. A summary of testing performed and results is presented in Table 3-8. A total of 1200 reentry cycles was performed. Seven panels were exposed for 100



PROFILE SIMULATION TEST FACILITY

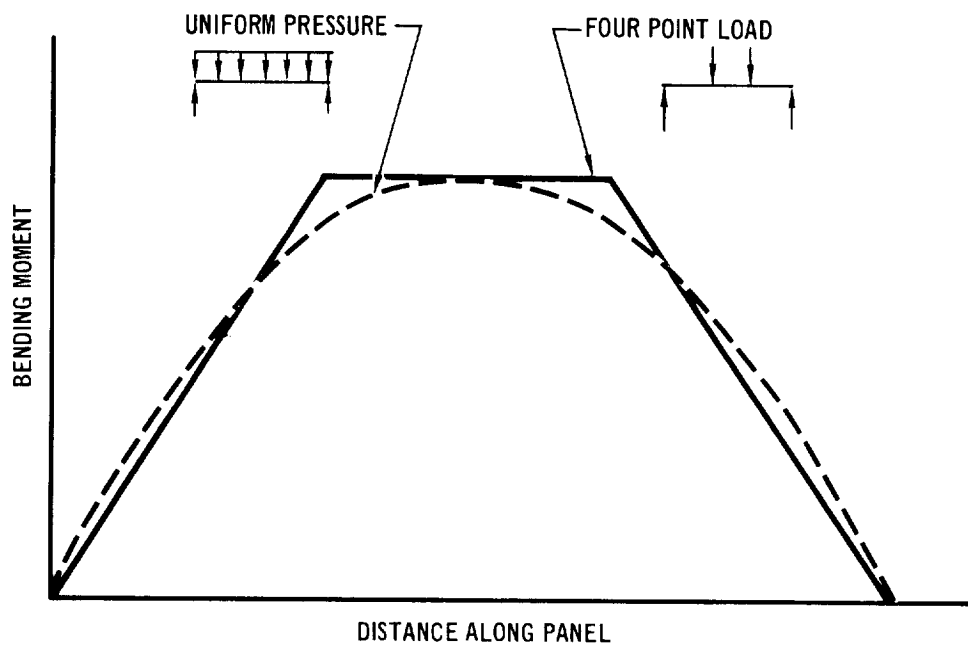
457-1201 A

FIGURE 3-34



457-1155

Four Point Loading Fixture



457-1156

Panel Bending Moment Distribution

PANEL LOADING DISTRIBUTION AND FIXTURE

FIGURE 3-35



TABLE 3-8

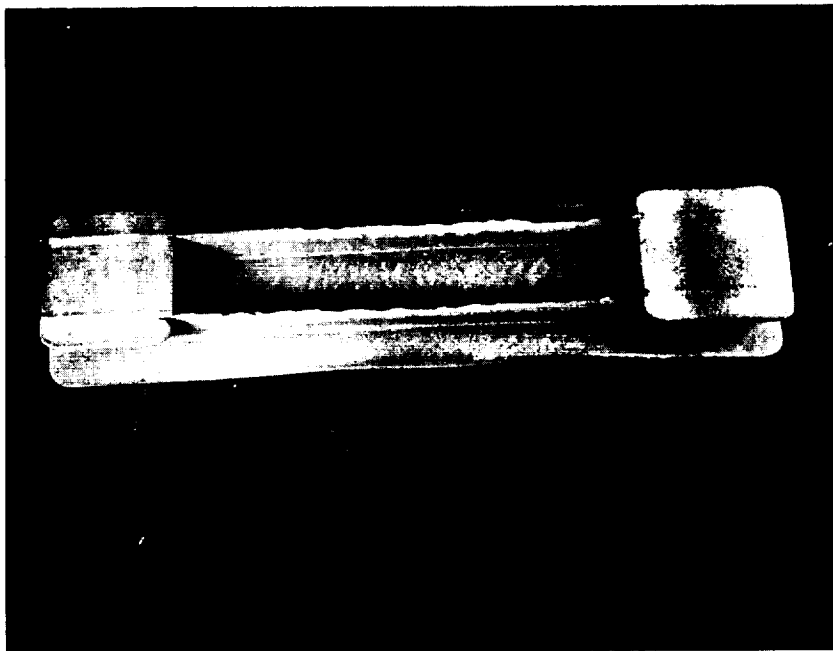
## MINIATURE RIB STIFFENED HEATSHIELD PANELS REUSE TESTING RESULTS

R-512E COATED ALLOY	ENVIRONMENTAL PRESSURE	NO. OF REENTRY CYCLES	AVERAGE CREEP DEFLECTION RATE		REMARKS
			(MILS/CYCLE)	( $\mu$ m)/CYCLE	
FS-85					
NO. 1	EXTERNAL	100	0.28	7.8	NO COATING FAILURES; SPECIMEN OVERLOADED ON 49TH CYCLE.
NO. 2	EXTERNAL	80	0.47	12	NO COATING FAILURE; COATING ACCIDENTLY DAMAGED ON RIBS AFTER 80 CYCLES, TESTING CON- TINUED, PANEL FAILED ON 2ND CYCLE.
NO. 3	EXTERNAL	59	0.47	12	NO COATING FAILURES; SPECIMEN OVERLOADED ON 18TH AND 59TH CYCLES, TESTING TERMINATED.
NO. 4	EXTERNAL	100	0.10	2.5	NO COATING FAILURES.
NO. 5	INTERNAL	100	0.11	2.8	NO COATING FAILURES.
AVERAGE: 0.29				8.4	
Cb-752					
NO. 1	EXTERNAL	100	0.90	23	NO COATING FAILURES; SPECIMEN OVERLOADED ON CYCLES 20 THRU 30.
NO. 2	EXTERNAL	80	0.40	10	NO COATING FAILURES; SPECIMEN OVER- LOADED ON 66TH CYCLE; REVERSE LOADED ON CYCLES 70 THRU 80; COATING DAMAGED ON RIBS DUE TO REVERSE LOADING, TEST- ING CONTINUED. PANEL FAILED ON 6TH CYCLE.
NO. 3	EXTERNAL	28	-	-	NO COATING FAILURES; SPECIMEN OVER- LOADED AND STRUCTURALLY FAILED ON 28TH CYCLE.
NO. 4	EXTERNAL	80	0.41	10.4	NO COATING FAILURES; FURNACE OVER- HEATED ON 85TH CYCLE, SPECIMEN DESTROYED.
NO. 5	INTERNAL	100	0.49	12.5	NO COATING FAILURES.
AVERAGE: 0.55				14	
C-129Y					
NO. 1	EXTERNAL	87	0.35	9	SKIN EDGE FAILURE AT 10 CYCLES. RIB EDGE FAILURES AT 40 CYCLES. NUMEROUS EDGE FAILURES AT 60 CYCLES. PANEL FRACTURED ASSENT LOADING 88TH CYCLE.
NO. 2	EXTERNAL	86	0.51	13	RIB EDGE FAILURE AT 20 CYCLES. NUMER- OUS EDGE FAILURES AT 40 CYCLES. PANEL FRACTURED ASSENT LOADING 87TH CYCLE.
NO. 3	EXTERNAL	100	0.34	8.6	RIB EDGE FAILURES AT 50 CYCLES. NUMER- OUS EDGE FAILURES AT 60 CYCLES.
NO. 4	INTERNAL	100	0.21	5.3	RIB EDGE FAILURES AT 60 CYCLES. NUMER- OUS RIB EDGE FAILURES AT 100 CYCLES.
AVERAGE: 0.35				9	

cycles each. Three of the seven 100 cycle panels were exposed in the internal pressure environment. The testing on five panels was terminated prior to reaching 100 cycles, due to equipment malfunctions and operational problems. The two remaining panels failed structurally after 87 cycles each in the external pressure environment. The structural failures were brought about by coating failures on the ribs. These two panels were of the C-129Y alloy. The extent of oxidation which was visually detectable is typified by the panel shown in Figure 3-36. This particular panel, made of C-129Y, survived 100 cycles structurally. The reason for the coating failures on the C-129Y panels is explained by a very thin coating on the rib edges. This is shown in Figure 3-37. Figures 3-38 and 3-39 show rib and skin edge coating thickness for the FS-85 and Cb-752 panels. The C-129Y skin edge thickness was examined to see if it had as thin a coating as the ribs did. As shown in Figure 3-37 it did not. The radius on the C-129Y ribs was not good, but this is not believed to be the full reason for the thin coating. Edge coverage during slurry dipping, which is inherently poor, was certainly a contributing factor. The manual overspraying of edges, particularly when the operator cannot be sure what has been sprayed and what has not been sprayed, creates a bad situation in trying to assure complete and uniform slurry coverage. The thin coating on the C-129Y ribs reveals dramatically one of the primary reasons this program sponsored work on slurry process optimization for full size heat shield panels. The problem of thin coating on edges was overcome by applying the slurry with a beading tool as discussed in Section 4.0.

However, the coating failures on the C-129Y panels did demonstrate that the occurrence of a coating failure does not mean immediate catastrophic structural failure. In this particular case the coating failures occurred in the most highly tension stressed area and a minimum of 50 reentry cycles after noticeable oxidation were required before structural integrity was affected. The panel area which experienced the highest tension stress was almost always located on the side of the panel which, during reentry, is exposed to low oxygen pressures. A C-129Y panel was tested in an internal pressure environment and survived 100 cycles of testing although coating failures showed up on the ribs after 60 cycles of exposure. This demonstrated that substandard coating can be tolerated on critically stressed areas in internal pressure environments and not prevent 100 flight reuse.

Panel creep deflection rates were determined from the portions of the testing of each panel which were not affected by overloading, operator error, or coating



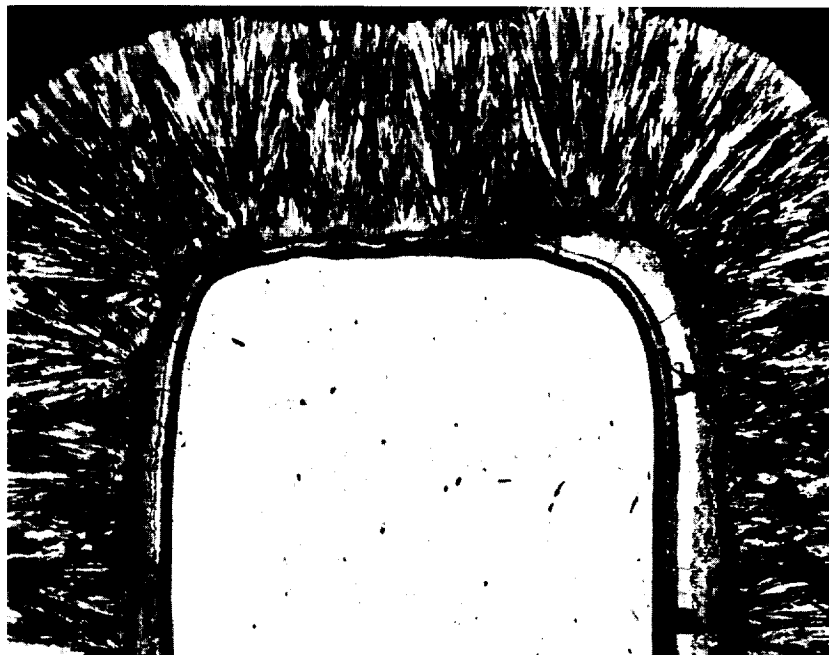
R-512E COATED C-129Y RIB STIFFENED HEAT SHIELD PANEL  
AFTER 100 SIMULATED SHUTTLE REENTRIES (EXTERNAL PRESSURE)

FIGURE 3-36

failures. The FS-85 exhibited the lowest average creep deflection rate of 0.29 mil (7.4  $\mu\text{m}$ )/cycle, the C-129Y second at 0.35 mil (8.9  $\mu\text{m}$ )/cycle, and the Cb-752 third at 0.55 mil (14.0  $\mu\text{m}$ )/cycle. Using the standard beam equation for the panel loading and the standard beam stress formula ( $\frac{Mc}{I}$ ) a strain-deflection equation was derived. Assuming uniform loading, which is valid since the 4 point loading fixture does a good job of duplicating uniform loading as was shown in Figure 3-35, the panel deflections for 100 cycles of exposure represent 0.57% creep for the FS-85, 0.68% for the C-129Y, and 1.07% for the Cb-752. Literature sources were not available for a direct comparison, but these creep percentages appear reasonable.

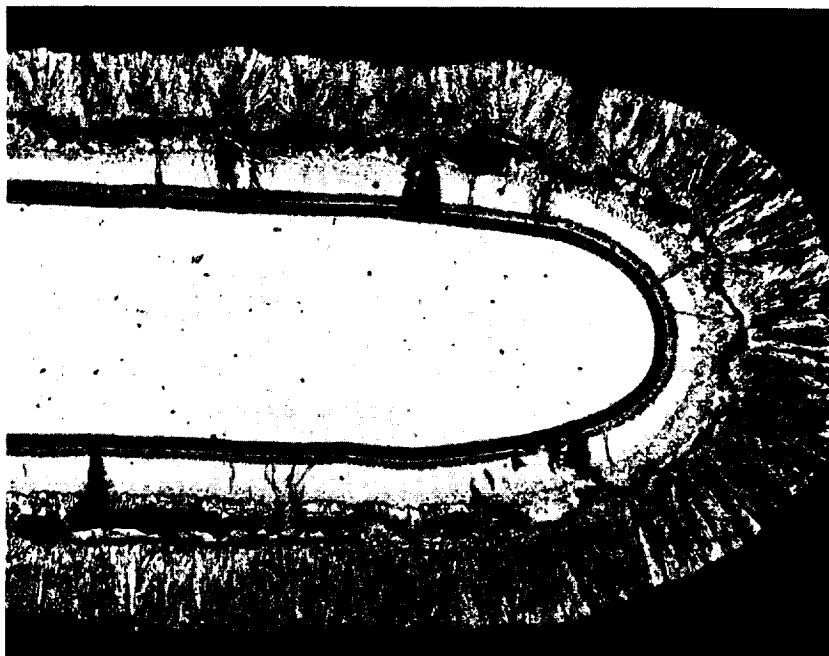
As with the tensile specimens, two nondestructive coating thickness measurement techniques were employed to determine and monitor coating thickness during cyclic reentry exposure of coated tensile and heat shield panel specimens. A thermoelectric device was used to determine coating thicknesses on edges in the "as coated" condition. The Dermatron eddy current device was used for surface thickness measurements before and after testing.

Table 3-9 presents a breakdown of the NDT data accumulated on the R-512E/C-129Y, R-512E/Cb-752, and R-512E/FS-85 rib stiffened heat shield panels before and



RIB CROSS-SECTION

150X

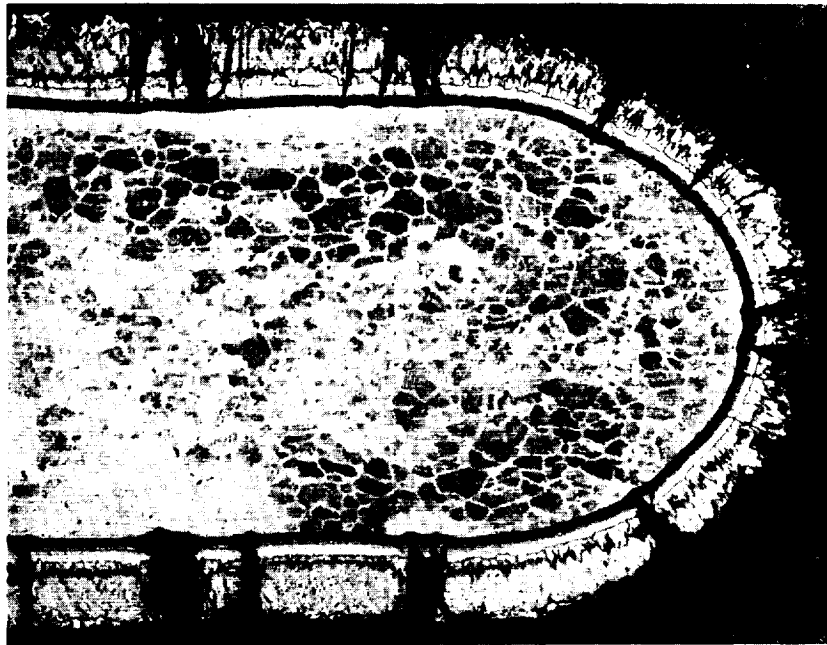


SKIN CROSS-SECTION

150X

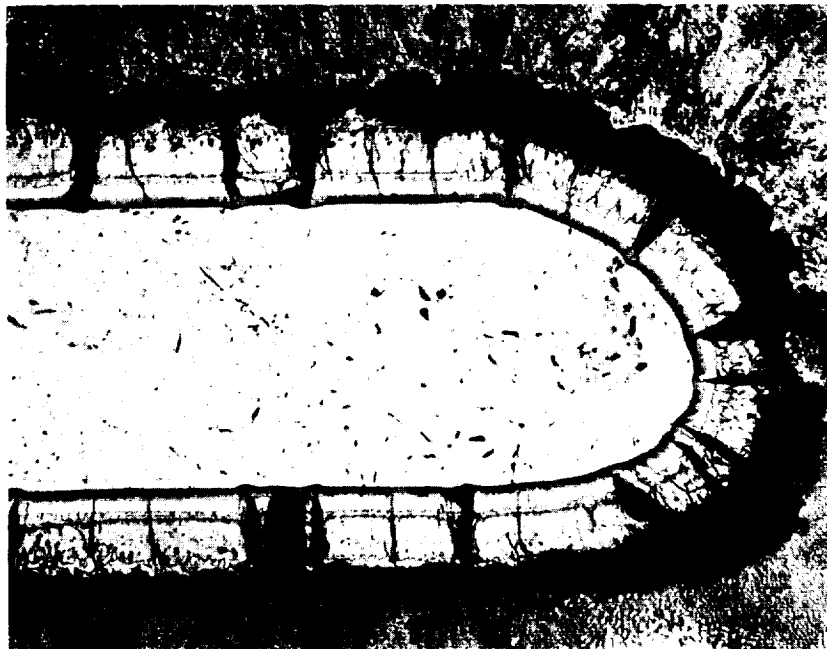
RIB AND SKIN CROSS-SECTIONS OF AN R-512E COATED C-129Y  
MINIATURE HEAT SHIELD PANEL IN THE AS COATED CONDITION

FIGURE 3-37



RIB CROSS-SECTION

150X

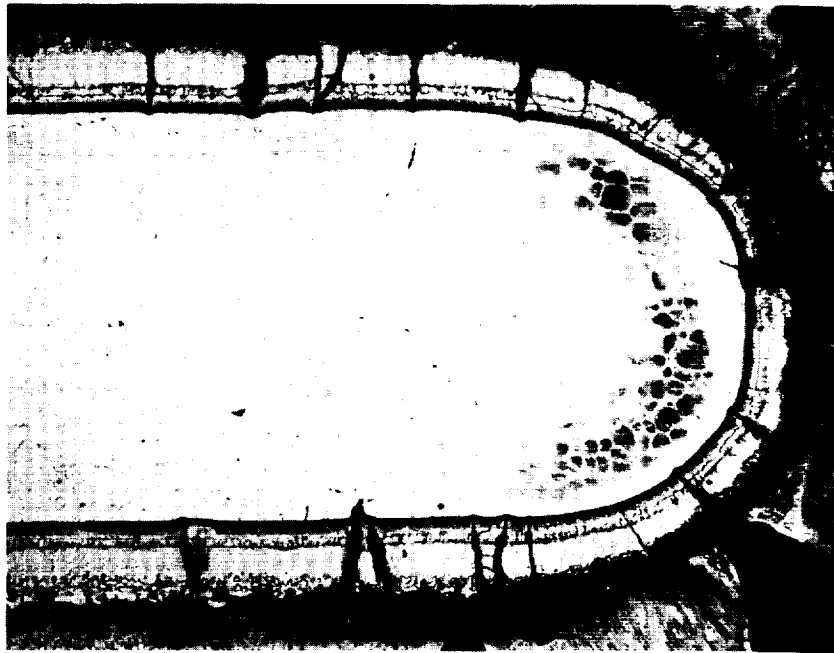


SKIN CROSS-SECTION

150X

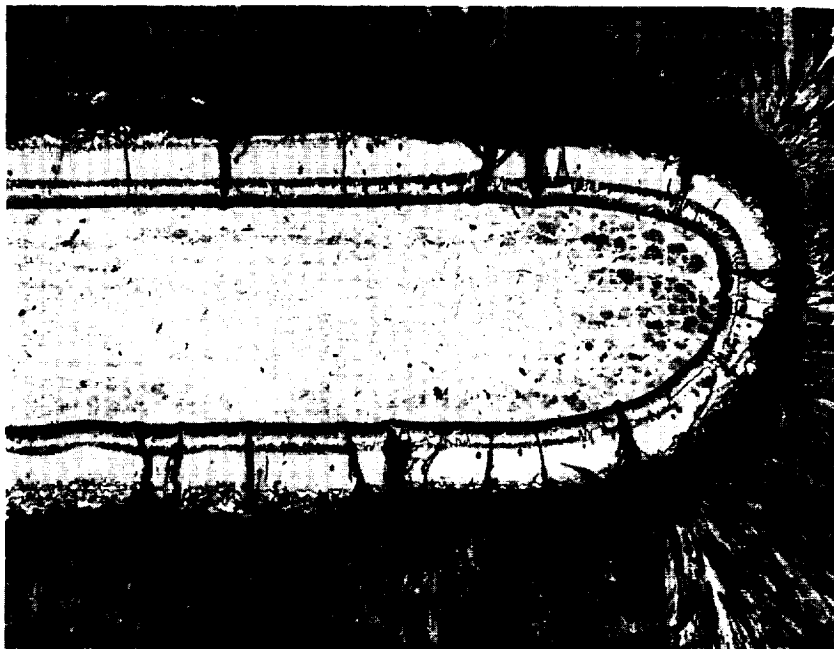
RIB AND SKIN CROSS-SECTIONS OF AN R-512E COATED FS-85 MINIATURE  
HEAT SHIELD PANEL AFTER 80 REENTRY EXPOSURES (EXT. PRESSURE)

FIGURE 3-38



RIB CROSS-SECTION

150X



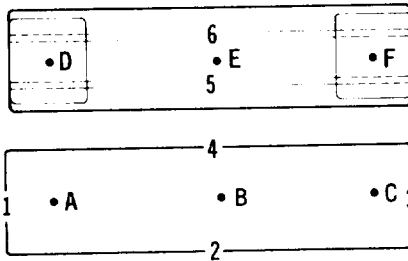
SKIN CROSS-SECTION

150X

RIB AND SKIN CROSS-SECTIONS OF AN R-512E COATED Cb-752  
MINIATURE HEAT SHIELD PANEL AFTER 28 REENTRY EXPOSURES (EXT. PRESSURE)

FIGURE 3-39

TABLE 3-9  
TYPICAL NDT COATING THICKNESS ON R-512E COATED RIB STIFFENED PANELS



\* THICKNESS CONVERSIONS TO METERS

1.0 MILS = 25  $\mu$ m  
2.0 MILS = 50  $\mu$ m  
3.0 MILS = 75  $\mu$ m  
4.0 MILS = 100  $\mu$ m  
5.0 MILS = 125  $\mu$ m  
6.0 MILS = 150  $\mu$ m  
7.0 MILS = 175  $\mu$ m

ALLOY/ COATING	NDT DEVICE	LOCATION	AS COATED THICKNESS (MILS)*			CHANGE FROM AS COATED THICKNESS (MILS/SIDE)* DUE TO CYCLING			
			LO	AVG	HI	INTERNAL PRESSURE		EXTERNAL PRESSURE	
						50 CYCLES	100 CYCLES	50 CYCLES	100 CYCLES
FS-85/R-512E	DERMITRON	A	3.7	4.0	4.1	-0.3	-0.2	+0.9	+2.2
		B	3.9	4.0	4.5	-0.1	-0.4	+1.1	+1.8
		C	4.2	4.2	4.3	+0.1	0	+0.7	+1.8
		D	3.1	3.6	3.8	+0.2	-0.1	+0.8	+1.4
		E	3.7	3.8	3.8	0	-0.3	+1.4	+2.0
		F	3.1	3.5	3.8	-0.1	-0.3	+1.3	+1.5
	THERMOELECTRIC	1	4.5	5.3	6.2	-	-	-	-
		2	3.2	3.5	3.9	-	-	-	-
		3	4.0	5.1	5.2	-	-	-	-
		4	3.1	3.6	4.0	-	-	-	-
		5	3.6	4.0	5.7	-	-	-	-
		6	3.6	4.0	5.2	-	-	-	-
C-129Y/R-512E	DERMITRON	A	3.1	3.2	3.5	0	-0.2	+1.5	+2.6
		B	2.7	3.0	3.7	-0.1	-0.2	+0.8	+1.7
		C	3.1	3.2	3.7	-0.3	-0.3	+0.9	+1.9
		D	2.4	2.5	2.5	+0.1	0	+1.0	+1.2
		E	2.8	3.0	3.7	0	-0.1	+0.6	+1.9
		F	2.5	2.7	3.2	-0.2	-0.3	+1.1	+1.5
	THERMOELECTRIC	1	5.6	6.0	7+	-	-	-	-
		2	6.1	6.5	6.8	-	-	-	-
		3	6.0	6.2	7+	-	-	-	-
		4	4.8	5.5	6.8	-	-	-	-
		5	2.7	3.2	5.0	-	-	-	-
		6	2.7	3.3	4.8	-	-	-	-
Cb-752/R-512E	DERMITRON	A	3.7	4.0	4.2	-0.1	-0.5	+0.9	+1.8
		B	3.7	3.8	4.0	-0.5	-0.8	+1.4	+2.4
		C	3.7	3.8	3.8	0	-0.1	+1.3	+2.5
		D	3.5	3.6	3.7	+0.2	+0.1	+1.0	+1.1
		E	3.1	3.3	3.5	-0.1	-0.4	+1.0	+1.7
		F	3.1	3.4	3.5	-0.1	-0.2	+0.9	+1.3
	THERMOELECTRIC	1	1.6	2.2	2.9	-	-	-	-
		2	0.4	0.7	1.2	-	-	-	-
		3	1.1	1.9	2.5	-	-	-	-
		4	0.2	0.8	2.6	-	-	-	-
		5	0.5	0.9	1.8	-	-	-	-
		6	0.6	0.9	1.5	-	-	-	-

after cycling. Nondestructive coating thickness measurements made on the miniature rib stiffened heat shield panels before cycling showed a much better coating thickness uniformity from end to end than that shown on the tensile specimens. Thin coating was detected by the thermoelectric device on the rib edges of the R-512E coated Cb-752 panels. However, no coating failures developed after exposure to 100 reentry cycles and later metallographic examination showed the coating was not thin. Reentry cycling caused failures and metallographic examination showed the R-512E/C-129Y panels to have thin (0.5 to 1.0 mil (12.5 to 25  $\mu\text{m}$ )) coatings on the ribs. Yet, the thermoelectric readings were not low, but there was a large relative difference between the rib and skin coating thicknesses with the rib coating thickness being about half that of the skin. These types of discrepancies were somewhat expected and caused a lack of confidence in the thermoelectric device for thickness measurement. Still another example is the 7+ mils (175  $\mu\text{m}$ ) of coating registered by the thermoelectric device when metallographic examination showed only 3.5 mils (89  $\mu\text{m}$ ) of coating.

The change in coating thickness as detected by NDT due to reentry cycling fell in line with those shown for the tensile specimens. There appears to be a slowdown in coating thickness loss after 50 reentry cycles in the internal pressure environment. Data did not permit a correlation to be made between coating thickness and coating life, as there were no wearout failures, nor were they expected at 100 cycles.

It was considered impossible to make a selection of the best columbium alloy based only on the results of the miniature heat shield panel testing. Therefore, the results of all screening tests were reviewed. After long and careful consideration, the FS-85 alloy was selected for the coating/alloy evaluations to be performed in subsequent tasks. The reuse performance differences between FS-85, C-129Y, and Cb-752 were relatively minor. Other considerations, such as alloy manufacturing, sensitivity to processing, and creep strength had to be considered for alloy selection to be made.



4.0 COATING PROCESS OPTIMIZATION AND SCALE-UP STUDIES FOR RIB STIFFENED HEAT SHIELD PANELS

4.1 Process Development - The objective of this study was to optimize coating slurries, using a lacquer and an acrylic based vehicle, so that full size 20" x 20" (50 cm x 50 cm) heat shield panels could be coated uniformly and reproducibly. The same basic R-512E, Si-20Cr-20Fe, metal powder composition was used throughout the program. Various additives were made to the slurries to give them thixotropic properties, primarily to promote suspension of the metal particles and also to prevent caking when settling occurs after long periods of nonuse. Materials used and the sources of supply are listed in Table 4-1.

TABLE 4-1  
MATERIALS USED FOR SLURRY PREPARATION

MATERIAL IDENTIFICATION	SUPPLIER
1. L-18 LACQUER	RAFFE AND SWANSON
2. B-66 ACRYLIC	ROHN AND HAAS
3. MPA 60	BAKER CHEMICAL CO.
4. THIXATROL ST	BAKER CHEMICAL CO
5. HIGH FLASH NAPHTHA (HFN)	HOGAN CHEMICAL
6. LACQUER THINNER (LT)	HOGAN CHEMICAL
7. XYLENE	HOGAN CHEMICAL
8. SILICON POWDER (-325)	UNION CARBIDE
9. CHROMIUM POWDER (ELCHROME)	UNION CARBIDE
10. IRON POWDER (K291)	GLIDDEN COMPANY

The L-18 nitrocellulose lacquer has been used as the basic vehicle for the R-512E slurry coating system since its inception; it was adopted because it is a low residue material with good "green" strength and it has a history of practical use in glass-to-metal seals and other applications at HiTemCo.

During a previous scale-up program (Reference 3) with Sn-Al slurry coatings for tantalum alloys and early work (Reference 4) with the R512 system coatings, certain qualitative relationships were established between slurry properties and coating deposition rate and uniformity. In dip-coating, slurry viscosity and withdrawal rates were found proportional to coating thickness. Viscosity could be increased by thixotropic additives or by increased metal powder ratios and decreased by increasing ambient temperatures.

It was found in general that withdrawal rates of approximately 1.0-6.0 in/min

(0.40-2.4 mm/sec) were most practical. Also, temperatures above 80°F (27°C) drastically decreased the stabilizing effect on thixotropic additives. Accordingly, these findings and experience were used as a guide in the present program.

4.1.1 Screening Slurry Compositions - In the primary stages of screening different slurry formulations, the slurries were made up in one-quart Mason jars. Batches of metal powders were made up separately and blended for 1-2 hours (36-72 h sec). The vehicle and additives were sheared together and then the metal powder mix sheared in. After cooldown, more vehicle (plus thinner) was mixed in by stirring in order to adjust the viscosity to some reasonable level.

Dip coating experiments were initially carried out using 0.017" (0.04 cm) thick x 1" (2.5 cm) x 6" (12.2 cm) stainless steel strips. These were grit blasted with G120 steel grit at 20-30 psi (138-207 kN/m<sup>2</sup>). The dip tanks were aluminum cylinders approximately 2" dia. x 8" (5 cm dia. x 20 cm) high. Later more definitive experiments were carried out with larger slurry quantities contained in steel cylinders approximately 3" dia. x 23" (7.5 cm dia. x 58 cm) high. Stainless steel strips 0.012" (0.03 cm) thick x 2" x 20" (5 cm x 50 cm) were used for these dipping tests.

Tables 4-2 and 4-3 list the slurry compositions screened and some of the typical dipping data obtained. Altogether 32 slurries were investigated. The results were evaluated on the basis of dipping and drying rates, coating thickness, coating uniformity top to bottom, streaking, sagging, and edge pull back.

An attempt was made to keep the amount of vehicle constant and to vary the thinners, control additives, and amount of metal powder. No attempt was made to control the ambient temperature. Dipping rates were varied somewhat in attempts to approximate the coating thickness desired. The objective was a weight of 22-24 mg/cm<sup>2</sup> at a rate of 1-4 in/min (0.4-1.7 mm/sec).

In general the acrylic base "A" slurries gave poor results until compositions utilizing 14 v/o LT (Lacquer Thinner) - 85 v/o HFN (High Flash Naphtha) were used. At higher HFN concentrations the coatings were slow drying and rather nonuniform top to bottom. The acrylic "B" slurries in general had higher LT contents but overlapped the "A" slurries somewhat in composition. These compositions were very fast drying and the coatings were not uniform or reproducible.

Four additional acrylic based slurries, designated "X," utilizing xylene as a thinner were also prepared and evaluated. However, these gave coatings slightly inferior to the better "A" compositions A-15, A-16, and A-17. Accordingly, the

TABLE 4-2  
ACRYLIC BASE SCREENING SURRIES

A. VEHICLE IS HFN PLUS 8 V/O B-66 ACRYLIC

SLURRY NO.	AMT. OF VEHICLE (CC)	MPA WT (g)	THIXATROL WT. (g)	POWDER WT (g) R512E	VISCOSITY $CP \times 10^2$ (Nsec/cm <sup>2</sup> )	AMBIENT TEMP °F (°C)	DIPPING SPEED IN MIN (mm/sec)	COATING WT. mg/cm <sup>2</sup>
A-1	200	20	0	500	36 (3.6)	80 (27)	1 (0.4)	23.5
A-2	400	20	0	600	9 (0.9)	85 (29)	2.5 (1.0)	9.0
A-3	200	0	0	500	26 (2.6)	78 (26)	1 (0.4)	19.8
A-4	200	10	0	500	14 (1.4)	76 (24)	4.5 (1.8)	12
A-5	200	10	0	600	24 (2.4)	80 (27)	6 (2.4)	17
A-6	200	10	5	600	35 (3.5)	78 (26)	6 (2.4)	32
A-7	300	10	5	600	18 (1.8)	74 (23)	8 (3.2)	16
A-8	200	16	0.25	500	16 (1.6)	78 (26)	6 (2.4)	15
A-9	200	16	0.75	500	28 (2.8)	74 (23)	4 (1.6)	25
A-10	200	16	0.75	550	37 (3.7)	74 (23)	6 (2.4)	13

B. VEHICLE IS HFN + LACQUER THINNER + 8V/O B-66 ACRYLIC

A-11	200 (50% HFN)	7.5	0	530	24 (2.4)	76 (24)	5 (2.0)	20
A-12	200 (50% HFN)	7.5	0	630	26 (2.6)	75 (24)	4 (1.6)	21
A-13	200 (60% HFN)	7	0.3	600	24 (2.4)	79 (26)	3 (1.6)	19.4
A-14	200 (60% HFN)	7	0.5	700	20 (2.0)	74 (23)	6 (2.4)	22
A-15	200 (85% HFN)	7	0.4	600	15 (1.5)	74 (23)	5 (2.0)	18
A-16	200 (85% HFN)	7	0.6	600	27 (2.7)	73 (23)	7 (2.8)	24
A-17	200 (85% HFN)	9	0.4	600	24 (2.4)	70 (21)	4 (1.6)	17
B-1	200 (100% LT)	20	0	500	19 (1.9)	80 (27)	(0.4)	21
B-2	400 (100% LT)	20	0	600	15 (1.5)	78 (26)	2.5 (1.0)	25
B-3	200 (100% LT)	5	0	500	17 (1.7)	76 (24)	2.5 (1.0)	15
B-4	220 (100% LT)	5	0	560	14 (1.4)	80 (27)	6 (2.4)	22
B-5	200 (50% HFN)	7.5	0	600	30 (3.0)	78 (26)	4 (1.6)	24
B-6	200 (50% HFN)	7.5	1.0	600	23 (2.3)	79 (26)	6 (2.4)	20

C. VEHICLE IS XYLENE + 8 V/O B-66 ACRYLIC

X-1	200	7	0	600	26 (2.6)	76 (24)	7 (2.8)	22
X-2	200	7	0	650	25 (2.5)	74 (23)	6 (2.4)	20
X-3	200	7	0.4	650	24 (2.4)	76 (24)	6 (2.4)	18
X-4	200 (50% HFN)	7	0.4	600	23 (2.3)	74 (23)	4 (1.6)	20

TABLE 4-3  
NITROCELLULOSE (L-18) LACQUER SLURRIES

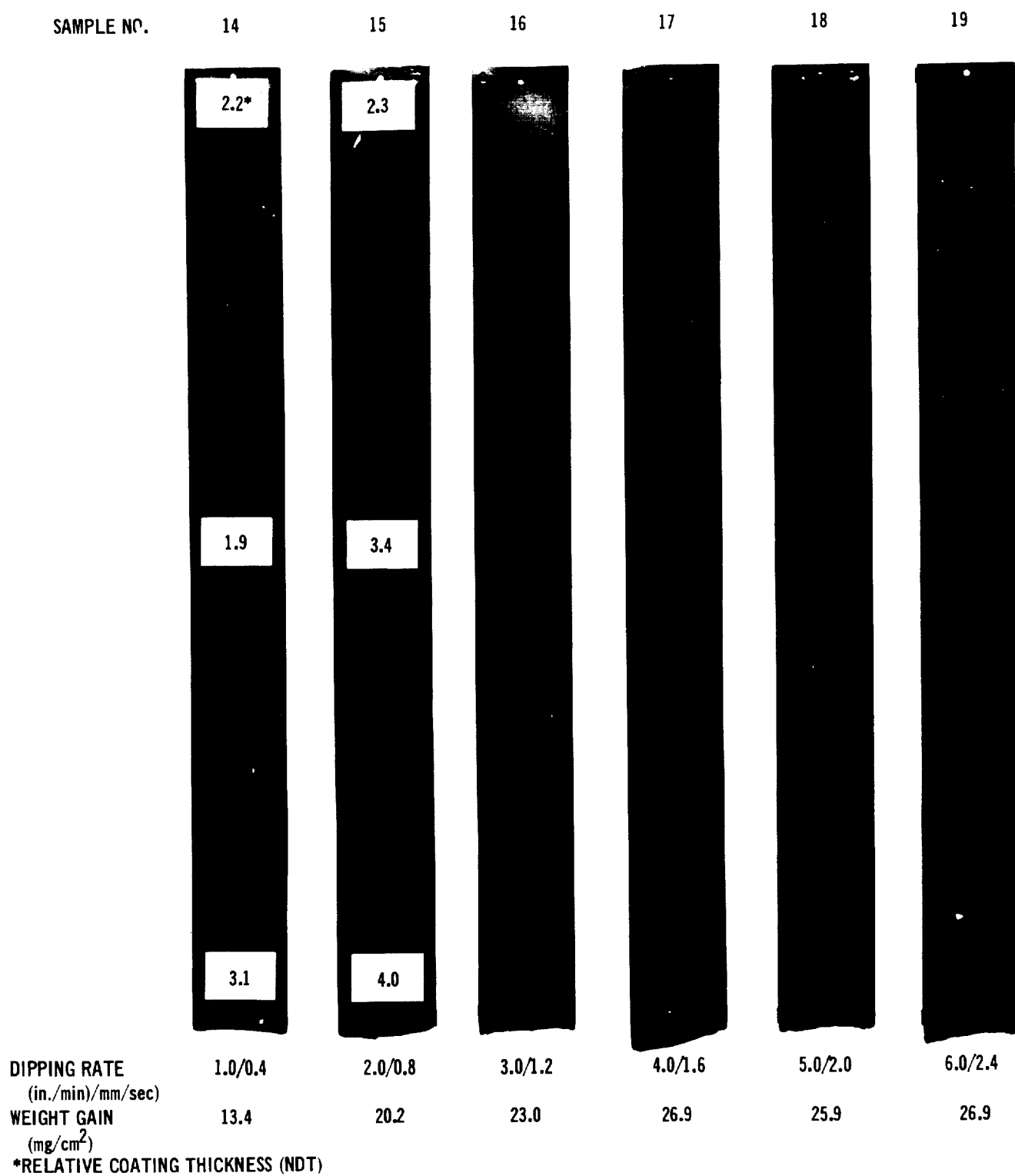
SLURRY NO.	AMT OF VEHICLE (g)	MPA WT (g)	THIXOTROL WT (g)	POWDER R512 WT (g)	VISCOSITY $CP \times 10^2$ (Nsec m <sup>-2</sup> )	AMBIANT TEMP, °F (°C)	DIPPING SPEED IN/MIN (mm/sec)	COATING WT. mg/cm <sup>2</sup>
C-1	200	16	0.25	500	15 (1.5)	79 (26)	4 (1.6)	18.5
C-2	200	16	0.75	500	13 (1.3)	73 (23)	6 (2.4)	16.5
C-3	200	16	0.75	600	20 (2.0)	75 (24)	0.75 (0.3)	18
C-4	200	16	0	600	18 (1.8)	74 (23)	2 (0.8)	20.1
C-5	200	16	1.0	600	21 (2.1)	73 (23)	2 (0.8)	21.1

three "A" coatings were selected for further study on longer test strips. It should be noted that, in general, smaller amounts of MPA 60 than used in the past with lacquer slurries, in conjunction with even smaller amounts of a second control additive, Thixatrol, appeared more effective in giving smoother, more uniform coatings with the acrylic based vehicle.

The lacquer vehicle or "C" slurries, shown in Table 4-3, were more closely related in composition to a known practical system, and they were more consistent and satisfactory in their behavior. Slurry C-4 is the composition used for coating most of the test samples used in this program. The other "C" slurries were variations based on use of a second additive, Thixatrol, in addition to the standard amount of MPA 60. Slurries C-3, C-4, and C-5 were selected for further study.

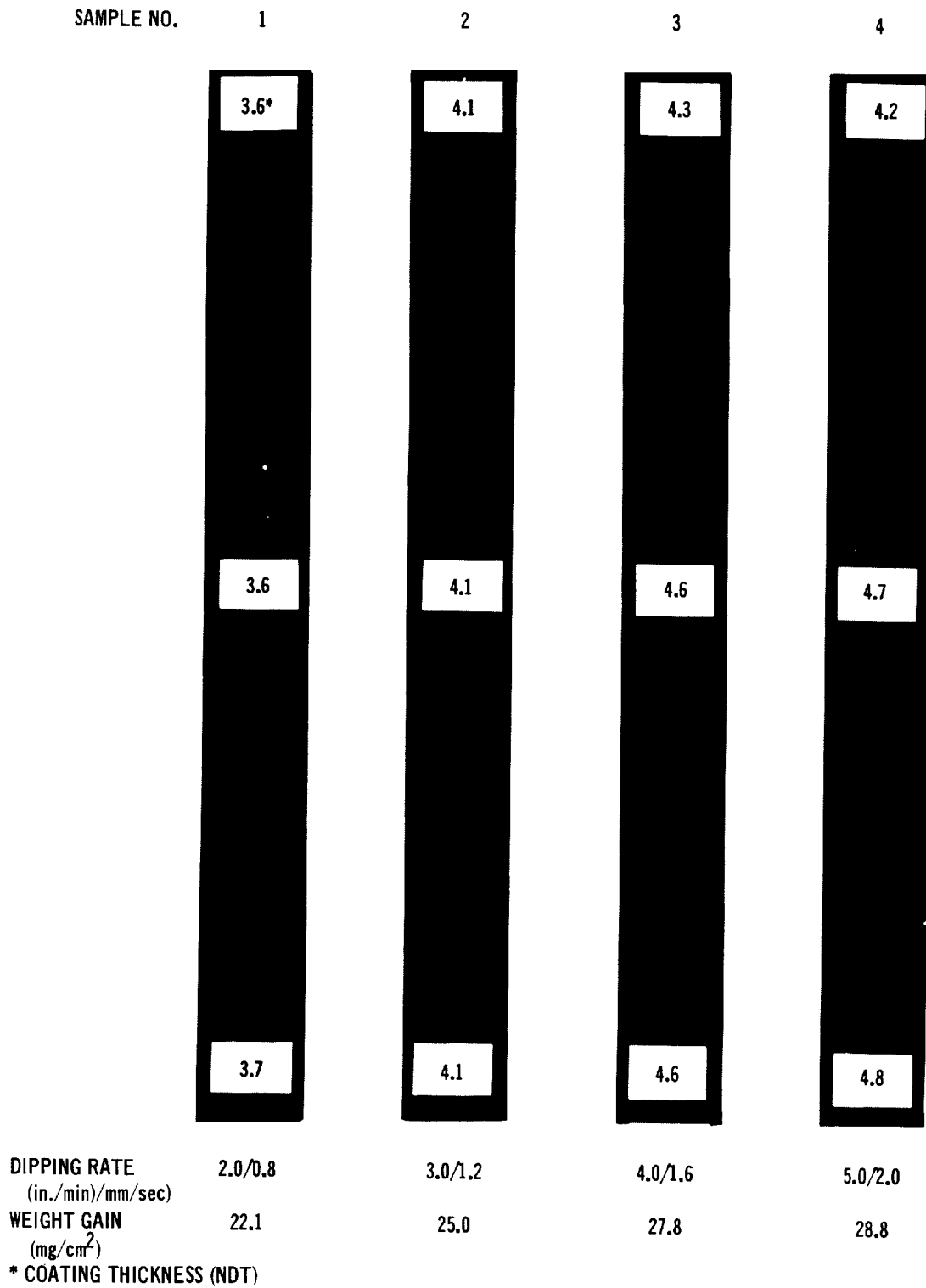
Some early qualitative comparisons could be made between the acrylic and lacquer based vehicle systems. In general the acrylic based system offered higher green strength, faster dipping rates, and apparently was less subject to edge pullback. Sufficient quantities of the six compositions selected (C-3, C-4, C-5, A-15, A-16, and A-17) from both systems were prepared to allow coating of 2" x 20" (5 cm x 50 cm) strips prior to selection of the slurries for full size scale-up.

Dipping studies were made on all six slurries and the coating uniformity was studied as a function of withdrawal rate. The results for three of these slurries are shown in Figures 4-1, 4-2 and 4-3. Coating thicknesses shown are relative measurements made with a Dermatron. The C-4 slurry is shown to produce uniform coatings at low coating thickness, and with increasing thickness, significant tapering of the coating takes place. At higher withdrawal rates the coating sags. The addition of a second viscosity control additive significantly increased the



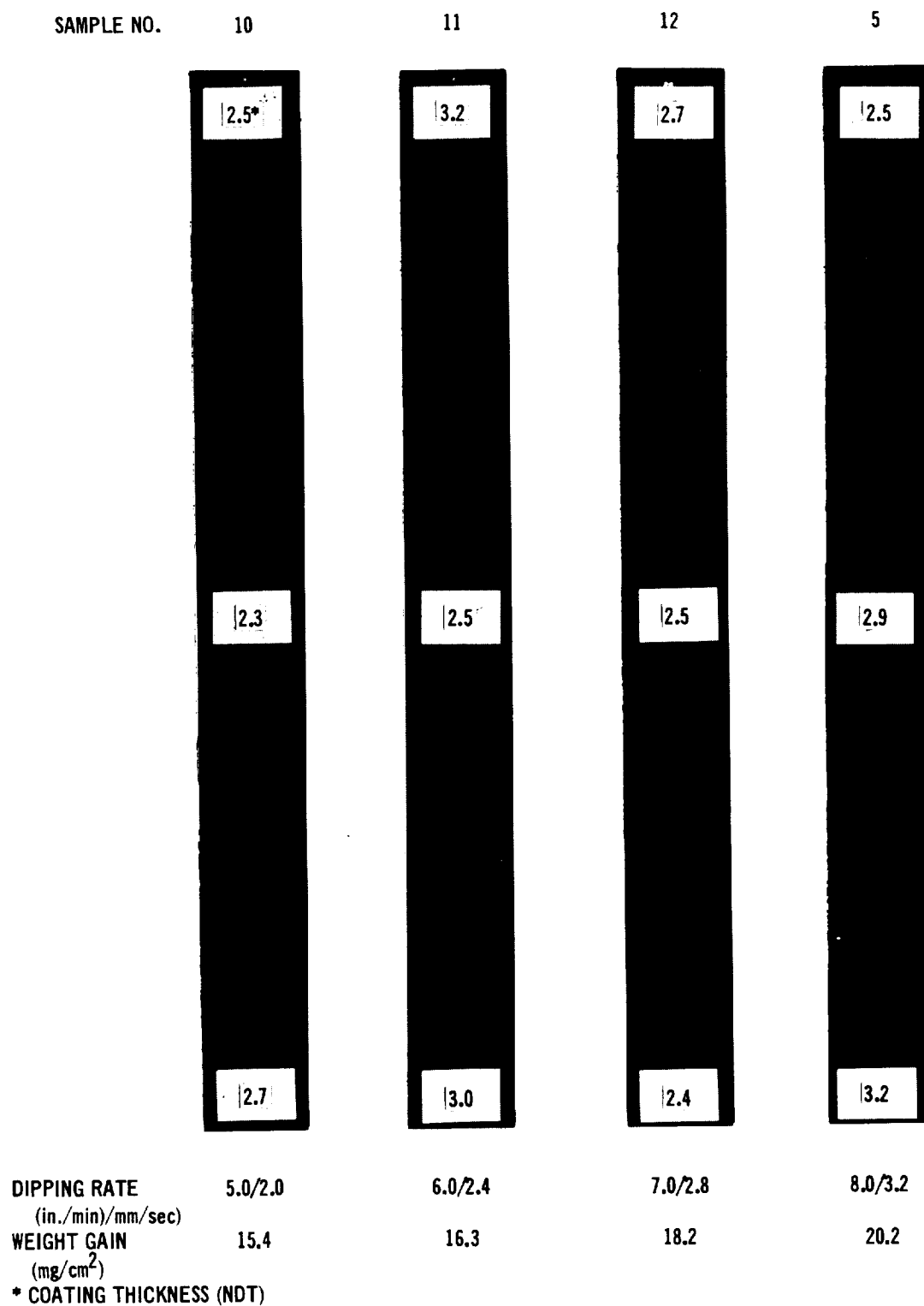
C-4 SLURRY COVERAGE

FIGURE 4-1



C-5 SLURRY COVERAGE

FIGURE 4-2



A-16 SLURRY COVERAGE

FIGURE 4-3

coating uniformity, and coatings up to  $27 \text{ mg/cm}^2$  could be produced without taper.

The A-15, 16 and 17 acrylic based slurries behaved erratically and further viscosity adjustment was required prior to obtaining satisfactory coatings. Of the A series, the A-16 slurry (highest concentration of the Thixatrol additive) performed best and the results are shown in Figure 4-3.

The uniformity of the A-16 slurry at the required coating thickness of  $19 \pm 3 \text{ mg/cm}^2$  was inferior to that obtained with C-5 slurry. However, edge coating coverage and green strength were superior to the C-5 slurry. More uniform coatings were obtained on this system at higher withdrawal rates than with the C-5 slurry. However, slurry stability problems were noted in the acrylic based systems; viscosity was found to change significantly with time.

In particular, A-16 slurries capable of producing the desired coating thickness of  $19 \text{ mg/cm}^2$  and with good uniformity were found several days later to produce either much thinner coatings of  $14 \text{ mg/cm}^2$  or a significant taper from top to bottom of the sample. These effects appeared to relate to a reaction between the acrylic binder and the thixotropic additives. Therefore, discussions were held with technical representatives of Rohm and Haas, suppliers of the acrylic binder, and Baker Castor Oil Company, supplier of the thixotropic additives. Rohm and Haas indicated that other people have also had viscosity stability problems using the Baker products and the acrylics and recommended bentonite thickeners from National Lead. This product was found to be a clay derivative which would not decompose on heating. The use of bentonite was therefore precluded as a control additive.

Baker Castor Oil Company recommended formulating slurries based on the addition of "Post 4" to the MPA and Thixatrol additives previously involved in these formulations. Five slurries were prepared as listed in Table 4-4 and the initial results were promising. A-22 slurry was then selected for uniformity studies. It should be noted that the A-20 slurry was of the same composition but was previously discarded because of a Quality Control question.

Strips 2" x 20" (5 cm x 50 cm) were dipped at various speeds, and in general the coating at the top 1" (2.5 cm) of the strips was somewhat thicker than for the rest of the strip. Thickness variations are illustrated in Table 4-5.

The results obtained were satisfactory at dipping rates of 5" and 7" per min (2.0 and 2.8 mm/sec). However, the uniformity was not equivalent to the results previously reported for the nitrocellulose based slurry C-5. The C-5 nitrocellulose



TABLE 4-4

## SLURRIES WITH POST 4 ADDED TO THE ACRYLIC VEHICLE

SLURRY NO.	AMT OF VEHICLE (cc)	MPA WT (g)	THIXOTROL WT (g)	POST 4 WT (g)	R512E POWDER WT (g)	VISCOSITY $CP \times 10^2$ (Nsec/m <sup>2</sup> )	AMBIENT TEMP °F (°C)	DIPPING SPEED IN/MIN (mm/sec)	COATING WT (mg/cm <sup>2</sup> )
A-18	200	7.5	0.6		625	20 (2.0)	72 (22)	6 (2.4)	15
A-19	200	9.0	0.4	5	625	28 (2.8)	70 (21)	5 (2.0)	15
A-20	200*	7.5	0.6	13.5	625	26 (2.6)	72 (22)	3 (1.2)	20
A-21	200	9.0	0.4	10.0	625	30 (3.0)	71 (21)	6 (2.4)	21
A-22	200*	7.5	0.6	13.5	625	29 (2.9)	74 (23)	3 (1.2)	21

\*VEHICLE IS 25 V/O LT, 75 V/O HFN + 8% B-66 ACRYLIC  
IN OTHER SLURRIES VEHICLE IS 15 V/O LT, 85 V/O HFN

TABLE 4-5

COATING UNIFORMITY STUDIES  
A-22 SLURRY, 2" x 20" (5 x 50 CM) STRIPS

WITHDRAWAL SPEED IN/MIN (MM/SEC)	4 (1.6)	5 (2.0)	6 (2.4)	7 (2.8)
COATING WEIGHT - MG/CM <sup>2</sup>	15.4	19.2	21.1	23
GREEN THICKNESS - MILS (μM)				
TOP	7.0 (178)	4.0 (101)	7.0 (178)	5.4 (137)
MIDDLE	3.0 (76)	5.1 (130)	4.2 (107)	4.0 (101)
BOTTOM	4.0 (101)	4.0 (101)	3.0 (76)	4.2 (101)

based slurry and A-22 acrylic based slurry were then selected for further study and large batches were prepared for study on 20" x 20" (50 x 50 cm) specimens.

4.1.2 Process Support Studies - A number of studies were performed in order to:

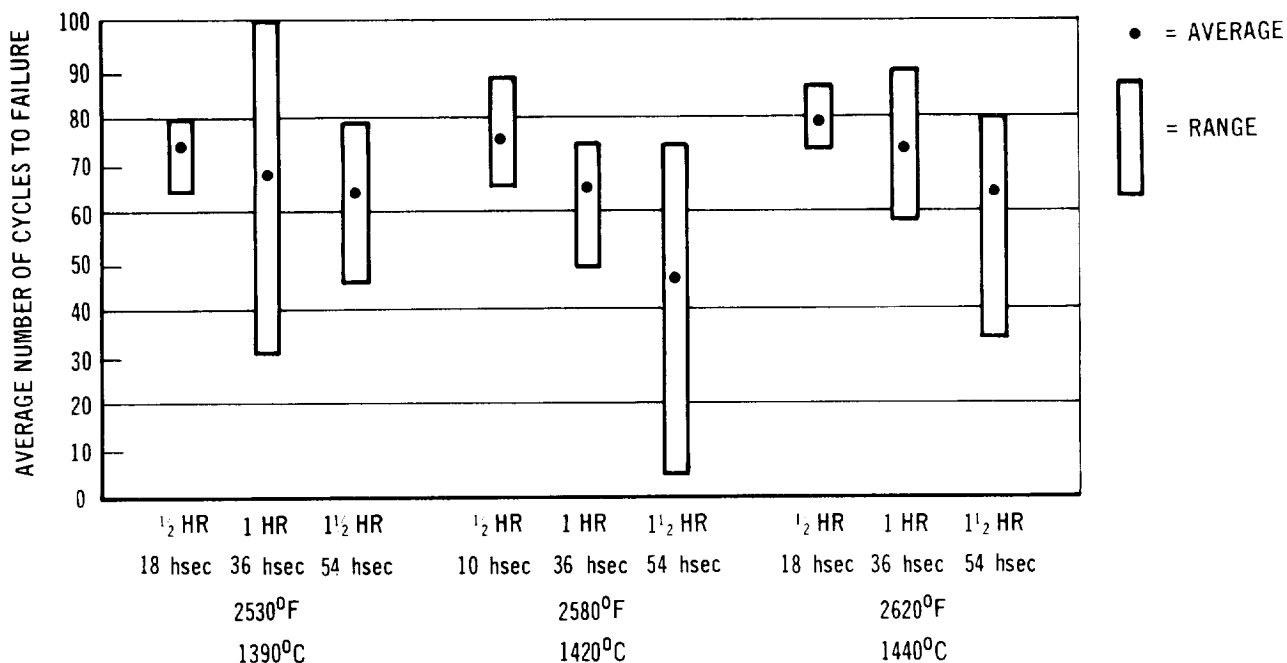
- (1) Determine the latitude available in the furnace cycle to be used in fusing the coating, and
- (2) Check for possible detrimental effects of slurry control additives on oxidation protection.

4.1.2.1 Fusion - Diffusion Cycle Latitude - The "normal" cycle is to heat parts at a pressure of  $10^{-4}$  torr to 2580°F (1420°C) and hold for one hour (36 h sec). The heating rate is as rapid as the vacuum pumping system will stand without choking. A series of experimental runs were made by bracketing the normal times and temperature to see what effects these variations had on oxidation performance.

Coupons of Cb-752, 0.013" x 1" x 1" (0.033 cm x 2.5 cm x 2.5 cm), were dip coated with the C-5 slurry and then fusion treated at 2530, 2580, and 2620°F (1390, 1420, and 1440°C) for 1/2, 1 and 1-1/2 hours (18, 36, and 54 h sec). Sample

preparation included drilling a 1/8" (0.32 cm) diameter hole in one end, rounding all edges manually on a rubber-abrasive wheel and then tumbling for 5 hours (18 k sec). Each sample was grit blasted before coating. A total of 90 samples were processed. Their performance was evaluated by oxidation testing in air at one atmosphere and in the external pressure reentry cycle. Both tests were similar in maximum temperature, 2400°F (1300°C). Five samples were tested for each fusion treatment.

The average and range of the protective lives obtained in the 1 atmosphere test, which is considered an accelerated test, are shown in Figure 4-4. Other data are listed in Table 4-6. In general, longer processing times at temperature gave decreased protection. Paradoxically there also appeared to be a tendency toward increased life with higher processing temperature. However, there are probably several competing systems at work. On the negative side are the coating weight losses which increase with time and temperature. The lost material is probably high in chromium and iron. Compositionwise, this increases the amount of  $\text{CbSi}_2$  at the outermost surface. On the positive side, the coating diffusion zone grows with time and temperature which probably improves reliability by giving more protection at crack roots in thinly coated areas.



EFFECT OF DIFFUSION TEMPERATURE AND TIME ON AIR SLOW CYCLE LIFE

FIGURE 4-4

TABLE 4-6  
EFFECT OF DIFFUSION TEMPERATURE AND TIME ON COATING LIFE

TEMPERATURE	TIME	AVERAGE COATING LOSS (MG/CM <sup>2</sup> )	AVERAGE COATING WT (MG/CM <sup>2</sup> )	ONE ATM AVERAGE LIFE, HRS (hSEC)	AVERAGE LIFE RED PRESSURE HRS (hSEC)
2530°F (1390°C)	1/2 HR (18 hSEC)	1.6	20.9	72 (260)	99 (360)
	1 HR (36 hSEC)	1.9	20.9	66 (240)	98 (350)
	1-1/2 HR (54 hSEC)	2.4	19.8	62 (220)	99 (360)
2580°F (1420°C)	1/2 HR (18 hSEC)	1.5	22.0	74 (270)	87 (310)
	1 HR (36 hSEC)	2.6	20.3	63 (230)	100+ (360+)
	1-1/2 HR (54 hSEC)	2.8	22.9	38 (140)	88 (320)
2620°F (1440°C)	1/2 HR (hSEC)	2.4	20.8	79 (280)	100+ (360+)
	1 HR (36 hSEC)	2.6	19.6	71 (260)	87 (310)
	1-2/2 HR (54 hSEC)	3.5	19.2	62 (220)	77 (280)

Longer lives were obtained in the reduced pressure tests; most samples lasted 100 cycles or more, at which point the tests were terminated. In both types of tests all of the failure sites were located on edges, holes, and corners. Accordingly, an interpretation and correlation of the quantitative results in optimizing the coating fusion cycle was not deemed as important as development of an improved and consistent edge coating technique. If anything, this work illustrated that fairly effective protection could be obtained over a broad range of processing time and temperature. Accordingly, for the balance of the program, no attempt was made to change the fusion cycle, particularly since a considerable data base had been obtained in the industry for the standard cycle.

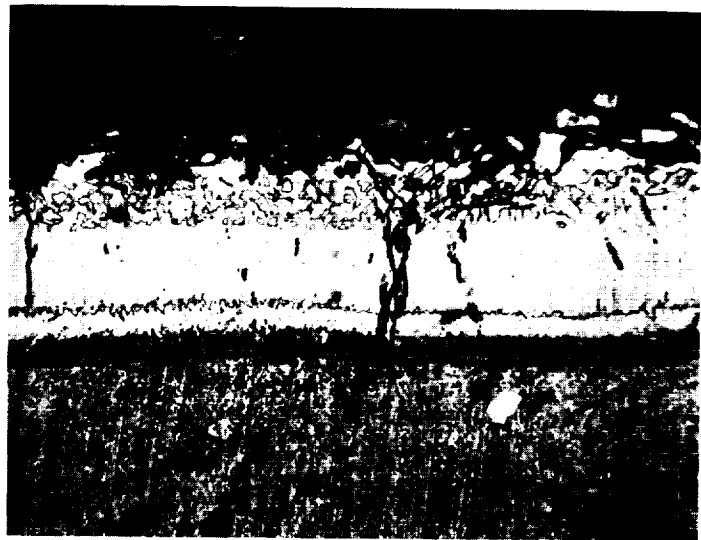
4.1.2.2 Slurry Additive - Effect on Performance - The possible effects on coating structure and performance caused by the use of the various binders and thixotropic additives were investigated by coating and evaluating Cb-752 specimens. The coating structures obtained, as shown in Figure 4-5, failed to show any significant differences attributable to the various binders or additives. The effects of these binders and additives on oxidation life in the accelerated slow cyclic air test, were also studied. The results shown in Table 4-7 failed to show any significant differences attributable to the various binders or additives. This result was anticipated because the binders and additives are reported to be residue-free and to decompose early in the diffusion cycle. It appeared feasible, therefore, to use these binders as additives in preparation of slurries for the large scale panels.



SLURRY COMPOSITION BASED ON 500g  
OF METAL POWDER  
MOUNT NO. - SLURRY NO.  
VEHICLE  
THIXOTROPIC ADDITIVES

G-122 C3  
167 cc, L-18  
13.3 gms MPA  
0.63 gms THIXITROL ST

400X



SLURRY COMPOSITION BASED ON 500g  
OF METAL POWDER  
MOUNT NO. - SLURRY NO.  
VEHICLE  
THIXOTROPIC ADDITIVES

G-125 AP-1  
145 cc 8% ACRYLIC IN HFN, 50 V/O XYLENE  
1.7 gms MPA  
1.7 gms POLY OX

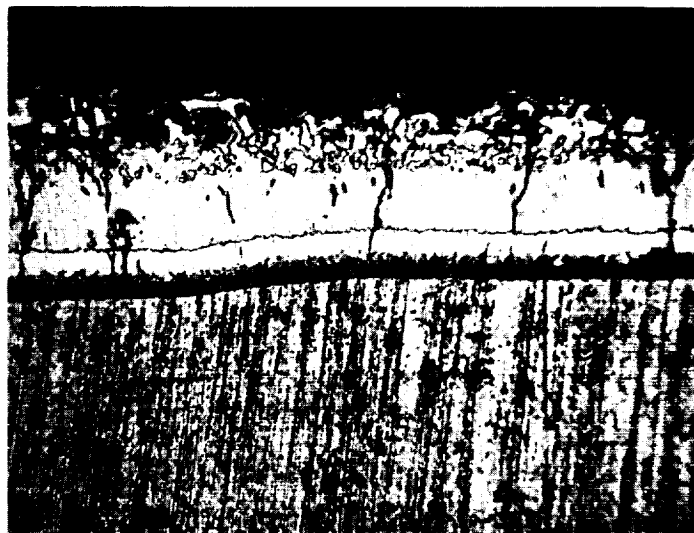
400X

EFFECT OF VEHICLE, BINDER AND THIXOTROPIC ADDITIVES ON THE  
COATING STRUCTURE OF R-512-E ON CB-752 ALLOY

FIGURE 4-5

SLURRY COMPOSITION BASED ON 500g  
OF METAL POWDER

MOUNT NO. - SLURRY NO.  
VEHICLE  
THIXOTROPIC ADDITIVES

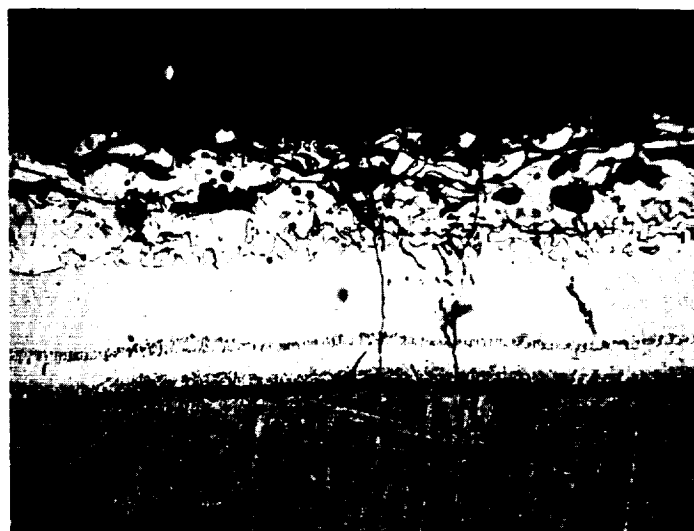


G-124 A-16  
185 cc, 8% ACRYLIC IN HFN, 25 -V/O LT  
5.8 gms MPA  
0.5 gms THIXITROL ST

400X

SLURRY COMPOSITION BASED ON 500g  
OF METAL POWDER

MOUNT NO - SLURRY NO.  
VEHICLE  
THIXOTROPIC ADDITIVES



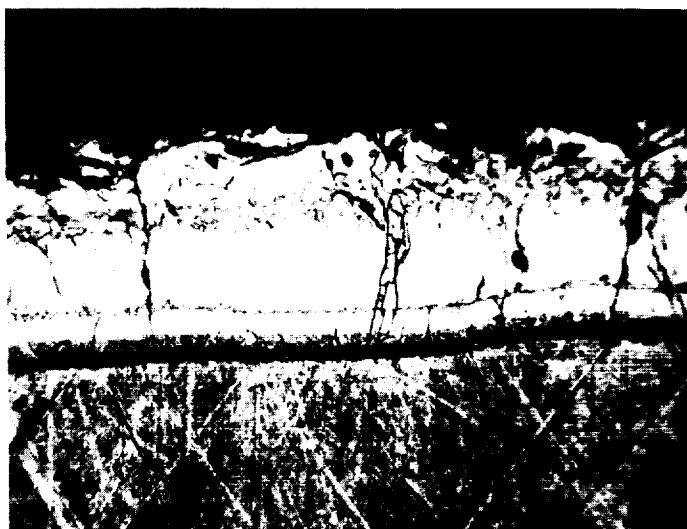
G-127 A-22  
185 cc, 8% ACRYLIC IN HFN, 25 V/O LT  
5.8 gms MPA  
0.5 gm THIXITROL ST  
11.3 gms POST 4

400X

EFFECT OF VEHICLE, BINDER AND THIXOTROPIC ADDITIVES ON THE  
COATING STRUCTURE OF R-512-E ON CB-752 ALLOY

FIGURE 4-5 (Continued)

SLURRY COMPOSITION BASED ON 500g  
OF METAL POWDER  
MOUNT NO. - SLURRY NO.  
VEHICLE  
THIXOTROPIC ADDITIVES



G-123 C6  
180 cc, L-18  
16.0 gms MPA  
1.5 gms THIXITROL ST

400X

SLURRY COMPOSITION BASED ON 500g  
OF METAL POWDER  
MOUNT NO. - SLURRY NO.  
VEHICLE  
THIXOTROPIC ADDITIVES



G-126 A-20  
180 cc 8% ACRYLIC IN HFN 25 V/O LT  
6.0 gms MPA  
0.5 gm THIXITROL ST  
11.0 gms POST 4

400X

EFFECT OF VEHICLE, BINDER AND THIXOTROPIC ADDITIVES ON THE  
COATING STRUCTURE OF R-512-E ON CB-752 ALLOY

FIGURE 4-5 (Continued)

TABLE 4-7

EFFECT OF SLURRY ADDITIVES ON SLOW CYCLIC AIR  
OXIDATION OF R512E COATED Cb-752 ALLOY

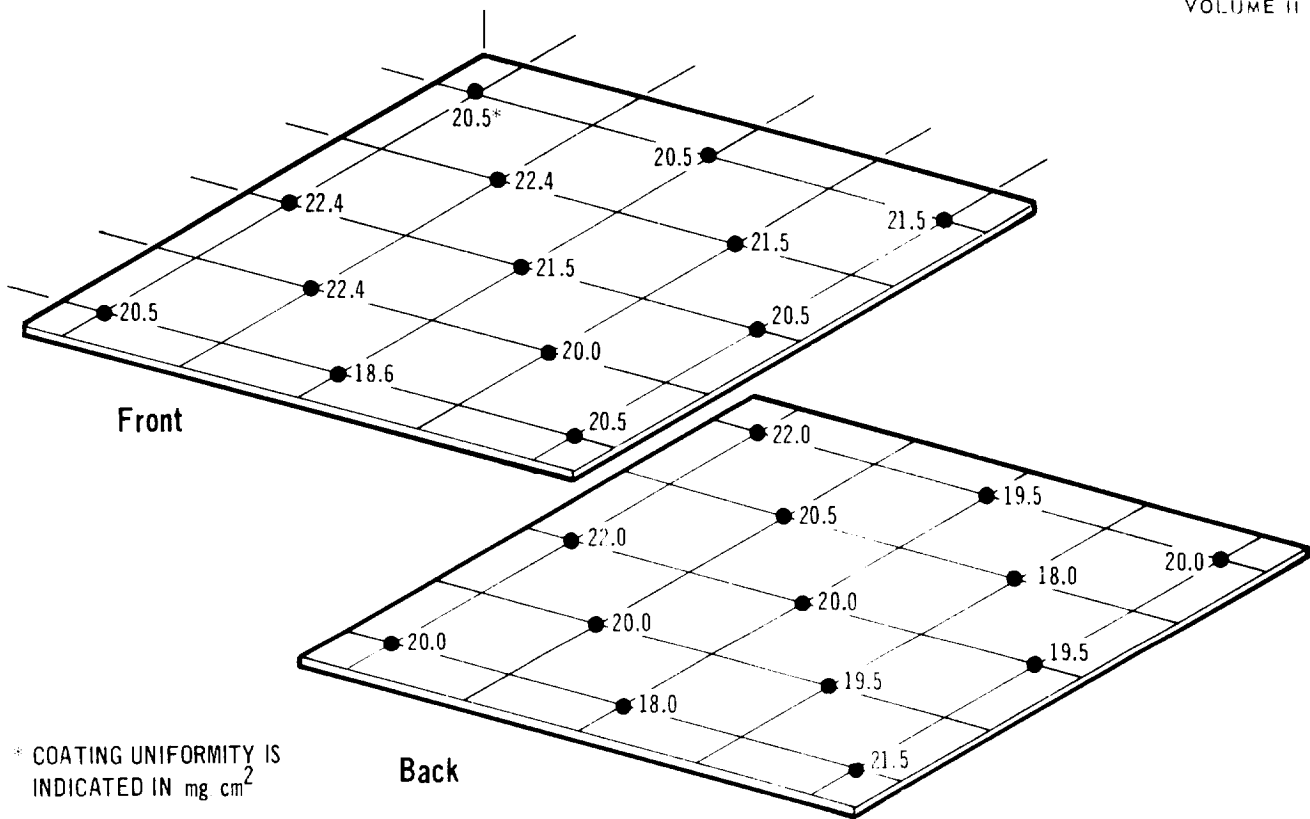
SLURRY	BINDER	ADDITIVES	OXIDATION LIFE (CYCLES)
C-3	NITROCELLULOSE	MPA + THIXATROL ST	66, 73, 73
C-5	NITROCELLULOSE	MPA + THIXATROL ST	70, 73, 73
A-16	ACRYLIC	MPA + THIXATROL ST	43, 73, 78
A-20	ACRYLIC	MPA + THIXATROL ST	60, 70, 70
A-22	ACRYLIC	MPA + THIXATROL ST + POST 4	80, 80, 82
AP-1	ACRYLIC	POLYOX	59, 73, 73

4.2 Process Scale-up

4.2.1 Slurry Preparation - As indicated, the C-5 nitrocellulose lacquer and A-22 acrylic based slurries were selected for scale-up evaluation. Several steel dipping tanks 3" (7.5 cm) wide x 23" (58 cm) long x 27" (69 cm) high were constructed and used for these trials and eventually for full scale panel dipping. Sheets of stainless steel 0.018" x 20" x 20" (0.5 cm x 50 cm x 50 cm) were used as panel mockups to check the uniformity of the coating thickness and slurry chemistry.

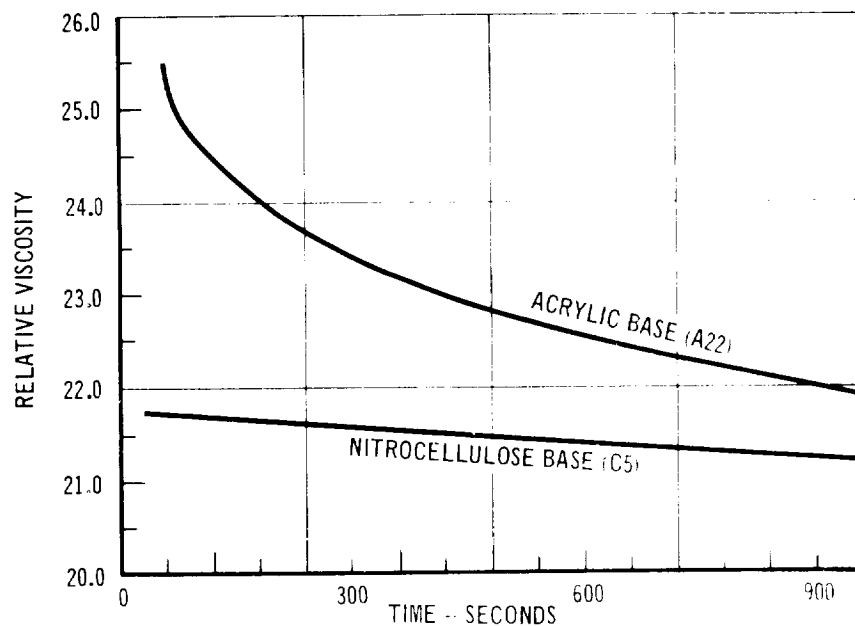
A large batch (20 gal. (0.076 m<sup>3</sup>)) of C-5 nitrocellulose base slurry was made up; it performed similarly to previous smaller batches after a minor viscosity adjustment was made. Figure 4-6 shows the coating uniformity obtained on one of the 20" x 20" (50 cm x 50 cm) panels. The average coating thickness was 20.5 mg/cm<sup>2</sup> and the Dermatron showed a thickness variation of 18 to 22 mg/cm<sup>2</sup>. This converts to a green coating thickness of 5.5 mils (140 μm) with a range of 5.0 to 6.0 mils (127 to 152 μm). After fusion, the finished coating is approximately one-half the green coating thickness. These values were well within the program goals.

Evaluation of the large batch of acrylic based slurry A-22 indicated that there were problems with settling and aging. In order to obtain uniform coatings, it is necessary for the viscosity of the slurry at the surface of the batch to be constant for the time required to coat the hardware. The viscosity of the A-22 slurry was determined just below the surface of the batch and compared to similar data on the C-5 slurry. The results of this test are shown in Figure 4-7. The C-5 slurry showed a constant viscosity whereas the A-22 slurry showed a considerable decrease with time. This change in viscosity indicates the lack of effectiveness of the



COATING UNIFORMITY STUDIES ON 20' x 20' (50 CM x 50 CM) FLAT PANEL MOCKUP

FIGURE 4-6



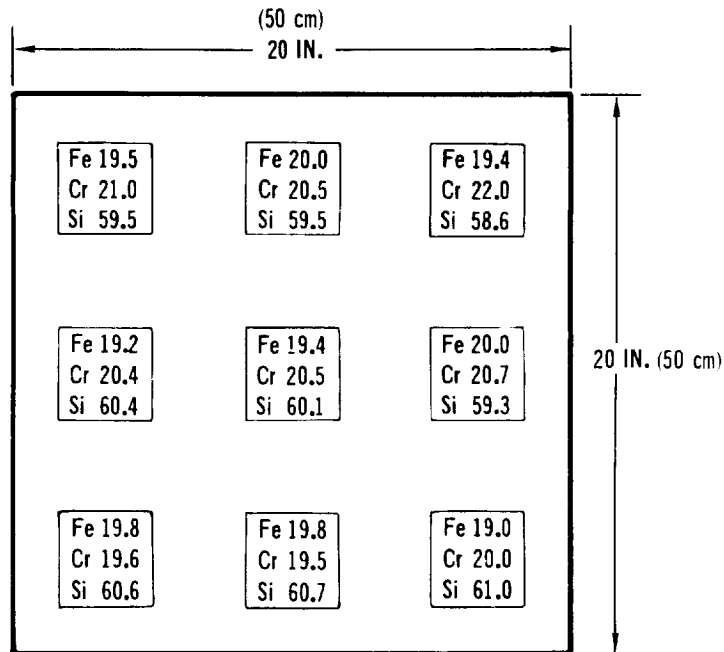
EFFECT OF SETTLING ON VISCOSITY 1/4 IN. (0.6 CM) BELOW SURFACE FOR  
ACRYLIC BASE (A22) AND NITROCELLULOSE BASE (C5) SLURRIES

FIGURE 4-7



viscosity control additives employed. Accordingly, further discussions were held with the manufacturers of the binders and additives and they confirmed the problems in stability of the viscosity control additives in this binder system. Suggestions made by the binder manufacturers were evaluated in a later portion of the program. In order to avoid major program delays, studies on the A-22 slurry were suspended and optimization studies were continued with the C-5 slurry.

The possible variations in coating chemistry obtained in this process at the slurry stage, were determined by coating a 20" x 20" (50 cm x 50 cm) flat stainless mockup in the C-5 slurry. The green coating was then selectively removed from 2" (5 cm) square areas in nine locations on the panel. The coating powder obtained was analyzed for Cr and Fe by x-ray fluorescence techniques, the results of which are shown in Figure 4-8. Silicon contents were determined by difference. The iron content was found to vary from 19.0 to 20.0%, chromium from 19.5 to 22%, and silicon from 58.6 to 61%. Since the normal slurry composition is 20% Fe, 20% Cr, and 60% Si, the analyzed values indicate the effectiveness of the viscosity control additive in minimizing relative settling of the metal powders.



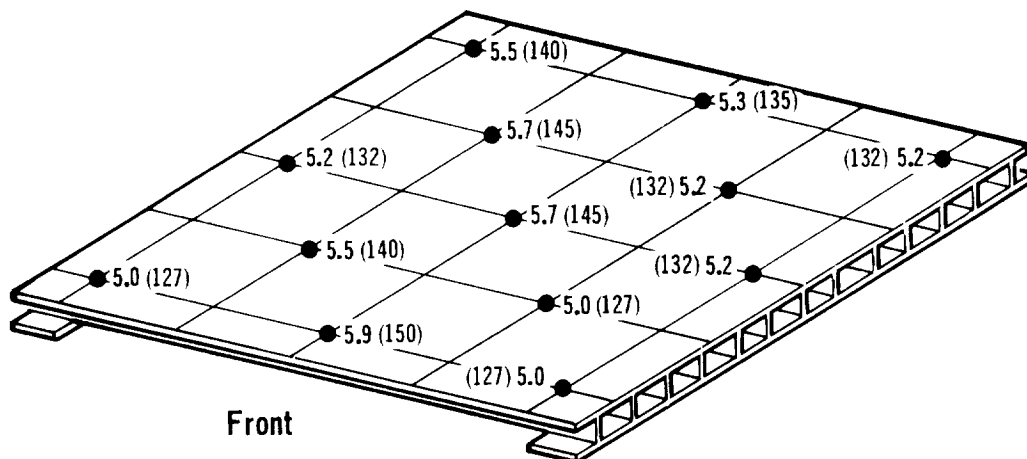
COATING COMPOSITION UNIFORMITY FROM C-5 SLURRY ON 20 IN. x 20 IN.  
(50 CM x 50 CM) FLAT STAINLESS MOCKUP

FIGURE 4-8

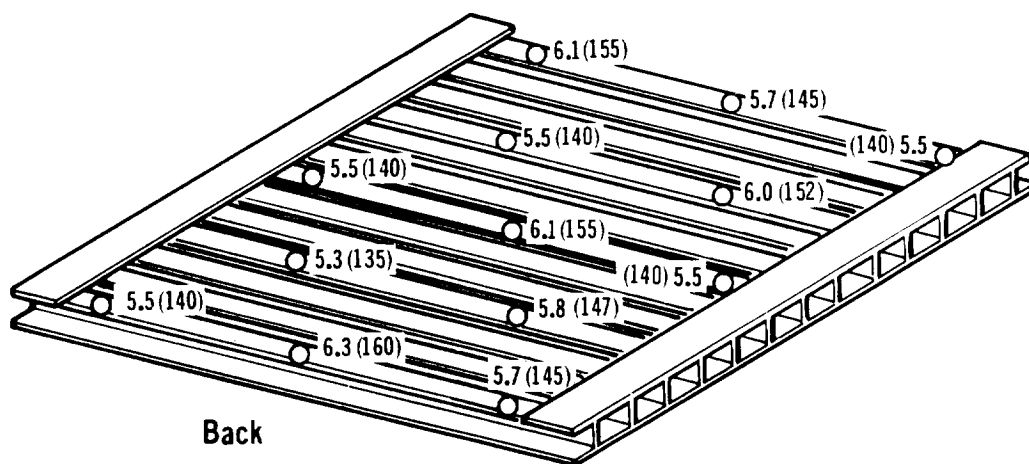
The possible effects of extreme compositional variations that might be obtained in the slurry were investigated by applying Si-18Cr-18Fe and Si-22Cr-22Fe to sample tabs of Cb-752 alloy. These samples were fused for one hour at 2580°F (36 h sec at 1420°C) and tested in the external pressure slow cyclic test. Five tabs of each composition were tested. All the specimens with the Si-22Cr-22Fe composition passed the 100 cycle goal of this program. However, samples coated with Si-18Cr-18Fe were found to exhibit oxidation failure between 36 to 52 cycles. The data obtained on as-deposited slurry compositional variations previously described indicates that the lowest Cr/Fe composition obtained was Si-19.5Cr-19.8Fe which is considerably above the Cr/Fe content of the poor performing Si-18Cr-18Fe. Although improved performance and an additional safety factor might be obtained by shifting the normal bath composition to higher Cr and Fe contents, considerably more information needed to be obtained before a recommendation was warranted to alter the basic Si-20Cr-20Fe composition with its large data base.

4.2.2 Coating Uniformity - The effects of complex geometry were investigated by dip-coating a 20" x 20" (50 cm x 50 cm) electron beam welded rib stiffened stainless steel panel in the same batch of slurry used for the 20" x 20" (50 cm x 50 cm) sheet. The panel picked up an average weight of 20.8 mg/cm<sup>2</sup> (the range was 19 to 22 mg/cm<sup>2</sup>). The average green coating thickness was 5.6 mils (142 μm). The front or skin side of the panel had an average coating thickness of 5.3 mils (135 μm), while the back side of the skin between the ribs was 5.7 mils (145 μm), and the ribs were 5.7 mils (145 μm). Green coating thickness distributions on the panel are shown in Figure 4-9. The coating uniformity (excluding edge coverage) was considered excellent for dipping and, in a fused state, would give a coating with a plus or minus variation in thickness of 0.3 mil (7.6 μm).

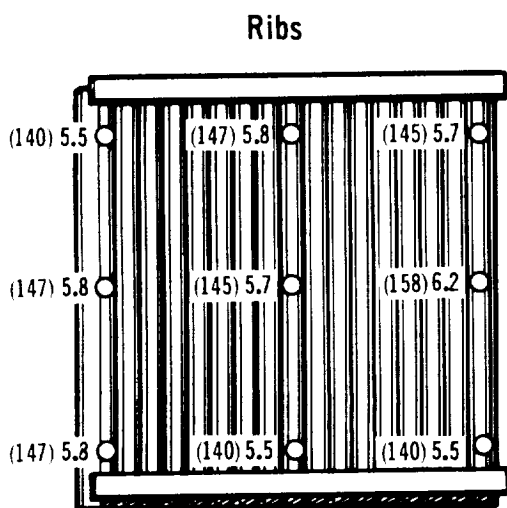
Further effects of complexity were studied using a 3" x 4" (7.5 x 10 cm) Cb-752 alloy electron beam welded rib stiffened corner detail which was coated using the same C-5 nitrocellulose based slurry. No attempt was made on this panel to improve the edge coverage by overspraying. After fusion, the Dermitron measurements indicated an average thickness of 19 mg/cm<sup>2</sup> with a range of 17 to 22 mg/cm<sup>2</sup>, as shown in Figure 4-10. The higher figures are for the green slurry. The panel was sectioned and extensively examined by metallography, as shown in Figure 4-11. The coating was found to average 3.5 mils (87 μm) with a range of 3.0 to 4.0 mils (75 to 100 μm) excluding edges. The edges uppermost on dipping were found to have a thickness of 1.5 mils (37 μm), side and lower edges had 2.0 and 3.2 mils (50-80 μm), respectively.



Front



Back



Ribs

COATING UNIFORMITY STUDY ON 20 IN. x 20 IN. (50 CM x 50 CM) RIB STIFFENED MOCKUP  
Slurry Thickness is in Mils ( $\mu m$ )

FIGURE 4-9

	50 (16) *	52 (17)	
	50 (19)	50 (19)	
	50 (18)	50 (20)	
	48 (18)	46 (17)	
	48 (17)	47 (18)	

54 (20)	54 (22)	56 (21)	56 (22)
50 (17)	50 (17)	50 (18)	50 (17)
	47 (17)	49 (20)	
55 (15)	47 (15)	49 (19)	50 (22)

Rib Sides

48 (19)	46 (21)	49 (19)	50 (20)	49 (19)	48 (17)
45 (20)	45 (18)	48 (20)	47 (20)	46 (18)	46 (18)
46 (19)	45 (17)	45 (19)	44 (18)	46 (19)	46 (17)

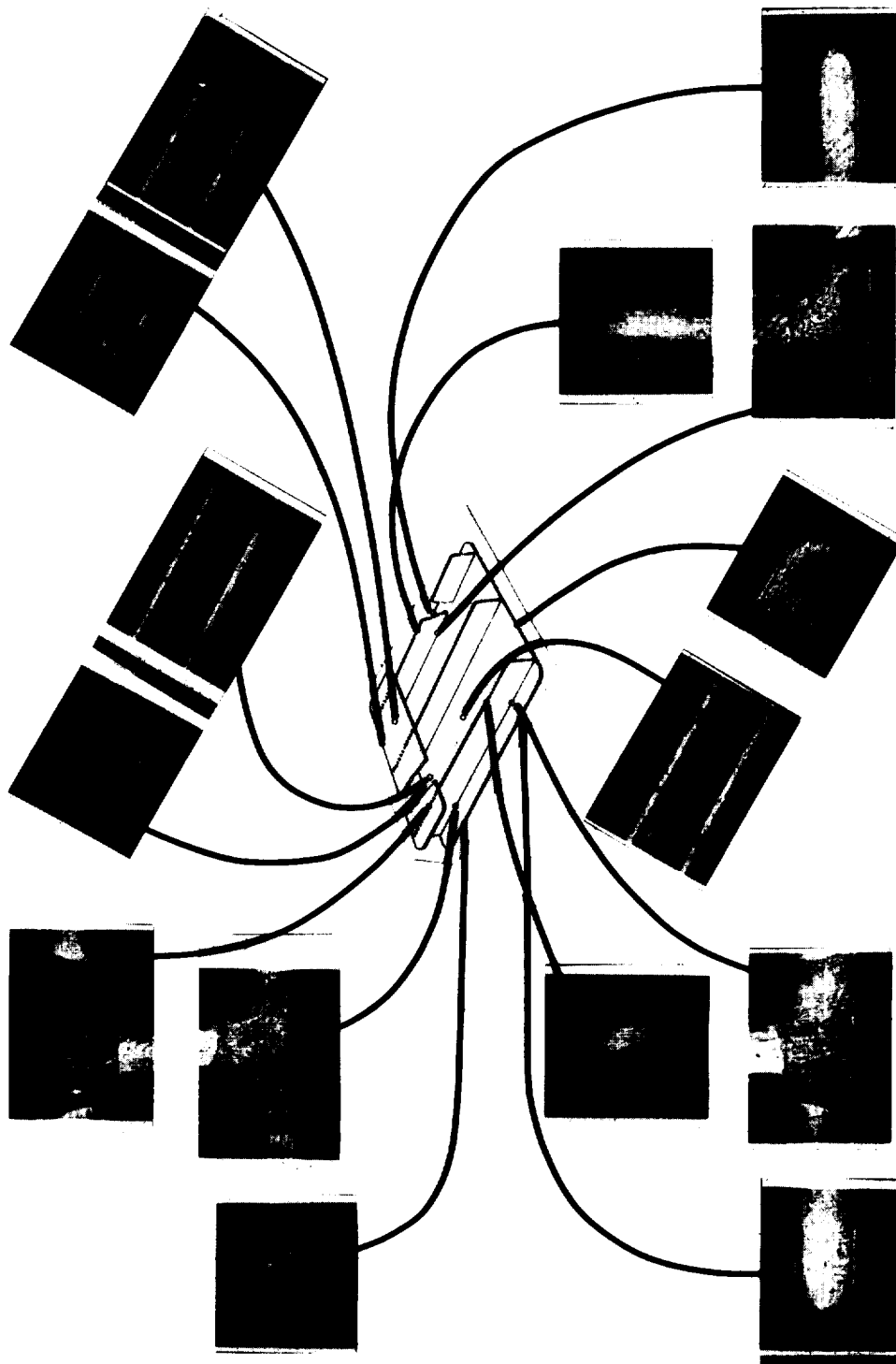
\*mg cm<sup>2</sup>

## DERMITRON UNIFORMITY STUDY AS DIPPED AND (AS DIFFUSED) R-512E ON Cb 752

FIGURE 4-10

4.2.3 Edge Coverage and Coating Reproducibility - The oxidation performance of the 3" x 4" (7.5 cm x 10 cm) panel would be questionable due to the thin edge coating. Normal procedure prior to this program included the application of additional coating to the edges by spraying with an air brush. Although excellent reproducibility was obtained by this coating method, it is a manual process and subject to operator error. It appeared desirable therefore to develop methods for improving slurry application to edges.

Double cycle coating application was investigated first in an effort to improve the edge coverage. The first processing sequence investigated consisted



METALLOGRAPHIC UNIFORMITY STUDY ON Cb 752 CORNER DETAIL

R512E COATED Cb 752 ALLOY  
3 IN. x 4 IN. (7.5 CM x 10 CM) CORNER DETAIL

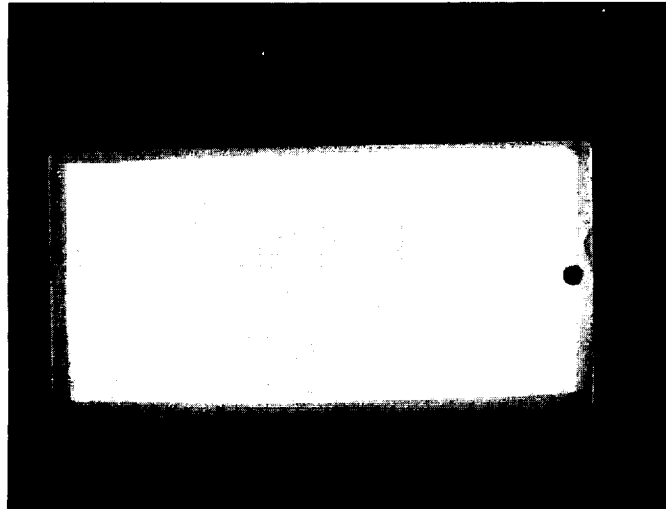
FIGURE 4-11

of two separate dip and fire cycles. The slurry employed was the C-5 nitrocellulose and the panel was rotated end for end between the coating cycles. The top and bottom edges showed considerable improvement, but the side edges were still thin and erratic. This processing sequence was applied to two Cb-752 alloy 3" x 4" (7.5 cm x 10 cm) panels, one of which was examined by NDT and metallographic sectioning, and the other panel was subjected to oxidation testing in the one atmosphere slow cyclic facility. NDT and metallographic examination showed coating uniformity similar to the panel in Figure 4-11, with the exception of improved coverage at the top and bottom edges. Slow cycle oxidation testing at one atmosphere confirmed that the coating was thin; the first evidence of substrate oxidation occurred at the side edge after the second cycle.

The second processing sequence utilized strips 1" x 4" (2.5 cm x 10 cm) of Cb-752 alloy and consisted of 2 green slurry coats followed by a single diffusion treatment. The first cycle dip was applied from the C-5 nitrocellulose based slurry ( $13 \text{ mg/cm}^2$ ); and, after thorough drying, additional coating ( $9 \text{ mg/cm}^2$ ) was applied by dipping in an acrylic based slurry. These specimens were also turned end to end in between the dip coats. These samples failed to show any significant improvement over either single cycle or the double diffusion coatings previously described.

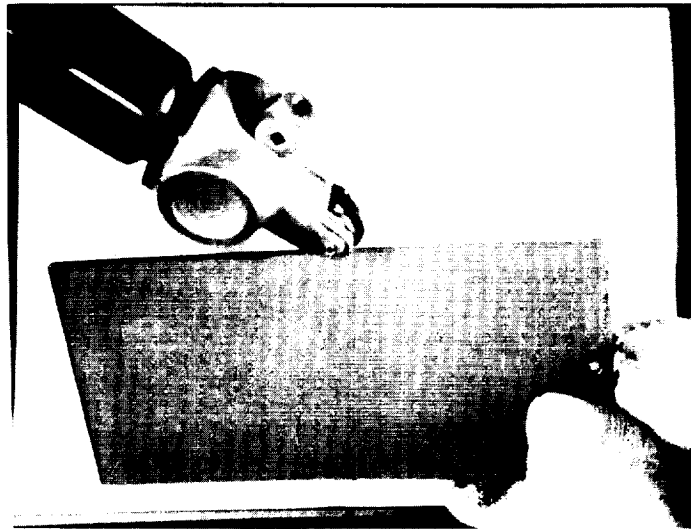
Efforts were then concentrated on alternative and, what proved to be, more reliable methods of applying additional slurry to the panel edges. The additional edge coating when applied by air brush spraying, on drying, blends into the dip coating and makes it hard visually to determine that all edges have been over-sprayed. The addition of coloring agents to the spray slurry was investigated, which would enable visual inspection for coverage. These coloring agents were selected from fully organic products which would decompose on diffusion treatment. Yellow, green and blue dyes were evaluated and found to decompose during diffusion, and they did not exhibit detrimental effects on 1 atmosphere slow cyclic oxidation performance. The yellow colorant was found to produce the most contrast, as shown in Figure 4-12. This method allows for easy visual inspection to ensure that all edges are covered. The color band does not show directly on the edge but rather on the flat surface adjacent to the edge.

Eventually a method for applying a bead of slurry directly to the edge was developed. A miniature paint striping tool was obtained as shown in Figure 4-13, and found to be adequate for applying the bead of slurry to the edge. Samples of



THE USE OF YELLOW COLORANT ON THE EDGE OVERSPRAY SLURRY

FIGURE 4-12



SLURRY BEAD APPLIED TO EDGE AFTER DIP COATING

FIGURE 4-13

Cb-752 were then dip coated and evaluated by NDT (thermoelectric) and by slow cycle oxidation testing at one atmosphere in the as-dipped, oversprayed, and beaded-edge conditions. The results of these tests are shown in Table 4-8.

TABLE 4-8  
EFFECT OF EDGE COATING METHOD ON PERFORMANCE  
ON R-512E COATING

CONDITION	EDGE THICKNESS NDT (MILLIVOLTS) COPPER PROBE	1 ATMOSPHERE SLOW CYCLIC OXIDATION LIFE
AS DIPPED	-0.2	2 CYCLES
AS DIPPED AND OVERSPRAYED	+0.2	20-50 CYCLES
AS DIPPED AND SLURRY BEADED	+0.4	75-150 CYCLES

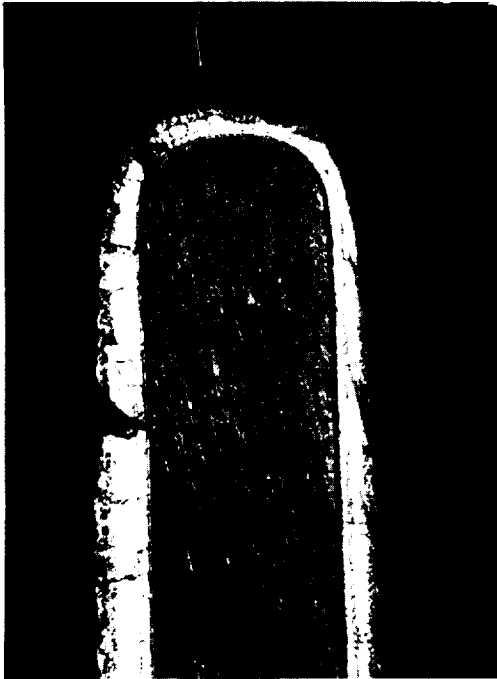
Metallographic examination of edge coverage is shown in Figure 4-14, for the as-dipped and as-dipped plus slurry-beaded samples. The results of these tests clearly show the performance advantage of the slurry-beading method. This method was selected for further study on 3" x 4" (7.5 cm x 10 cm) Cb-752 alloy panels.

The thermoelectric probe was modified to allow for easier inspection of coating thickness at the edges as shown in Figure 4-15. A nickel roller and heater extension were machined and attached to the standard heating tip. This modification provides for rapid edge coating inspection, limited only by the accuracy of the thermoelectric NDT method. Some minor problems exist such as binding of the nickel roller, which requires a high temperature conductive lubrication.

Based on the excellent performance of the tabs coated with an extra bead of slurry applied to the edges after dipping, a 3" x 4" (7.5 cm x 10 cm) Cb-752 panel was coated and examined by NDT and metallography. The coating was found to be very uniform on all surfaces with thickness ranging from 3 to 4 mils (75 to 100  $\mu$ m) determined by metallography. Good correlation was obtained between Dermatron eddy current NDT and metallography. The thermoelectric probe showed edges to vary from 1.9 to 2.2 millivolts with 1.2 mv obtained on uncoated columbium alloy. Metallographic examination of the edges showed the coating to vary from 2.2 to 4.0 mils (56 to 100  $\mu$ m). A typical edge of the ribs is shown in Figure 4-16.

Additional 3" x 4" (7.5 cm x 10 cm) Cb-752 panels were coated and oxidation tested in the 1 atmosphere slow cyclic tester. The results are listed in Table 4-9. The first panel tested (S/N 5) had a life of 20 cycles before the first evidence of substrate oxidation was noted on the inside of the stiffening strap. This is the





100X

As Dipped

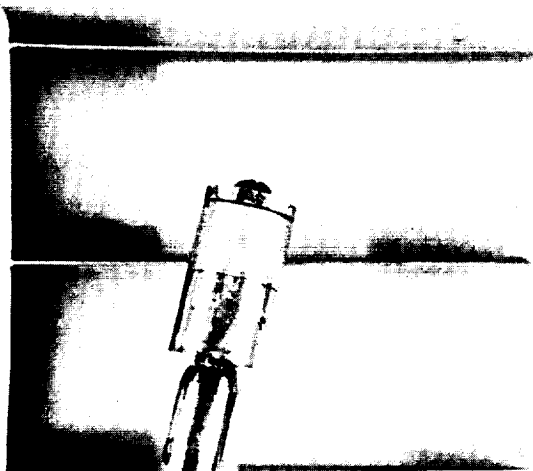


100X

As Dipped and Beaded

EDGE COVERAGE R512E ON Cb-752 ALLOY

FIGURE 4-14



ROLLER PROBE FOR THERMOELECTRIC  
NDT OF EDGE COATING THICKNESS

FIGURE 4-15



COATING AT RIB EDGE ON  
3 IN. x 4 IN. (7.5 CM x 10 CM) Cb-752 PANEL

FIGURE 4-16

TABLE 4-9  
COATING THICKNESS AND CYCLIC LIFE OF  
PANEL SECTIONS

PANEL NO.	COATING THICKNESS (MG/CM <sup>2</sup> )	1 ATMOSPHERE SLOW CYCLE LIFE (NO. CYCLES)
5	19.3	19
6	19.8	50
7	20.8	90
8	21.0	113
9	19.3	90
11	21.6	100*

\*TEST STOPPED WITHOUT FAILURE.

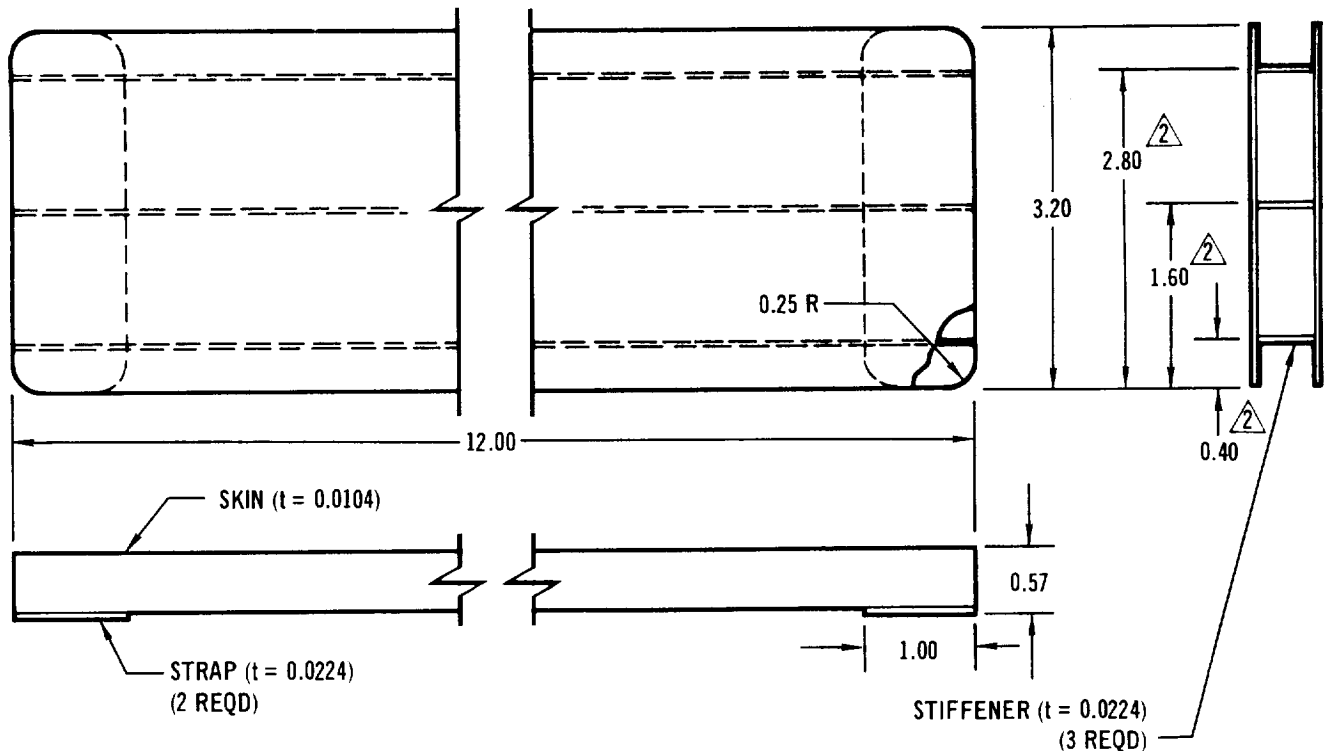
area most difficult to reach with the slurry beading tool. Panel S/N 6 was then coated using additional care in this area; and, again, the first evidence of substrate oxide occurred in the same location but after 50 cycles. The third panel (S/N 8) had additional slurry brushed on this area and survived over 100 slow cycles without failure. It should be noted that the 1 atmosphere air test is a highly accelerated exposure in which 10 cycles are equivalent to approximately 100 reduced pressure cycles. Three additional panels tested had lives of 90 to over 100 cycles.

#### 4.3 Process Verification

##### 4.3.1 Subsize Panels

4.3.1.1 Fabrication - Rib stiffened panels, 3 by 12" (7.5 x 30 cm) were used to verify effectiveness and reproducibility of the optimized coating. The panel specimen is shown in Figure 4-17. It was designed to be representative of a full-size rib stiffened panel in all respects except the overall dimensions, which were selected to fit into a load fixture used in conjunction with a 7" (18 cm) diameter tube furnace.

The fabrication of the 3 x 12" (7.5 x 30 cm) panel specimens shown in Figure 4-17 was accomplished using the FS-85 columbium alloy selected in Section 3.0. The required sheet material was chemically milled or chemically cleaned to indicated gages within 1 mil (25  $\mu$ m). Detail parts were sheared and the ribs were machined to final dimensions to insure parallel edges. The tool for electron beam welding was designed to align the welding beam with the center of one rib and the rib was then blind welded through the skin. Subsequent ribs were joined to the skin by moving the initial rib to an adjacent locating slot without changing the location



## NOTES:

- 1 - EB WELD STIFFENERS TO SKIN AND STRAPS
- 2 - DIMENSIONS LOCATE  $\phi$  OF STIFFENERS
- 3 - DIMENSIONS ARE IN INCHES

## RIB STIFFENED COLUMBIUM PANEL SPECIMEN

457-1709

FIGURE 4-17

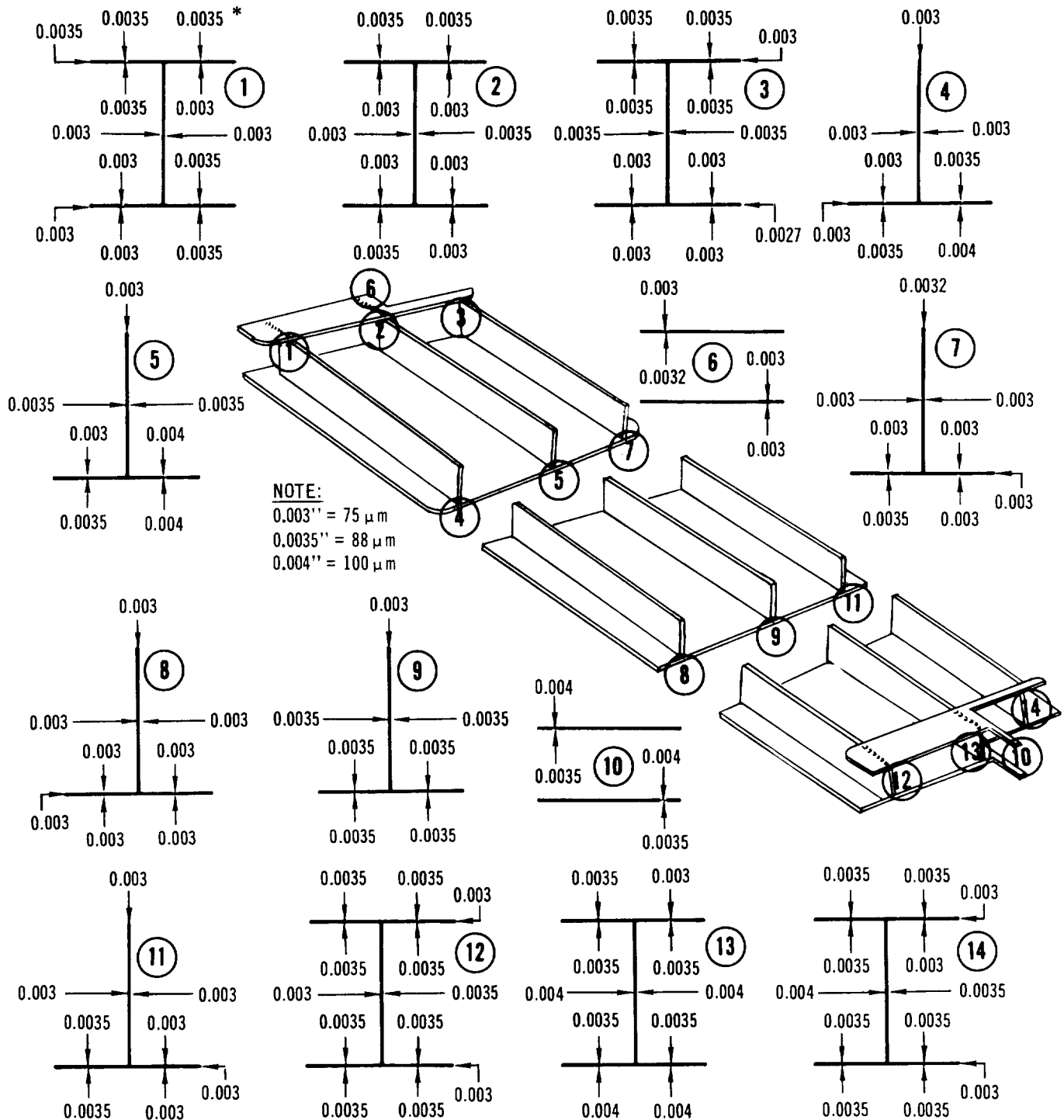
of the tool with respect to the welding beam. The second rib was then secured in the identical tooling position as the first rib and then welded to the skin. Subsequent ribs were then added to the panel assembly in a similar fashion. After the ribs had been joined to the skin, the straps on the reverse side of the ribs were electron beam welded in place. The final step was to radius the edges to enhance good coating quality.

The fusion welding of the skin to the ribs caused a noticeable amount of skin distortion. The longitudinal bowing of the panels produced a nominal deflection of 0.06" (0.15 cm) in the center of the span and a series of ripples, or buckling of the skin, between the ribs. The maximum depth of the buckles, 0.08" (0.2 cm) occurred in the center of the panel and the buckling of the skin was not noticeable on the unsupported edges. While the appearance of the panels was less than desirable, the panels were considered structurally acceptable and it was decided to proceed with the coating and profile testing of the panels to the conditions described in Section 1.0.

4.3.1.2 Coating - Based on the excellent performance and consistency of the dip plus slurry beading coating process obtained on the 3" x 4" (7.5 cm x 10 cm) panels, it was decided to coat the 3" x 12" (7.5 cm x 30 cm) FS-85 alloy subscale panels employing the same slurry application procedures. The diffusion treatment was for 1 hour at 2580°F (36 h sec at 1420°C). Panel #1 was coated and metallographically examined after a thorough NDT inspection for coating uniformity; the numerical results are shown in Figure 4-18, and metallographic sections in Figure 4-19. The coating thickness was found to vary between 3.0 and 4.0 mils (75 and 100  $\mu$ m) and averaged approximately 3.2 mils (81  $\mu$ m) on all surfaces and edges, well within the program goals. This coating process was then approved for the balance of the 3" x 12" (7.5 cm x 30 cm) rib stiffened FS-85 alloy panels which were processed for tests. The coating weight and thickness measurements are summarized in Table 4-10. The NDT thickness measurements were affected by the ripples in the panel skin which are a result of stresses created by welding shrinkage as previously discussed.

4.3.1.3 Testing - Subsize, 3" x 12" (7.5 cm x 30 cm), heat shields were utilized in flight simulation testing to demonstrate the effectiveness of the optimized fused slurry coating and to determine the reuse capability of the heat shield. Five subsize heat shield panels were subjected to simultaneous simulation of temperature, pressure, and stress profiles and acoustic exposures representative of a Space Shuttle reentry flight. Pressure conditions representative of both internal and external surfaces were simulated. Flight simulations were accomplished using the modified Astrotube Furnace and the loading fixture shown in Figure 4-20. The temperature, pressure and stress conditions are those that were presented in Section 1.0, Figure 1-2, for subsize panel testing. A total of 412 reentry cycles were conducted; three panels were exposed for 100 cycles each. Creep and elastic deflection measurements were made prior to and during testing. Elastic deflection measurements were made under four-point loading of the panels at a load (141 lbs (64 kg)) which produced a stress in the outermost portion of the ribs equal to 77% of room temperature yield. Creep deflection measurements made with a straight bar and micrometer over an 11" (28 cm) span were also recorded for each panel at various intervals during cycling.

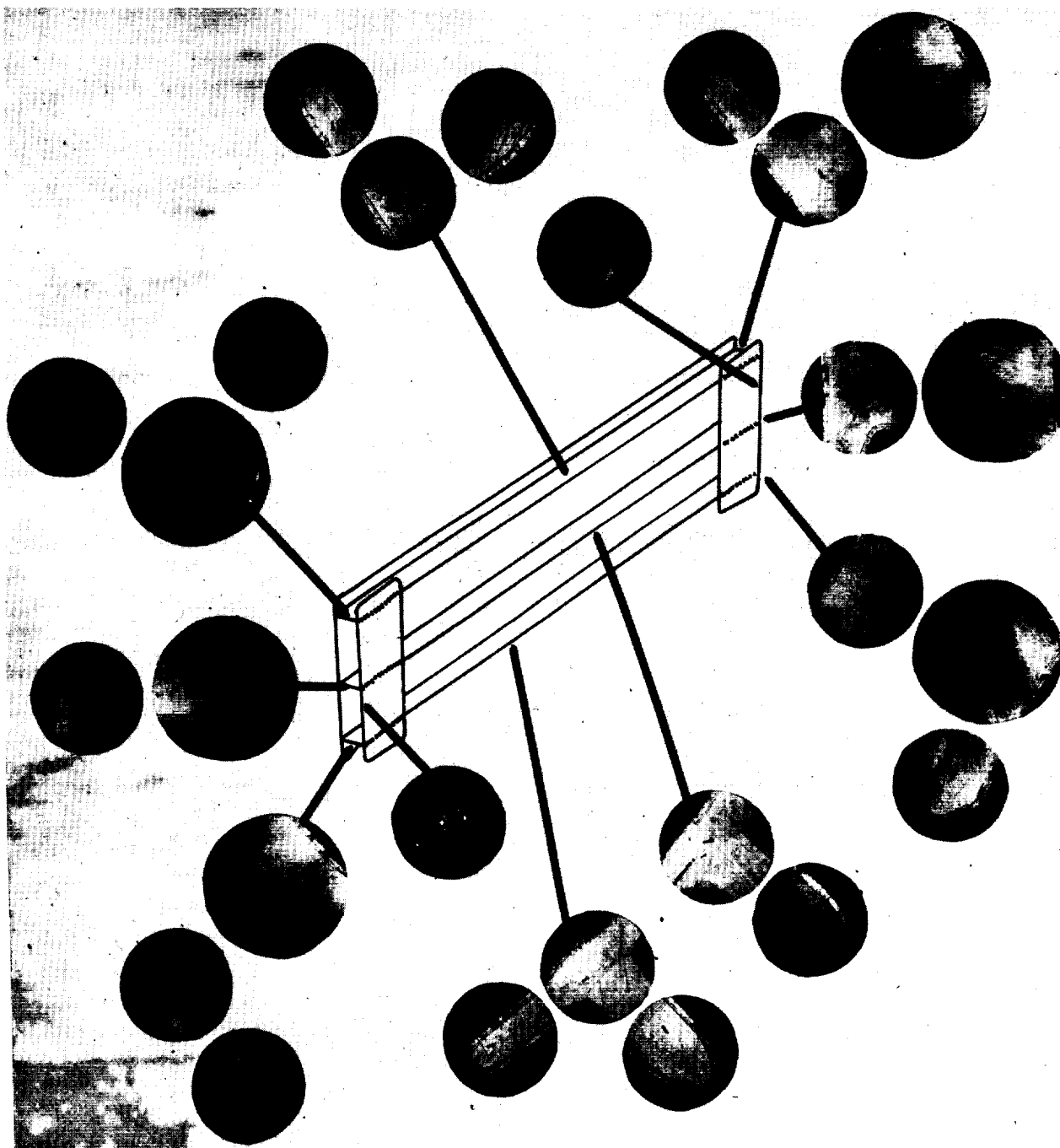
Results of creep and elastic deflection measurements are shown in Table 4-11. Creep deflections are expressed in average deflection rate (mils/cycle and  $\mu$ m/cycle) for each group of cycles conducted per panel and in cumulative average deflection



\*COATING THICKNESS IN INCHES

METALLOGRAPHIC COATING UNIFORMITY STUDY ON  
R512E COATED FS-85 ALLOY SUB-SIZE RIB STIFFENED HEAT SHIELD PANEL

FIGURE 4-18



PHOTOS ARE 20X

UNIFORMITY STUDY-R512E COATED FS-85 ALLOY 3" x 12"  
(7.5 CM x 30 CM) RIB STIFFENED PANEL

FIGURE 4-19

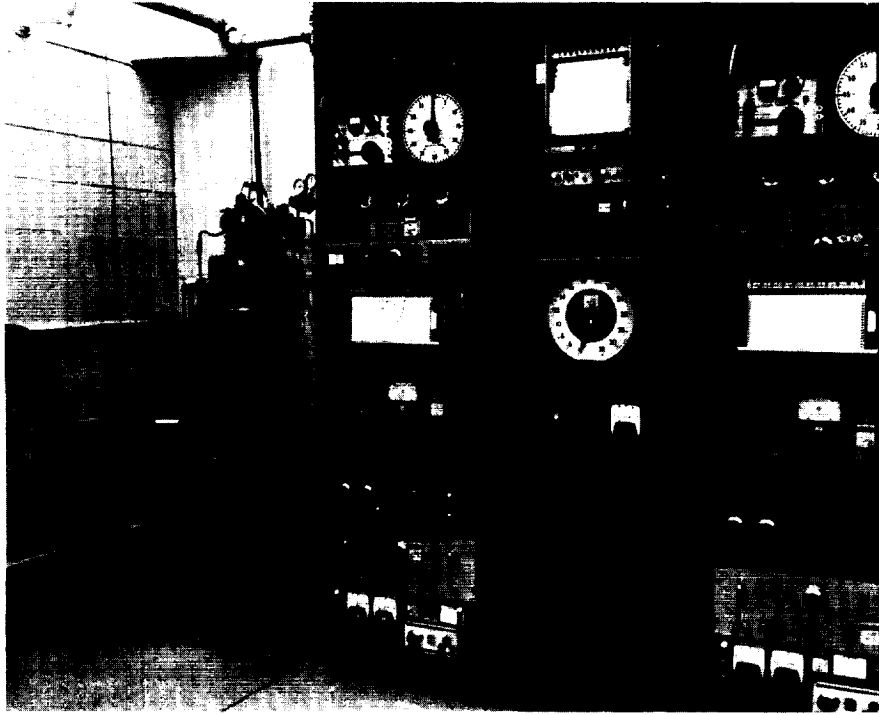
TABLE 4-10  
COATING WEIGHT AND THICKNESS  
SUMMARY FOR SUB-SIZE FS-85 RIB STIFFENED PANELS

PANEL NO.	DIFF WT (MG/CM <sup>2</sup> )	SLURRY THICKNESS DERMITRON NDT (MG/CM <sup>2</sup> )		EDGE THICKNESS THERMOELECTRIC NDT (MILLIVOLTS)
		SKIN	RIB	
1	19.1	21-23	22-28	2.0-2.5
2	19.2	20-24	20-26	2.0-2.5
3	19.8	25-27	23-30	2.0-2.5
4	20.1	23-29	23-28	2.0-2.5
5	21.0	25-28	24-29	2.0-2.5

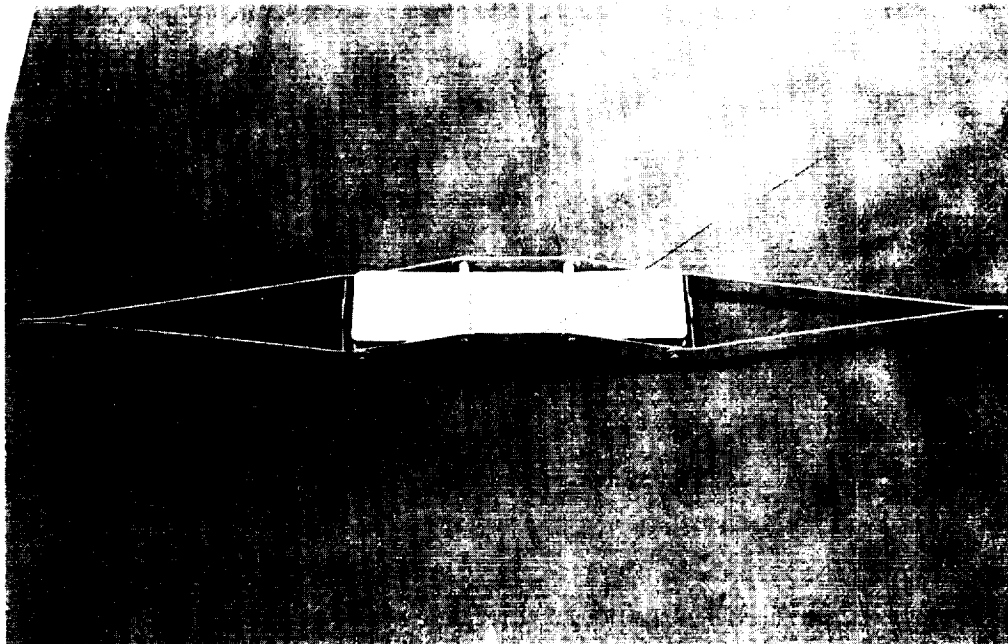
rate (mils/cycle and  $\mu\text{m}/\text{cycle}$ ) for each group of cycles conducted per panel. Elastic deflection measurements are shown in inches and centimeters measured at the center of an 11" (28 cm) span.

The most noticeable phenomenon was the large decrease (from 30 to 50%) in the measured creep and elastic deflection rates after the first group of cycles. This decrease in deflection is believed to be due to a prestressing of the coating during the first few cycles which results from cooling while under load. The zero point for creep deflection measurements is made on the panel in an "as coated" condition which is basically stress free. The panel is then heated to 2400°F (1300°C) and a bending load is applied. The deflection in the panel while it is at temperature is primarily elastic with some creep occurring. The initial coating and the additional coating growth which forms while at temperature, are in a stress-free state because of their plasticity. Cooling the coated panel under load and then releasing the load produces a compressive stress in the coating on the rib side of the panel. The compression strength of the coating at room temperature is such that it will not allow full elastic recovery, thus resulting in a larger creep deflection measurement. This explanation also holds for the elastic deflection measurements. The decrease in amount of deflection from the "as coated" condition, for the same applied load, results from the residual compressive stress remaining after reentry cycling which must be overcome before the panel starts to deflect. The elastic deflections remain fairly constant after the first group of reentry cycles. Additional coating growth, by diffusion, which would add to residual compressive strength is possibly balanced by the lower load carrying cross section of the panel due to columbium consumption by diffusion growth of the coating.

Creep deflections versus number of reentry cycles for panels tested in the



Astro Tube Furnace (Model 60-280) Modified for Reentry Simulation



Heat Shield Loading Fixture with Panel Installed for Testing  
ASTRO FURNACE AND LOADING FIXTURE USED FOR REENTRY SIMULATION

FIGURE 4-20



TABLE 4-11  
DEFLECTION MEASUREMENTS FOR SUB-SIZE RIB STIFFENED PANELS

PANEL NO.	PRESSURE	CYCLE NO.	DEFLECTION MEASUREMENTS		
			CREEP		ELASTIC
			GROUP RATE MILS( $\mu$ m)/CYCLE	CUMULATIVE AVERAGE RATE MILS( $\mu$ m)/CYCLE	AFTER EACH GROUP REENTRY CYCLES IN. (cm)
1	EXTERNAL	0			
		14	0.71 (18)	0.71 (18)	
		28	0.22 (5.6)	0.46 (11.7)	
		41	0.15 (3.8)	0.38 (9.7)	
		57	0.57 (14.5)	0.40 (10.2)	
		70	0.54 (13.7)	0.43 (11)	
		86	0.50 (12.7)	0.43 (11)	
		100	0.43 (11)	0.43 (11)	
2	EXTERNAL	0			
		13	0.61 (15.5)	0.61 (15.5)	
		28	-0.27 (-6.9)	0.14 (3.6)	
		40	0.17 (4.3)	0.15 (3.8)	
		56	0.75 (19)	0.32 (8.1)	
		70	0.50 (12.7)	0.36 (9.2)	
		86	0.38 (9.7)	0.36 (9.2)	
		100	0.50 (12.7)	0.38 (9.7)	
5	EXTERNAL	0			0.107 (0.272)
		15	1.30 (33)	1.30 (33)	0.083 (0.210)
		30	0.67 (17)	0.97 (24.6)	0.082 (0.208)
		45	0.33 (8.4)	0.76 (19.3)	
3	INTERNAL	0			0.091 (0.230)
		22	0.73 (18.5)	0.73 (18.5)	0.076 (0.193)
		47	0.60 (15.2)	0.66 (16.8)	0.075 (0.190)
		71	0.00 (0)	0.43 (11)	0.075 (0.190)
		86	0.33 (8.4)	0.42 (10.7)	0.076 (0.193)
		100	0.50 (12.7)	0.43 (11)	
4	INTERNAL	0			0.092 (0.234)
		25	0.80 (20.2)	0.80 (20.2)	0.082 (0.208)
		45	0.05 (1.3)	0.47 (12)	0.089 (0.226)
		67	0.09 (2.3)	0.34 (8.6)	

external and internal pressure environments are shown in Figure 4-21. It can be seen that after the panels become stabilized they have a linear creep deflection rate of approximately 0.45 mil/cycle (11.5  $\mu$ m/cycle). This amount of deflection is equivalent to 0.15" (0.38 cm) on a full size 20" (50 cm) rib stiffened heat shield panel after 100 reentry cycles.

Figure 4-22 shows the cumulative average creep deflection rate of all panels reentry cycled, grouped into pressure environments. As expected, the pressure

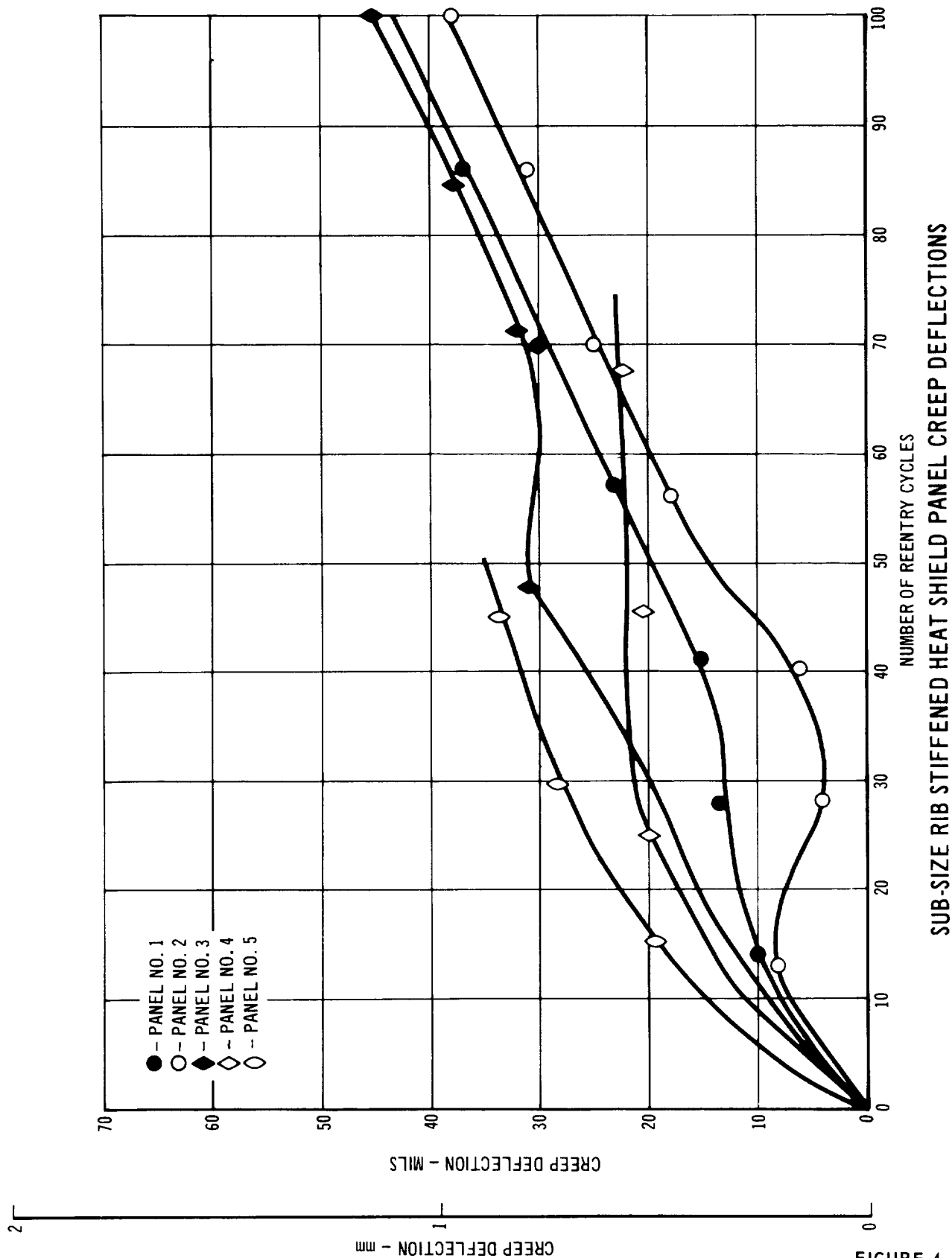
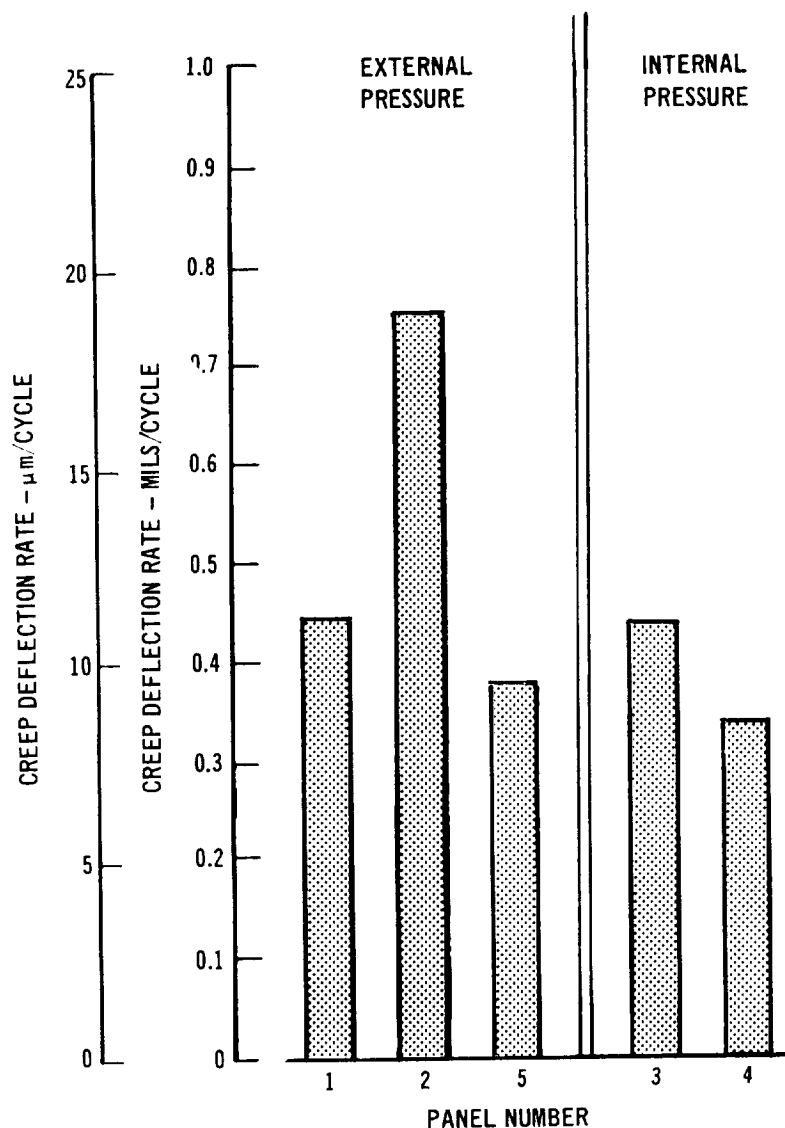


FIGURE 4-21



CREEP DEFLECTION RATE OF SUB-SIZE RIB STIFFENED HEAT  
SHIELD PANELS

FIGURE 4-22

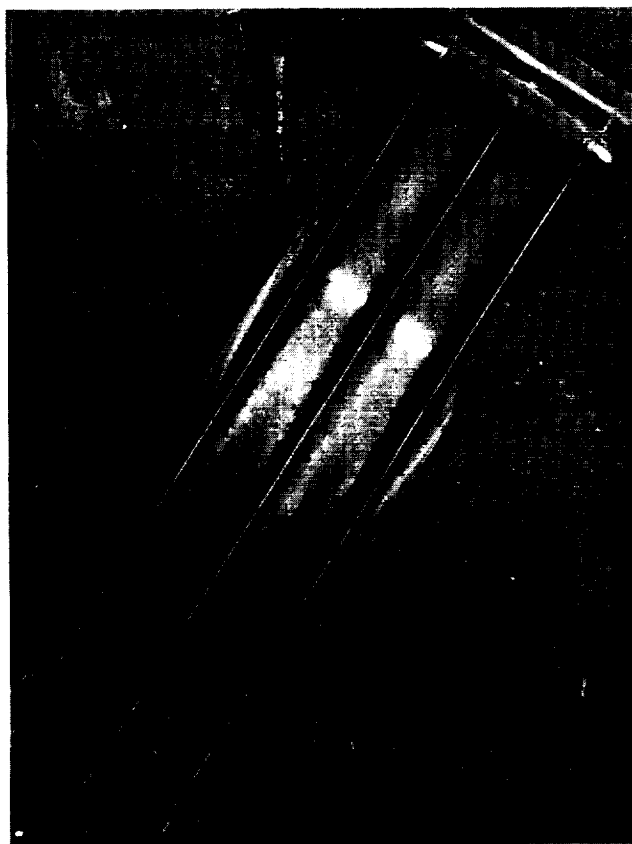
environment had no effect.

There was not one breakdown of coating produced by the environment and thus no oxidation of the substrate during reentry testing of the five subsize rib stiffened heat shield panels. These five panels contained approximately 360 linear inches (9m) of edges of 12 and 20 mil (0.03 and 0.05 cm) sheet. The one oxidation failure which was observed resulted from damage sustained on one end of Panel No. 2 during acoustic exposure. This phenomenal oxidation performance is attributed to the good edge coating procedures and optimized processing developed and employed

during this program.

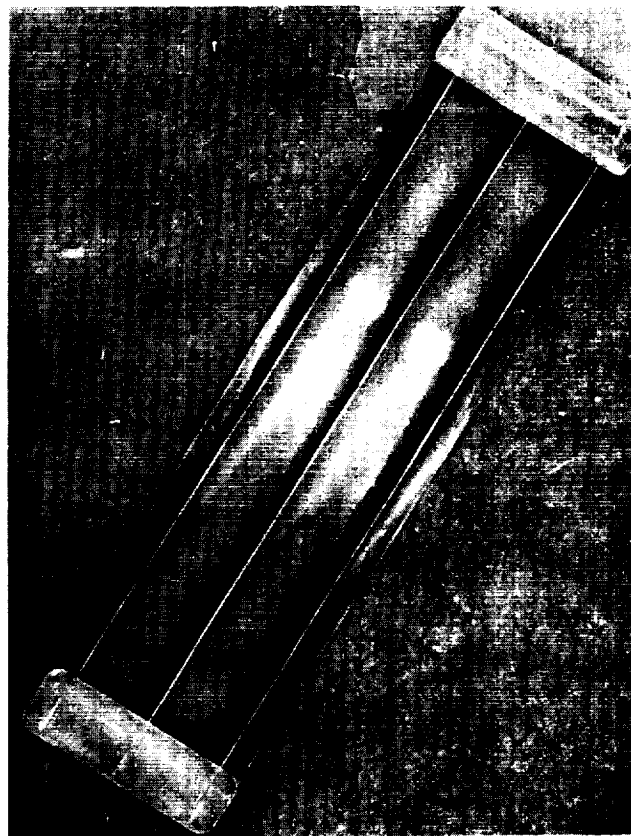
Photographs of each of the five panels are shown at various stages of testing in Figures 4-23 through 4-27. All panels structurally failed during acoustic testing. Out of five panels, three survived for 86 cycles of acoustic exposure (86 x 28.6 sec) but failed to withstand the last few hundred seconds of exposure. The remaining two panels failed structurally during acoustic testing after 30 and 77 cycles, respectively, had been completed successfully. Based on the results of these panel tests, the average fatigue life of typical R-512E coated FS-85 heat shield structure at 10,000 psi ( $69 \text{ mN/m}^2$ ) lies somewhere between 650,000 and 760,000 cycles. Fatigue life was estimated at 760,000 cycles prior to testing. The early fatigue failure of Panel No. 5 at this time can only be attributed to a possible fabrication flaw which acted as a stress riser. Photomicrographs of Panel No. 2 and Panel No. 5, after structural failure, are shown in Figures 4-28 and 4-29. Close examination reveals micro cracks in the substrate at the base of the typical spikes of coating oxide. These are typical fatigue cracks and in most instances appear to exist within small areas of substrate contamination at the base of the oxide spikes.

Table 4-12 presents the results of nondestructive coating thickness measurements made on the five subsize heat shield panels before and after reentry cycling. The Dermatron eddy current device was used for thickness measurements. Excellent coating uniformity for each panel was revealed in the "as coated" condition. Panels No. 1 and No. 2 showed lower overall coating thickness compared to Panels No. 3, No. 4 and No. 5. However, this does not agree with average weight change due to coating. The changes in coating thickness, as detected by NDT, due to reentry cycling are shown for 12 of the 16 measurement locations. Panels tested in the external pressure environment had larger coating thickness increases than the panels tested in the internal pressure environment. This would appear due to larger coating oxide build-up, which occurs because of more available oxygen in the external pressure environments. The NDT thickness data for the subsize panels compares favorably with the NDT data for the miniature panels in the external pressure environment. The NDT data for the subsize panels tested in the internal pressure environment shows a slight increase in thickness after 100 cycles of exposure, whereas slight thickness losses were shown for the miniature heat shield panels. This indicates some slight variation in environments between the small and large reentry simulators.



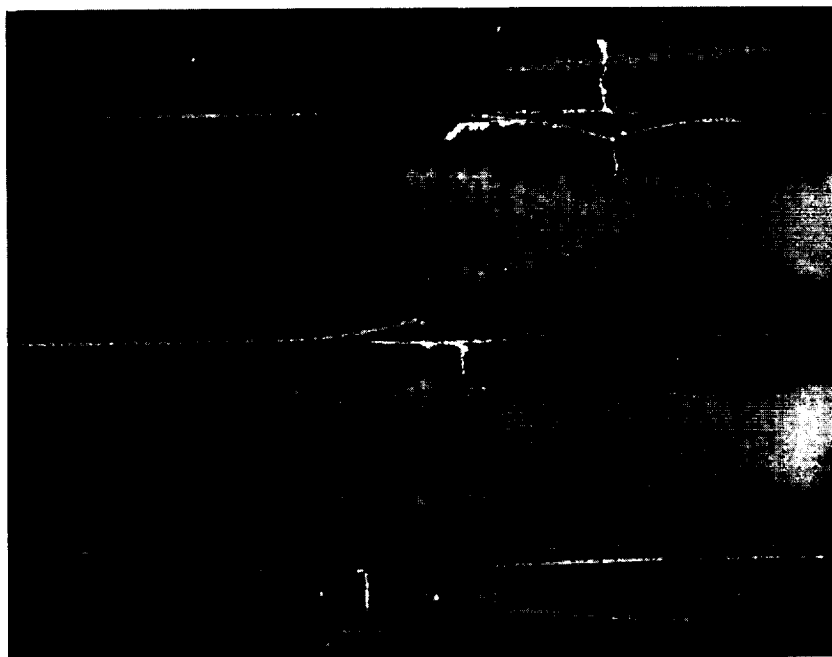
A) AFTER 70 REENTRY AND ACOUSTIC CYCLES

.38X



B) AFTER 100 REENTRY CYCLES AND 86 ACOUSTIC CYCLES

.38X

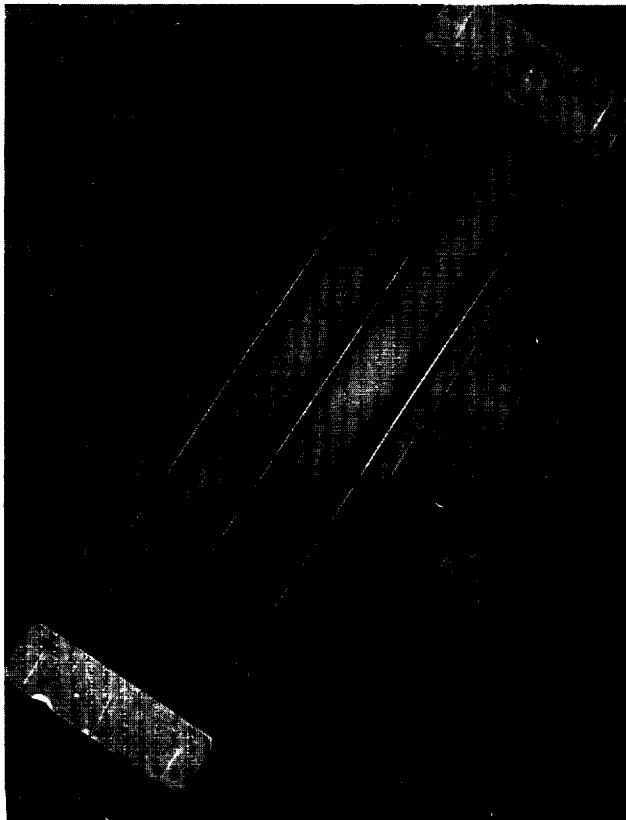


C) AFTER 100 REENTRY AND ACOUSTIC CYCLES

1X

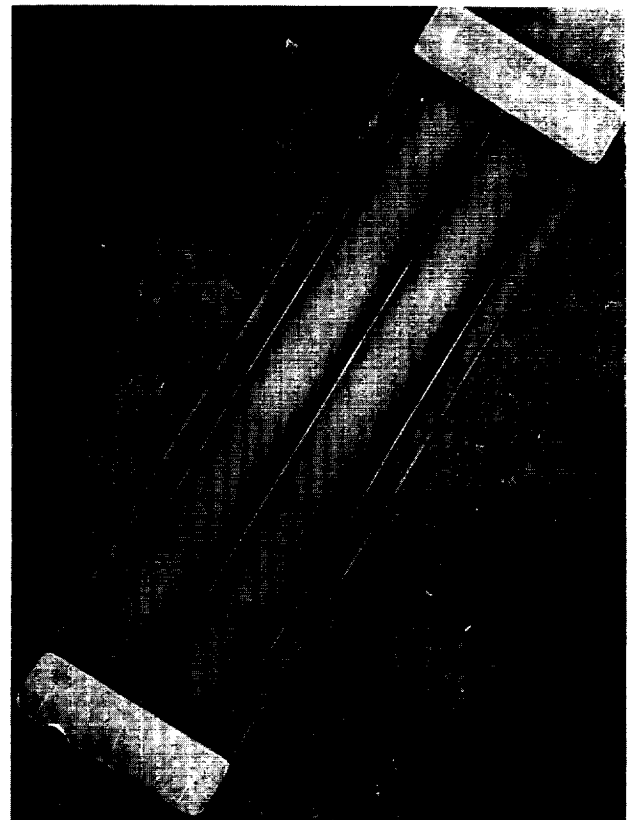
FLIGHT SIMULATION TESTING OF PANEL NO. 1

FIGURE 4-23



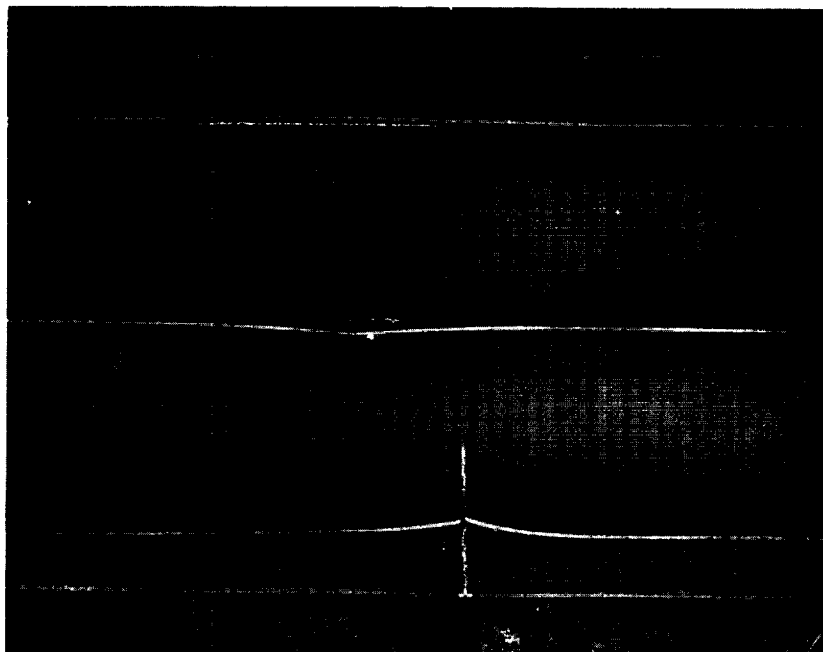
A) AFTER 86 REENTRY AND ACOUSTIC CYCLES

.38X



B) AFTER 100 REENTRY CYCLES AND 86 ACOUSTIC CYCLES

.38X

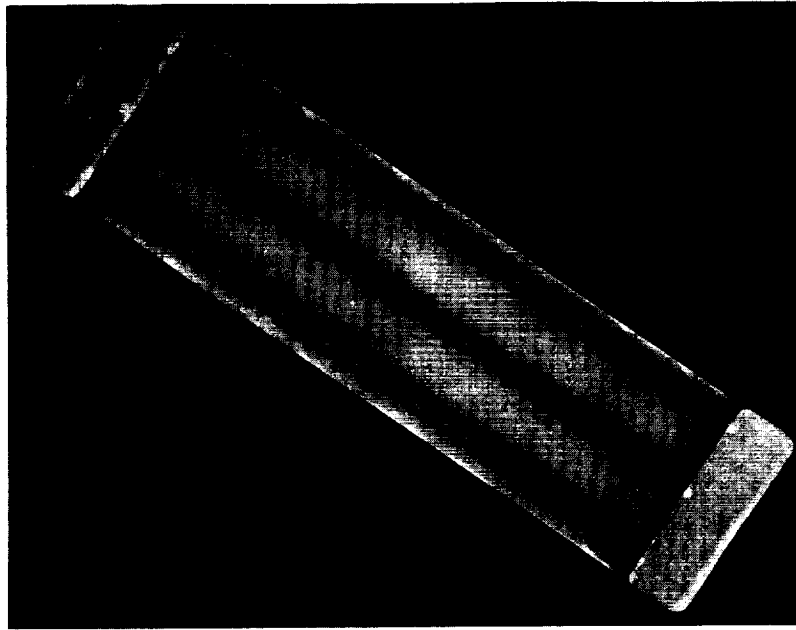


C) AFTER 100 REENTRY AND ACOUSTIC CYCLES

.9X

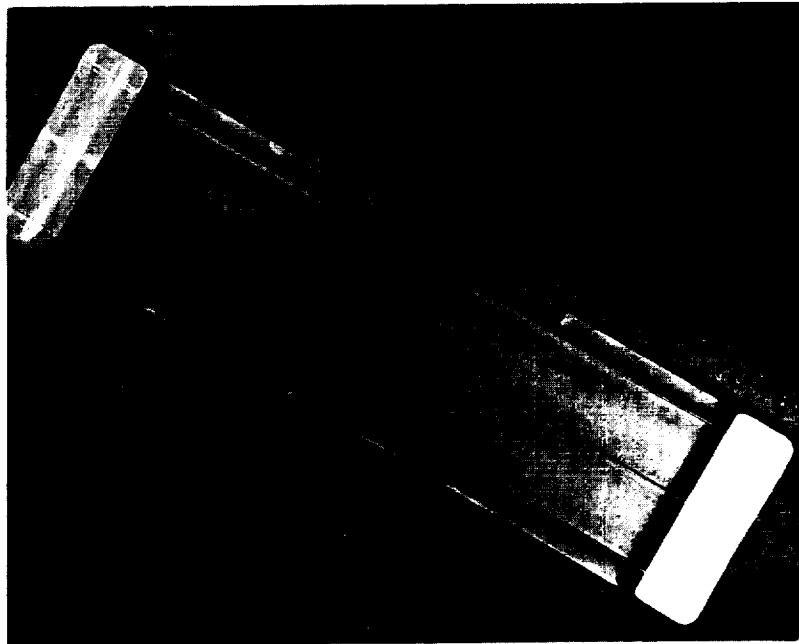
FLIGHT SIMULATION TESTING OF PANEL NO. 2

FIGURE 4-24



.38X

A) AS COATED PRIOR TO TESTING

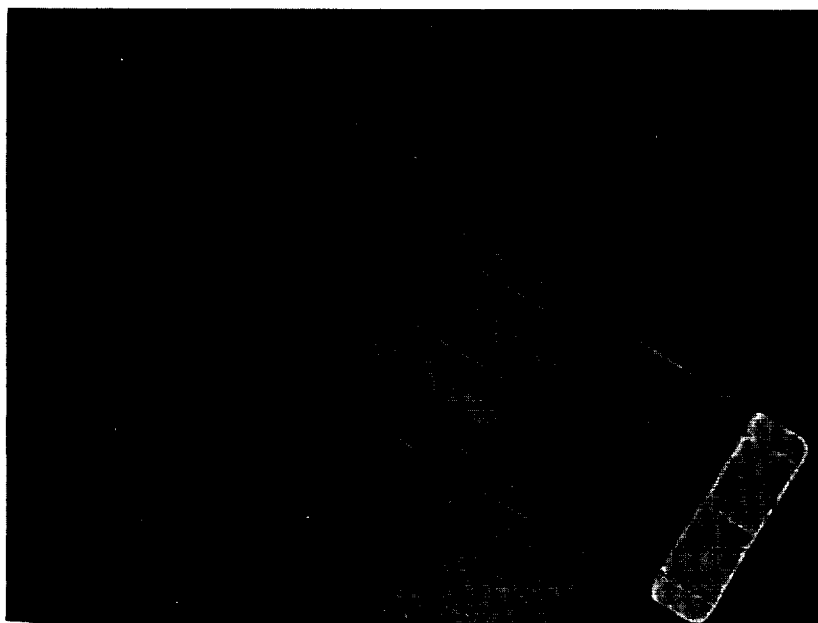


.38X

B) AFTER 100 REENTRY CYCLES AND 86 ACOUSTIC CYCLES

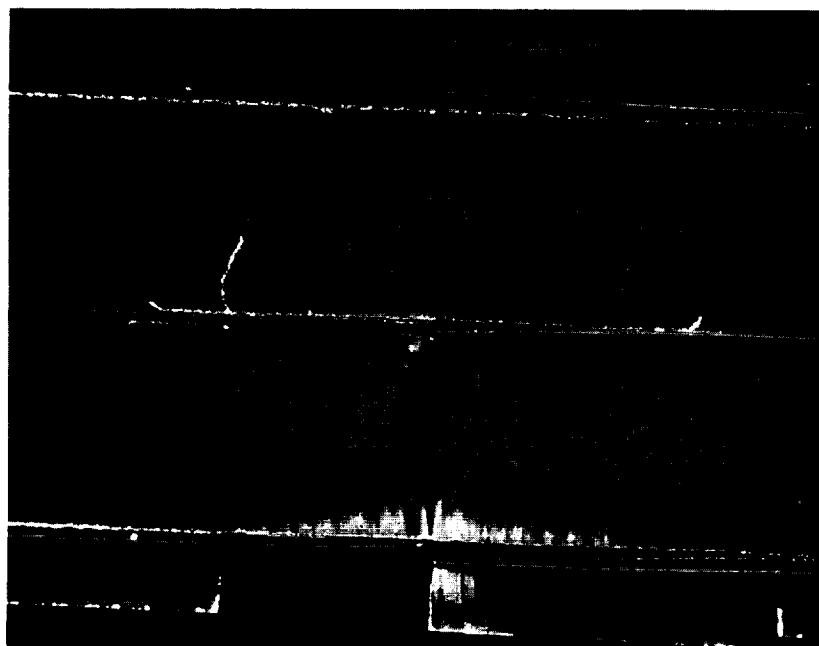
### FLIGHT SIMULATION TESTING OF PANEL NO. 3

FIGURE 4-25



.38X

A) AFTER 67 REENTRY CYCLES AND 45 ACOUSTIC CYCLES



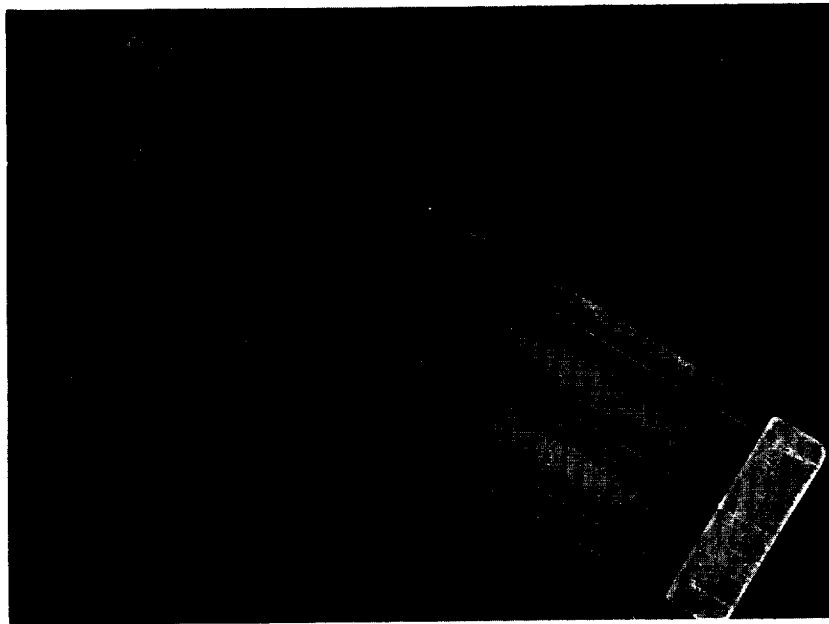
1X

B) AFTER 67 REENTRY AND ACOUSTIC CYCLES

### FLIGHT SIMULATION TESTING OF PANEL NO. 4

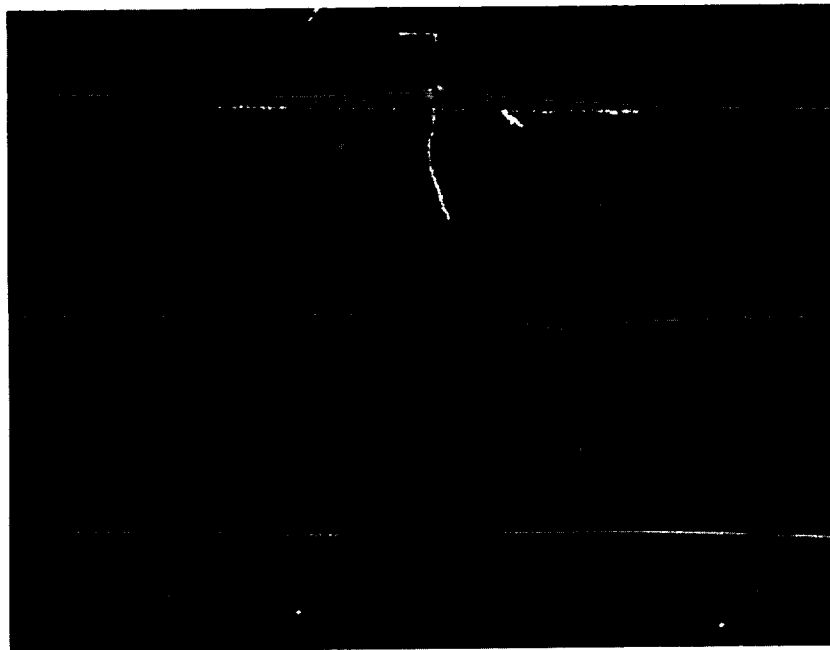
FIGURE 4-26





.36X

A) AFTER 45 REENTRY CYCLES AND 30 ACOUSTIC CYCLES

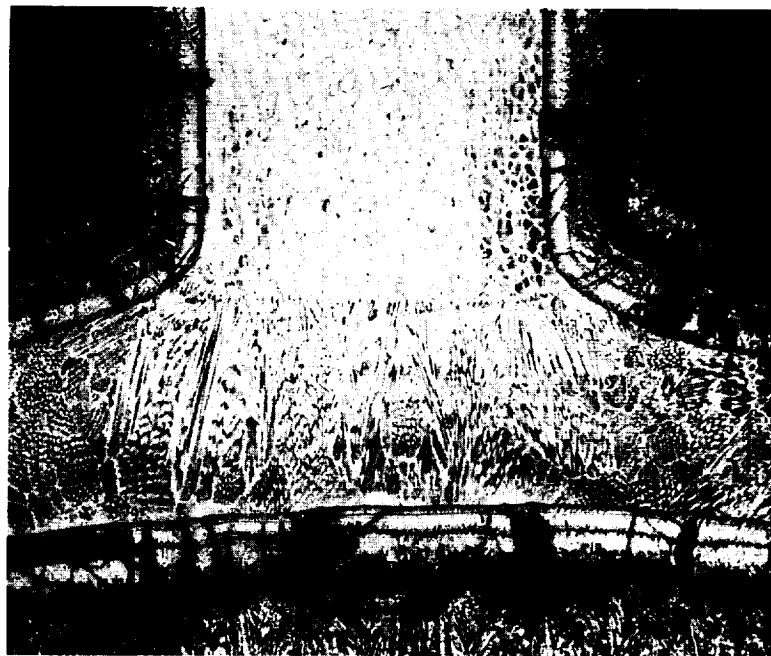


.9X

B) AFTER 45 REENTRY AND ACOUSTIC CYCLES

FLIGHT SIMULATION TESTING OF PANEL NO. 5

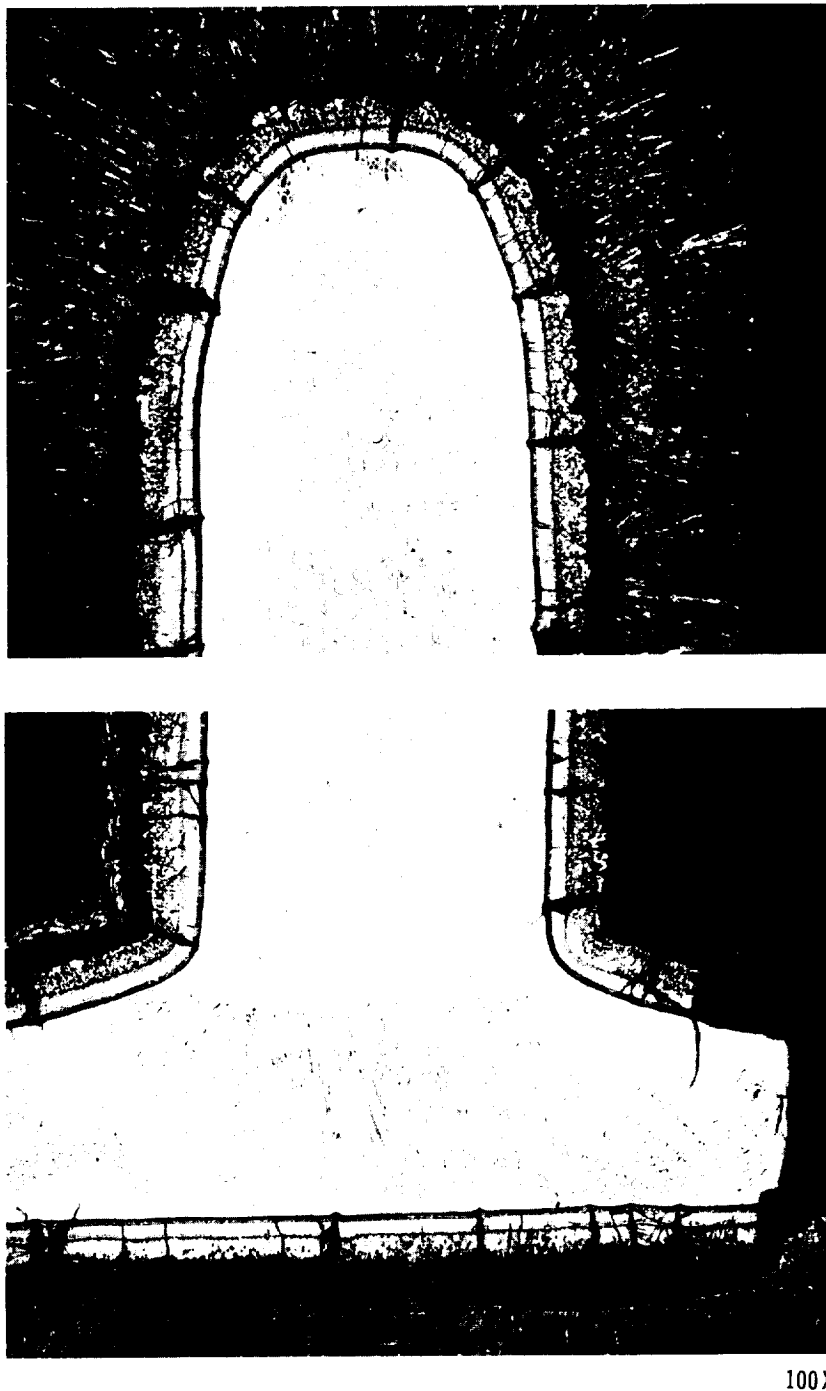
FIGURE 4-27



100 X

HEAT SHIELD PANEL NO. 2 AFTER 100 CYCLES – EXTERNAL PRESSURE  
1/4" (0.6 CM) FROM RIB FRACTURE

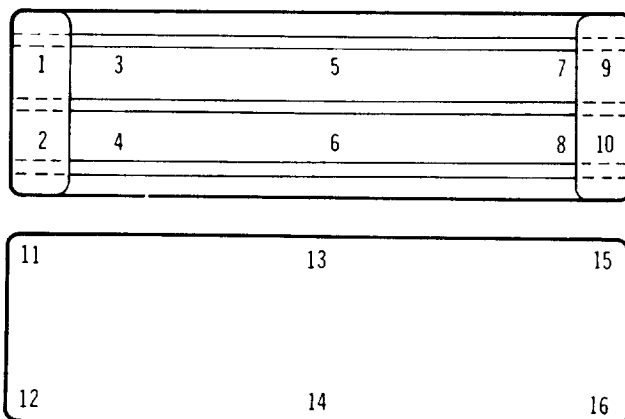
FIGURE 4-28



HEAT SHIELD PANEL NO. 5 AFTER 45 CYCLES – EXTERNAL PRESSURE  
1/4 IN. (0.6 CM) FROM RIB FRACTURE

FIGURE 4-29

TABLE 4-12  
NDT DERMITRON COATING THICKNESS ON R-512E COATED FS-85  
SUB-SIZE PANELS



PANEL NO.	NO. OF REENTRY CYCLES	COATING THICKNESS MILS/ $\mu$ m AT LOCATION															
		1	2	3	4	5	6	7	8	9	10	11	12	13	14	15	16
1	0	$\frac{2.9}{74}$	$\frac{2.9}{74}$	$\frac{3.2}{81}$	$\frac{3.5}{89}$	$\frac{3.7}{94}$	$\frac{3.6}{91}$	$\frac{3.2}{81}$	$\frac{3.5}{89}$	$\frac{2.9}{74}$	$\frac{3.2}{81}$	$\frac{2.9}{74}$	$\frac{3.1}{79}$	$\frac{3.1}{79}$	$\frac{2.9}{74}$	$\frac{3.1}{79}$	$\frac{2.8}{71}$
	100			$\frac{4.5}{114}$	$\frac{4.7}{119}$	$\frac{4.3}{109}$	$\frac{3.7}{94}$	$\frac{3.6}{91}$	$\frac{4.0}{101}$			$\frac{3.6}{91}$	$\frac{3.6}{91}$	$\frac{5.3}{136}$	$\frac{4.4}{111}$	$\frac{4.0}{101}$	$\frac{3.3}{84}$
2	0	$\frac{2.7}{69}$	$\frac{2.9}{74}$	$\frac{2.9}{74}$	$\frac{3.2}{81}$	$\frac{2.9}{74}$	$\frac{2.9}{74}$	$\frac{3.2}{81}$	$\frac{3.1}{79}$	$\frac{2.9}{74}$	$\frac{3.1}{79}$	$\frac{2.7}{69}$	$\frac{2.7}{69}$	$\frac{2.9}{74}$	$\frac{2.8}{71}$	$\frac{2.7}{69}$	$\frac{2.7}{69}$
	100			$\frac{4.5}{114}$	$\frac{4.5}{114}$	$\frac{4.7}{119}$	$\frac{4.8}{121}$	$\frac{4.0}{101}$	$\frac{3.3}{84}$			$\frac{3.1}{79}$	$\frac{3.3}{84}$	$\frac{3.3}{84}$	$\frac{3.3}{84}$	$\frac{3.3}{84}$	$\frac{3.2}{81}$
5	0	$\frac{3.6}{91}$	$\frac{3.7}{94}$	$\frac{3.6}{91}$	$\frac{3.9}{99}$	$\frac{3.2}{81}$	$\frac{3.5}{89}$	$\frac{3.6}{91}$	$\frac{3.7}{94}$	$\frac{3.2}{81}$	$\frac{3.2}{81}$	$\frac{3.5}{89}$	$\frac{3.3}{84}$	$\frac{3.7}{94}$	$\frac{3.5}{89}$	$\frac{3.5}{89}$	$\frac{3.6}{91}$
	45			$\frac{3.7}{94}$	$\frac{4.1}{104}$	$\frac{3.9}{99}$	$\frac{4.0}{101}$	$\frac{3.9}{99}$	$\frac{4.1}{104}$			$\frac{3.6}{91}$	$\frac{3.5}{89}$	$\frac{4.0}{101}$	$\frac{3.7}{94}$	$\frac{3.6}{91}$	$\frac{3.7}{94}$
3	0	$\frac{3.6}{91}$	$\frac{3.3}{84}$	$\frac{3.9}{99}$	$\frac{4.0}{101}$	$\frac{3.3}{84}$	$\frac{3.5}{89}$	$\frac{3.1}{79}$	$\frac{3.3}{84}$	$\frac{3.5}{89}$	$\frac{3.6}{91}$	$\frac{3.6}{91}$	$\frac{3.6}{91}$	$\frac{3.5}{89}$	$\frac{3.5}{89}$	$\frac{3.5}{89}$	$\frac{3.6}{91}$
	100			$\frac{4.4}{111}$	$\frac{4.5}{114}$	$\frac{4.8}{121}$	$\frac{4.5}{114}$	$\frac{4.7}{119}$	$\frac{4.0}{101}$			$\frac{4.4}{111}$	$\frac{4.4}{111}$	$\frac{4.1}{104}$	$\frac{4.1}{104}$	$\frac{3.6}{91}$	$\frac{3.5}{89}$
4	0	$\frac{3.5}{89}$	$\frac{3.6}{91}$	$\frac{3.5}{89}$	$\frac{3.1}{79}$	$\frac{3.3}{84}$	$\frac{3.2}{81}$	$\frac{3.2}{81}$	$\frac{3.7}{94}$	$\frac{3.2}{81}$	$\frac{3.3}{84}$	$\frac{3.9}{99}$	$\frac{3.7}{94}$	$\frac{3.5}{89}$	$\frac{3.7}{94}$	$\frac{3.6}{91}$	$\frac{3.6}{91}$
	67			$\frac{3.7}{94}$	$\frac{3.6}{91}$	$\frac{3.5}{89}$	$\frac{3.6}{91}$	$\frac{3.3}{84}$	$\frac{3.9}{99}$			$\frac{4.0}{101}$	$\frac{4.0}{101}$	$\frac{3.6}{91}$	$\frac{3.9}{99}$	$\frac{3.7}{94}$	$\frac{3.7}{94}$

The fused slurry silicide coating applied to subsize rib stiffened heat shield panels utilizing optimized processing techniques developed in this program performed outstandingly. The good coating quality was evidenced by the absence of any coating failures during reentry testing; 60% of the tests were conducted for 100 reentry cycles.

The reuse evaluation testing was also designed to determine structural performance under service conditions which would be expected on Space Shuttle vehicles for 100 flights. From this aspect the coating and panel were treated as an integral unit. The failure criterion was structural life. There were no structural failures due to the application of flight loads; the structural failures were induced by acoustic exposure. However, acoustic environment simulation was designed to produce fatigue failures in 100 flights. Reasons for this were explained in Section 1.0. In actual practice, heat shield panel design factors would include allowances for fatigue life in order to obtain reliable structural performance for 100 flights.

4.3.2 Full Size Panels - Two full size 20" x 20" (50 cm x 50 cm) rib stiffened heat shield panels were fabricated from FS-85 alloy sheet. Material gages, rib spacing and height were the same as those utilized on the subsize panels. Fabrication procedures were also identical, except that the full size panels were subjected to a creep flattening procedure to remove the skin distortion between the welds. The undesirable skin distortion was caused by shrinkage of the electron beam fusion weld which joined the ribs to the skin. The creep flattening was successfully performed using machined molybdenum tooling and a vacuum heat cycle of one hour (36 h sec) at 2700°F (1480°C).

The two full size rib stiffened FS-85 columbium alloy heat shield panels were prepared for slurry coating using the processes optimized on the subsize panels. The slurry bath was checked for correct weight pickup and coating uniformity using 20" (50 cm) stainless strips. Slight adjustments to the slurry viscosity were made to produce a coating thickness of 21 mg/cm<sup>2</sup> of green coating. A weight loss of approximately 2 mg/cm<sup>2</sup> was expected during diffusion which should have brought the final coated weight to 19 mg/cm<sup>2</sup>. The program goal was 19 ±3 mg/cm<sup>2</sup>.

The first large FS-85 panel was dipped and had an average weight gain of 20 mg/cm<sup>2</sup>. However, NDT (Dermitron) analysis of the green slurry after drying indicated that the rib side averaged 2 mg/cm<sup>2</sup> heavier than the skin side and the skin side had some areas as low as 13 mg/cm<sup>2</sup>. These results were not consistent

with those obtained on flat rib stiffened stainless steel mockups previously coated. Recoating of the stainless mockups was then performed to check on slurry performance. The results showed excellent coating uniformity - as good as that obtained earlier in the program.

The FS-85 alloy panels had a slight warp or twist resulting from welding the end straps to the ribs after creep flattening, which changed the angle at which the skin exits from the slurry surface during dip coating. A review of the NDT data showed a correlation between the coating nonuniformities and the panel twist. These nonuniformities were also possibly related to the narrow slurry tank 3" (7.5 cm) wide and the resultant difficulties in centering the twisted panel, causing it to be within 1/4" (0.6 cm) of the tank wall during part of the withdrawal procedure.

Experiments were run with flat stainless steel sheets close to the tank wall, and a nonuniformity of approximately  $1 \text{ mg/cm}^2$  was noted, indicating the major problem to be in the twist of the panel.

To avoid another creep flattening of the panel it was decided to apply a slightly heavier coating to the panel which would reduce the effects of nonuniformity due to panel twist. A rigid clamp fixture was also used. This fixture held the panel closer to a perpendicular exit angle than suspension wire hooks used on the first trial coat. The panel was cleaned and the withdrawal speed adjusted to produce a heavier pickup, and the panel was dipped. An average green coating weight of  $24 \text{ mg/cm}^2$  was achieved. This should produce a fired coating weight of  $22 \text{ mg/cm}^2$ . The green coating on the skin side was found to range from 21 to  $25 \text{ mg/cm}^2$  and on the rib side ranges from 22 to  $27 \text{ mg/cm}^2$ . The NDT inspection data on the green coated panel is shown in Figure 4-30.

The panel was diffusion treated for 1 hour at  $2580^\circ\text{F}$  (36 h sec at  $1420^\circ\text{C}$ ). The average coating weight after firing was  $22 \text{ mg/cm}^2$  as determined by weight change. Approximately  $7 \text{ mg/cm}^2$  is equivalent to 1 mil (25  $\mu\text{m}$ ) of final coating thickness. NDT (Dermatron) measurements were taken at 60 locations and the average of the NDT measurements was found to be  $23 \text{ mg/cm}^2$ , showing a good correlation between this NDT method and coating thickness. The NDT average for the rib side was  $23.8 \text{ mg/cm}^2$ , and for the skin side it was  $22.1 \text{ mg/cm}^2$ . The differential, though insignificant, is attributed to the geometry of the panel which affects the slurry deposition as the part is withdrawn from the slurry bath. The results of the NDT thickness studies on the completed panel are shown in

24		22				23	
26	23	23	24	23	23	23	22
27	24	24	25	24	24	24	24
26	24	25	25	24	25	25	24
25		25				25	

22	23	22	22	22	22	22	23
23	23	23	22	22	22	23	22
21	23	22	22	22	22	22	22

GREEN COATING UNIFORMITY STUDY BY DERMITRON NDT - PANEL 8C0

FIGURE 4-30

Figure 4-31. The coating was found to have local thickness variations of from 20 to 26 mg/cm<sup>2</sup>, which is within the program goal of  $\pm 3$  mg/cm<sup>2</sup>. This is better than a 50% reduction in the  $\pm 7$  mg/cm<sup>2</sup> variation typical prior to this process optimization study.

Additional slurry was applied to all the edges on this panel by the slurry-beading technique previously described. NDT inspection of the coating on the edges using the thermoelectric roller showed a reading of 2.0 to 2.4 millivolts, which is equivalent to readings previously obtained on the subscale subsize panels. Typical readings are shown in Figure 4-32.

The second 20" x 20" (50 cm x 50 cm) rib stiffened panel was dipped and found to have coating variations similar to those found on the first panel. It was decided to clean the panel of the green coating and attempt to flatten it by strain relieving at 2600°F (1425°C). This treatment was not successful; the panel retained its slight twist. Some slight handling damage was sustained during the strain relieving operation which was repaired by EB welding.

The panel was processed through coating and sustained an additional slight damage in the repair zone due to handling. A decision was reached to coat the panel in its damaged condition. The slurry was applied by the methods employed for the first panel and 24.7 mg/cm<sup>2</sup> average green coating was obtained, compared to 24.0 for the first panel coated. The skin side averaged 24.8 mg/cm<sup>2</sup> and the rib side 24.3 mg/cm<sup>2</sup> prior to firing, as determined by NDT. After diffusion the panel had an average coated weight of 22.2 mg/cm<sup>2</sup> as determined by weight change. The skin side averaged 22.6 mg/cm<sup>2</sup> and the rib side 22.4 mg/cm<sup>2</sup>, as determined by Dermatron NDT, and shown in Figures 4-33 and 4-34.

The edges were overcoated using the techniques employed on the first panel and NDT (thermoelectric) showed some edges having a coating thickness equivalence of 1.9 millivolts. An acceptance standard of 2.0 millivolts had been arbitrarily set and therefore the edges were recoated and diffusion treated for an additional 5 minutes at 2580°F (300 sec at 1420°C). After this treatment the NDT measurement indicated acceptable values of 2.0 to 2.5 millivolts at all the edges, as shown in Figure 4-35. Further work is required to optimize the edge coating process, so that a reproducible amount of coating can be applied.

The 20" x 20" (50 cm x 50 cm) rib stiffened panels were coated by the process developed on this program, and a significant improvement in coating uniformity, edge coverage and slurry stability were demonstrated. The process specification



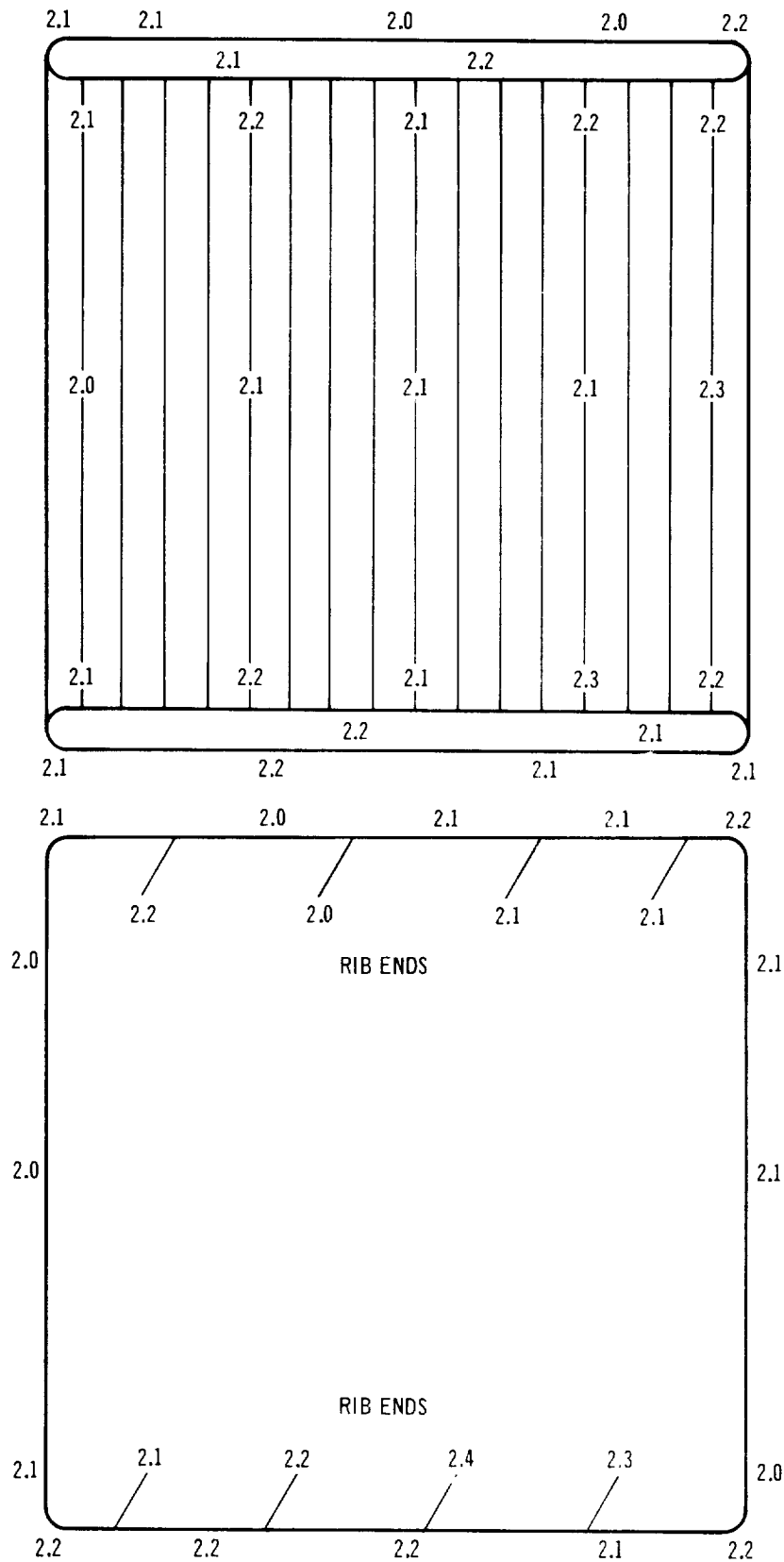
# FINAL REPORT

24		21						22						
25		21		21		22		21		20		21		21
26		24		25		24		24		24		24		24
25		25		25		25		24		25		25		24
25		25						25						

22	22	22	22	21	21	23	22
22	23	23	22	22	22	23	22
21	23	22	23	22	22	22	21

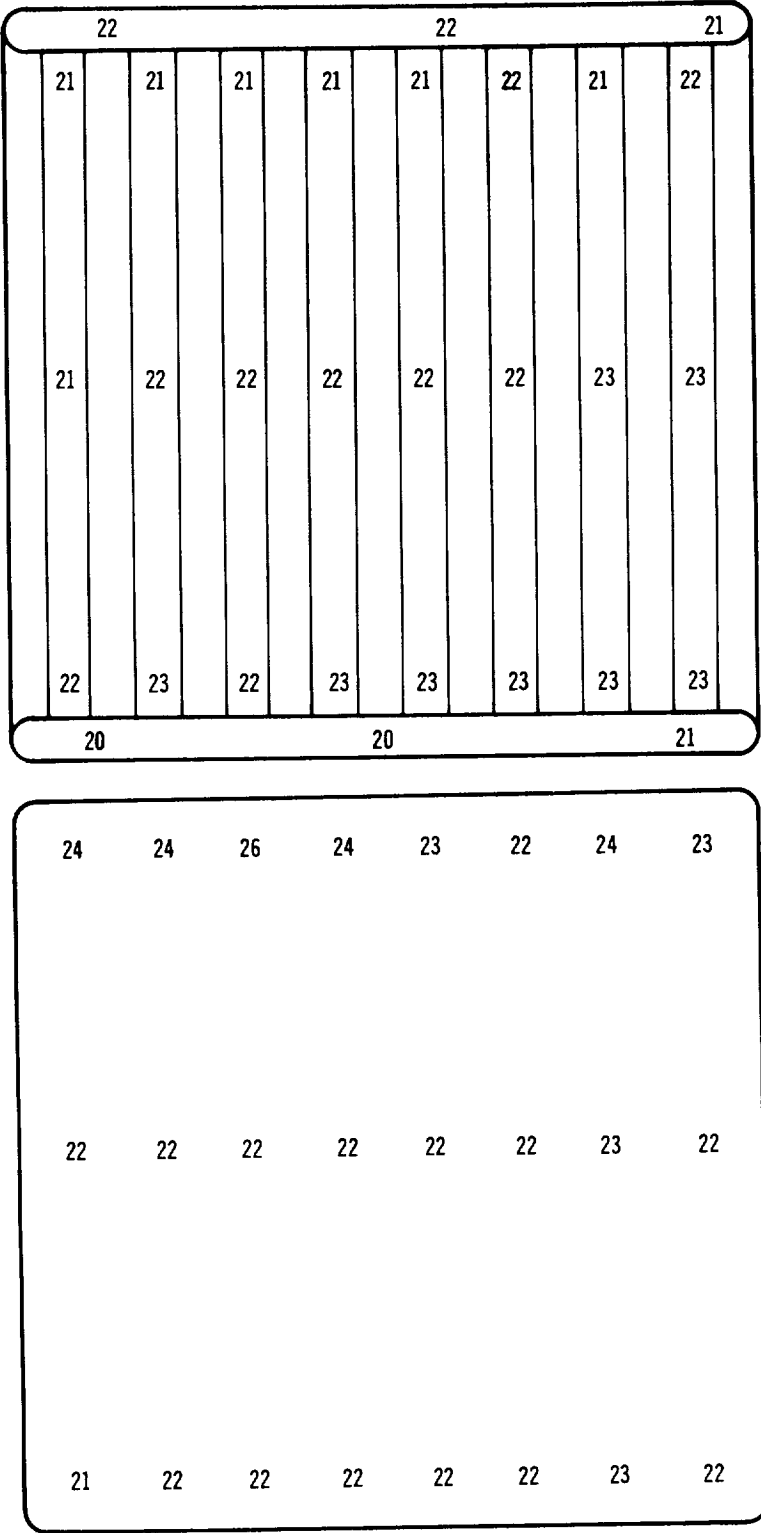
FINAL COATING UNIFORMITY STUDY BY DERMITRON NDT - PANEL 8C0

FIGURE 4-31

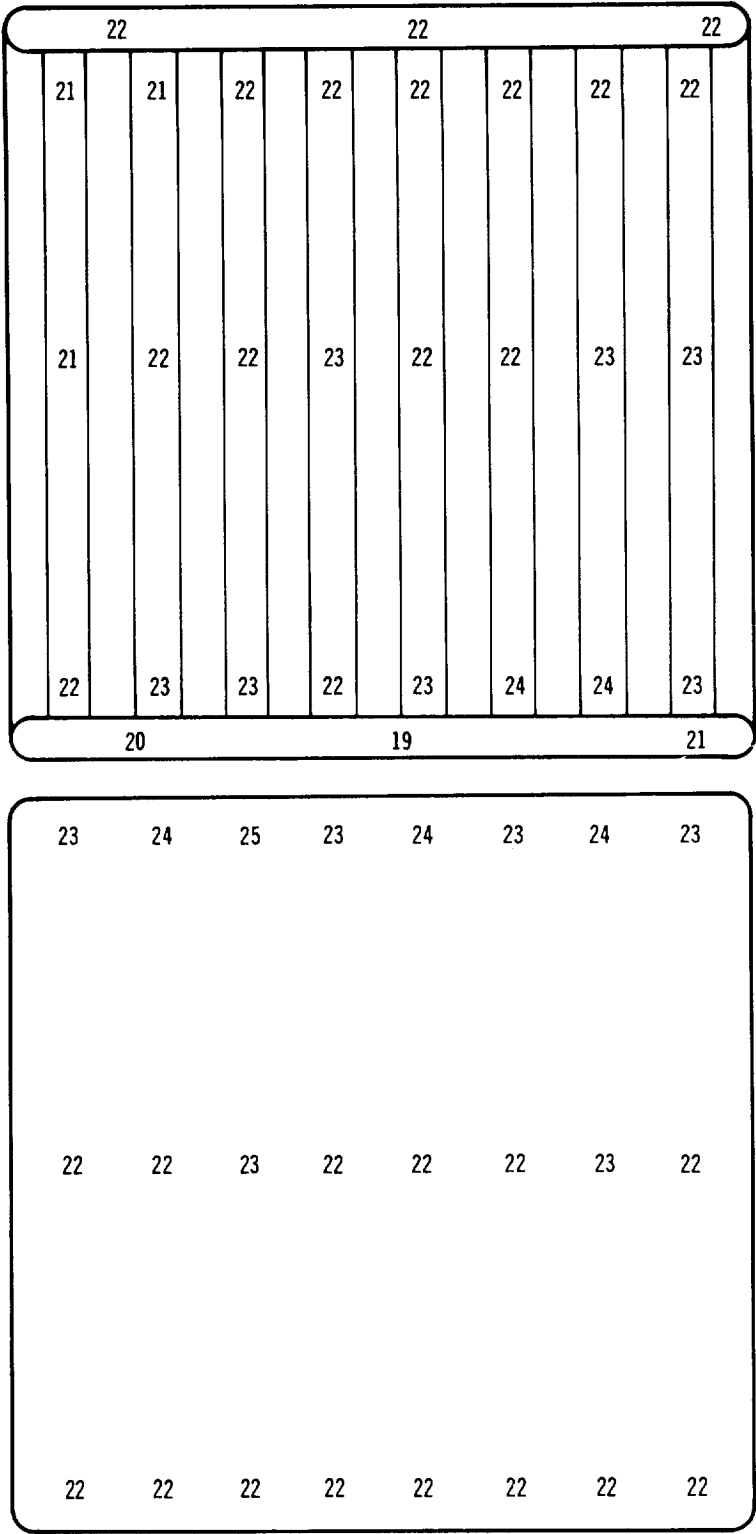


FINAL EDGE COATING THICKNESS UNIFORMITY STUDY  
BY THERMOELECTRIC NDT - PANEL 8C0

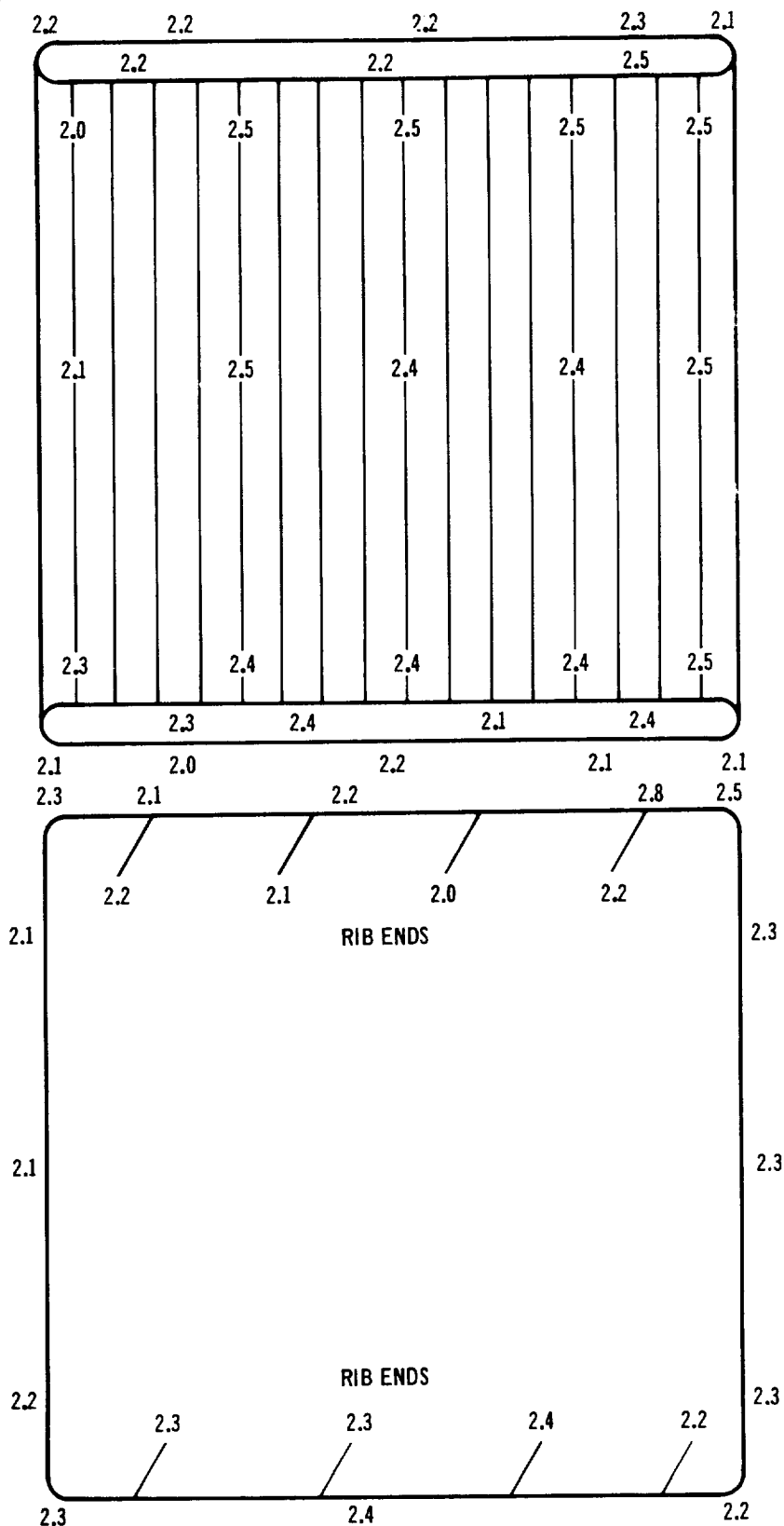
FIGURE 4-32



GREEN COATING UNIFORMITY STUDY BY DERMITRON  
NDT - PANEL 8



FINAL COATING UNIFORMITY STUDY BY DERMITRON  
NDT - PANEL 8

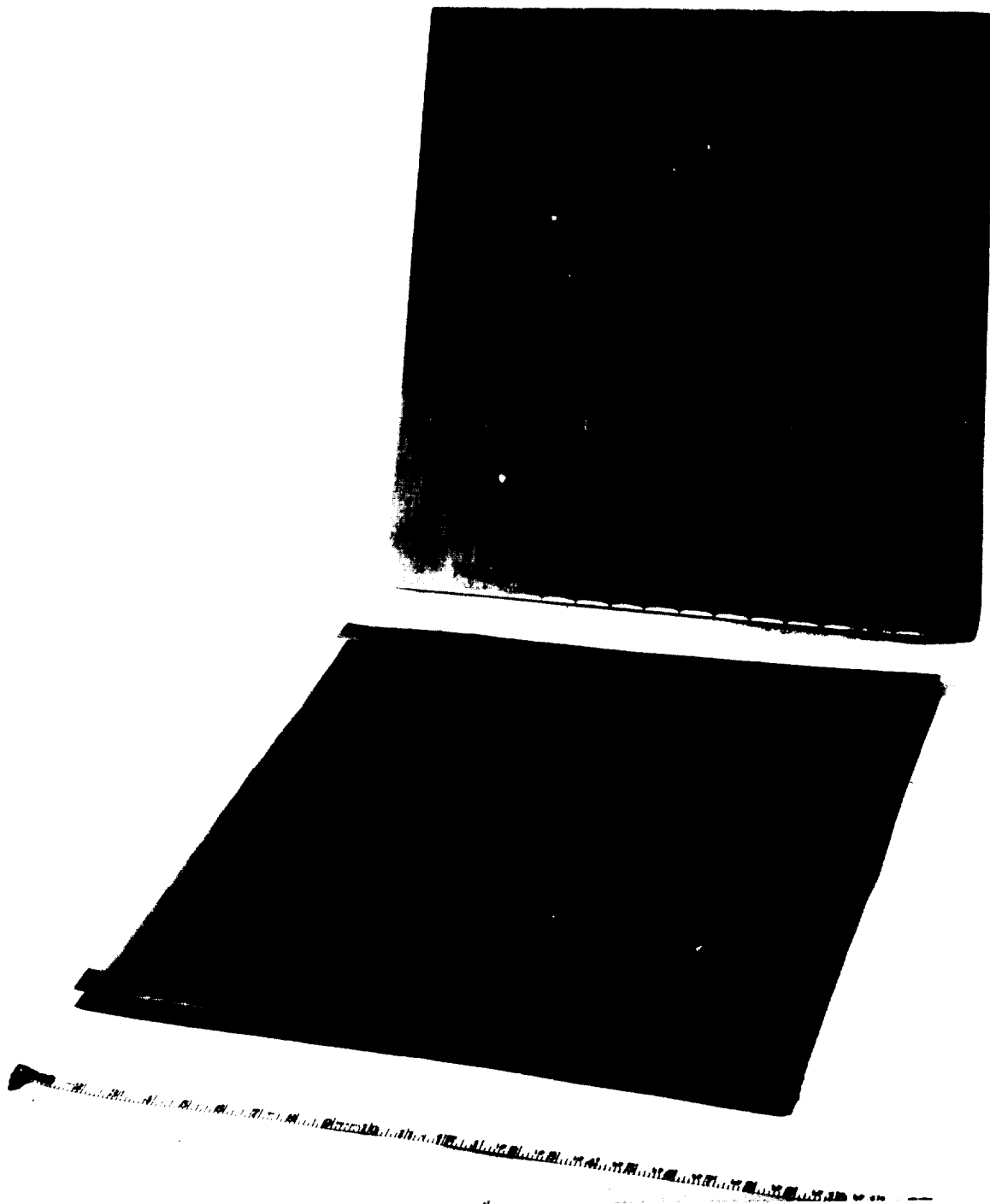


FINAL EDGE COATING THICKNESS UNIFORMITY STUDY  
BY THERMOELECTRIC NDT - PANEL 8

457-3177

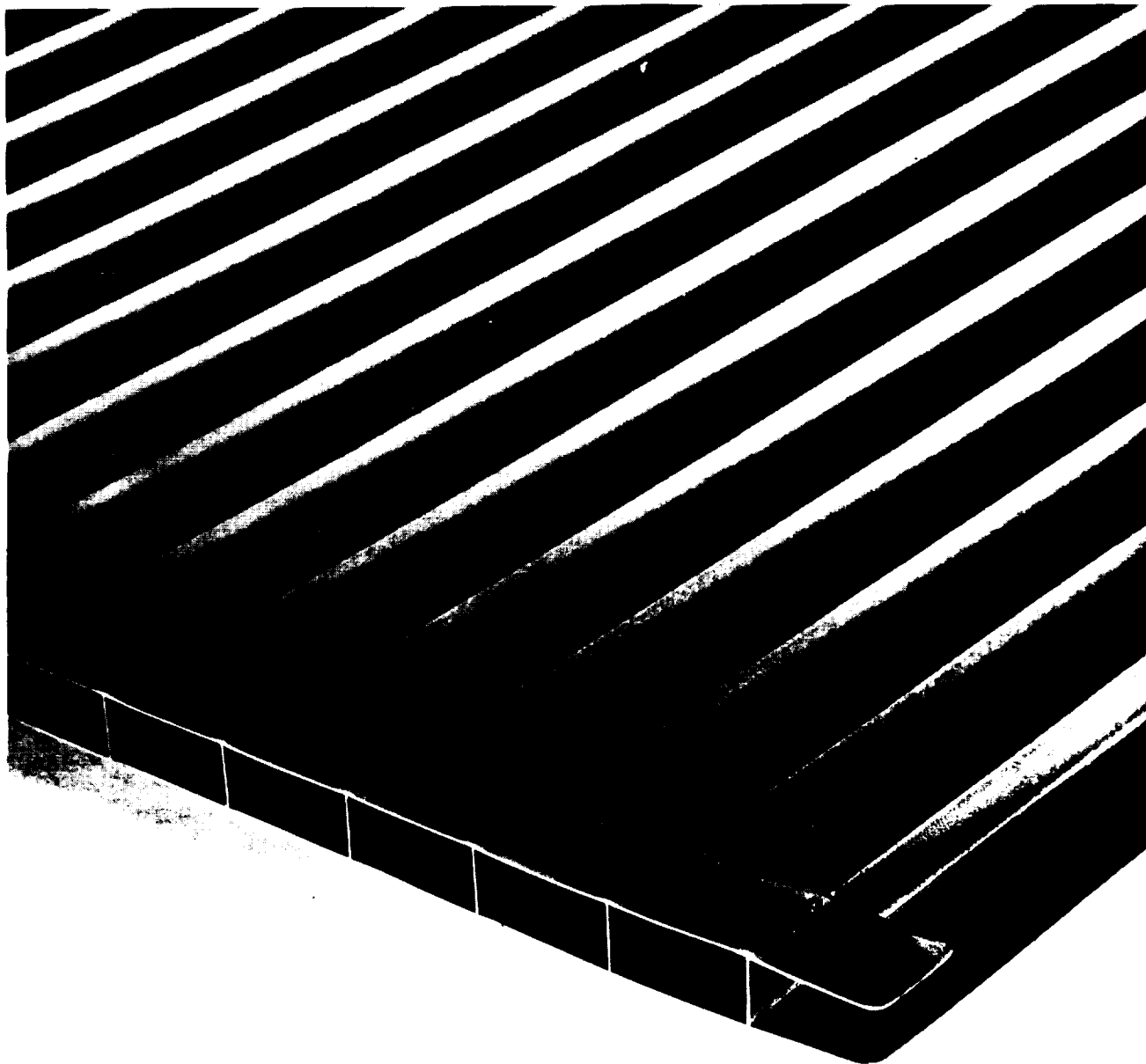
FIGURE 4-35

for application of the R-512E coating to rib stiffened panels using the C-5 slurry is presented in Section 3.0. The full size coated panels are shown in Figure 4-36 with a closeup view in Figure 4-37.



20" x 20" (50 CM x 50 CM) RIB STIFFENED FS85 ALLOY HEAT SHIELD PANEL

FIGURE 4-36



CORNER DETAIL OF 20" x 20" (50 CM x 50 CM) RIB STIFFENED FS85  
ALLOY HEAT SHIELD PANEL

FIGURE 4-37

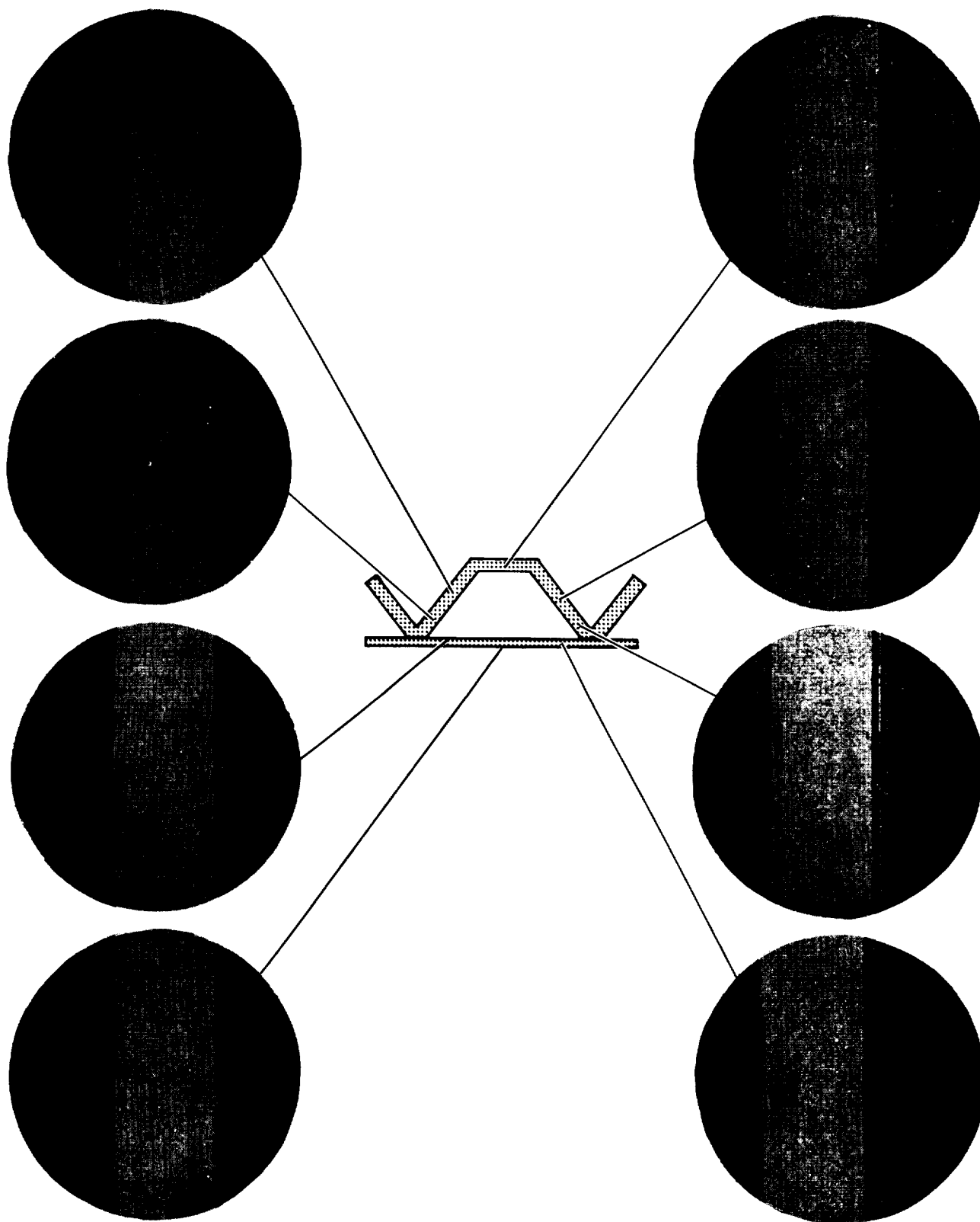


## 5.0 COATING PROCESS OPTIMIZATION AND SCALE-UP STUDIES FOR CORRUGATION STIFFENED HEAT SHIELD PANELS

5.1 Process Development - The use of corrugation stiffening of structural skins to improve efficiency has been a popular design for some time. Past hardware programs utilizing refractory metals utilized corrugation stiffening almost exclusively for heat shielding. The rib stiffened heat shield design was selected as the initial configuration for this program because it offered increased inspectability which is considered important in 100 multimission reuse. However, the strength to weight efficiency of the corrugation design cannot be overlooked because of the important role that weight plays in space vehicle systems. The corrugation design will undoubtedly be utilized in future columbium hardware systems, and because of this it was considered important to optimize and scale-up the fused slurry coating process for corrugation stiffened heat shield panels.

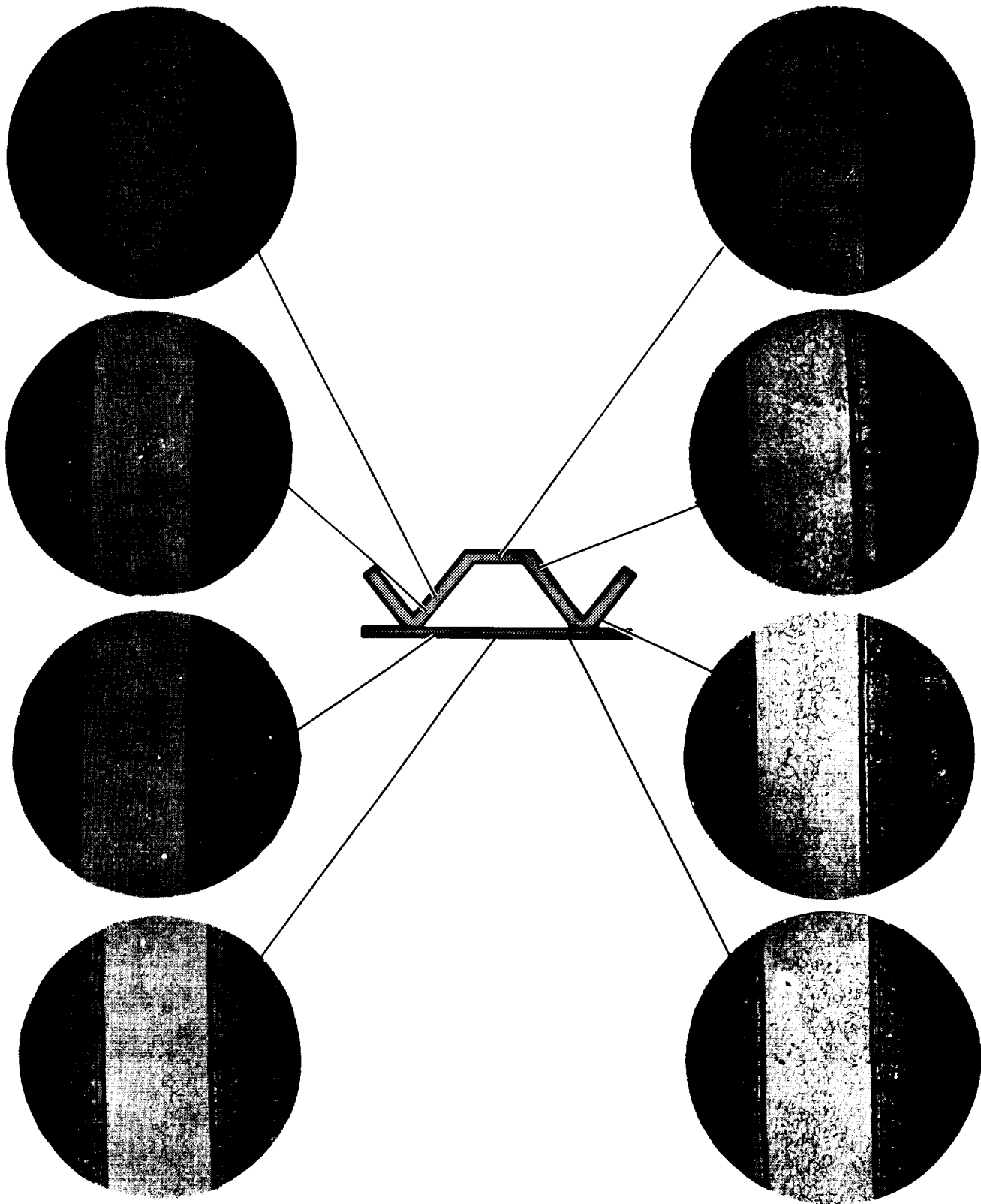
5.1.1 Slurry Formulation - Prior to initiating process development studies for the single faced corrugation configuration, preliminary work was done to determine the feasibility of using the optimized C-5 nitrocellulose based slurry which was so successful with the rib-stiffened panel design. It was anticipated that one of the major problems would be to get equal coating thickness on the inside and outside of the corrugations. Due to restricted access of air, the drying rate of the slurry is lower on the inside. There were also some questions regarding the general effect the geometry would have on coating uniformity.

To verify this behavior and to develop a base on which improvements could be made, an 18" (46 cm) long electron beam welded single faced corrugated FS-85 specimen was coated with the C-5 nitrocellulose base slurry. The specimen was subjected to several slow oxidation cycles to check for any gross lack of oxidation protection and was then sectioned in three locations, top, center, and bottom with respect to dipping direction. No gross oxidation was observed. Metallographic sections of these locations are shown in Figure 5-1, 5-2, and 5-3. The coating thickness taper from top to bottom on the inside or outside was not of a magnitude to be considered a significant problem. However, there was an interior coating thickness distribution range of 1.2 mils (30.5  $\mu\text{m}$ ) to 2.7 mils (68.6  $\mu\text{m}$ ) for the top location. The thinning occurred as the coating approached the acute angle at the weld. The same trend was evident in the center and bottom cross sections but there was not as large a range in coating thickness.



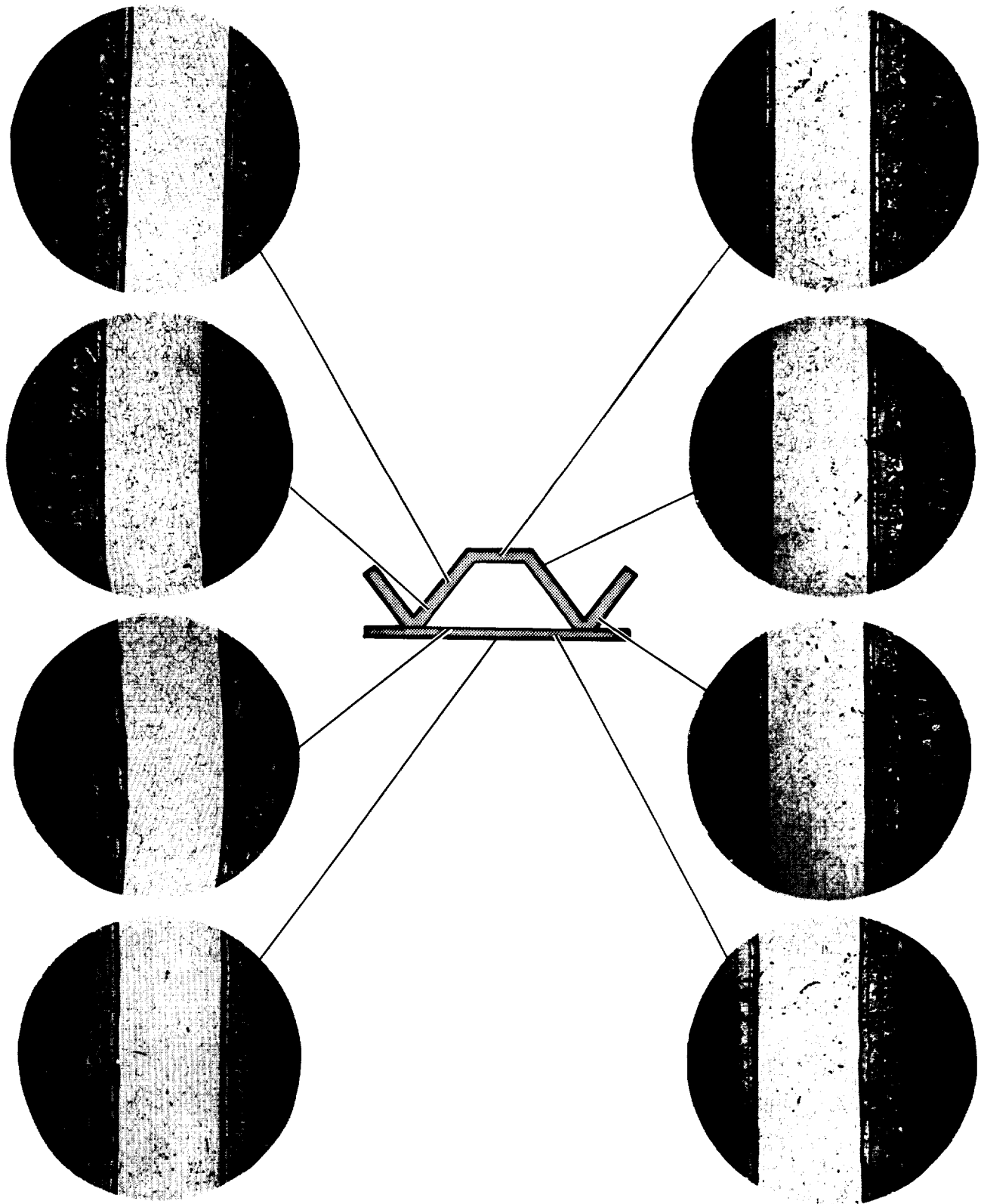
CROSS-SECTION OF 20'' (50 CM) LONG CORRUGATED SPECIMEN MADE 1''  
(2.5 CM) FROM TOP WITH RESPECT TO DIPPING DIRECTION OF SPECIMEN

FIGURE 5-1



CROSS-SECTION OF 20'' (50 CM) LONG CORRUGATED SPECIMEN MADE 9''  
(23 CM) FROM TOP WITH RESPECT TO DIPPING DIRECTION OF THE SPECIMEN

FIGURE 5 2



CROSS-SECTION OF 20'' (50 CM) LONG CORRUGATED SPECIMEN MADE 15''  
(38 CM) FROM TOP WITH RESPECT TO DIPPING DIRECTION OF SPECIMEN

FIGURE 5-3

Because of the above problem with the nitrocellulose slurry and the desire to obtain a high green slurry strength, it was decided to further the development of an acrylic based slurry having long term stability. Initial efforts performed during processing studies for rib stiffened panels, failed to produce an acrylic slurry which did not degrade within a few weeks. Apparently a reaction takes place between the thixotropic additives and the acrylic resin which decreases the effectiveness of the thixotropic additives with time. However, it was later discovered through continuing investigations, after the C-5 nitrocellulose was selected, that by using a high solids content slurry and by substituting more acrylic resin for the thixotropic agents, the slurries become more stable. A list of the slurry compositions used in the balance of the program is shown in Table 5-1.

For example, Figure 5-4 shows the slurry viscosity as a function of time for the optimized C-5 nitrocellulose based slurry and the acrylic slurries, A-22 and A-28. The A-22 slurry is based on a resin content of 4.0% and thixotropic additives MPA and Thixatrol ST. The A-28 is based on an acrylic resin content of 40% and minor amount of MPA as an agglomerate preventive. The A-22 slurry shows a decreasing viscosity with time, whereas the A-28 shows a constant viscosity after a 5 min (300 sec) stabilizing period.

The weight loss on the acrylic based slurry during the diffusion treatment is approximately  $7 \text{ mg/cm}^2$  compared to  $2 \text{ mg/cm}^2$  for the nitrocellulose slurry, C-5. This is due to the higher resin content in the dried film. It is therefore necessary to apply  $27\text{--}29 \text{ mg/cm}^2$  green instead of  $22\text{--}24 \text{ mg/cm}^2$  to obtain a coating of the desired final thickness.

5.1.2 Application Parameters - The effect of dipping speed on the coating uniformity and thickness of 2" x 20" (5 cm x 50 cm) stainless strips was then evaluated for the A-28 slurry. Good uniformity was obtained at 1-1/2" per minute (0.6 mm/sec), as shown in Figure 5-5. However, at the desired coating weights, significant coating taper was produced with this slurry. The A-28 slurry was modified to increase its viscosity by increasing the solids content, and the results obtained are shown in Figure 5-6 for the A-29 slurry. Excellent uniformity at the desired coating thickness was obtained.

Stainless steel single faced corrugated panels 2.4" wide x 18" long (6 cm x 46 cm) with a corrugation pitch of 1.2" (3 cm) and a corrugating height of 0.55" (1.4 cm) were fabricated for further processing studies. The corrugation was

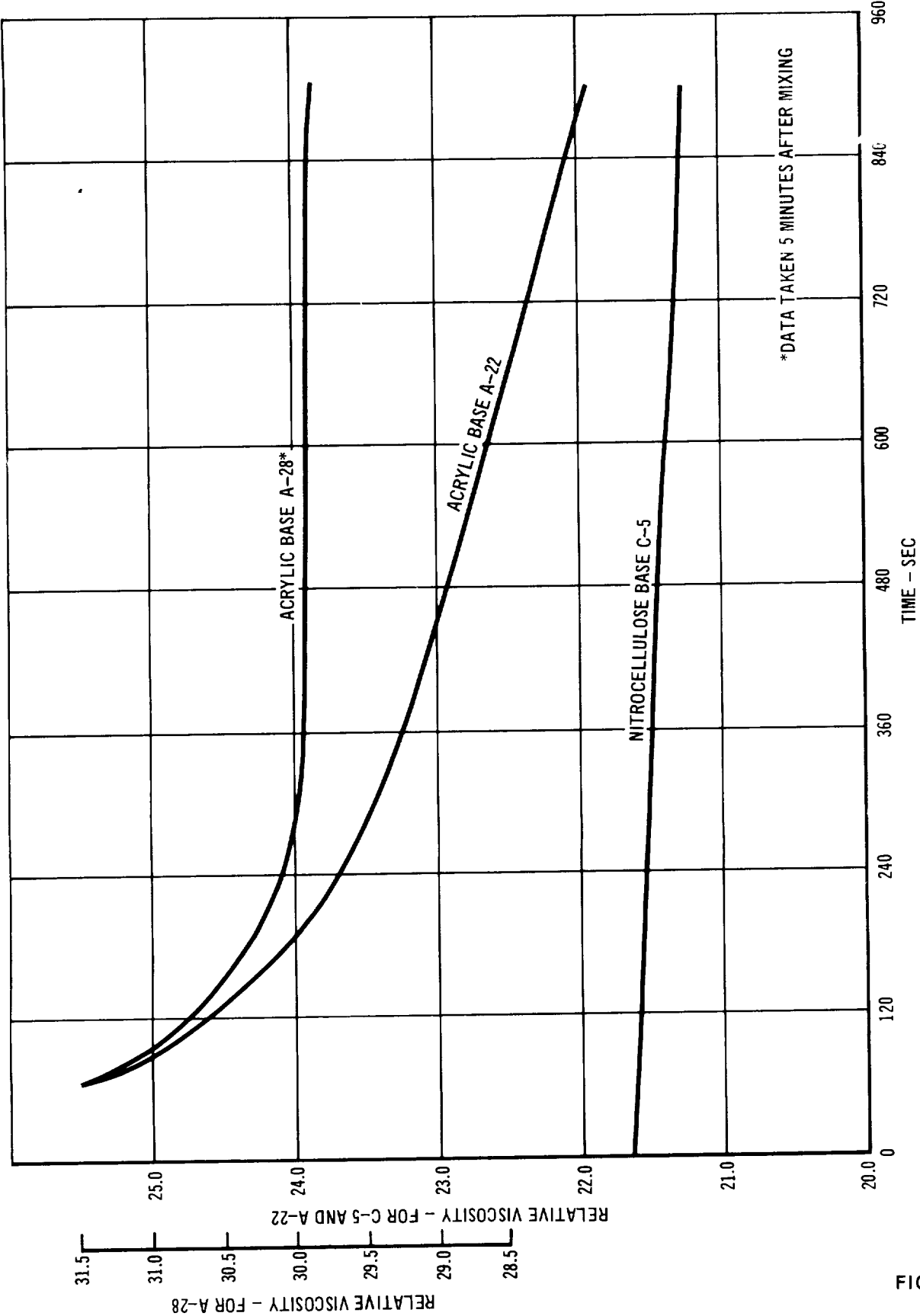
TABLE 5-1  
MODIFIED AND SCALED UP ACRYLIC BASE SLURRY COMPOSITIONS  
(Vehicle is HFN Plus B-66)

SLURRY NO.	MPA WT (G)	R-512E METAL POWDERS WT (G)	VEHICLE	
			TOTAL WT (G)	% B-66 ACRYLIC RESIN
28	50	3600	1140	43
29	50	3860	1140	43
30	50	3600	1190	43
31	100	3600	1240	38
32	150	3600	1190	39

joined to the skin by a Forged Upset Diffusion Joining (FUDJ) process, similar to seam welding. The panels are shown in Figure 5-7. These mockup panels could be dip coated and NDT measurements made on the exterior surface. Subsequently they could be cut open in order to perform an NDT evaluation on the inside.

A series of stainless steel corrugated mockups were dipped in the acrylic based A-29 and the nitrocellulose based C-5 slurries for comparison. The slower drying A-29 slurry showed a considerable spread in coating thickness from the inside surface to the outside surface. The C-5 nitrocellulose based lacquer produced more uniform results, as shown in Table 5-2; however, average coating thickness was somewhat low for both slurries. Two 18" (46 cm) long stainless steel corrugated mockups, one coated with the C-5 slurry and the other with the A-29 slurry, were cross sectioned at the upper end with respect to dipping direction and examined by metallographic techniques. The green coating thickness is shown in Figures 5-8 and 5-9. The minimum coating thickness in the acute angle approaching the weld was 0.5 mils (13  $\mu$ m) for the C-5 slurry and 0.68 mils (17  $\mu$ m) for the A-29 slurry compared to 4.0 and 5.0 mils (102 to 127  $\mu$ m) typical in adjoining areas. The use of vacuum drying was then evaluated as a means to accelerate drying of the slurry in the interior of the corrugations to improve the coating thickness. Vacuum drying produced excellent results for both the nitrocellulose and acrylic slurry systems as can be seen in Table 5-3.

5.1.3 Slurry Control Methods - The effects of viscosity control additives on slurry thinning on the interior of corrugations were investigated. Two new acrylic slurries were made with double and triple the MPA concentration in the A-29 slurry. The effects of increased MPA concentration on the uniformity of air dried acrylic



EFFECT OF SETTLING ON VISCOSITY 1/4" (0.6 CM) BELOW SURFACE FOR  
ACRYLIC BASE A-22, A-28 AND NITROCELLULOSE BASE C-5 SLURRIES

FIGURE 5-4

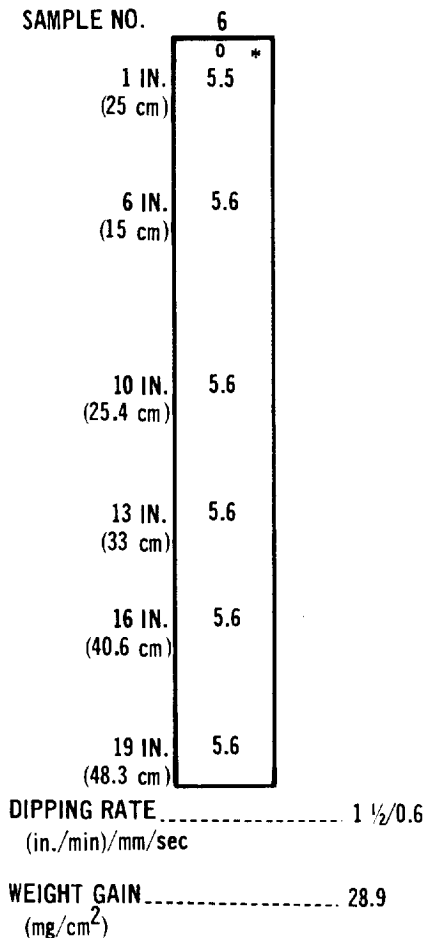
SAMPLE NO.	1	2	3	4
1 IN. (2.5 cm)	4.7*	5.0	4.7	5.1
6 IN. (15 cm)	4.7	5.5	6.3	7.5
10 IN. (25.4 cm)	4.7	5.3	6.2	7.0
13 IN. (33 cm)	4.9	5.3	6.2	7.0
16 IN. (40.6 cm)	4.9	5.5	6.2	7.0
19 IN. (48.3 cm)	4.9	5.7	6.3	7.1
DIPPING RATE (in./min)/mm/sec	1 1/2/0.6	2 0.8	2 1/2/1.0	3 1.2
WEIGHT GAIN (mg./cm <sup>2</sup> )	23.9	26.8	30.1	33.8

\* RELATIVE SLURRY COATING THICKNESS (NDT)

EFFECT OF WITHDRAWAL SPEED ON COATING THICKNESS AND  
UNIFORMITY OF 2" x 20" (5 cm x 50 cm) STRIPS IN ACRYLIC SLURRY A 28

FIGURE 5-5





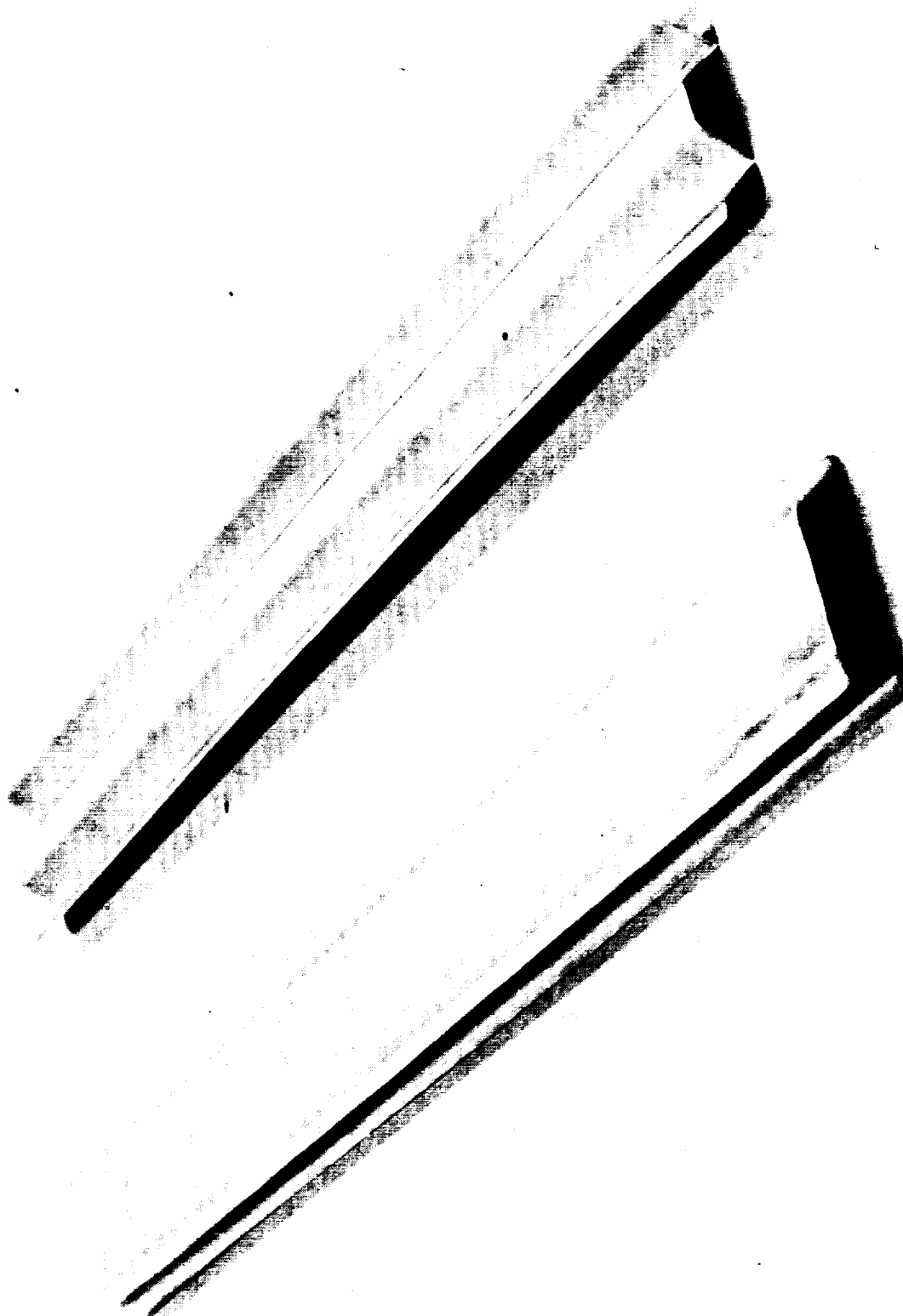
☐ RELATIVE SLURRY COATING THICKNESS (NDT)

UNIFORMITY STUDY OF 2" x 20" (5 CM x 50 CM) STRIP  
IN ACRYLIC BASED SLURRY A 29

FIGURE 5-6

based slurry are shown in Table 5-4. As the MPA content was increased, additional sag control was obtained which improved the inside versus outside surface coating uniformity. Caution on this point was advisable because the higher MPA content of acrylic slurries investigated during rib stiffened panel process optimization studies suffered from a lack of stability. However, the acrylic slurries from the earlier work were different in that they contained much lower resin contents.

A series of stainless steel 18" (46 cm) long corrugation mockups were dipped in the C-5 and A-32 slurries, air and vacuum dried, cut open and NDT inspected. Results are shown in Figure 5-10. A stainless steel 18" (46 cm) long corrugation mockup was dipped in the high MPA content A-32 slurry, air dried and sectioned. A cross section of this sample, as shown in Figure 5-11, had a minimum green



18" (46 CM) LONG STAINLESS STEEL CORRUGATED SPECIMENS

TABLE 5-2

COMPARISON OF AN ACRYLIC VS. NITROCELLULOSE BASED SLURRY  
ON COATING UNIFORMITY OF SINGLE FACED CORRUGATED PANELS

PANEL NO.	SLURRY	WITHDRAWAL SPEED (IN/MIN)/(MM/SEC)	DRYING	COATING THICKNESS (MG/CM <sup>2</sup> )		
				AVERAGE	INSIDE	OUTSIDE
1	A29	1.25/0.5	AIR	22.9	14.9	25.5
2	A29	1.50/0.6	AIR	23.6	-	-
3	A29	1.75/0.7	AIR	24.4	14.9	27.7
4	C-5	1.25/0.5	AIR	16.8	17.9	16.4
5	C-5	1.50/0.6	AIR	17.5	-	-
6	C-5	1.75/0.7	AIR	19.0	17.9	19.5

coating thickness of 1.8 mils (46  $\mu$ m), which was a considerable improvement over the lower MPA additive slurry. Viscosity checks made on a daily basis revealed that approximately 3 weeks was required for complete slurry stability. The A-32 slurry produced excellent uniform coatings after stabilization with a slight increase in withdrawal speed to obtain the desired weight pickup.

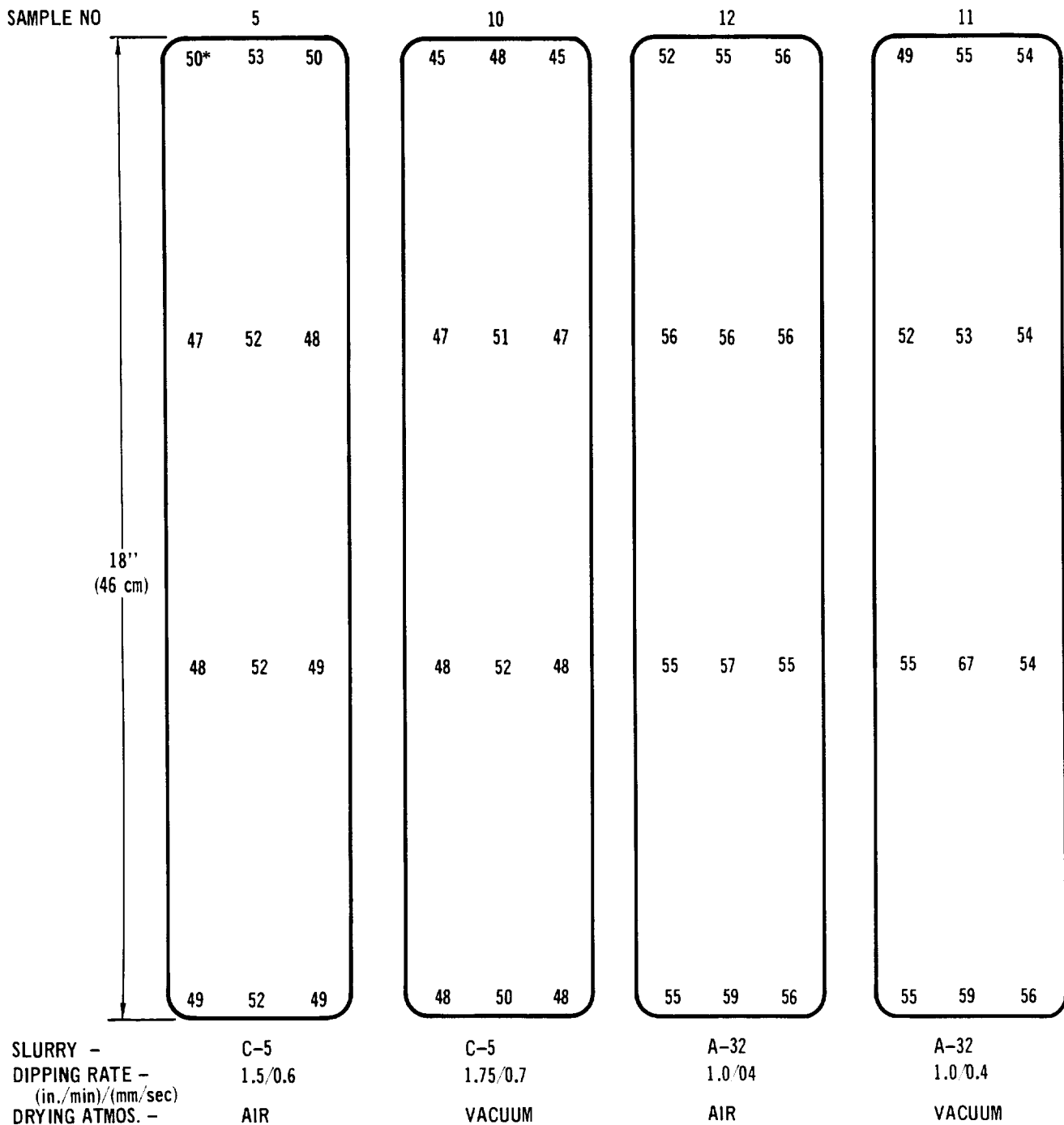
The effect of "Post 4", a wetting agent, was investigated by its addition to the A-29 slurry, and metallographic examination showed that it essentially eliminated the slurry thinning in the acute angle approaching the weld, as shown in Figure 5-12. However, on standing, this slurry degenerated and in less than one week, no longer provided suspension of the coating powders.

## 5.2 Process Scale-Up

5.2.1 Coating Uniformity - The thinning of the slurry in the corrugation in the acute angle approaching the weld was greatly improved by using the higher MPA content in the A-32 slurry. It was decided to assess whether further improvement would be realized during the normal diffusion or firing cycle due to flow-out while in the molten phase.

This was done by coating and sectioning 2" (5 cm) long electron beam welded corrugation stiffened mockups of FS-85 columbium alloy. The A-32 slurry was chosen for this work because it showed the best results of the stable slurries. The results after firing are shown in Figure 5-13, compared to green coating previously shown in Figure 5-11. The coating was found to flow out sufficiently to minimize the thinning effect on 2" (5 cm) long samples.

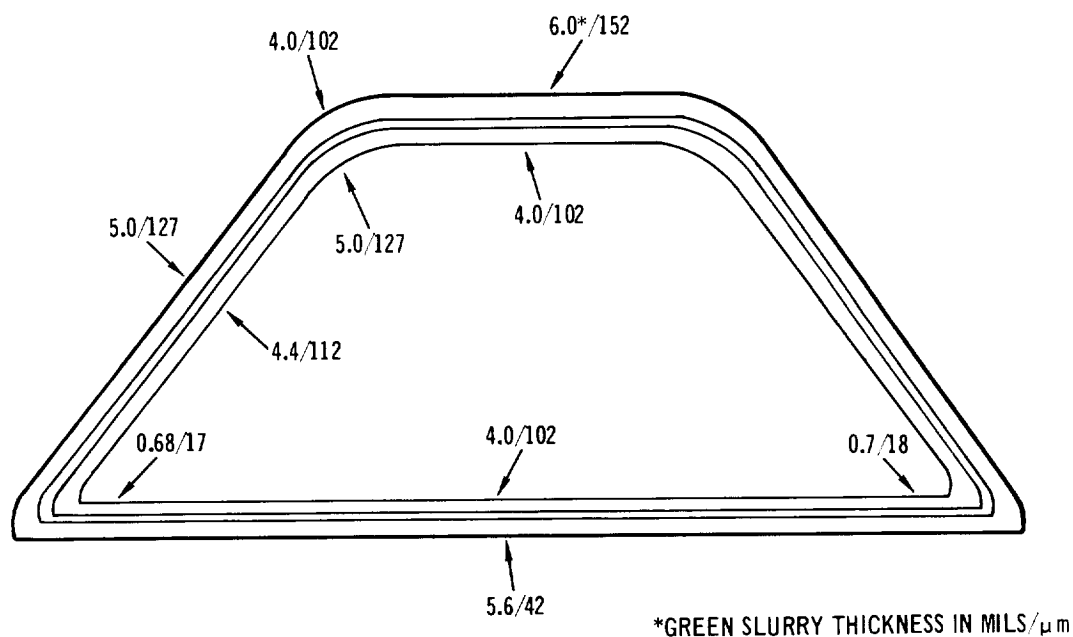
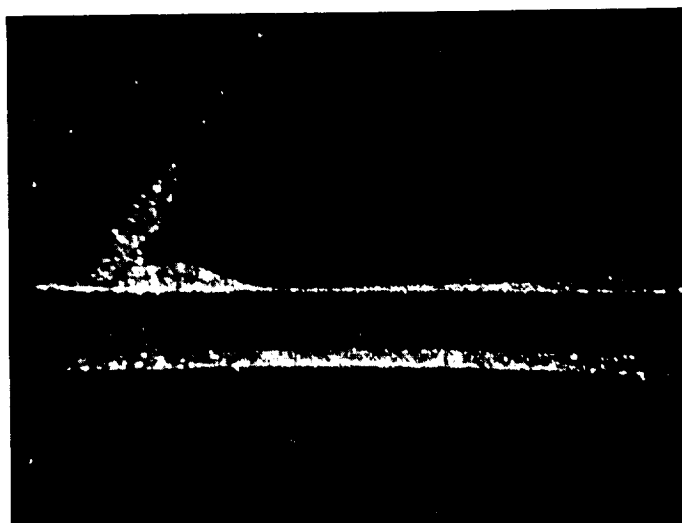
Further studies were made on several 3" x 12" (7.5 cm x 30 cm) subsize and 3" x 4" (7.5 cm x 10 cm) subscale electron beam welded FS-85 columbium corrugated panels. Corrugation configurations for these subscale and subsize panels were the



\*DERMITRON READING

GREEN COATING UNIFORMITY STUDY ON INSIDE SURFACE OF SKIN,  
SINGLE FACE CORRUGATED PANELS. FOR NITROCELLULOSE AND  
ACRYLIC BASED SLURRY AIR AND VACUUM DRIED (NOTE COATING  
THINNING TOWARDS EDGE).

FIGURE 5-8



COATING UNIFORMITY STUDY ON CORRUGATED MOCKUP PANEL  
PANEL 18 - A29 ACRYLIC BASED SLURRY

TABLE 5-3

COMPARISON OF AIR VS. VACUUM DRYING ON COATING UNIFORMITY  
OF SINGLE FACED CORRUGATED PANELS

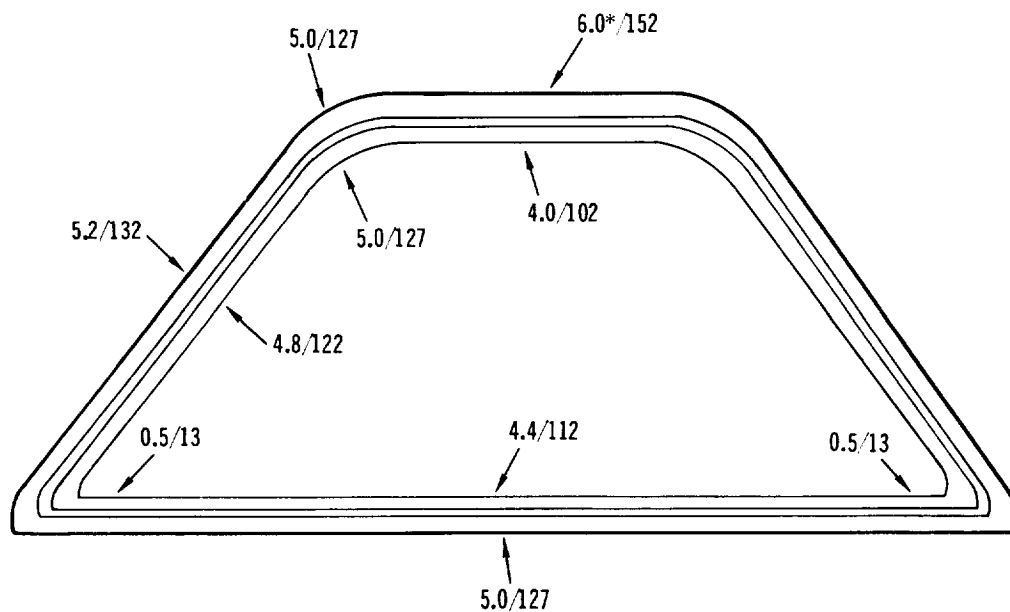
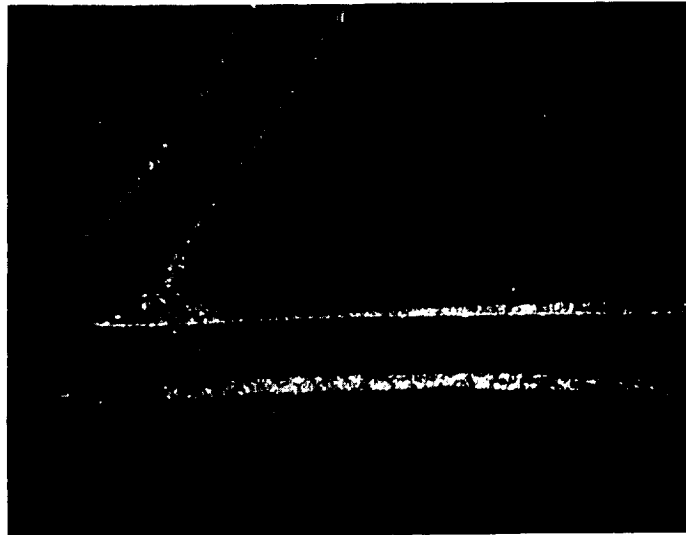
PANEL NO.	SLURRY	WITHDRAWAL SPEED (IN/MIN)/(MM/SEC)	DRYING	COATING THICKNESS (MG/CM <sup>2</sup> )		
				AVERAGE	INSIDE	OUTSIDE
1	A29	1.25/0.5	AIR	22.9	14.9	25.5
7	A29	1.50/0.6	VACUUM	27.4	27.4	27.4
6	C-5	1.75/0.7	AIR	19.0	17.9	19.5
10	C-5	1.75/0.7	VACUUM	20.6	20.9	20.5

TABLE 5-4

EFFECT OF THIXOTROPIC ADDITIVE CONCENTRATION ON COATING UNIFORMITY  
OF SINGLE FACE CORRUGATED PANELS WITH ACRYLIC BASED SLURRY

PANEL NO.	SLURRY	MPA CONTENT (GM)	WITHDRAWAL SPEED (IN/MIN)/(MM/SEC)	DRYING	COATING THICKNESS (MG/CM <sup>2</sup> )		
					AVERAGE	INSIDE	OUTSIDE
1	A29	50	1.25/0.5	AIR	22.9	14.9	25.5
8	A31	100	1.0 /0.4	AIR	25.2	20.9	29.8
12	A32	150	1.0 /0.4	AIR	25.2	23.9	25.7

same as those of the stainless steel mockups, 1.2" (3 cm) pitch and 0.55" (1.4 cm) corrugation height. These panels were of a size that would allow oxidation testing in the 1 atmosphere slow cycle tester. Initially one 3" x 4" (7.5 cm x 10 cm) and one 3" x 12" (7.5 cm x 30 cm) panel were dip-coated in the A-32 slurry and vacuum dried. During vacuum drying, severe blistering on the 3" x 4" (7.5 cm x 10 cm) panel was experienced. This blistering was observed during the final drying stages and was traced to an excessively fast drying rate. The outer coating dried and formed a skin which blistered as the solvent tried to evaporate too fast from the wet coating underneath. The drying rate was reduced by throttling the vacuum system; however, slow drying can cause excessive coating nonuniformity on the interior of the corrugation. The 3" x 4" (7.5 cm x 10 cm) panel was redipped after stripping and the NDT results are shown in Figure 5-14. The NDT results on the 3" x 12" (7.5 cm x 30 cm) panel are shown in Figure 5-15. The edges were overcoated by the slurry beading method, and the panels were diffusion treated. Excellent uniformity was obtained on both panels as shown by the NDT analysis after firing in Figures 5-16 and 5-17. The 3" x 12" (7.5 cm x 30 cm) panel was sectioned in sixteen locations and typical metallographic cross sections are shown in Figure 5-18. Thickness measurements are shown in Figure

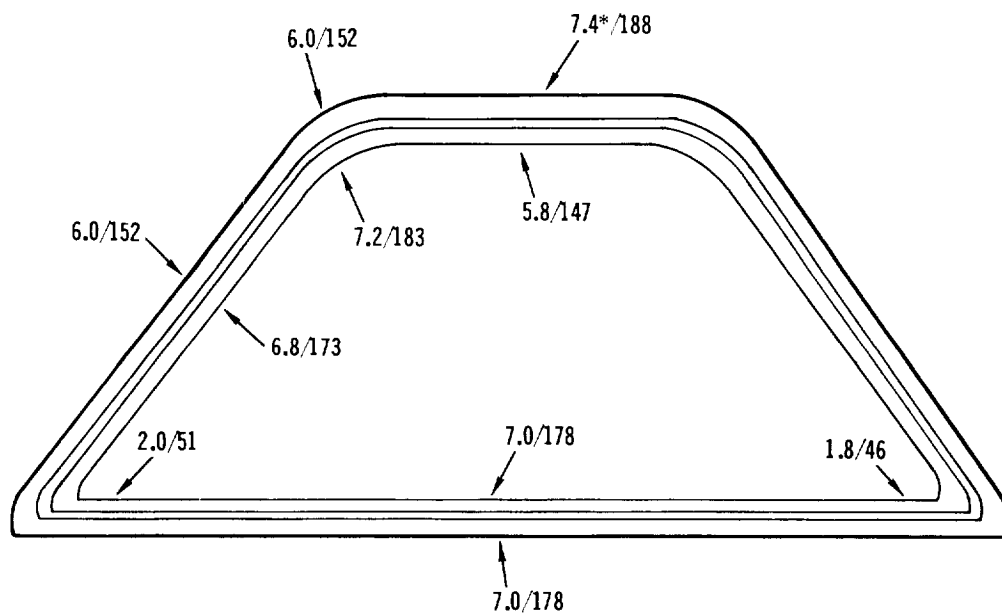
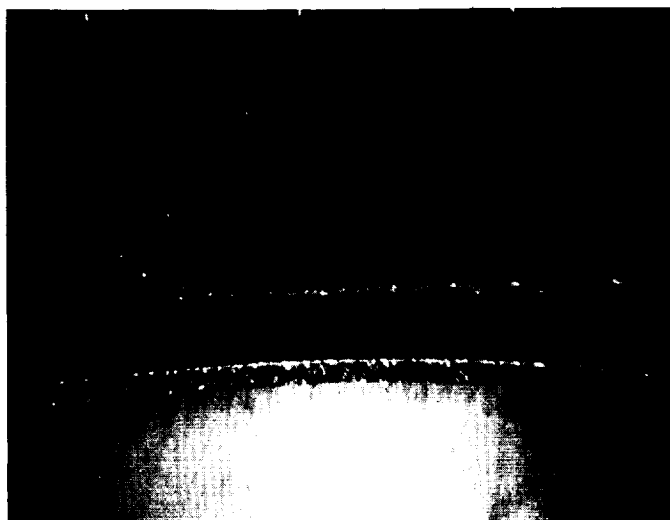


\*GREEN SLURRY THICKNESS IN MILS/ $\mu$ m

COATING UNIFORMITY STUDY ON CORRUGATED MOCKUP PANEL  
PANEL 19 - C-5 NITROCELLULOSE BASED SLURRY

457-3181

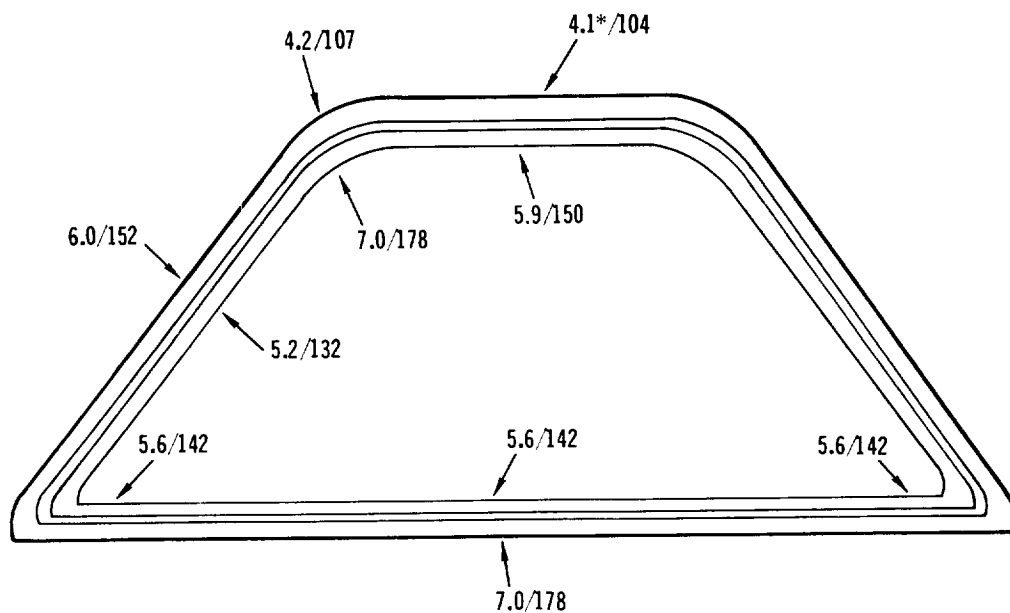
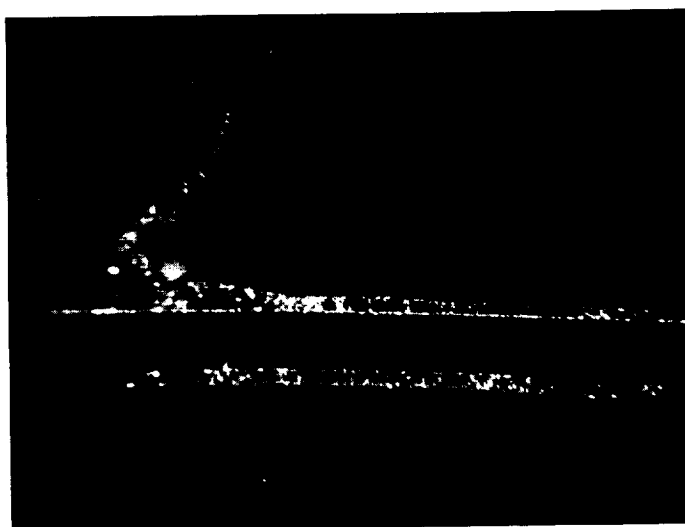
FIGURE 5-10



\*GREEN SLURRY THICKNESS IN MILS/ $\mu\text{m}$

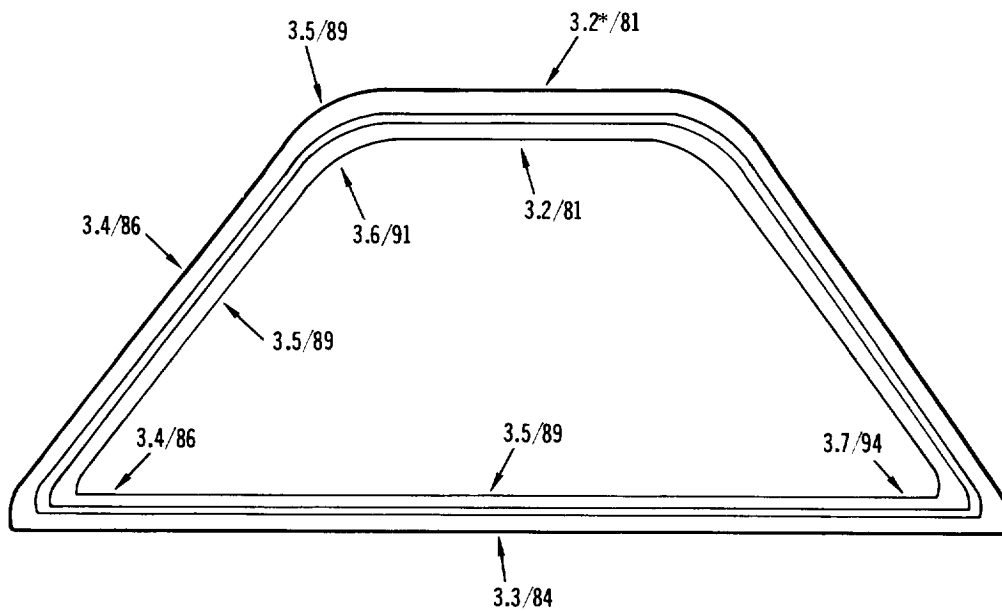
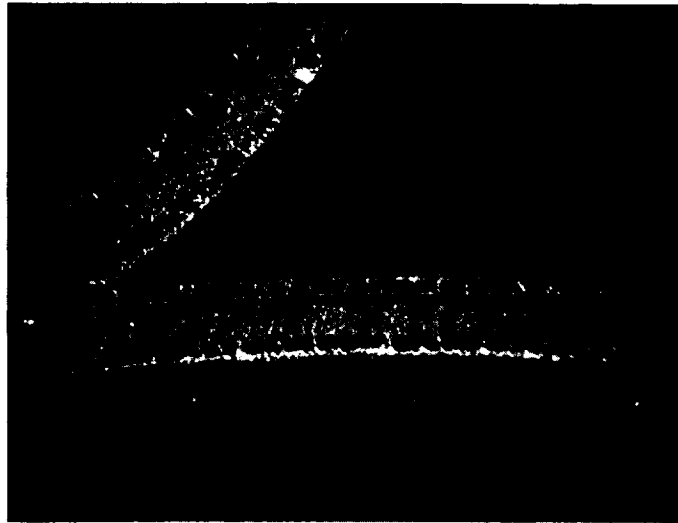
COATING UNIFORMITY STUDY ON CORRUGATED MOCKUP PANEL  
PANEL S-1 - A32 (HIGH ADDITIVE) ACRYLIC BASED SLURRY





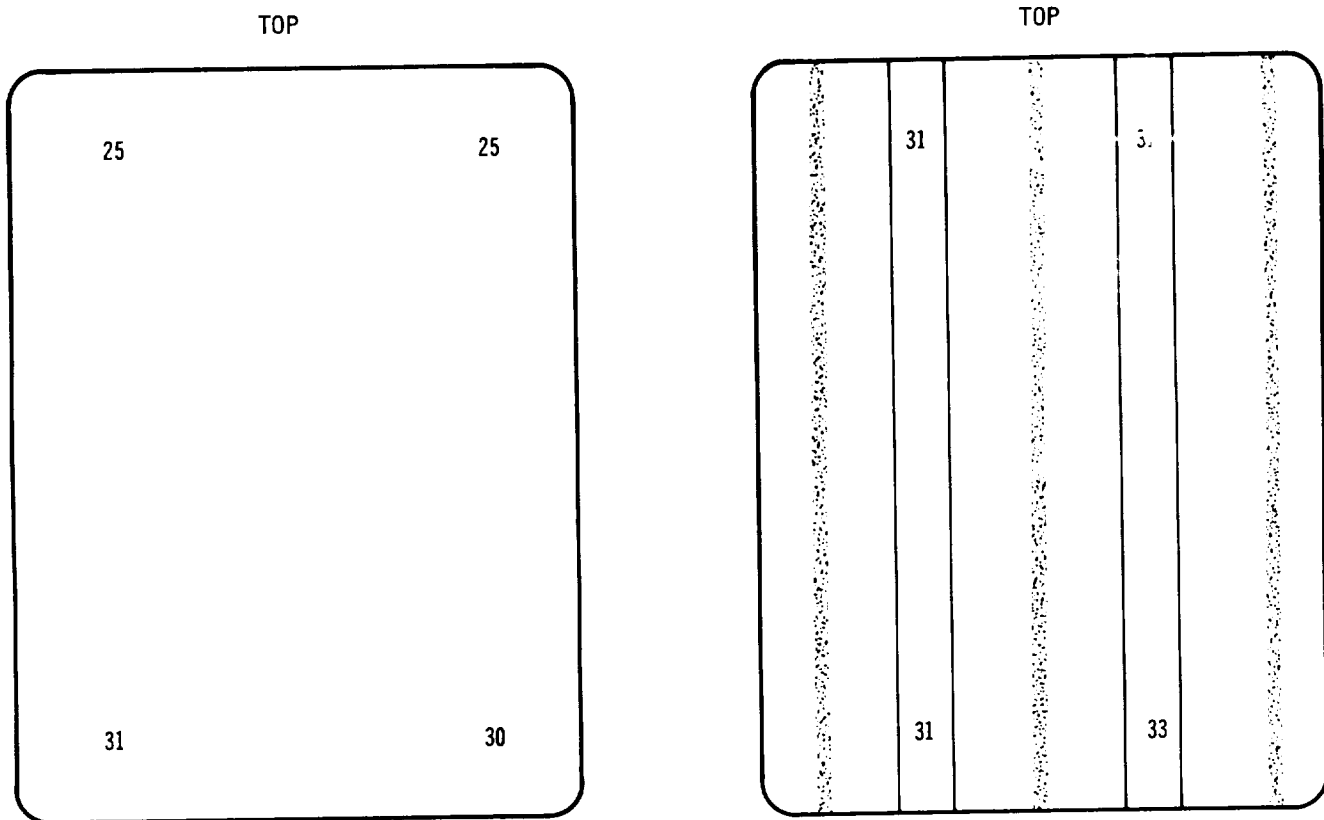
\*GREEN SLURRY THICKNESS IN MILS/ $\mu\text{m}$

COATING UNIFORMITY STUDY ON CORRUGATED MOCKUP PANEL  
PANEL 21 - A-29 ACRYLIC BASED SLURRY WITH POST 4 WETTING AGENT



\*DIFFUSED COATING THICKNESS IN MILS/ $\mu$ m

COATING UNIFORMITY STUDY ON FS85 ALLOY  
Si-20Cr-20Fe COATED CORRUGATED PANEL DETAIL  
A-32 ACRYLIC BASED SLURRY



# GREEN COATING UNIFORMITY STUDY ON 3'' x 4'' (7.5 CM x 10 CM) CORRUGATED FS85 ALLOY

457-3185

FIGURE 5-14

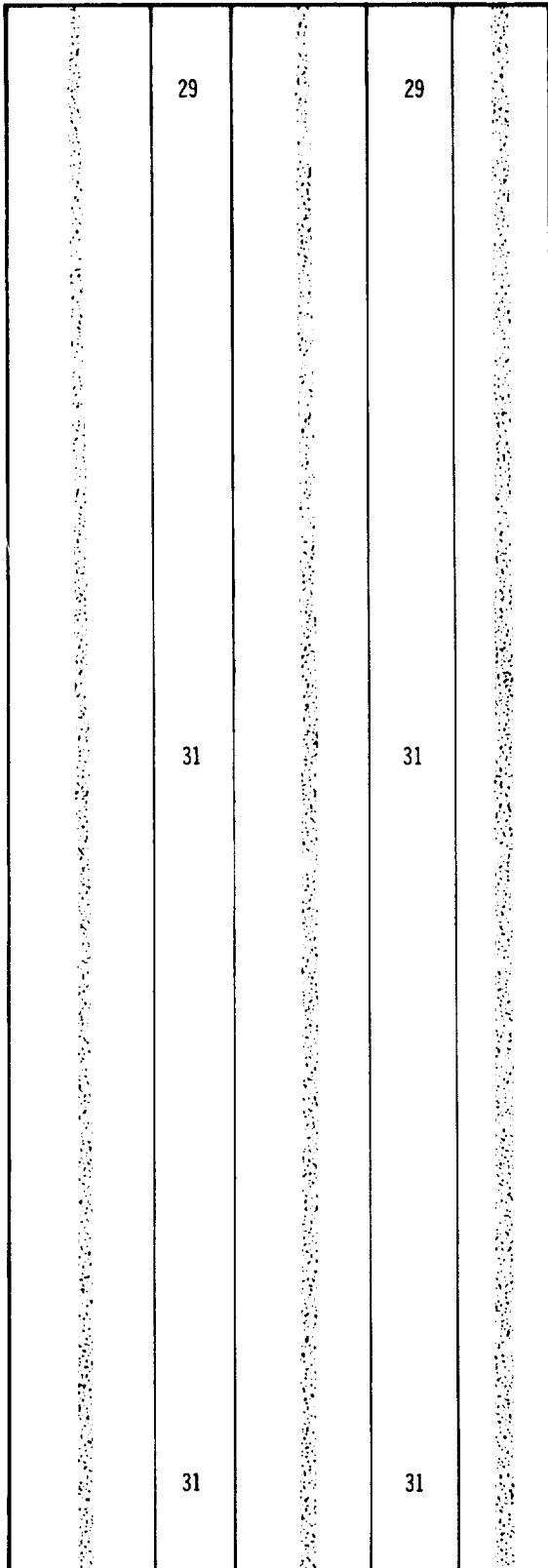
5-19 for the same locations.

5.2.2 Coating Reproducibility - Additional 3'' x 4'' (7.5 cm x 10 cm) panel sections were slurry coated, fired, and were slow cycle oxidation tested along with the first panel section that was coated. The results are listed in Table 5-5.

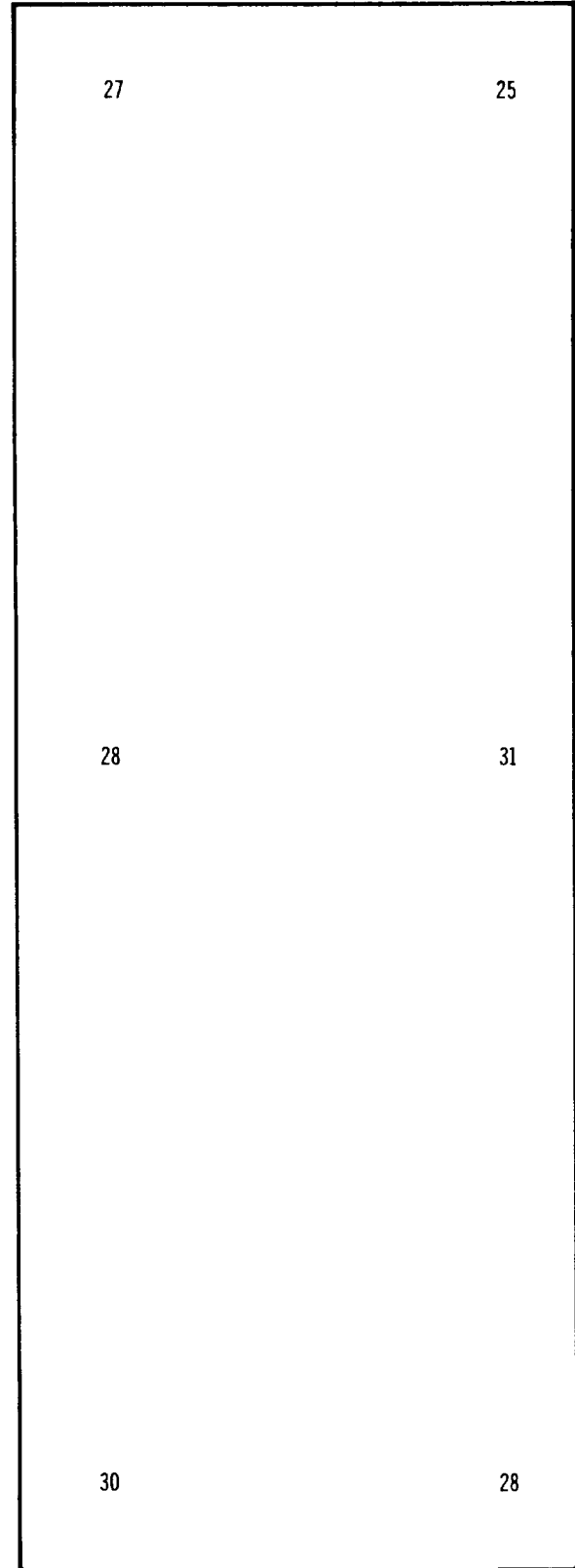
One of the panels, 3T, was coated with the nitrocellulose based slurry for comparison with the acrylic. The A-32 acrylic slurry was used for the other four panels. In general the only major coating problem encountered was with the end edges of the panel specimens. This was understandable since there was no complete access for rounding off these irregular edges, particularly in the vicinity of the welds.

Although a small oxidation spot developed on the outer surface in the weld area on panel 2T, there was no other evidence of oxidation or attack in the

TOP

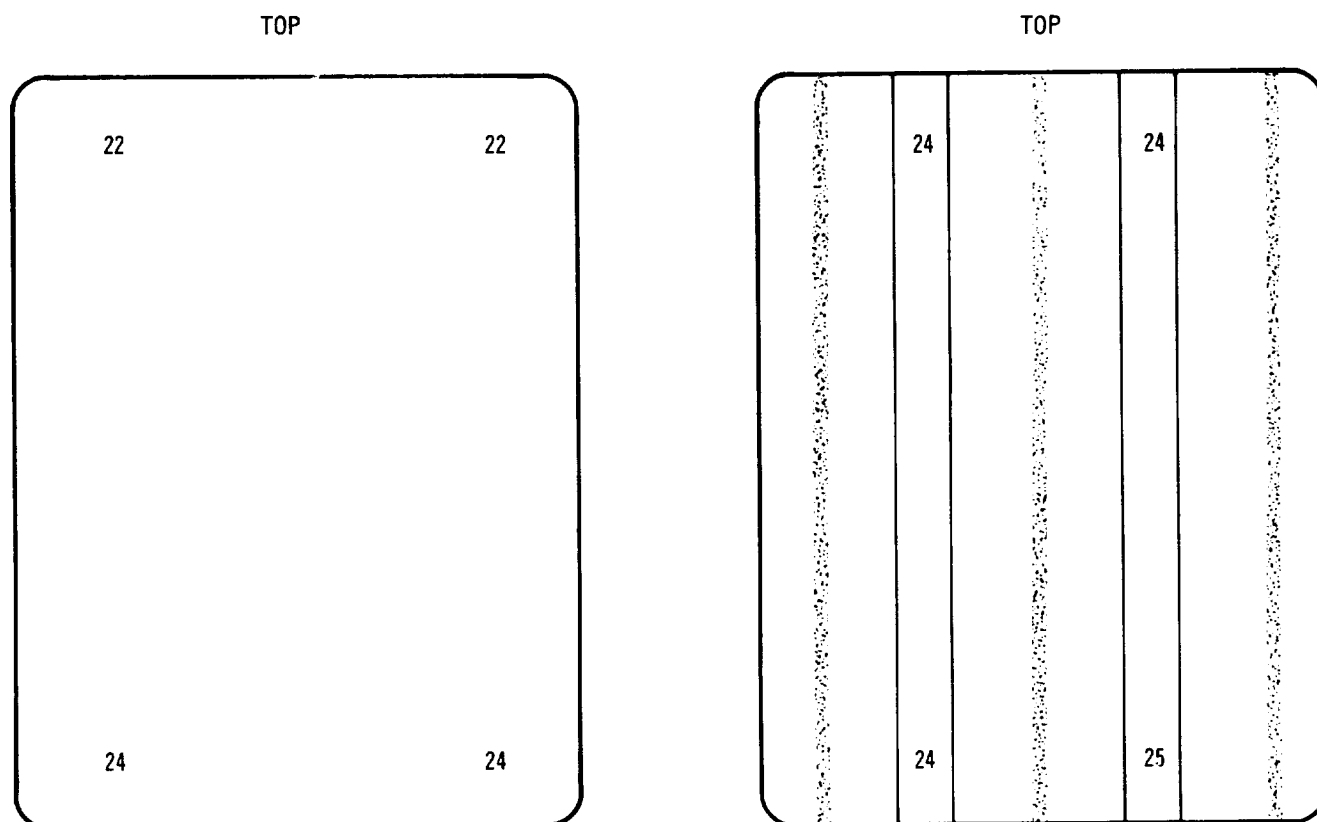


TOP



GREEN COATING UNIFORMITY STUDY ON SUB-SIZE CORRUGATED FS85 ALLOY

457-3186



FIRED COATING UNIFORMITY STUDY ON 3' x 4' (7.5 CM x 10 CM) CORRUGATED  
FS85 ALLOY PANEL - DERMITRON NDT

457-3187

FIGURE 5-16

vicinity of welds on any panel. More significantly there were no signs of coating failures on the inside of the corrugations at any location. Panel 3T fell out of the test holder during testing and the edge may have been damaged by impact and/or interaction with surrounding construction materials.

Panel 4T lasted over 100 cycles without any sign of oxidation failure. Accordingly, these test results gave assurance that the corrugations could be well enough coated with the A-32 slurry to proceed with the subscale and full panel coating process verification.

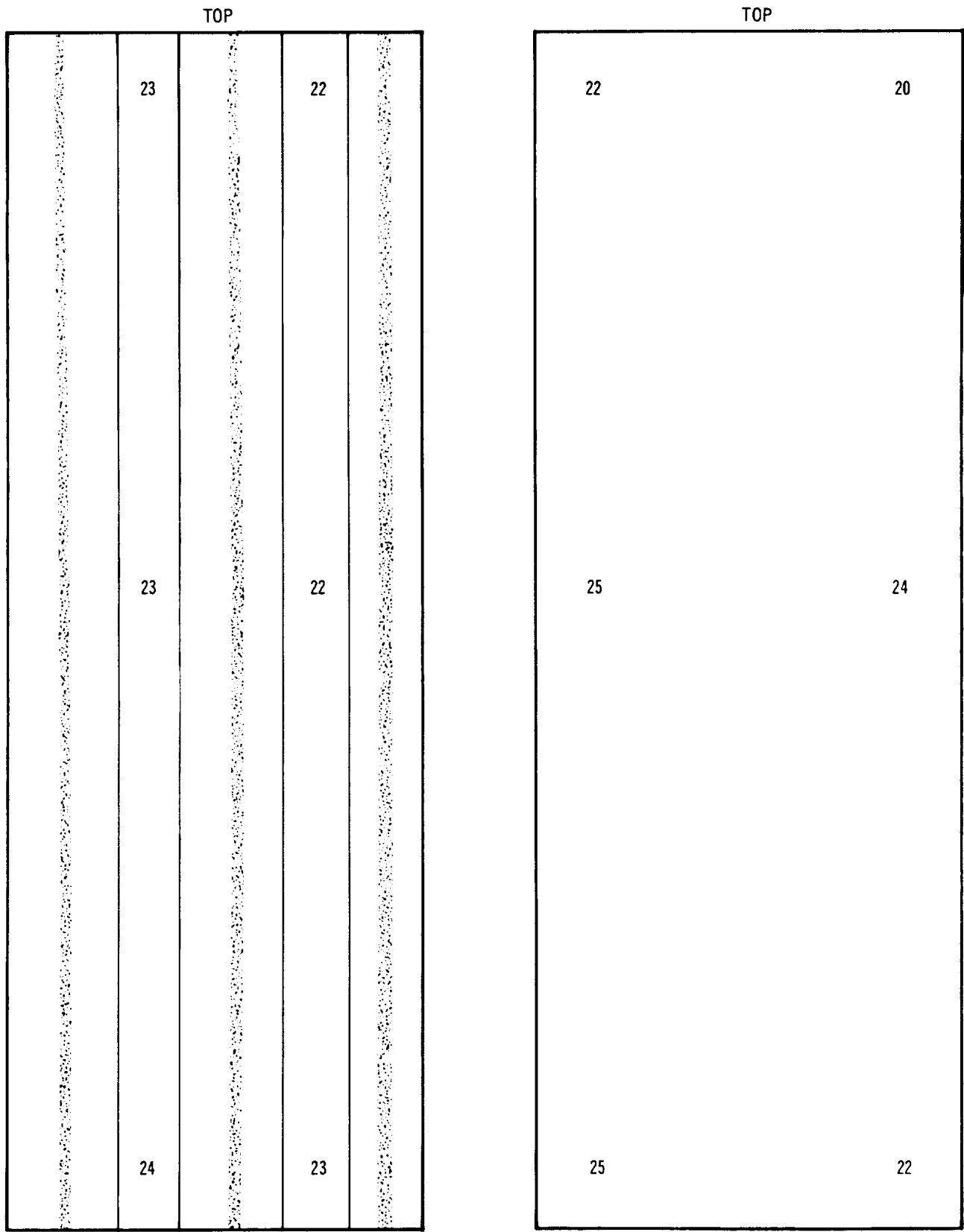
### 5.3 Process Verification

#### 5.3.1 Subsize Panels

5.3.1.1 Fabrication - Subsize heat shield panels of the corrugation stiffened configuration were fabricated from the FS-85 columbium alloy. The subsize panels were 3.2" wide x 12" long x approximately 1/2" deep (8 cm x 30 cm x 1.25 cm).

FUSED SLURRY SILICIDE  
COATED COLUMBIUM

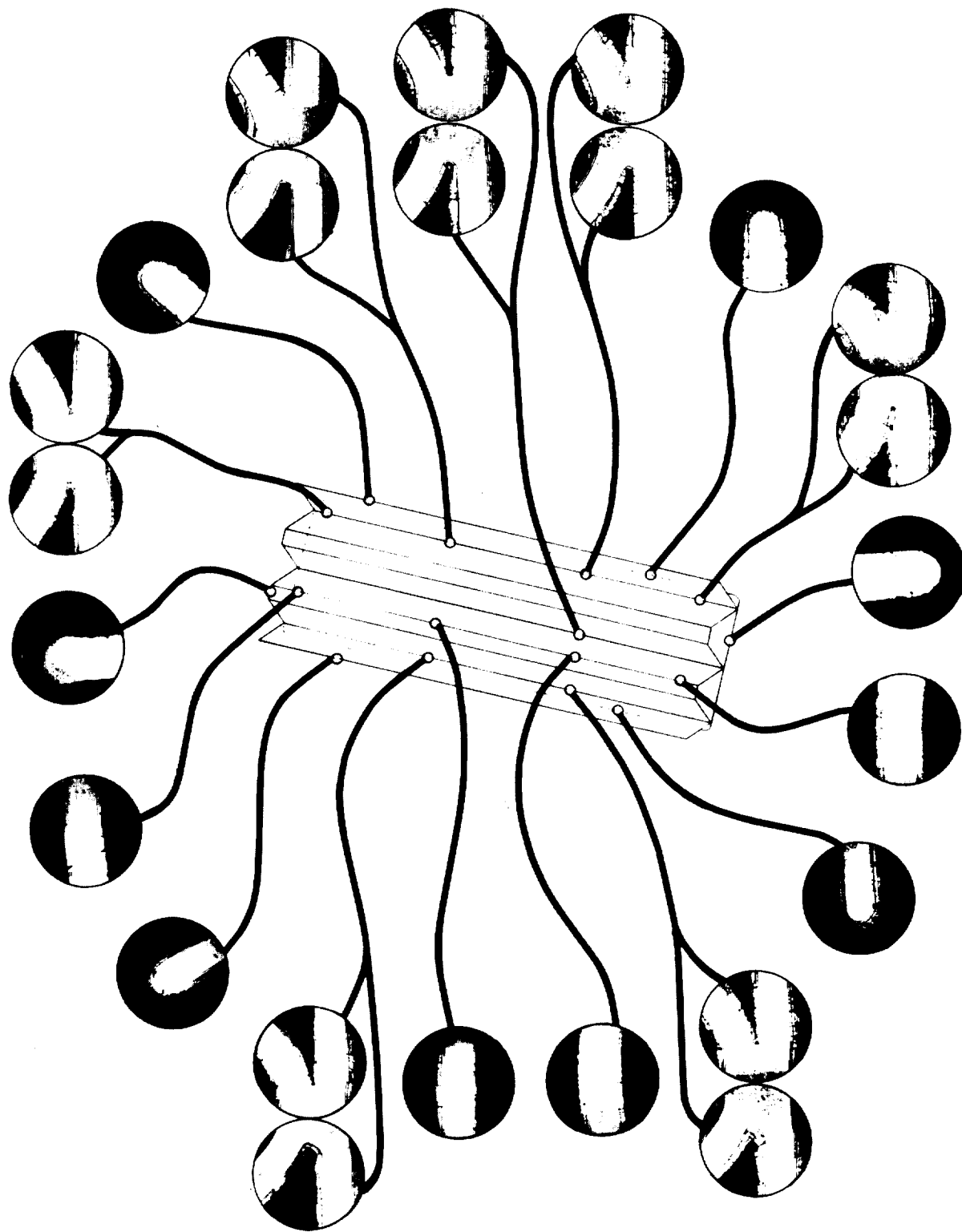
FINAL REPORT



457-3188

FIRED COATING UNIFORMITY STUDY ON SUB-SIZE CORRUGATED FS85 ALLOY  
PANEL - DERMITRON NDT

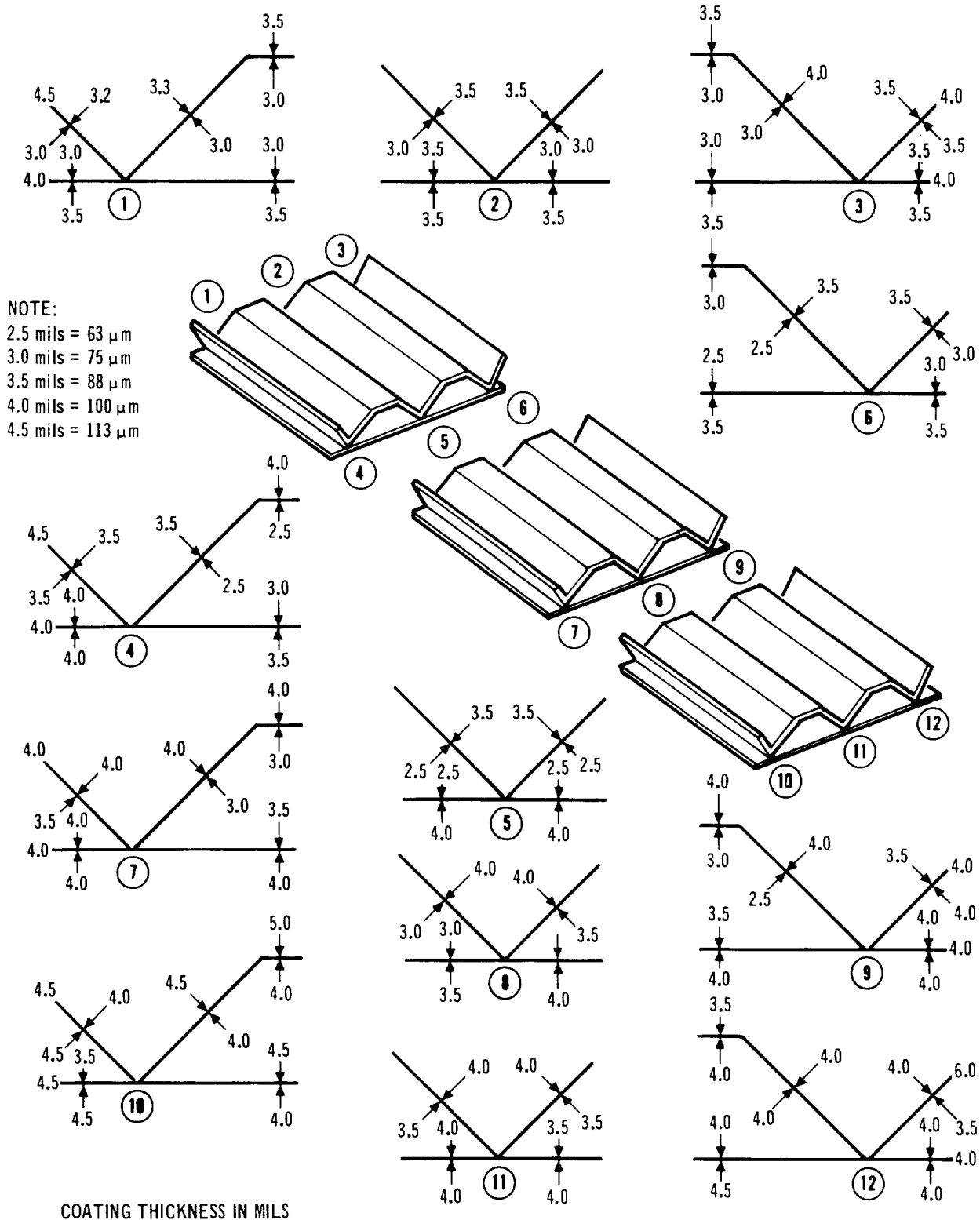
FIGURE 5-17



UNIFORMITY STUDY - R512E COATED FS85 ALLOY SUB-SIZE CORRUGATED PANEL

457-3189

FIGURE 5-18



COATING UNIFORMITY STUDY ON SUB-SIZE CORRUGATED HEAT SHIELD PANEL

FIGURE 5-19



TABLE 5-5  
COATING STUDIES ON 3" x 4" (7.5 CM x 10 CM) PANEL SECTIONS

PANEL NO.	COATING THICKNESS (MG/CM <sup>2</sup> )	1 ATMOSPHERE SLOW CYCLE LIFE (CYCLES)	FAILURE SITES
1 T	21.3	36	TOP EDGE AND WELD AREA
2 T	19.8	50	TOP EDGE AND CENTER WELD AREA
3 T*	20.8	77	BOTTOM EDGE**
4 T	23.0	107	NONE
5 T	20.7	53	TOP EDGE

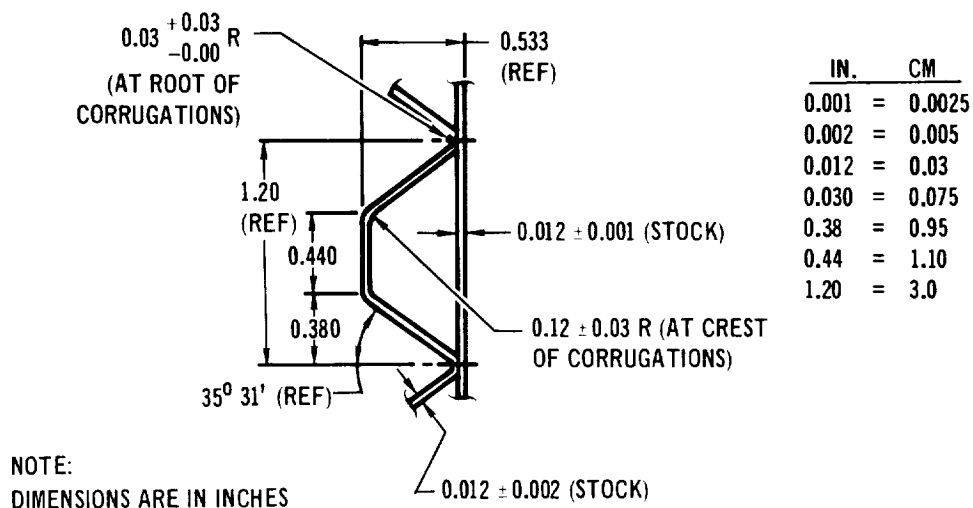
\*COATED WITH C-5 SLURRY FOR COMPARISON

\*\*FELL OUT OF TESTER DURING TESTING

The corrugation stiffened panels had both the corrugation and skin made from .012" (.03 cm) gage sheet. The skins were joined to the corrugations by electron beam welding through the skin into the corrugation. The electron beam width and penetration were adjusted to produce a weld joint which did not create or leave any faying surfaces. Five subsize corrugated heat shield panels, with the corrugation cross-section dimensions shown in Figure 5-20 were fabricated. The final operation was to radius the edges to enhance good coating quality.

5.3.1.2 Coating - During the coating of the 3" x 4" (7.5 cm x 10 cm) sub-scale panels the vacuum drying of the slurry was somewhat variable and difficult to control to prevent blistering of the coating. Even though the bubbling or blistering encountered with fast drying could be overcome, it was found with panel 1T that a blister could occur later during the high temperature fusion treatment. This blister was repaired but the incident raised a question about the use of vacuum drying for the larger subsize and full size panels where the volume of material would be much greater and therefore even more difficult to control. Accordingly it was decided that it would be preferable to air dry slowly with panels in the horizontal position. This would prevent the more slowly drying slurry on the inside of the corrugations from flowing out and being lost by dripping.

Five 3" x 12" (7.5 cm x 10 cm) subsize panels were dip coated in the A-32 slurry at 1"/min (0.4 mm/sec) and at a viscosity of .56 Nsec/m<sup>2</sup> at 75°F (24°C). Upon exit from the slurry each panel was placed in the horizontal position, skin side down, so that it was supported directly by resting on metal pins inserted in



SINGLE PITCH OF CORRUGATED HEAT SHIELD PANEL CROSS-SECTION  
DRAWING SHOWING SHAPE AND DIMENSIONS

FIGURE 5-20

a wooden support structure. The pins were in contact with the skin side of the panel only, two horizontal at one end and one vertical at the other end. These contact points were readily touched up with a dab of slurry later.

Drying took place during one working day period after which time the panels appeared completely dry, including the inside of the corrugations. The loss of volatiles was monitored intermittently by weighing. Edge-beading was performed on the free sides of the panel. However, the end edges were overcoated by dipping in the slurry so that only a 1/8" (0.32 cm) length of the panel was immersed. This technique is more applicable to the corrugation-welded junctures at the ends than edge-beading.

Dermatron measurements of the green slurry coating indicated excellent uniformity and reproducibility from panel to panel as shown in Table 5-6. This was also confirmed by weight measurements after the diffusion treatments. Thermo-electric probe measurements after diffusion treatment indicated the edges were well covered.

The diffusion treatment was carried out in a single batch of all five panels, for 1 hour at 2580°F (36 hsec at 1420°C). It was found that the much larger volatilization losses of the acrylic compared to the nitrocellulose slurries at this large batch size caused some vacuum pumping difficulties and slowed down the

TABLE 5-6

## DATA SUMMARY FOR SUB-SIZE FS-85 CORRUGATED PANELS

PANEL NO.	DIFF WT (MG/CM <sup>2</sup> )	SLURRY THICKNESS DERMITRON NDT (MG/CM <sup>2</sup> )		EDGE THICKNESS THERMOELECTRIC NDT (MILLIVOLTS)
		SKIN	CORRUGATION	
16426-49-2	21.5	26-27	26-28	2.2-2.6
-5	21.4	26-28	27-28	2.2-2.6
-7	22.2	28-29	28-29	2.1-2.5
-10	21.3	27-28	27-28	2.2-2.6
-12	21.4	27-28	27-29	2.2-2.5

heating time. There was also a more noticeable amount of surface residue compared to small samples and parts.

5.3.1.3 Testing - Subsize, 3" x 12" (7.5 cm x 30 cm) corrugation stiffened heat shields were utilized in flight simulation testing to demonstrate the effectiveness of the optimized fused slurry coating and to determine the reuse capability of the heat shield. Five panels were subjected simultaneously to temperature, pressure, and stress profiles and acoustic exposures representative of a Space Shuttle flight. Pressure conditions representative of both internal and external surfaces were simulated. Flight simulations were accomplished using the modified Astro tube furnace and the loading fixture shown in Figure 4-20. The temperature, pressure and stress conditions are the same as those that were utilized for the rib stiffened panels; they were presented in Section 4.0 for subsize panel testing. A total of 488 reentry cycles were conducted; four panels were exposed for 100 cycles each. Elastic deflection measurements were made under four-point loading of the panels at a load of 216 lbs (98.5 kg) which produced a stress in the outermost portion of the corrugation equal to 77% of room temperature yield. Creep deflection measurements made with a straight bar and micrometer over an 11" (28 cm) span were also recorded for each panel at various intervals during cycling.

Results of creep and elastic deflection measurements are shown in Table 5-7. Creep deflections are expressed in deflection rate (mils (μm)/cycle) for each group of cycles conducted per panel and in cumulative average deflection rate (mils (μm)/cycle) for each group of cycles conducted per panel. Elastic deflection measurements are shown in inches and centimeters measured at the center of an 11" (28 cm) span.

TABLE 5-7  
DEFLECTION MEASUREMENTS FOR SUB-SIZE CORRUGATION  
STIFFENED HEAT SHIELD PANELS

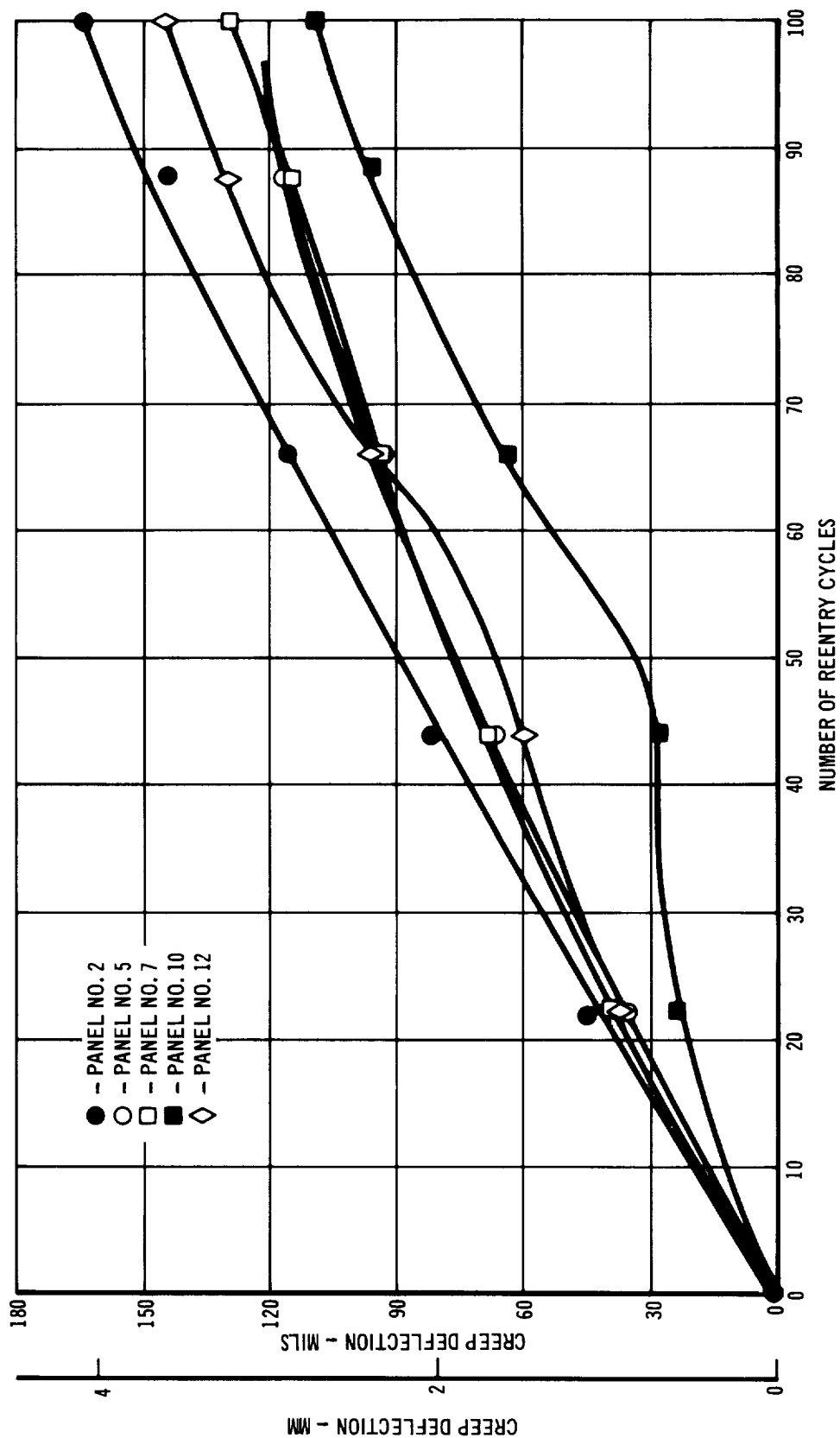
PANEL NO.	PRESSURE	CYCLE NO.	DEFLECTION MEASUREMENTS		
			CREEP		ELASTIC
			GROUP RATE MILS ( $\mu$ m)/CYCLE	CUMULATIVE AVERAGE RATE MILS ( $\mu$ m)/CYCLE	AFTER EACH GROUP REENTRY CYCLES IN. (cm)
2	EXTERNAL	0			0.118(0.300)
		22	2.04(52)	2.04(52)	0.095(0.242)
		44	1.68(43)	1.86(47)	0.102(0.259)
		66	1.55(39)	1.75(45)	0.102(0.259)
		88	1.32(33)	1.65(42)	0.103(0.262)
		100	2.42(61)	1.64(42)	
5	EXTERNAL	0			0.112(0.284)
		22	1.59(40)	1.59(40)	0.090(0.228)
		44	1.45(37)	1.52(39)	0.099(0.252)
		66	1.23(31)	1.42(36)	0.104(0.264)
		88	1.09(28)	1.34(34)	
7	INTERNAL	0			0.114(0.290)
		22	1.86(47)	1.86(47)	0.092(0.234)
		44	1.18(30)	1.52(39)	—
		66	1.23(31)	1.42(36)	0.091(0.232)
		88	1.00(25)	1.32(33)	0.092(0.234)
10	INTERNAL	100	1.25(32)	1.31(33)	
		0			0.106(0.269)
		22	1.14(29)	1.14(29)	0.106(0.232)
		44	0.18(5.0)	0.66(17)	0.088(0.224)
		66	1.59(40)	0.97(25)	0.090(0.228)
		88	1.45(37)	1.09(28)	0.099(0.252)
12	INTERNAL	100	1.25(32)	1.11(28)	
		0			0.122(0.310)
		22	1.77(45)	1.77(45)	0.096(0.244)
		44	1.00(25)	1.57(40)	0.094(0.239)
		66	1.55(39)	1.44(37)	0.098(0.249)
		88	1.64(42)	1.49(38)	0.101(0.256)
		100	1.08(27)	1.44(37)	

The most noticeable phenomenon in the measured creep and elastic deflection rates was the large decrease (from 10 to 20%) after the first group of cycles. This decrease in deflection rate is believed to be due to a prestressing of the coating during the first few cycles due to cooling while under load. This same phenomenon was experienced with the rib stiffened panels.

Creep deflections versus number of reentry cycles for panels tested in the external and internal pressure environments are shown in Figure 5-21. It can be seen that after the panels become stabilized they have an almost linear creep deflection rate of approximately 1.25 mils/cycle (31.8  $\mu\text{m}$ /cycle). This amount of deflection is equivalent to 0.42" (1.06 cm) on a full size 20" (50 cm) corrugation stiffened heat shield panel after 100 reentry cycles.

The creep deflection rate for the corrugation stiffened panels was approximately three times the creep rate of the rib stiffened panels. Both types of panels were loaded to the same stress level in the outermost portion of the stiffeners (the edge of the ribs for the rib stiffened panels and the flat of the corrugations for the corrugation stiffened panels). To achieve the same stress level in the outermost portion of the stiffeners the corrugation design required a load 53% higher than for the rib stiffened design. The difference in amount of creep experienced for one design versus the other design can be attributed to different stress distributions within the panels, which are generated simply by the different cross-sectional geometries. The rib stiffened design has a tension to compression neutral axis that is much closer to the skin or compression side of the cross section than the corrugation design. This means higher stresses in the skin for the corrugation design. Compressive stresses contribute just as much to creep strain as the tensile stresses. Thus the corrugation design should show a higher creep deflection.

There were only two small spots of coating breakdown produced by the environment during reentry testing of the 5 subsize corrugation stiffened panels. These occurred on Panel No. 2 directly on the weld on the corrugation side of the panel after 44 reentry exposure cycles but did not lead to or cause any structural failure of the panel. The occurrence of coating failure at this location was unusual. Although the cause was not determined, it appears the most likely explanation is blistering during the diffusion cycle because of excessive slurry buildup or some contaminant or inclusion picked up during the forming or welding of the panels. Corners and ends of Panel No. 2, Panel No. 5 and Panel No. 10 revealed some coating failures but these were a result of accidental damage incurred during acoustic exposure and did not result in any structural failure of the panels. The areas which were accidentally damaged early were repair coated. There were no indications of coating breakdown on the interior of the corrugations in the areas (acute angle approaching the welds) where there was



SUB-SIZE CORRUGATION STIFFENED HEAT SHIELD PANEL CREEP DEFLECTIONS

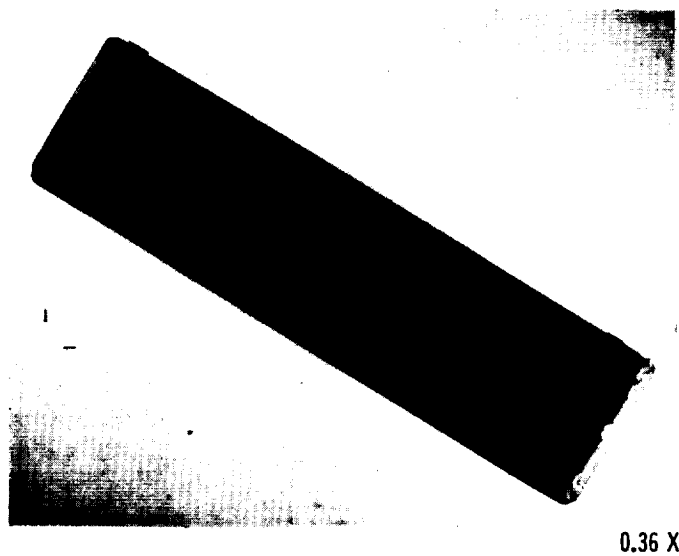
FIGURE 5-21

some concern of reliable performance. Overall, the R-512E coating performance produced from the acrylic base slurry was equivalent to that produced from the nitrocellulose base slurry and evaluated on the rib stiffened panels.

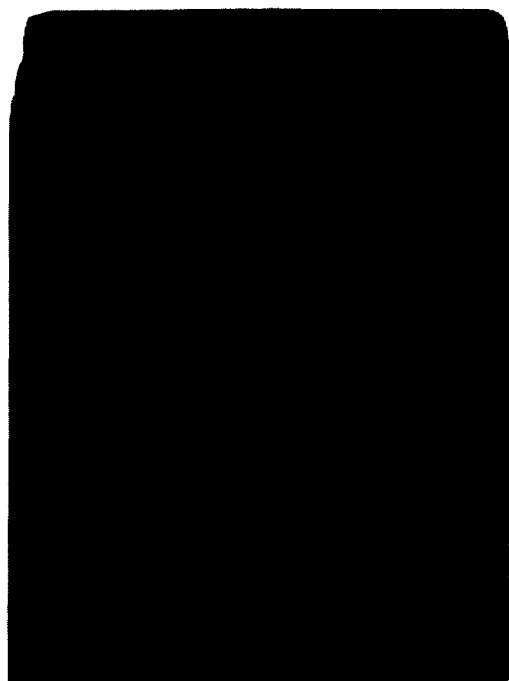
Photographs of each of the five panels are shown at various stages of testing in Figures 5-22 through 5-26. Only one panel, Number 5, structurally failed during acoustic testing. Out of five panels, four survived for 100 cycles of acoustic exposure (100 x 28.6 sec). The remaining panel failed structurally during acoustic testing after 88 cycles had been completed successfully. Based on the results of these panel tests, the average fatigue life of typical R-512E coated FS-85 corrugation heat shield structure at 10,000 psi ( $69 \text{ MN/m}^2$ ) is approximately 760,000 cycles. Fatigue life for the rib stiffened panels is between 650,000 and 760,000 cycles. The fatigue life of the corrugated panels would be expected to be slightly better than that of the rib stiffened panels because the rib edge is more likely to provide a stress riser than the flat top portion of the corrugation. Photomicrographs of Panel No. 10 after 100 reentry exposures are shown in Figures 5-27 and 5-28. The uniform coating coverage on the interior of the corrugation including the acute angle approaching the weld should be noted.

Table 5-8 presents the results of nondestructive coating thickness measurements made on the five subsized heat shield panels before and after reentry cycling. The Dermitron eddy current device was used for thickness measurements. Excellent coating uniformity for each panel was revealed in the as-coated condition.

Panels tested in the external pressure environment showed about the same coating thickness increase as the panels tested in the internal pressure environment. This is not consistent with thickness changes observed on the rib stiffened panels. Rib stiffened panels tested in the internal pressure environment had less thickness increase than those tested in the external pressure environment. The same test conditions were used for both types of panels. The only known difference, which shouldn't have had much influence, was that an acrylic based slurry was used for coating the corrugation panels and a nitrocellulose based slurry was used for the rib panels. However, as can be observed in Figure 5-27 there is a considerable amount of oxide scale for an internal pressure test.



(A) As Coated Prior to Testing



SKIN SIDE

1 X



CORRUGATION SIDE

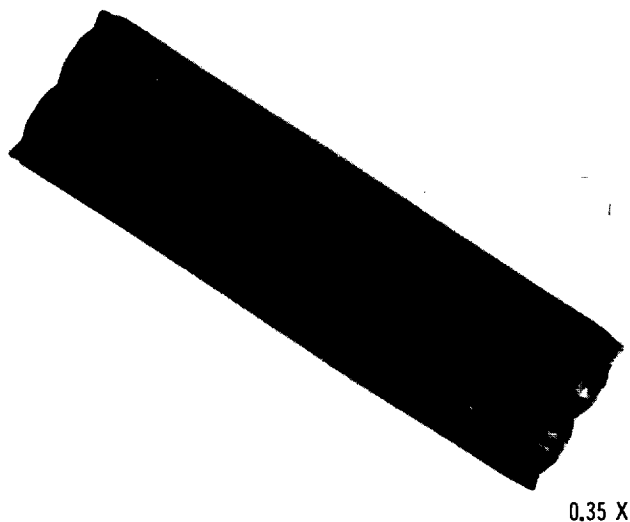
1 X

(B) After 100 Reentry and Acoustic Cycles

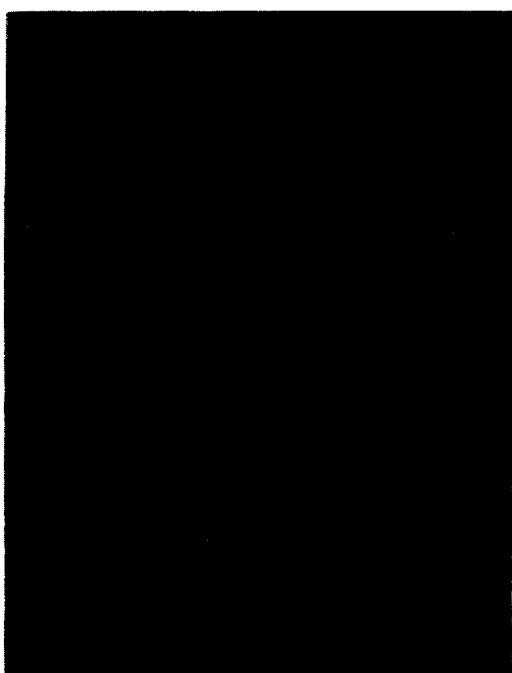
FLIGHT SIMULATION TESTING OF PANEL NO. 2

FIGURE 5-22



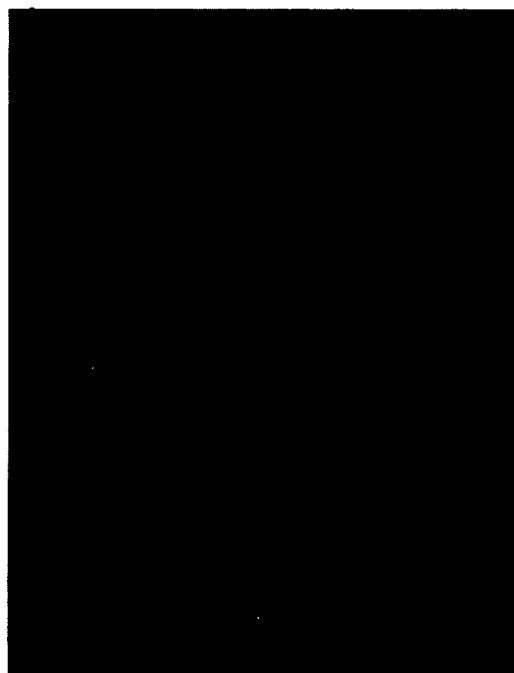


(A) After 44 Reentry and Acoustic Cycles



PANEL CENTER SECTION  
SKIN SIDE

(B) After 88 Reentry Cycles and  
66 Acoustic Cycles

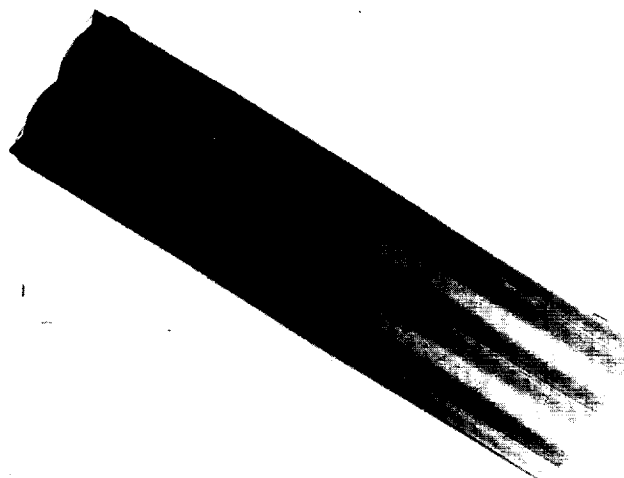


PANEL CENTER SECTION  
CORRUGATION SIDE

(C) After 88 Reentry and  
Acoustic Cycles

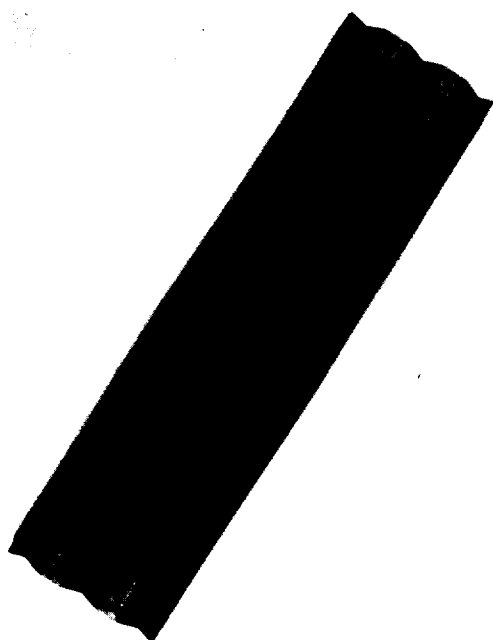
FLIGHT SIMULATION TESTING OF PANEL NO. 5

FIGURE 5-23



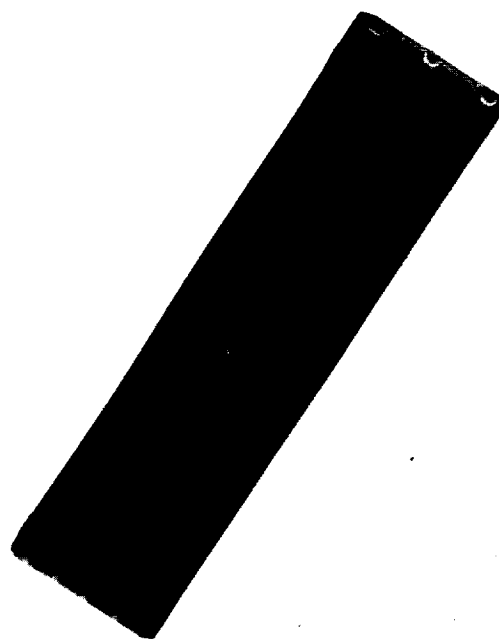
0.38 X

(A) As Coated Prior to Testing



CORRUGATION SIDE

0.38 X



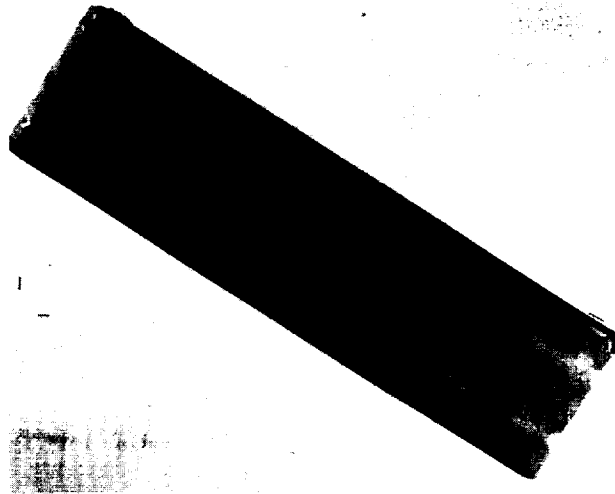
SKIN SIDE

0.38 X

(B) After 100 Reentry and Acoustic Cycles

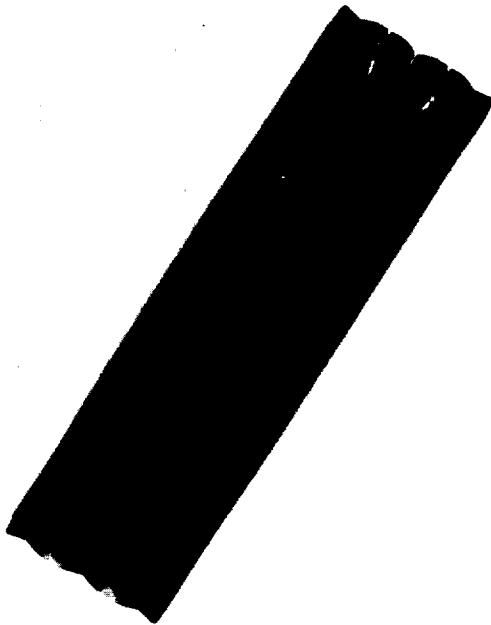
FLIGHT SIMULATION TESTING OF PANEL NO. 7

FIGURE 5-24



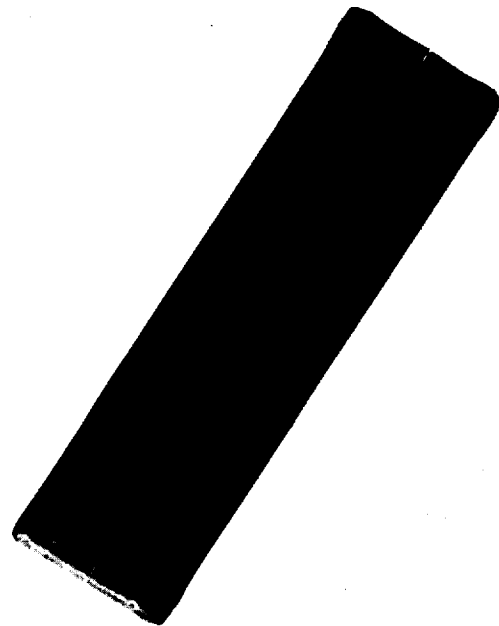
0.37 X

(A) As Coated Prior to Testing



0.37 X

CORRUGATION SIDE



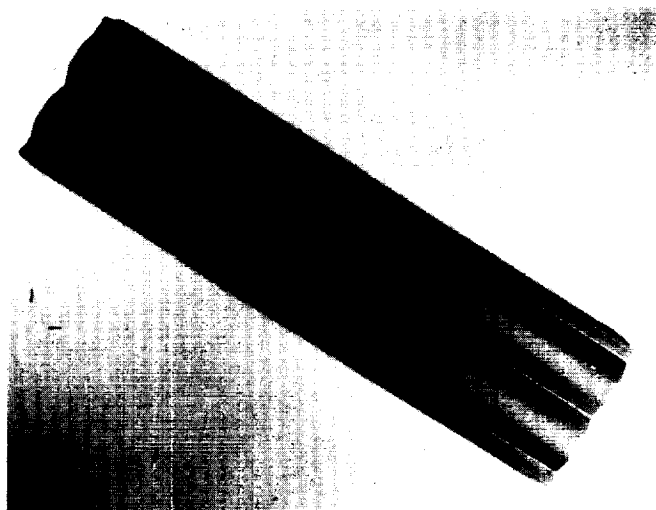
0.37 X

SKIN SIDE

(B) After 100 Reentry and Acoustic Cycles

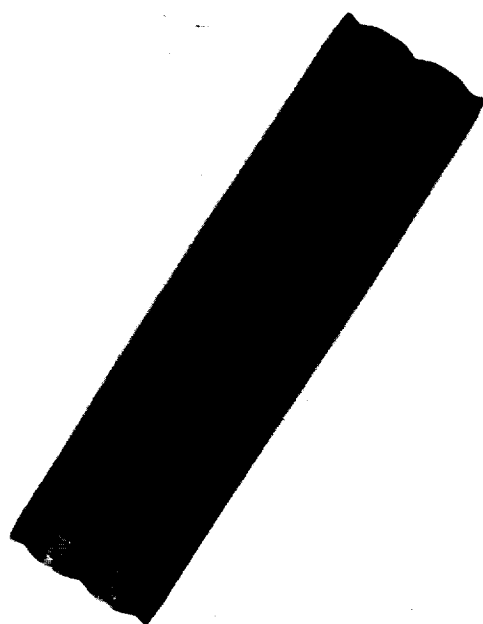
FLIGHT SIMULATION TESTING OF PANEL NO. 10

FIGURE 5-25



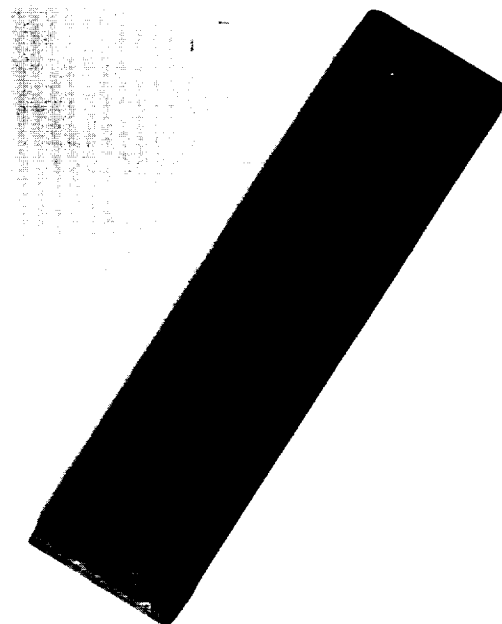
0.37 X

(A) As Coated Prior to Testing



CORRUGATION SIDE

0.37 X



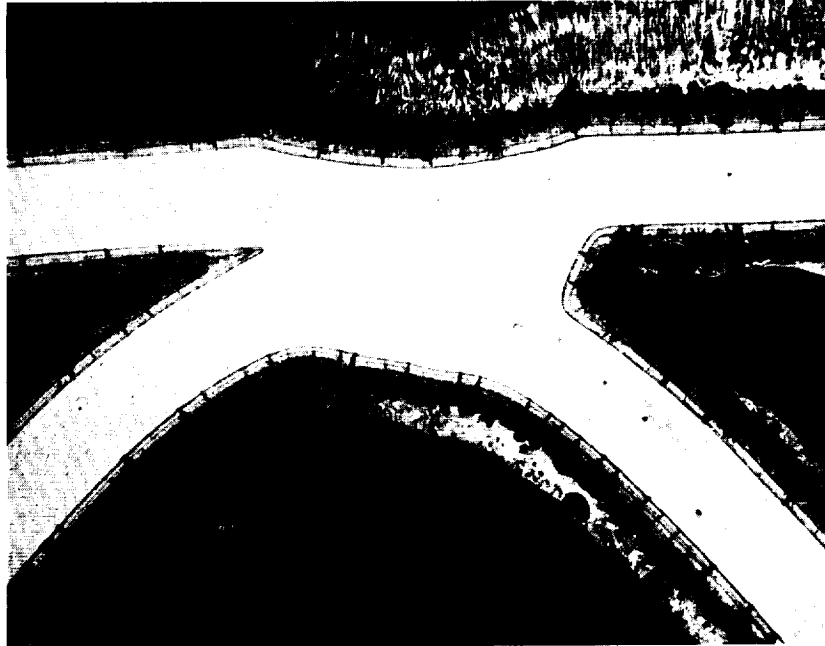
SKIN SIDE

0.37 X

(B) After 100 Reentry and Acoustic Cycles

FLIGHT SIMULATION TESTING OF PANEL NO. 12

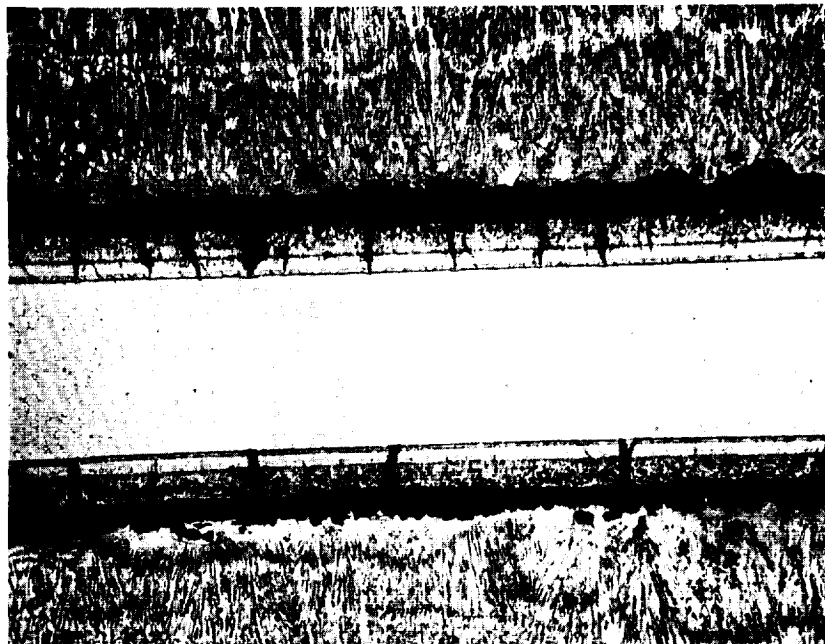
FIGURE 5-26



50 X

CORRUGATION-SKIN JOINT OF PANEL NO. 10 AFTER 100 REENTRY  
CYCLES - INTERNAL PRESSURE ENVIRONMENT

FIGURE 5-27



100 X

SKIN CROSS-SECTION BETWEEN WELDS OF PANEL NO. 10 AFTER 100  
REENTRY CYCLES - INTERNAL PRESSURE ENVIRONMENT

FIGURE 5-28

TABLE 5-8  
NDT DERMITRON COATING THICKNESS ON R-512E COATED FS-85  
SUB-SIZE CORRUGATION STIFFENED PANELS

1	3	5
2	4	6

7	9	11
8	10	12

PANEL NO.	NO. OF REENTRY CYCLES	COATING THICKNESS MILS/ $\mu$ m AT LOCATION											
		1	2	3	4	5	6	7	8	9	10	11	12
2	0	$\frac{2.9}{74}$	$\frac{2.9}{74}$	$\frac{2.9}{74}$	$\frac{2.9}{74}$	$\frac{3.1}{79}$	$\frac{3.1}{79}$	$\frac{2.9}{74}$	$\frac{2.9}{74}$	$\frac{2.9}{74}$	$\frac{2.9}{74}$	$\frac{2.9}{74}$	$\frac{2.9}{74}$
	100	$\frac{4.3}{109}$	$\frac{4.3}{109}$	$\frac{3.7}{94}$	$\frac{4.8}{121}$	$\frac{3.2}{81}$	$\frac{3.2}{81}$	$\frac{4.0}{101}$	$\frac{4.7}{119}$	$\frac{4.3}{109}$	$\frac{3.7}{94}$	$\frac{3.9}{99}$	$\frac{4.0}{101}$
5	0	$\frac{2.8}{71}$	$\frac{2.8}{71}$	$\frac{2.8}{71}$	$\frac{2.9}{74}$	$\frac{2.9}{74}$	$\frac{2.9}{74}$	$\frac{2.8}{71}$	$\frac{2.7}{69}$	$\frac{2.9}{74}$	$\frac{2.8}{71}$	$\frac{2.8}{71}$	$\frac{2.8}{71}$
	88	$\frac{3.9}{99}$	$\frac{3.7}{94}$	$\frac{4.1}{101}$	$\frac{4.1}{104}$	$\frac{4.1}{104}$	$\frac{4.1}{104}$	$\frac{3.9}{99}$	$\frac{3.7}{94}$	$\frac{6.4}{164}$	$\frac{3.7}{94}$	$\frac{6.1}{157}$	$\frac{5.7}{146}$
7	0	$\frac{2.9}{74}$	$\frac{2.9}{74}$	$\frac{3.1}{79}$	$\frac{3.1}{79}$	$\frac{2.9}{74}$	$\frac{3.1}{79}$	$\frac{2.9}{74}$	$\frac{2.8}{71}$	$\frac{2.9}{74}$	$\frac{2.9}{74}$	$\frac{2.9}{74}$	$\frac{2.9}{74}$
	100	$\frac{4.8}{121}$	$\frac{4.5}{114}$	$\frac{4.1}{104}$	$\frac{4.1}{104}$	$\frac{3.7}{94}$	$\frac{3.9}{99}$	$\frac{4.3}{109}$	$\frac{4.0}{101}$	$\frac{4.5}{114}$	$\frac{4.0}{101}$	$\frac{4.0}{101}$	$\frac{4.0}{101}$
10	0	$\frac{2.8}{71}$	$\frac{2.8}{71}$	$\frac{2.8}{71}$	$\frac{2.8}{71}$	$\frac{2.8}{71}$	$\frac{2.8}{71}$	$\frac{2.9}{74}$	$\frac{2.9}{74}$	$\frac{2.9}{74}$	$\frac{2.8}{71}$	$\frac{2.8}{71}$	$\frac{2.9}{74}$
		NOT MEASURED											
12	0	$\frac{2.8}{71}$	$\frac{2.8}{71}$	$\frac{2.8}{71}$	$\frac{2.8}{71}$	$\frac{2.8}{71}$	$\frac{2.9}{74}$	$\frac{2.8}{71}$	$\frac{2.9}{74}$	$\frac{2.8}{71}$	$\frac{2.8}{71}$	$\frac{2.8}{71}$	$\frac{2.8}{71}$
	100	$\frac{4.3}{109}$	$\frac{4.3}{109}$	$\frac{3.6}{91}$	$\frac{3.6}{91}$	$\frac{3.5}{89}$	$\frac{3.6}{91}$	$\frac{4.0}{101}$	$\frac{4.0}{101}$	$\frac{3.6}{91}$	$\frac{4.0}{101}$	$\frac{3.3}{84}$	$\frac{3.3}{84}$

It was determined that the fused slurry silicide coating applied to subsize corrugation stiffened heat shield panels utilizing optimized processing techniques developed in this program was of outstanding quality. The good coating quality was evidenced by the low incidence of coating failures; 80% of the tests were conducted for 100 reentry cycles.

The reuse evaluation testing was also designed to determine structural performance under service conditions which would be expected on Space Shuttle vehicles for 100 flights. From this aspect the coating and panel were treated as an integral unit. The failure criterion was structural life. There were no structural failures due to the application of flight loads. The only structural failure was induced by acoustic exposure. However, acoustic environment simulation was designed to produce fatigue failures in 100 flights. This was explained in Section 4.0. In actual practice heat shield panel design factors would be applied for fatigue life in order to obtain reliable structural performance for 100 flights.

The coating performance demonstrated with the subsize corrugation stiffened heat shield panels was satisfactory and go-ahead was given for coating of the full size panels for final verification of the coating application process.

5.3.2 Full Size Panels - Two full size 20" x 20" (50 cm x 50 cm) corrugation stiffened heat shield panels were fabricated from FS-85 columbium alloy sheet. Material gages, corrugation shape, pitch, and height were the same as those utilized on the subsize panels. Fabrication procedures were also identical, except for a skin beading operation prior to welding. The beads are 0.8" (2 cm) wide and 0.080" (0.2 cm) deep and were formed in the skin so there will be one between all welds. The beads are parallel to the welds and run the full length of the panel. The beading prevents the warping which occurs during welding of a flat skin. The skin warping between welds was evident with the rib stiffened panels.

The two 20" x 20" (50 cm x 50 cm) panels were prepared and dipped in the same A-32 slurry as the subsize panels and following the same general handling procedures. However, the residual stresses from welding curved these panels which meant having a minimum clearance between the panel and the dip tank walls during dipping. Therefore, a steel straightening bar was used as a support fixture during the dipping process. When this bar was used, there were three contact points where pins in the bar bore against the outer surfaces of the panel

as shown in Figure 5-29. Two C-clamps were used in suspending the panel during dipping. The five contact points made by the pins and C-clamps were later touched up readily with a dab of slurry applied by brush.

Although the A-32 slurry was approximately three months old, its viscosity was relatively stable. Accordingly the two panels were dipped at 1"/min (0.4 mm/sec) at a viscosity of 5.3 Nsec/m<sup>2</sup> and a temperature of 73°F (23°C).

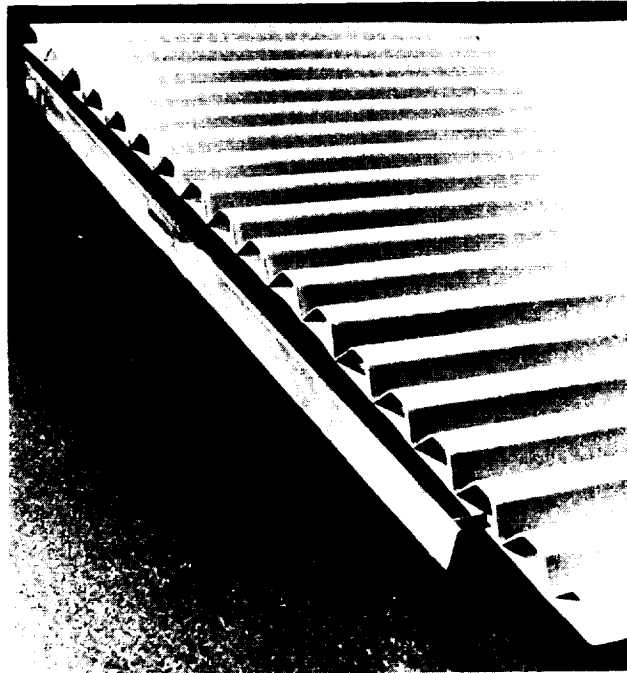
While processing the first panel F-1, it was noted that complete drying was not achieved inside the corrugations during an overnight period. When the panel was turned to a vertical position, it dripped. Therefore the slurry was stripped using methylene chloride, ultrasonically cleaned in acetone and hot vapor degreased. Subsequently, it was recoated, followed by overnight drying in still air plus a one hour period in moving air under a drying hood. Panel F-2 was coated in a similar fashion.

The straight edges on both panels were overcoated using the edge beading tool. To overcoat the edges of the corrugations, these ends were redipped to a depth of approximately 1/8" (0.32 cm) into the slurry bath and air dried. Each panel was vacuum diffusion treated in a separate run at 2580°F for one hour (1420°C for 36 h sec). It was difficult to maintain a reasonable heating rate without allowing the pressure in the furnace to rise above  $1 \times 10^{-5}$  torr. The total furnace cycle was about five hours (18 ksec) in each case, compared to about three hours (10.8 ksec) needed with C-5 slurry coated similar size panels processed in previous work.

There was a powdery residue on the surfaces of the panels after heat treatment. The finished coating weights for panels F-1 and F-2 were 22.7 and 23.0 mg/cm<sup>2</sup>, respectively, compared to their green coating weights of 27.8 and 27.6 mg/cm<sup>2</sup>. The weight losses during firing were about 2 mg/cm<sup>2</sup> less than was expected from the work done on the subsize panels. This difference appears to be related to the residue, although some effort was made to remove it by brushing prior to weight measurements.

Dermatron and thermoelectric probe measurements before and after firing are shown for panel F-1 in Figures 5-30, 5-31 and 5-32 and for panel F-2 in Figures 5-33, 5-34 and 5-35. Coating uniformity from top to bottom and from skin side to corrugation side appears to be very good for both panels. The minimum edge thickness indications were equal to or exceeded the 2.0 millivolts level required, and the general thickness variation appear to be well within plus or minus 10%.



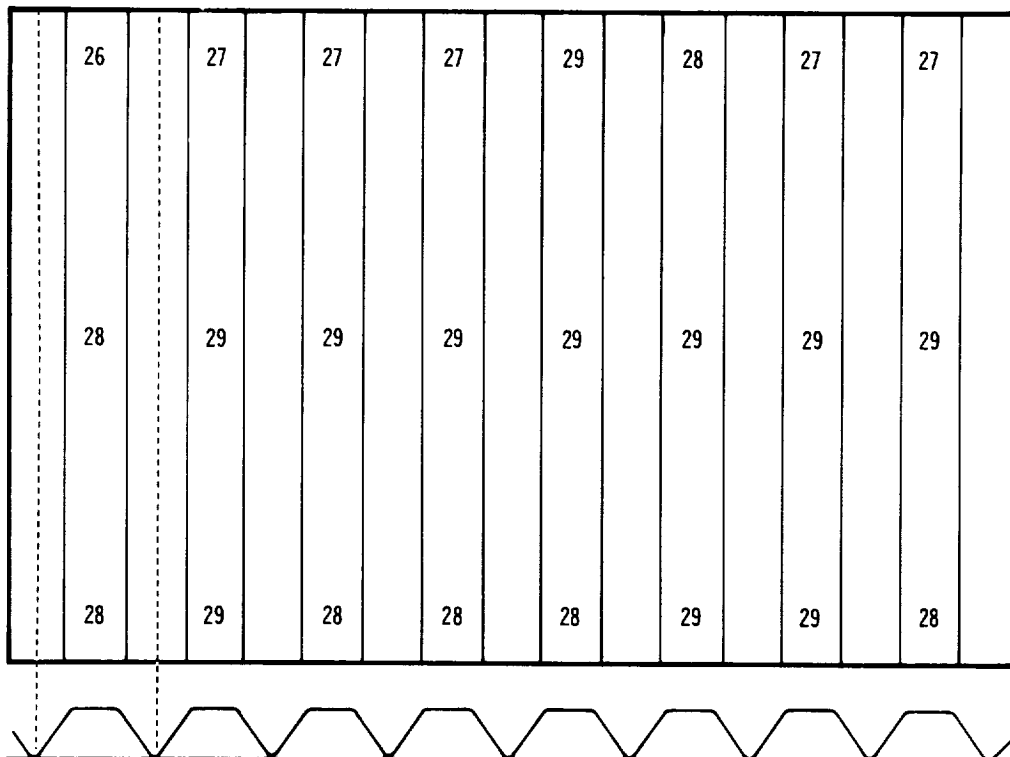


STRAIGHTENING BAR FIXTURE IN PLACE OF PANEL F-1 PRIOR TO DIPPING

FIGURE 5-29

The general appearance of the two panels after coating is illustrated in Figures 5-36 and 5-37. Both have uniform texture over all surfaces with a slight exception. On the bottom half of each panel (dipping direction), in the valleys between corrugations, which correspond to the weld line, the coating is somewhat shiny. Under a low power microscope it appears the coating may be somewhat thicker here than in other areas.

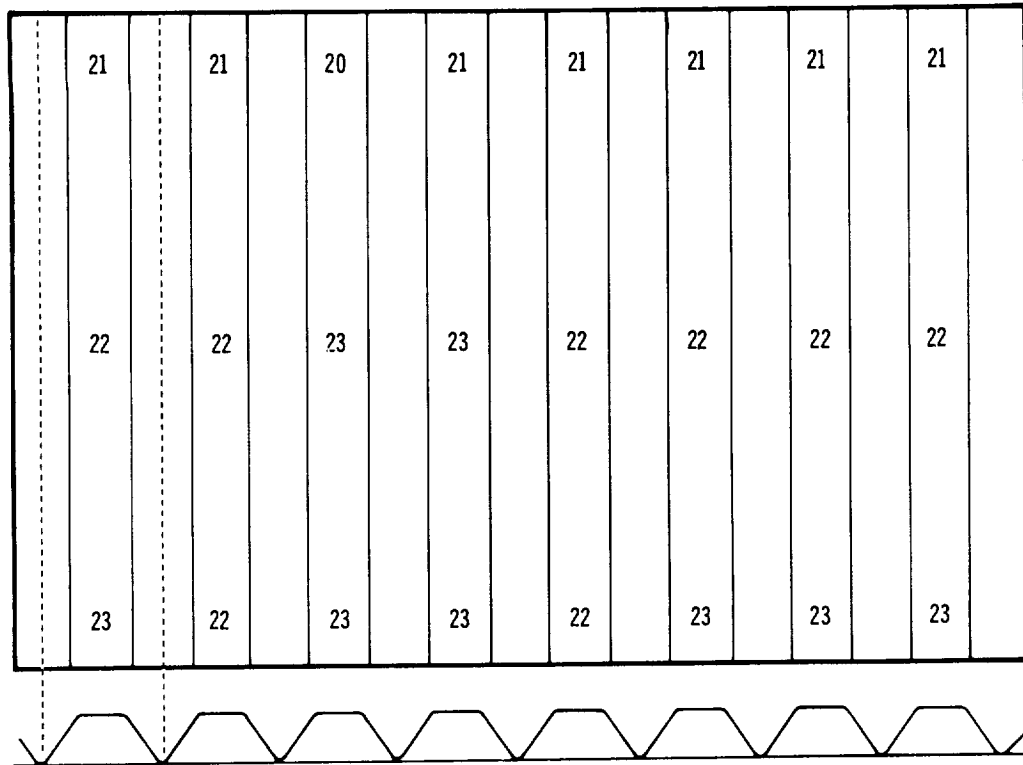
In summary the coating process utilizing the acrylic based vehicle can be used to obtain good, adherent, uniform and reproducible coatings on corrugated panels. The process specification for application of the R-512E coating using the A-32 slurry is presented in Section IV.



28	28	28	28	28	28	29	29
29	29	29	29	29	29	28	29
28	29	29	29	29	29	29	29

GREEN COATING UNIFORMITY BY DERMITRON NDT – PANEL F-1

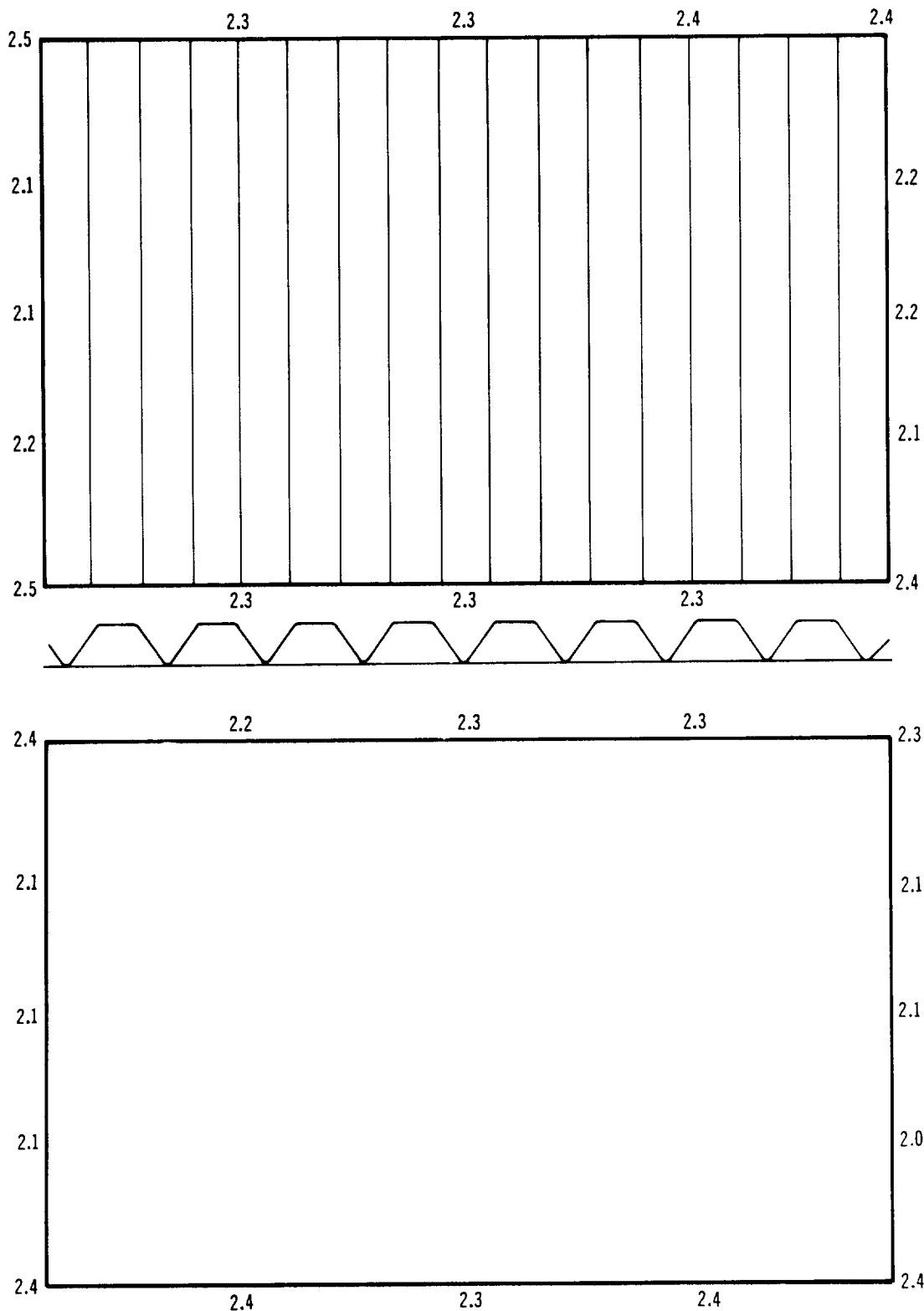
FIGURE 5-30



21	21	21	21	21	22	21	21
22	22	22	21	22	23	22	22
23	22	22	23	23	22	23	23

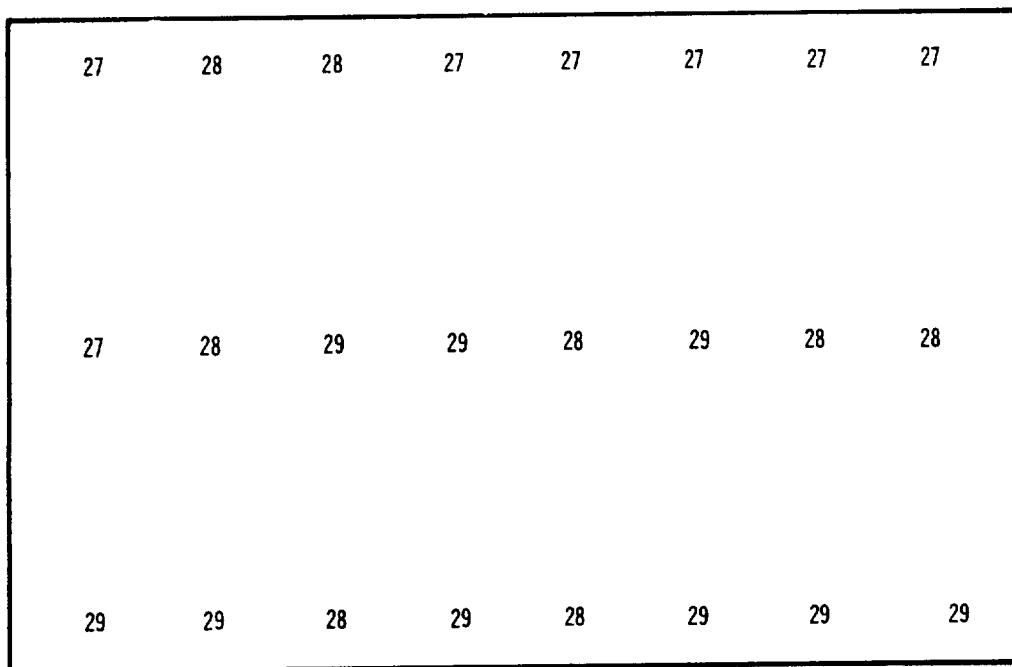
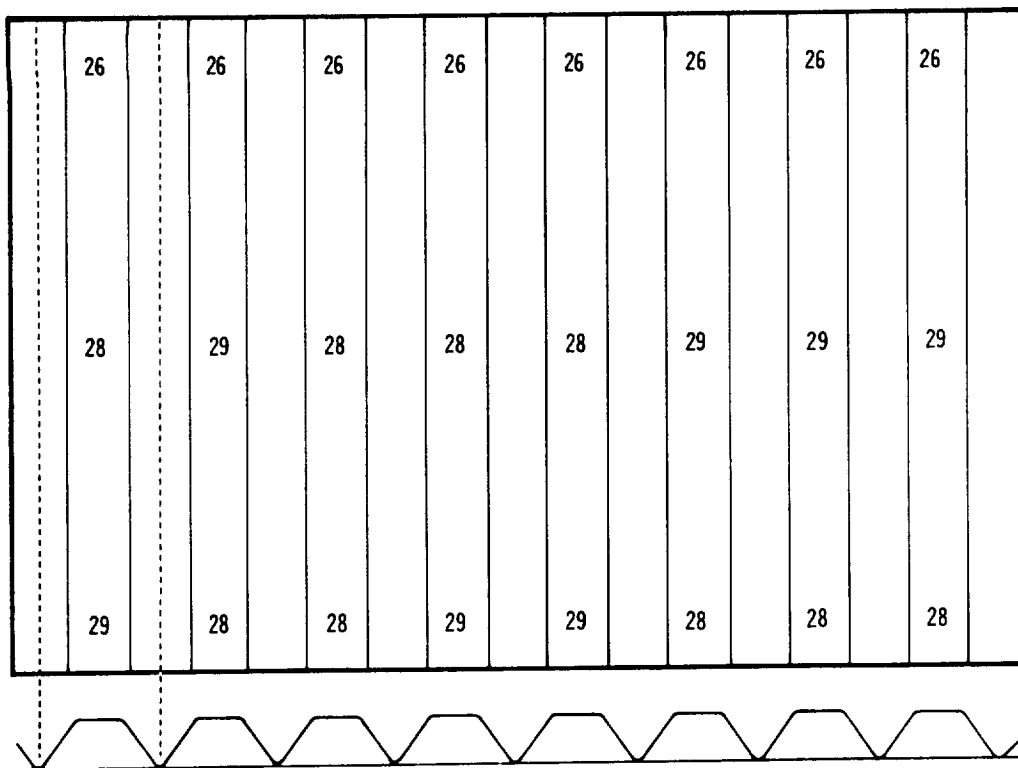
FINAL COATING UNIFORMITY BY DERMITRON NDT – PANEL F-1

FIGURE 5-31



FINAL EDGE COATING THICKNESS UNIFORMITY BY  
THERMOELECTRIC NDT - PANEL F-1

FIGURE 5-32



GREEN COATING UNIFORMITY BY DERMITRON NDT - PANEL F-2

FIGURE 5-33

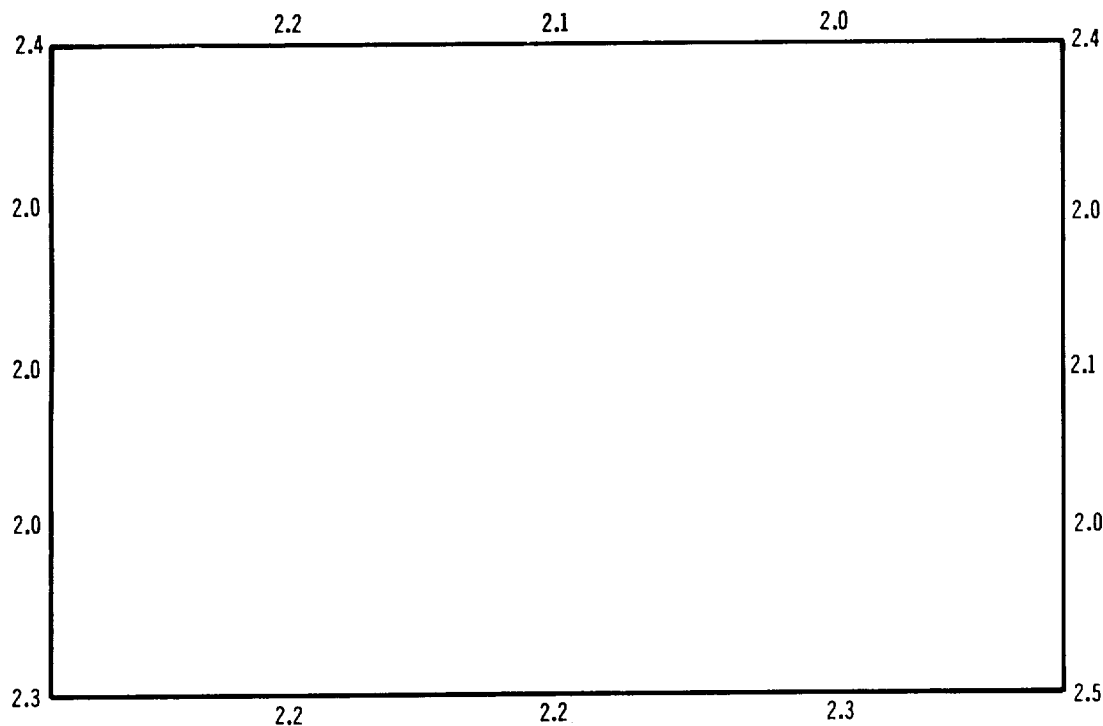
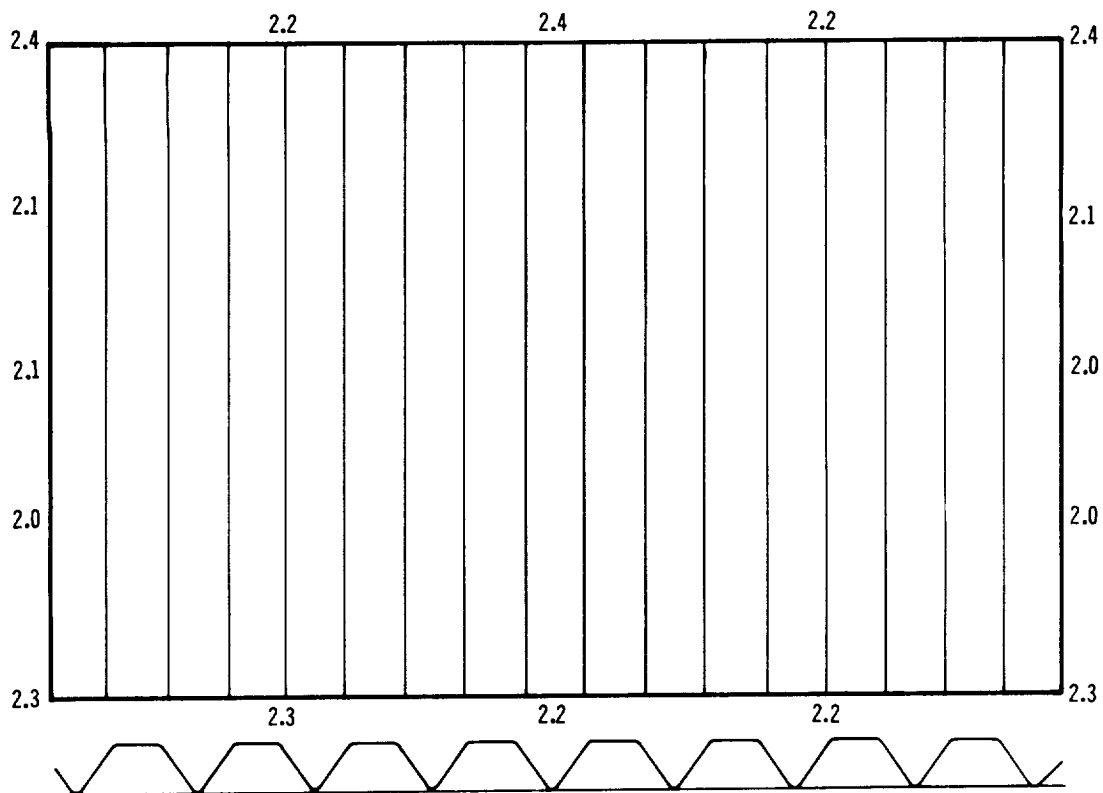
	20		20		20		21		21		21		20		21	
	22		22		22		22		22		21		21		22	
	22		22		23		22		23		22		22		22	



22	22	21	22	22	21	21	22
22	22	23	22	22	23	22	22
23	23	23	23	23	22	23	23

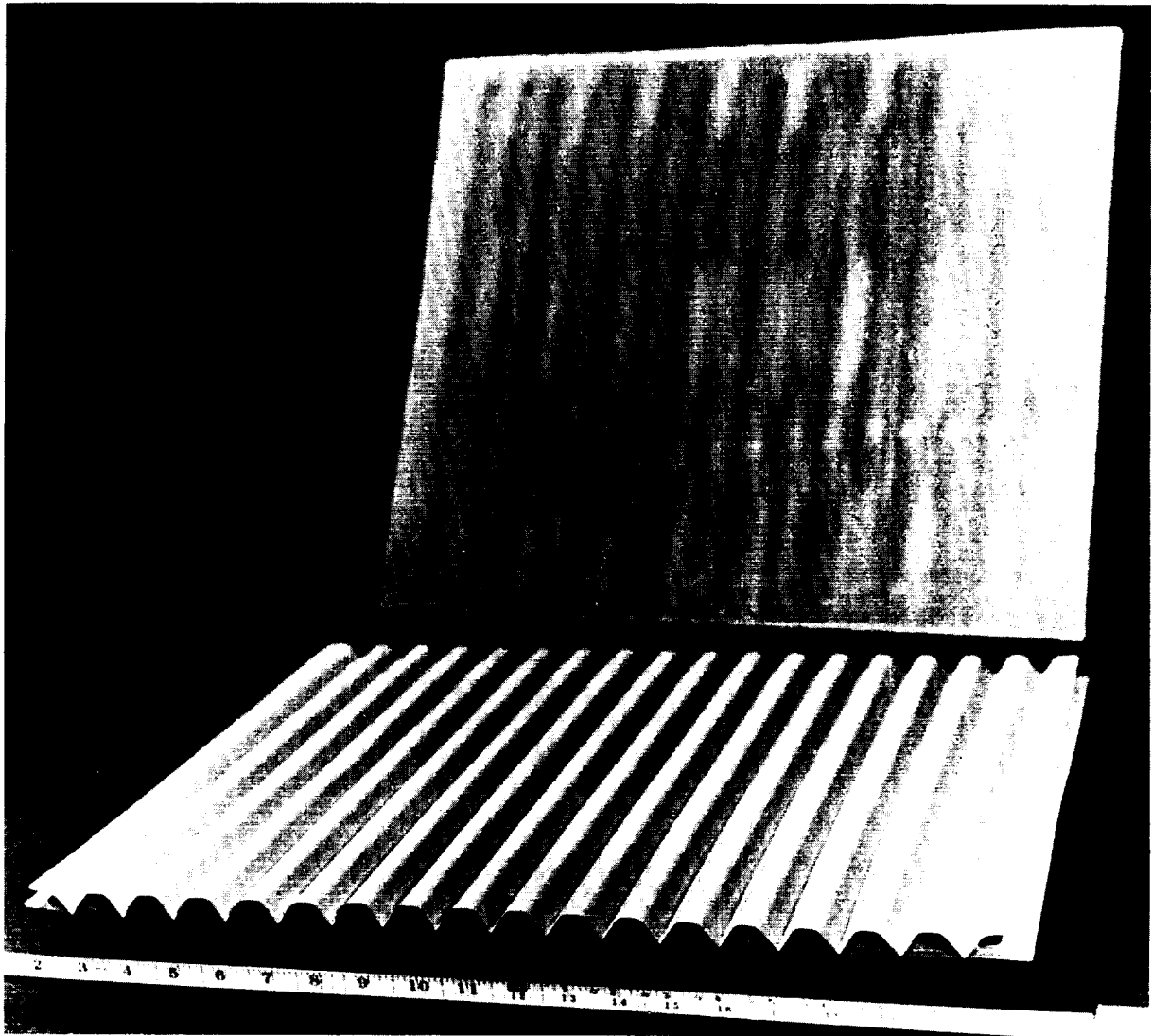
FINAL COATING UNIFORMITY BY DERMITRON NDT - PANEL F-2

FIGURE 5-54



FINAL EDGE COATING UNIFORMITY BY THERMOELECTRIC NDT - PANEL F-2

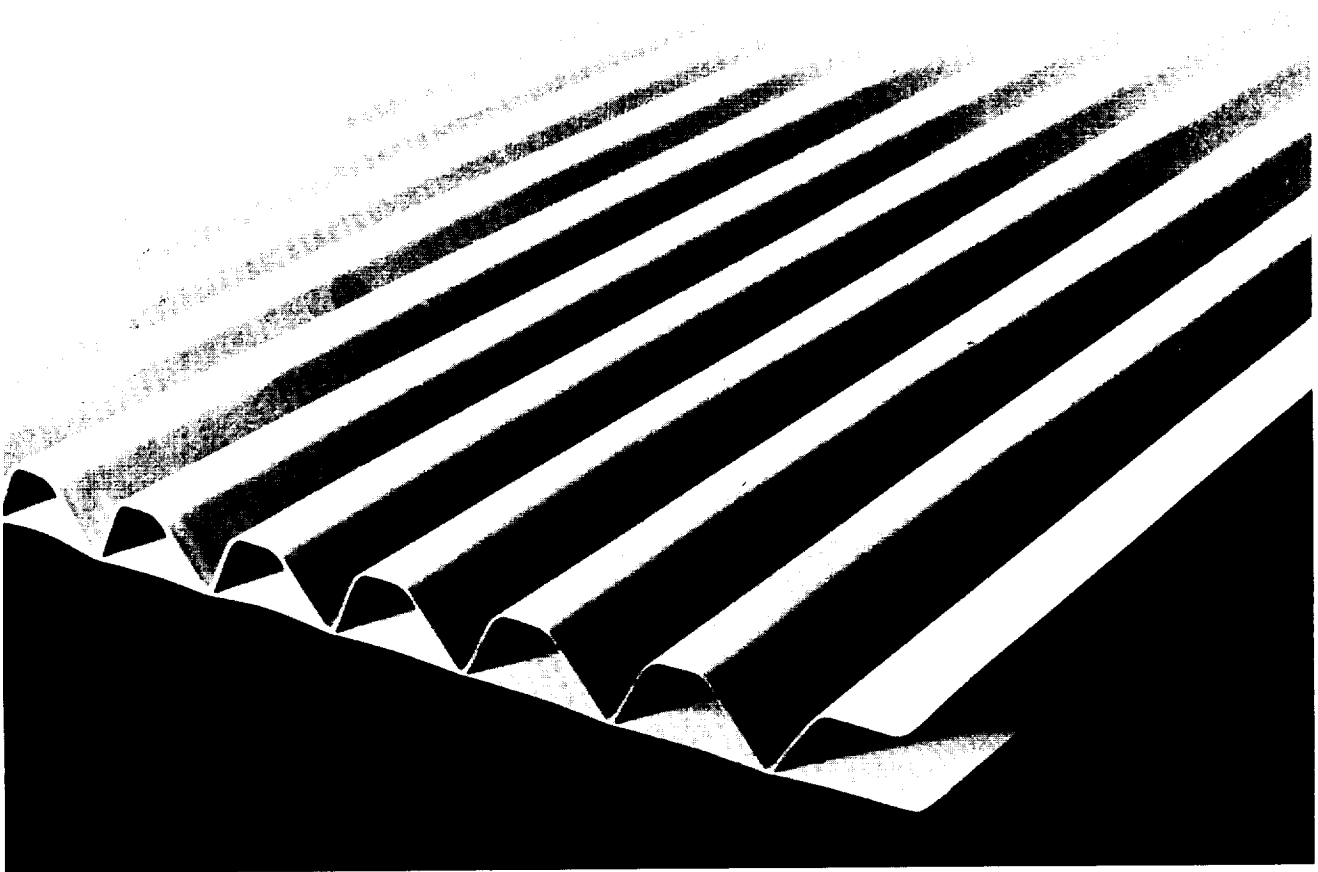
FIGURE 5-35



GENERAL APPEARANCE OF PANELS F-1 AND F-2 AFTER COATING

FIGURE 5-36





CLOSEUP VIEW OF CORNER AREA OF PANEL F-1 AFTER COATING

FIGURE 5-37

II

C-5 COATING PROCESS SPECIFICATION

Section II contains the process specification for application of the R-512E coating to rib stiffened columbium alloy heat shield panels, utilizing a nitro-cellulose lacquer base slurry.

C-5 COATING PROCESS SPECIFICATION

Application of R-512E Coating to Heat Shield Panels of Rib Stiffened Design

1.0 SCOPE

This specification covers the application of R-512E (Si-20Cr-20Fe) Fused Slurry Silicide Coating to rib stiffened columbium alloy heat shield panels.

2.0 MATERIALS

- 2.1 Silicon metal powder - 325 mesh - 99% pure
- 2.2 Chromium metal powder - 325 mesh - 99% pure
- 2.3 Iron metal powder - 325 mesh - 99% pure
- 2.4 MPA 60 - lacquer additive
- 2.5 Thixatrol ST - lacquer additive
- 2.6 Lacquer - L18 or equivalent
- 2.7 Lacquer thinner - commercial

3.0 R-512E COMPOSITION

Silicon	60.0	wt. %
Chromium	20.0	wt. %
Iron	20.0	wt. %

4.0 PROCEDURE - SLURRY PREPARATION

4.1 Weigh out to the nearest gram the following quantities of material to make 1000 g of R-512E.

Silicon	600 g
Chromium	200 g
Iron	200 g

Multiples of the above batch can be prepared.

- 4.2 Dry blend for 1-2 hours in a V-type blender.
- 4.3 Weigh out 300 g L18 lacquer and pour into shearing mixing container.
- 4.4 Weigh out 32 g MPA 60 and add to blending container.
- 4.5 Weigh out 2 g Thixatrol ST and add to blending container.
- 4.6 Blend lacquer and additives (Premier Dispersator Series 2501 or equivalent) and after 60 sec slowly add preblended R-512E powder charge. Blend 600 sec after powder has been added.

4.7 Transfer to dipping container and cool, and age at least 24 hours (86.4 ksec) prior to use.

4.8 Check viscosity temperature and specific gravity prior to use - adjust if necessary with lacquer thinner.

4.9 Slurry Requirement -

Viscosity	2300 cp ( $2.3 \text{ Nsec/m}^2$ )
Temperature	72-73°F (22.2-22.8°C)
Specific gravity	1.673

5.0 PRECOATING PREPARATION

5.1 Visually check general condition of part. Any flaws which will affect the performance of the final hardware shall be cause for rejection.

5.2 Degrease part.

5.3 Weigh part to nearest gram and record.

6.0 COATING APPLICATION

6.1 Stir slurry thoroughly. Check viscosity and temperature. Adjust, if required, and record.

6.2 Place part in dipping rack.

6.3 Slowly immerse part in rack into the slurry tank.

6.4 Withdraw part at 2.0 to 2.5 in/min (0.8 to 1.0 mm/sec).

6.5 Dry part in still air.

6.6 Weigh part.

6.7 Calculated weight change/unit area is to be  $22 \pm 3 \text{ mg/cm}^2$ .

6.8 If part meets 6.7 then NDT inspect for thickness; if not, strip in lacquer thinner and recoat, adjusting withdrawal rate to meet requirement of 6.7.

7.0 NDT INSPECTION

7.1 NDT inspection for thickness uniformity is carried out with a Dermatron Model D5 or equivalent.

Probe C

Operating position 3

The machine is standardized by adjusting the balance and sensitivity controls. Green coated coupons 1" x 1" (2.5 cm x 2.5 cm) of the same base alloy and

thickness of the part shall be used as standards. These coupons have approximately 15, 20 and 25 mg/cm<sup>2</sup> thickness and the Dermitron is set to read 30, 40, and 50, respectively.

Data should be taken on a minimum grid of 3" x 3" (7.5 cm x 7.5 cm) on the facing sheet. The back of the facing sheet between the ribs is also to be measured in 20 locations. The sides of the ribs do not lend themselves to this treatment. NDT measurements should indicate coating of  $22 \pm 3$  mg/cm<sup>2</sup> on all measured areas.

7.2 If the panel fails to meet the requirements of 7.1, then it is to be stripped and recoated as per 6.1 to 6.8, adjusting viscosity and withdrawal rate to produce a more uniform coating.

#### 8.0 EDGE COATING

- 8.1 Fill edge roller tube with slurry, viscosity 3500 cp (3.5 Nsec/m<sup>2</sup>).
- 8.2 Slowly roll edge coater along each edge.
- 8.3 Air dry.

#### 9.0 DIFFUSION TREATMENT

9.1 Load panels into vacuum furnace capable of 2600°F (1425°C) and 1 torr absolute pressure.

9.2 Evacuate furnace below 0.5 torr before starting run.

9.3 Bring furnace to  $2580 \pm 30^\circ\text{F}$  ( $1420 \pm 1^\circ\text{C}$ ) and hold at temperature for 1 hour (36 h sec).

9.4 Do not allow pressure in furnace to rise above 1 torr during heating cycle. If pressure exceeds 1 torr then shut power and allow for pressure recovery.

9.5 Record time, temperature, pressure at least every 10 min (6 ksec) during heating and holding cycle.

9.6 Cool furnace to below 500°F (260°C) before unloading parts.

#### 10.0 INSPECTION

- 10.1 Weigh part and record. Calculate final weight.
- 10.2 Check for coating uniformity with Dermitron.
- 10.3 Check for edge thickness with thermoelectric roller probe.

11.0 REQUIREMENTS

11.1 Final coating weight shall be  $19 \pm 3 \text{ mg/cm}^2$ .

11.2 Final NDT by Dermitron shall indicate local coating thickness to be  $19 \pm 6 \text{ mg/cm}^2$ .

11.3 The thermoelectric reading (nickel probe) on edge shall be 20 millivolts minimum.

III

A-32 COATING PROCESS SPECIFICATION

Section III contains the process specification for application of the R-512E coating to corrugation stiffened columbium alloy heat shield panels utilizing an acrylic resin base slurry.

A-32 COATING PROCESS SPECIFICATION

Application of R-512E Coating to Heat Shield Panels of Corrugation  
Stiffened Design

1.0 SCOPE

This specification covers the application of R-512E (Si-20Cr-20Fe) Fused Slurry Silicide Coating to corrugation stiffened columbium alloy heat shield panels.

2.0 MATERIALS

- 2.1 Silicon metal powder - 325 mesh - 99% pure
- 2.2 Chromium metal powder - 325 mesh - 99% pure
- 2.3 Iron metal powder - 325 mesh - 99% pure
- 2.4 MPA
- 2.5 B-66 Acrylic Resin
- 2.6 High Flash Naphtha (HFN) Thinner - Solvent
- 2.7 Methylene Chloride
- 2.8 Acetone

3.0 R-512E COMPOSITION

Silicon	60.0	wt. %
Chromium	20.0	wt. %
Iron	20.0	wt. %

4.0 PROCEDURE - SLURRY PREPARATION

4.1 Weigh out to the nearest gram the following quantities of material to make 3600 g of R-512E:

Silicon	2160 g
Chromium	720 g
Iron	720 g

4.2 Dry blend for 1-2 hours (36-72 h sec) in a V-type blender.

4.3 Weigh out 464 g of B-66 Acrylic.

4.4 Weigh out 726 g of HFN.

4.5 Pour Acrylic and HFN into one quart ( $9.5 \times 10^{-4} \text{ m}^3$ ) shearer and shear for 3 minutes (180 sec).



- 4.6 Weigh out and add 150 g MPA and shear for 3 min (180 sec).
- 4.7 Age for 16 hours ( $5.76 \times 10^4$  sec).
- 4.8 Pour mixture into blender (Premier Dispenser Series 2501 or equivalent) and slowly add R-512E powder.
- 4.9 Add another 150 g HFN and shear for 8-10 min (29-36 ksec) until temperature reaches 140-150°F (60-66°C).
- 4.10 Cool to room temperature.
- 4.11 Add HFN until viscosity reaches 7000-7500 cp ( $7.0-7.5 \text{ Nsec/m}^2$ ).
- 4.12 Age for 1 week and check viscosity. Should be 5000-5500 cp ( $5.0-5.5 \text{ Nsec/m}^2$ ).
- 4.13 If too high add HFN to lower viscosity to desired level.
- 4.14 Slurry Requirement:
- |                  |                                    |
|------------------|------------------------------------|
| Viscosity        | 5300 cp ( $5.3 \text{ Nsec/m}^2$ ) |
| Temperature      | 72-73°F (22.2-22.8°C)              |
| Specific Gravity | 1.906                              |

## 5.0 PRECOATING PREPARATION

- 5.1 Visually check condition of part. Any flaws which will affect the performance of the final hardware shall be cause for rejection.
- 5.2 Vapor degrease part.
- 5.3 Weigh part to nearest gram and record.

## 6.0 COATING APPLICATION

- 6.1 Stir slurry thoroughly. Check viscosity and temperature. Adjust, if required, and record.
- 6.2 Place part in dipping fixture.
- 6.3 Slowly immerse part in fixture into the slurry tank.
- 6.4 Withdraw part at  $3/4"$  to 1 in/min (0.3 to 0.4 mm/sec).
- 6.5 Place part in drying rack on pins and dry in still air for 16 hours ( $5.76 \times 10^4$  sec).
- 6.6 Dry in moving air for at least one hour (36 h sec).
- 6.7 Weigh part.
- 6.8 Calculate weight change/unit areas should be  $25 \pm 3 \text{ mg/cm}^2$ .
- 6.9 If part meets 6.8 then NDT inspect for thickness; if not strip in methylene chloride, ultrasonically clean in acetone and wipe down all surfaces with a soft cloth. Then recoat, adjusting withdrawal rate to meet requirement of 6.8.

## 7.0 NDT INSPECTION

7.1 NDT inspection for thickness uniformity is carried out with a Dermatron Model D5 or equivalent.

Probe C

Operating Position 3

The machine is standardized by adjusting the balance and sensitivity controls. Green nitrocellulose vehicle R-512E coated coupons 1" x 1" (2.5 cm x 2.5 cm) of the same base and thickness columbium alloy can be used as standards. These coupons have approximately 15, 20 and 25 mg/cm<sup>2</sup> thickness and the Dermatron is set to read 30, 40 and 50 respectively.

Data should be taken at a minimum of 24 locations on the skin side and on the outer crest of every other corrugation. NDT measurements should indicate a coating of  $25 \pm 3$  mg/cm<sup>2</sup>.

7.2 If coating does not meet thickness requirements then it is to be stripped as per 6.9 and recoated as per 6.1 to 6.8.

## 8.0 EDGE COATING

8.1 Fill edge roller tube with slurry, viscosity 3000-3500 cp (3.0-3.5 Nsec/m<sup>2</sup>).

8.2 Slowly roll edge coater along each edge.

8.3 Air Dry.

## 9.0 DIFFUSION TREATMENT

9.1 Load panels into vacuum furnace capable of 2600°F (1425°C) and 1 torr.

9.2 Evacuate furnace below 0.5 torr before starting run.

9.3 Bring furnace to 2580°F  $\pm$  30°F (1420  $\pm$  1°C) and hold at temperature for 1 hour (36 h sec).

9.4 Do not allow pressure in furnace to rise above 1 torr during heating cycle. If pressure exceeds 1 torr then shut power and allow for pressure recovery.

9.5 Record time, temperature, pressure at least every 10 min (6 ksec) during heating and holding cycle.

9.6 Cool furnace to below 500°F (260°C) before unloading parts.

10.0 INSPECTION

- 10.1 Weigh part and record. Calculate final unit weight gain.
- 10.2 Check for coating uniformity with Dermatron.
- 10.3 Check for edge thickness with thermoelectric roller probe.

11.0 REQUIREMENTS

- 11.1 Final coating weight shall be  $19 \pm 3 \text{ mg/cm}^2$ .
- 11.2 Final NDT by Dermatron shall indicate local coating thickness to be  $19 \pm 6 \text{ mg/cm}^2$ .
- 11.3 The thermoelectric reading (nickel probe) shall be 20 millivolts minimum.

IV

REFERENCES

- (1) Christensen, H. E., "Entry Thermal Environment for Shuttle TPS High Temperature Insulation," Technical Memo E242-324, 29 September 1970.
- (2) Fitzgerald, B. G. and Rusert, E. L., "Evaluation of the Fused Slurry Silicide Coating Considering Component Design and Reuse," Technical Report AFML-TR-70-154, December 1970.
- (3) Sama, L. and Reznik, B., "Development of Production Methods for High-Temperature Coating of Tantalum Parts." AFML-TR-66-217, Sylcor Division of Sylvania to Air Force Materials Lab on AF33(657)11272, August 1966.
- (4) Priceman, S. and Sama, L., "Development of Fused Slurry Silicide Coatings for the Elevated Temperature Oxidation Protection of Columbi-um and Tantalum Alloys," AFML-TR-68-210, dated December 1968.